ABSTRACT

Title of thesis: SCALE MODELING OF THE TRANSIENT BEHAVIOR OF WOOD CRIB FIRES IN ENCLOSURES

Jonathan Andrew Perricone, Master of Science, 2005

Thesis directed by: John L. Bryan Chair Professor James G. Quintiere
Department of Fire Protection Engineering

Scale modeling affords engineers the ability to appreciate the dynamic enclosure fire environment of larger than life structures in the laboratory. Conventional approaches to scaling have expressed results in terms of time-averaged values. Transient scaling accuracy must be achieved in order to reasonably assess the interaction of the fire environment with the structural components of a prototype building. A wood crib is used to represent a typical fuel arrangement. The parameters of the wood crib and its surrounding enclosure are designed based on length scale relationships derived from the governing conservation equations. Experiments conducted at three model scales, in ventilation limited enclosures, demonstrate a high degree of both transient and spatial accuracy in the prediction of burning rates, temperatures and gas concentrations. Although it seems that a global energy balance is achieved, some inconsistencies in the scaling of local radiant heat fluxes are highlighted for future attention.

SCALE MODELING OF THE TRANSIENT BEHAVIOR OF WOOD CRIB FIRES IN ENCLOSURES

by

Jonathan Andrew Perricone

Thesis submitted to the Faculty of the Graduate School of the
University of Maryland, College Park in partial fulfillment
of the requirements for the degree of
Master of Science
2005

Advisory Committee:

Professor James G. Quintiere, Chair
Professor Andre Marshall
Professor Arnaud Trouve

DEDICATION

On September 11, 2001, an act of evil was vanquished by the legacy of one of the most powerful displays of courage and sacrifice in all of history. A total of 343 firemen gave their lives in an attempt to carry themselves and their equipment 80 stories to fight a battle against a raging inferno. As engineers, we design the fire environment. We hold the power to identify the challenges that it presents and the potential to eradicate them altogether. May the courage of these heroes ignite a furious determination among us to seize our potential. We are called to sacrifice our own lives in a different way, but for the same ideals. May the depth of our sacrifices demonstrate the immortality of our spirit.

ACKNOWLEDGEMENTS

This research effort has been a journey that has been filled with love and support from family, friends and colleagues. During my education at The University of Maryland, I have been so very fortunate to receive educational and professional guidance from an outstanding faculty in the Department of Fire Protection Engineering. Most notably among these men is my mentor, teacher and friend, Dr. James G. Quintiere. His tireless dedication and consistent innovation are the lifeblood of Fire Protection Engineering at the University of Maryland. For many years, Dr. Quintiere has shaped the minds of both professionals and students from all backgrounds with a well deserved confidence in his own abilities that is the product of unparalleled expertise. During my time in graduate school, Dr. Quintiere has reached out to me like so many others, with limitless patience and gentle guidance. Thank you, Dr. Quintiere, for your work and your teaching. They are an immeasurable gift to our profession and the public that is serves.

During my time in graduate school I have also cherished the opportunity to be a part of a very special group of students in the Potomac Laboratory. I thank Yunyong (Pock) Utiskul, Joe Panagiotou and Xin Liu for teaching me the ropes in the lab. Thank you, Pock and Joe especially, for your willingness to lend a hand at a moment's notice, including weekends. Such care comes only from genuine friendship.

Among this group in the Potomac Laboratory is my partner Peter Veloo, for whom I am forever grateful. Peter is responsible for the continuation of this research and I could not be more confident in the mind that will continue to shape this work. Thank you, Peter, for keeping me sane throughout so many difficult challenges. Thank you for

working in the lab with me until all hours of the morning to construct giant fire compartments. Your thirst for challenges will carry you very far in your career.

Thank you to Ming Wang and Dr. Peter Chang of the Department of Civil Engineering at the University of Maryland. Their concurrent development of scaled steel structures to implement into these fire compartments has provided valuable insight into the design of the fire models.

I am very thankful for the help of the staff at the ATF Fire Research Laboratory in Beltsville, MD, particularly agent Scott Dillon. Thank you, Scott for opening your doors to us and giving so much of your time to supervise our testing. Your generosity contributed directly to the success of this project.

Throughout the many long nights in the lab and weekends in the office I have been so fortunate to have the love and support of my wife, Kara. Kara, you are my source of strength in this and in all that I do. Thank you for your constant encouragement and the sacrifices that you have made, which have allowed me to give the necessary attention to this research. My love for you gives me an unwavering motivation and understanding of what protecting the public is and what it must become. Thank you to Barry, Cindi and Vaughn Warren for your love and support. I would like to particularly acknowledge the countless sacrifices of Barry and Vaughn who have served our country so proudly for so many years.

Thank you to my parents, Joe and Elaine, who have sacrificed so much to provide me with an outstanding education so that I could reach this point of accomplishment. You have instilled in me the importance of having dreams and given me the tools necessary to follow them. Your constant love and support have shaped me into who I am

today. I am especially thankful for that same love and support from my grandparents. Thank you, Grammy, Poppops and Grandma for your generosity, your willingness to listen and your desire to always be an integral part of my life. I am blessed to have been surrounded in my youth by role models of strong, hard-working men in my father and grandfather. Your examples have demonstrated the importance of integrity and sacrifice through many years of confronting life's challenges.

No list of acknowledgements would be complete without my older brother Matthew. Matthew, you are my oldest and truest friend. I have admired you in many ways for many years. As Dr. Matthew Perricone, you have earned my utmost professional respect. You are a remarkably talented young leader in engineering. Sharing my engineering experiences with you through graduate school has reinforced my determination and given an invaluable confidence during particularly difficult challenges. Knowing that I have your love, support and professional respect is priceless to me.

TABLE OF CONTENTS

LIST OF TABLES

LIST OF FIGURES

NOMENCLATURE

a	Ratio of Burning to Total Fuel Surface Area
A_c	Char Surface Area
A_o	Enclosure Vent Area
A_s , A_f	Total Exposed Surface Area of Crib
A_T	Total Enclosure Surface Area (Internal)
A_v	Area of Vertical Shafts within Crib
B	Spalding Transfer Number
b	Stick Cross Sectional Dimension
C	Material Constant
C_d	Flow Coefficient
c_p	Specific Heat
D	Height of Thermal Discontinuity
$d_{orifice}$	Fuel Bed Diameter
E	Elevation of Crib
F	Thermal Diffusivity Ratio
F_{ij}	View Factor Relationship
Fr	Froude Number
f	Friction Factor
G	Geometric Factor
G_o	Initial Crib Mass
Gr	Grashof Number
g	Gravitational Acceleration
H	Height of Enclosure
H_0	Enclosure Vent Height
ΔH_c	Heat of Combustion of Fuel
ΔH_{O_2}	Heat of Combustion of Oxygen
h_c	Height of Crib
h_{flame}	Height of Flame Above Crib
I	Flow Enthalpy per Unit Area
j	Exponential Constant
K	Constant of Proportionality
k	Thermal Conductivity
L	Stick Length
L_{enc}	Length of Enclosure
L_{vap}	Latent Heat of Gasification
l	Characteristic Length
l_m	Mean Beam Length
MW_f	Molecular Weight of Fuel
MW_a	Molecular Weight of Air
m_f	Fuel Mass
$\dot{m}_f$, $\dot{m}_v$	Fuel Mass Loss Rate
$\dot{m}_a$	Mass Flow Rate of Air

$\dot{m}_{O_2}$	Mass Flow Rate of Oxygen
N	Number of Layers
n	Number of Sticks Per Layer
Nu	Nusselt Number
P	Crib Porosity
P_s	Shaft Perimeter
Pr	Prandtl Number
p	Absolute Pressure
$\dot{Q}$	Heat Release Rate
$\dot{q}$	Rate of Heat Transfer
$\dot{q}_{conv}$	Rate of Convective Heat Transfer
$\dot{q}_{rad}$	Rate of Radiant Heat Transfer
$\dot{q}_{cond}$	Rate of Conductive Heat Transfer
$\dot{q}_{incident}$	Total Incident Rate of Heat Transfer
$\dot{q}_{net}$	Net Rate of Heat Transfer
$\dot{q}''$	Rate of Heat Transfer per Unit Area
R, R_r	Mass Loss Rate
$\bar{R}$	Steady State Mass Loss Rate
r	Stoichiometric Air to Fuel Ratio
Ra	Rayleigh Number
Re	Reynolds Number
s	Stick Spacing
S	Control Volume Surface Area
T	Temperature
$\tilde{T}$	Characteristic Temperature
T_g	Gas Temperature
T_a, T_∞	Ambient Temperature
T_w	Wall Temperature
t	Time
$\tilde{t}$	Characteristic Time
t_b	Total Burn Time
u	Flow Velocity
$\tilde{u}$	Characteristic Velocity
U_a	Rate of Mass Airflow
$U_{a,c}$	Rate of Mass Airflow to Charred Fuel
$\bar{U}_v$	Steady State Rate of Volatilization

V	Volume
W	Compartment Width
X_{O_2}	Mole Fraction of Oxygen
X_{CO_2}	Mole Fraction of Carbon Dioxide
X_{CO}	Mole Fraction of Carbon Monoxide
x	Linear Distance
Y_{O_2}	Mass Fraction of Oxygen
Y_{CO_2}	Mass Fraction of Carbon Dioxide
Y_{CO}	Mass Fraction of Carbon Monoxide
y_i	Chemical Yield of Species i
z	Height Above Enclosure Floor
α	Thermal Diffusivity
δ	Wall Thickness
$\delta_{thermal}$	Thermal Thickness
ε	Emissivty
ε_g	Gas Emissivity
ϕ	Mass Flow Rate of Air Entering Enclosure
φ	Crib Porosity (Complex Version)
κ_g	Spectral Absorption Coefficient of the Gas
κ_f	Spectral Absorption Coefficient of the Flame
λ	Ratio of Mass Flow Entering versus Exiting Crib Shaft
μ	Dynamic Viscosity
ν	Kinematic Viscosity
π	Dimensionless Group Notation
θ	Gas Temperature Rise
ρ	Density
ρ_a, ρ_∞	Density of Ambient Air
σ	Stefan Boltzmann Constant
T	Shear Stress
τ	Dimensionless Time
ω	Dimensionless Height in the Enclosure
ξ	Ratio of Volatile Fuel Produced to Solid Fuel Burned
ψ_{real}	Transducer Voltage Indicative of Instantaneous Values
ψ_{meas}	Measured Transducer Voltage
ψ_{steady}	Steady State Transducer Voltage

1. Introduction

There is a tremendous need for an accurate method of utilizing design variables to predict a complete set of fire effects on a surrounding enclosure. Fire Protection Engineers have awakened to that need, so horrifically demonstrated by the collapse of the World Trade Center's Twin Towers. An accurate modeling scheme will afford engineers with a means to confidently implement performance based fire protection in proposed structures. In the case of the World Trade Center where only pictures and blueprints remain, such a model could analytically reconstruct the fire environment and offer a variety of lessons to be learned from a tragedy. Although a great deal of progress in fire research is necessary before such an ideal model is fully realized, the need is clear and it is being met with an equal clarity of purpose from engineers.

To date, scale modeling has proven to be an engineering tool with several useful applications. Aerospace engineers have made use of wind tunnel testing for almost 200 years dating back to the revolutionary experiments of the Wright brothers. Oceanographers have learned to harness the linearity of wave propagation to predict features of oceanic waves based on attributes of scale models. Civil Engineers benefit from the insight provided by scale models of structural assemblies, particularly with respect to stress and strain. Ironically, the design team for the World Trade Center conducted wind tunnel tests on scale models of the Twin Towers to evaluate unusual wind loading on the structures during the design phase[1]. These were the first known scale model tests applied to high-rise construction.

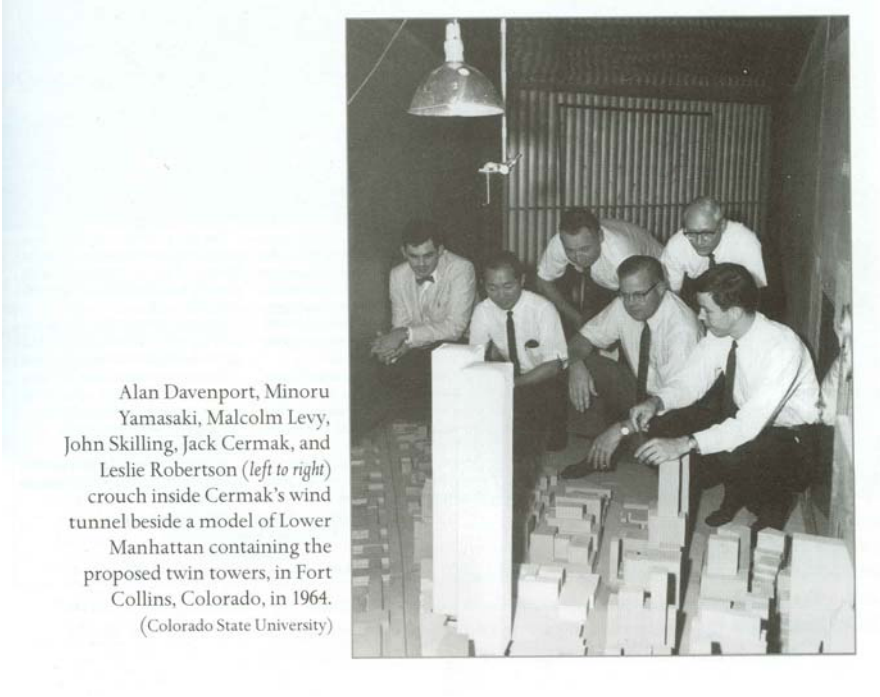

Alan Davenport, Minoru Yamasaki, Malcolm Levy, John Skilling, Jack Cermak, and Leslie Robertson (*left to right*) crouch inside Cermak's wind tunnel beside a model of Lower Manhattan containing the proposed twin towers, in Fort Collins, Colorado, in 1964. (Colorado State University)

Figure 1.1: World Trade Center Scale Model[1]

As with all of the above applications, manipulating the length scale of a system produces a variety of consequences to a population of dependent variables. It is generally accepted that the roles of all such dependent variables in the prototype will not be fully reproduced in the scale model. The key to producing a successful model is the selection of those dependent variables in the prototype whose roles must be appropriate captured in the model in order to conclude analogous behavior. The nature of this process dictates that the designer must run the risk that some less significant effects of background variables will be lost in translation.

Although all of the aforementioned methods of scaling lack the ability to reproduce a complete set of dependent variable behavior, this has not impeded successful implementation of model analysis into full scale designs. The tests conducted by the World Trade Center design team provided the project engineers with the insight necessary to evaluate the wind loading performance of the Vierendeel trusses for which

the towers were famous. Wind tunnel testing has consistently provided Aerospace Engineers with advancements in aerodynamic designs of aircraft features. Critics of scale modeling cite the variable selection process as evidence of the domination of art over science. What they fail to acknowledge is that the behavior of the model and prototype are both fully dictated by science. The inability to completely synchronize the two is only a shortcoming of our own understanding. What appears to be art is truly science that is not yet fully appreciated.

The problem at hand for Fire Protection Engineers is manifested in the physical and monetary size of conducting full scale enclosure fire experiments. The nature of the discipline requires engineers to work with structures that are larger than life and as a result must exist outside of the laboratory environment. Even the largest of fire laboratories will never be able to house full scale replicas of high rise buildings. Without the development of scaling, such structures will be forced to rely on sophisticated computer models for performance based design. Although these models are rich in mathematical detail, the size of the prototype prohibits validation by laboratory data.

To date, the field of Fire Protection Engineering has invested significant resources in the development of scale models. Approaches to scaling the fire environment have thus far taken on many identities. One approach known as pressure modeling satisfies the complete set of Navier-Stokes combustion equations by manipulating the pressure field in the model[2]. Another more common laboratory approach is to satisfy the same governing equations by conserving the Froude number (*Fr*), a dimensionless quantity that relates length scale to buoyancy[3]. The current effort derives several critical variable relationships to length scale from the governing conservation equations. Previously

published scaling efforts have been applied to areas such as fire growth and development of the smoke layer. Although the techniques for model design and analysis may vary, the effort to reproduce burning rates, heat fluxes, gas temperatures, wall temperatures and gas species concentrations is common.

Despite sharing many commonalities in model development and testing, the current research effort is unique in its focus on the transient accuracy of scale modeling. Until now, scale modeling has been used largely as a tool for yielding order of magnitude estimates. The literature is filled with experiments represented by single data points obtained by averaging quantities over the steady state duration of a fire. The introduction of a steel structure into the fire environment requires far greater clarity in the model results. The thermally induced yielding and failure of a steel frame is determined by transient heating of its elements. An order of magnitude estimate for the time to failure of the steel structures in any real building environment is simply inadequate.

The challenge that must be met is the determination of an appropriate design fire for a given occupancy with an unknown fuel load. Achieving transient accuracy for such a fire requires the ability to distinguish the effects of its magnitude and duration on the features of the surrounding enclosure. Out of a desire to produce a fundamental model, this research focuses on the scale modeling of wood crib fuel loads. These geometric configurations of sticks are commonly used in laboratory analysis and have an excellent reputation for producing repeatable data.

Ultimately this work will serve as a foundation for experimentation with a fire-structure scale model. This report focuses exclusively on the development of the fire scale model. Research efforts to address the fire-structure interaction are ongoing.

2. Literature Review

The following is a survey of research efforts regarding topics that are pertinent to the development of the present work. The topics addressed are free-burning wood crib fires, enclosure fires with a wood crib fuel source and the scaling of wood crib fires in an enclosure.

2.1 Free-Burning Wood Crib Fires

2.1.1 Why Wood Cribs?

The earliest known research effort to focus on the burning of cross piles of wood sticks was undertaken by Chief Officer F. Folk of the Fredericksburg, Denmark Fire Brigade in 1931. Folk recognized that although attention had been paid to classifying fire resistance of materials and structures, not much thought had been given to methods of fire extinguishment. With this in mind, Folk designed a series of experiments to investigate the extinguishment of burning piles of wood[4].

The research was aimed at quantifying the effectiveness of various means of extinguishment. As such, the effort required a highly reproducible fire source. Folk settled on a pile of air-dried fir sticks ignited from underneath by a pan of gasoline. The sticks were all of uniform dimensions and spacing. After conducting several preliminary experiments varying the number and orientation of the sticks, three critical issues were identified. First, in order to ensure both a repeatable orientation of the wood pile and sufficient access of the extinguishing agent to the fuel surface, it was decided to orient successive layers of sticks perpendicularly. In addition, each of the wood sticks within a given pile had to possess the same density and moisture content in order to attain the desired level of reproducibility. Folk's cross piles of wood sticks would eventually come

to be known as wood cribs. A representation of Folk's final wood crib design for his extinguishment experiments is given in Figure 2.1.

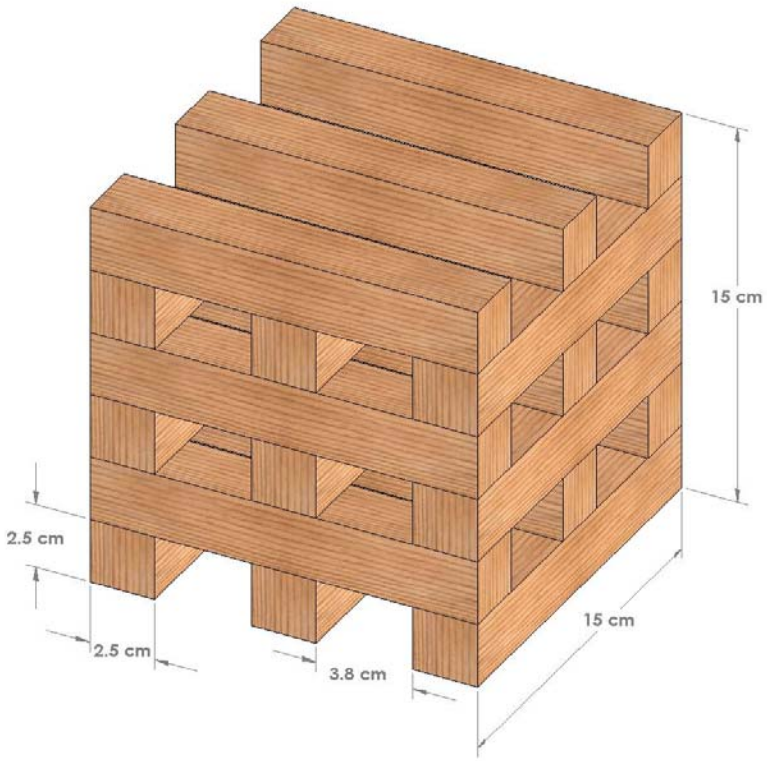

Figure 2.1: Replica of Folk's Wood Crib

Prior to conducting extinguishment experiments, Folk collected data for the burning of his wood cribs. The data collected was recorded by visual observation of an insulated scale placed underneath the crib. These experiments yielded data for the mass the wood over time, which was also used to determine a rate of mass loss. These curves are shown in Figure 2.2.

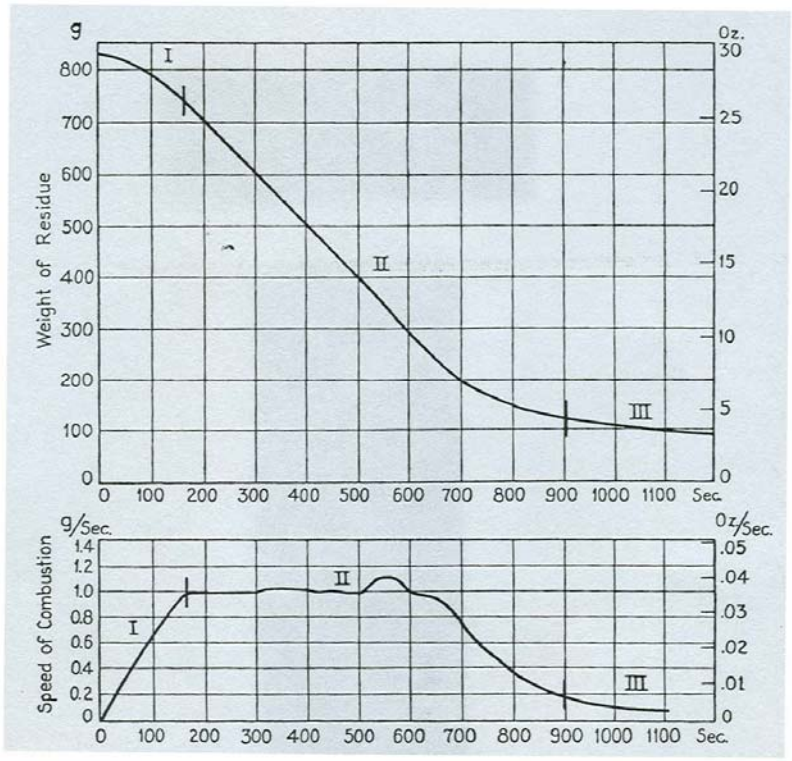

Figure 2.2 : Folk's Transient Mass and Mass Loss Rate Data[4]

The change in slope of the transient mass data coupled with visual observation of the experiments enabled Folk to identify three stages in the burning of his wood cribs. Ignition was identified as the initial period of spread leading up to gas combustion. The gas combustion referred to what is today known as steady state combustion during which the rate of change of the mass of the fuel with respect to time is relatively constant. It is during this phase that Folk noted the significance of the predominantly upward flow of gas through the chimney spaces of the pile. The third and final stage of glow identified what is commonly referred to today as smoldering combustion. The relatively short-lived peak in the second stage is identified by Folk as the point at which an optimal mixture of air and fuel for combustion is achieved[4]. The presence of this peak will be seen again in the current research and a more thorough explanation of its appearance will be offered in Chapter 4.

2.1.2 An Empirical Model for the Free-Burning Rate

In 1962, a scientist at the National Bureau of Standards took Folk's analysis of free-burning wood cribs a few steps further. Gross recognized the need for a more fundamental understanding of the enclosure fire environment in order to evaluate the fire resistance of building materials. At the same time he realized that the cost of full scale testing was prohibitive. As a result he focused on developing a means to evaluate the mechanism of fire spread in wood cribs at a manageable geometric scale[5].

In the design and preparation of his fuel source, Gross made use of Folk's analysis. He used the same wood specie for each element of a single crib (Douglas fir) in an effort to keep the density of the wood as uniform as possible. To control moisture content, prior to testing the wood was conditioned in an atmosphere that was maintained at 23^{o}C and 50% relative humidity until equilibrium was reached at approximately 9.2%. Gross' design criteria for his cribs included a square cross section for each stick and a length of the sticks that was proportional to 10 times the cross section. Thus he created a series of geometrically scaled cribs. Gross also identified the following nomenclature for identification of critical design parameters of his cribs, which has since become an unofficial standard:

b = cross section of a single square stick

L = length of a single stick

n = the number of sticks in a single layer, same for every layer

N = the total number of layers of sticks

A schematic of the experimental setup is shown in Figure 2.3.

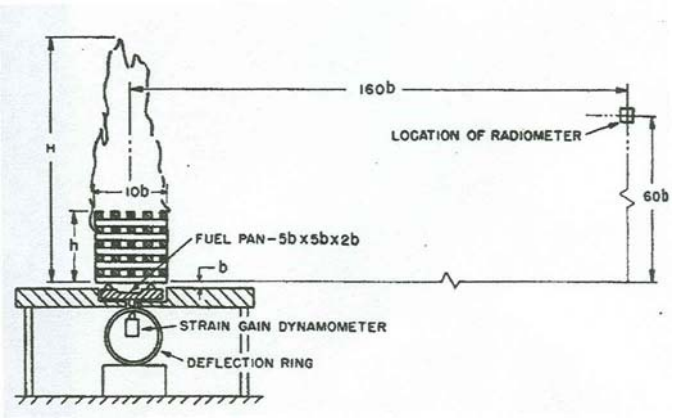

Figure 2.3: Gross' Experimental Setup[5]

The most important features to notice in this setup are the fuel pan below the crib and the elevation of the crib above the pan. The square metal pan was smaller in footprint area than the crib and was centered below the crib. The crib was then elevated above the lip of the pan by a distance equal to the cross section *b* of a single stick. Tests began by igniting a pool of either heptane or alcohol, which had been poured into this fuel pan. Gross noted in his results that only the quantity and not the type of starter fuel had an effect on the recorded burning rate. He also recognized the same three stages of burning identified by Folk. Although transient data was taken in his experiments, Gross chose to focus on a time averaged peak mass loss rate evaluated as the maximum slope of the transient mass data[5].

Perhaps the greatest contribution from the results of these tests was the quantification of the internal air flow through the crib structure by an empirical parameter φ, which Gross defined as the porosity of the crib. To define this parameter, he derived expressions for the total exposed surface area of the crib prior to ignition A_s, and the area of the vertical shafts within the cross-pile A_v. The latter of these areas is calculated as a

summation of the area of the vents along the surface plane of each side of the rectangular prism.

$$A_s = 2nb^2\left[N\left(2L-n\right)+n\right] \tag{2.1}$$

$$A_v = b^2\left(10-n\right)^2 \tag{2.2}$$

$$\varphi = N^{0.5}b^{1.1}A_v/A_s \tag{2.3}$$

Gross appreciated the existence of a critical value of the crib porosity, below which insufficient gas flow through the vertical shafts of the pile results in a decreased peak mass loss rate. In addition he observed that the burning rate data for the set of geometrically scaled cribs seemed to follow a power law relationship with the stick cross section. He populated his plots with different wood species by multiplying each data point by a thermal diffusivity ratio *F*. He therefore expressed his data in the form $FRb^{1.6}$. The power law for the stick cross section was chosen based on heat conduction data taken from experiments in which various materials were exposed to a standard fire exposure curve. In these tests, Gross claimed that a one-dimensional steady state heat conduction analysis could be conducted using Fourier's law of conduction. As a result, the conduction resistance time was proportional to the material thickness (represented here as the cross section of a stick) raised to the power 1.6.

The importance of the stick cross section is that it is used in these cribs to characterize a length scale. Keep in mind that Gross' cribs contained an in-built correlation between the length of the crib and the cross section of its sticks. Thus, the size of the cross section had additional subtle effects on the burning rate of the cribs. Results from Gross' experiments are shown in Figure 2.4. Note that data from Folk's experiments have been included.

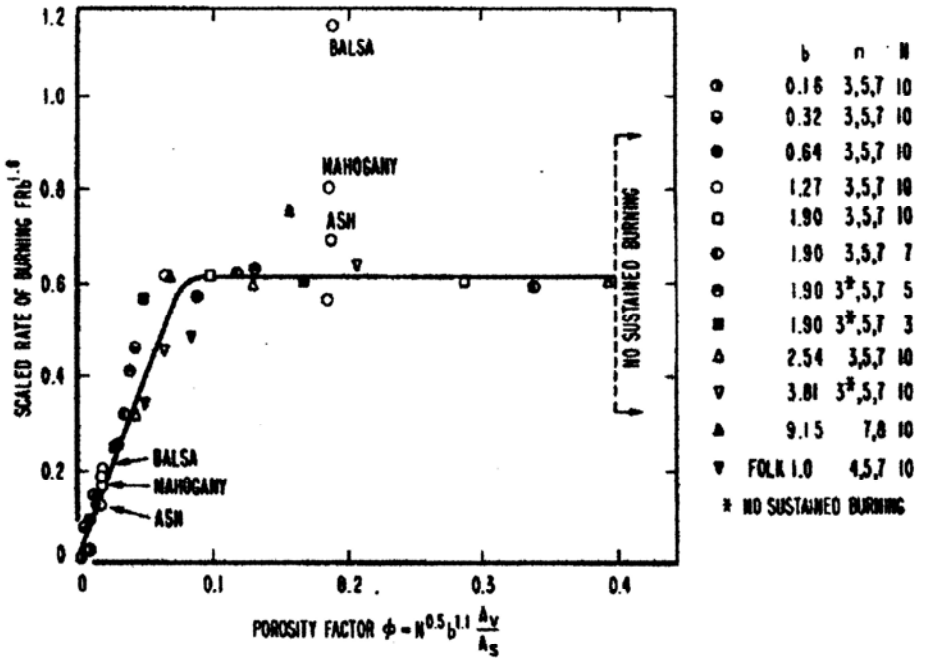

Figure 2.4: Gross' Effect of Porosity on the Scaled Crib Mass Loss Rate[5]

From the above data, three distinct regions of combustion were identified. The first region exists for low values of porosity where the combustion is diffusion limited. The second regime shows complete independence of the burning rate from the porosity of crib. As the porosity is further increased, eventually a point is reached at which the sticks burn as individual members incapable of sustaining combustion as a unit.

2.1.3 A Search for Statistical Correlations

Despite the attempt by Gross to correlate his data with that of Folk, other research efforts were unable to collect data and make a similar comparison based on Gross' parameters. A statistical analysis was conducted in an attempt to isolate the effects of individual design variables of the crib. Recognizing that the gas velocity in the interior shafts of the crib was governed by buoyancy and the inertia of the gas, the variable

$A_v\sqrt{H}$ was used as a way to express the volumetric flow rate of this vertical interior flow. The effort was focused on the investigation of relationships presented in Equation 2.4.

$$R/\left(A_v\sqrt{H}\right) \propto A_v^y A_s^z \tag{2.4}$$

Note that Gross' parameters can be substituted above by expressing the height of the crib as the product of the cross section of a stick and the number of layers in the crib. The result of such a substitution yields a result that is similar in form to Gross' correlation.

$$R \propto A_v^{y+1} A_s^z N^{0.5} b^{0.5} \tag{2.5}$$

Ultimately, it was realized that there were too many relationships between variables to confidently separate the effect of one design parameter over another with respect to the burning rate[6]. The final result was the following empirical formula in cgs units for crib lengths in the range of 30-200 cm.

$$\frac{R}{\sqrt{A_v A_s N b}} = 0.0017/\left(A_s A_v\right)^{0.052} \tag{2.6}$$

2.1.4 The Role of the Flame Height

Further efforts for determining dominant influences on the burning rate of free burning wood cribs led to consideration of the thermal radiation of the flame above the crib. Thomas' hypothesis was that the radiation delivered to the crib surface is determined by the burning rate of the fuel and that this radiation is related to the height of the flame[7]. In forming this hypothesis, he noted the work of Burke and Schumann with laminar gas burner diffusion flames. In this classical work, it was determined that the height of a diffusion flame is directly related to the flow rate of fuel supplied[8].

Thomas recognized the difference between the forced convection flames of a gas burner and the free convection flames produced by a typical wood crib; however, he sought to substantiate a similar relationship between the flame height, the dimensions of the fuel bed and the fuel supply rate. A set of dimensionless quantities was produced from the conservation equations. From these quantities, the desired relationship was determined[7].

$$\frac{h_{flame}}{d_{orifice}} \propto \frac{\dot{Q}^{2}}{d_{orifice}^{5}} \tag{2.7}$$

Attempts were made to verify this relationship experimentally. Although it appears that this was done successfully, the technique for measuring flame heights relies on visual observation of photographs of turbulent flames. Therefore, the validation for Equation 2.7 is not considered as valuable as the relationship itself.

2.1.5 Internal Radiation as a Driving Mechanism

In 1965, researchers at the US Department of Agriculture focused their efforts on the dominant mechanism of fire spread throughout a wood crib structure. They sought to harness the significance of radiant and convective energy in wood crib fires. In doing so, they cited Thomas' finding that the burning rate was influenced by the height of the flame above the crib. Taking this model one step further, they claimed that the radiation exchange internal to the crib structure was an additional significant influence on the burning rate. To support their hypothesis, McCarter and Broido focused on the radiant energy emanating from the wooden members of the crib located outside the flame zone[9].

The wood species used in these experiments was western hemlock. The moisture content of the cribs was accounted for by conditioning the samples in a desiccator prior to

experimentation. Seven different designs were used with the common features of wood species and a square stick cross section of 1.3 cm. All other design parameters varied between cribs. It should be noted that previous studies had required the equal length of all sticks within a single crib so that a square base is obtained. This particular research effort instead utilized a rectangular crib base. Lengths of sticks residing in adjacent layers of the crib were thus unequal. This design choice was made out of a desire to measure flame propagation in a predetermined direction. Also note that Figure 2.5 shows crib types B and G oriented in a manner that is perpendicular to the more common design orientation[9].

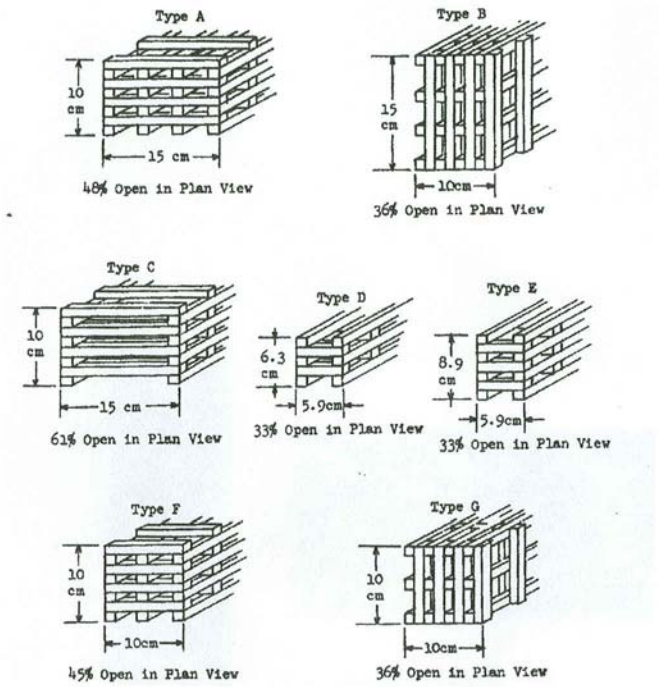

Figure 2.5: McCarter and Broido Crib Designs[9]

Experiments began by igniting an interval of predefined thickness on the side of the crib with a strip of asbestos soaked in ethyl alcohol. The fire was then allowed to spread freely throughout the structure as data was taken. As the fire propagated from

zone to zone along the length of the crib, the support system underneath the crib was moved in a way that allowed smoldering embers to fall off of the structure onto a catch below. Although somewhat vague in description, it is known that cribs were suspended with the use of reflective supports. The supports were designed to minimize conduction losses. Among the data presented in the report were the rate of steady state combustion, the rate of flame propagation through the crib and the rate of radiant energy emitting from the crib at various spherical angles from the fuel bed[9].

One of the most unique measurements taken during these experiments were achieved by shielding the radiometer from either the glowing embers, burning crib structure or the diffusive flame so as to isolate the rate of radiant energy emitting from each contributing source.

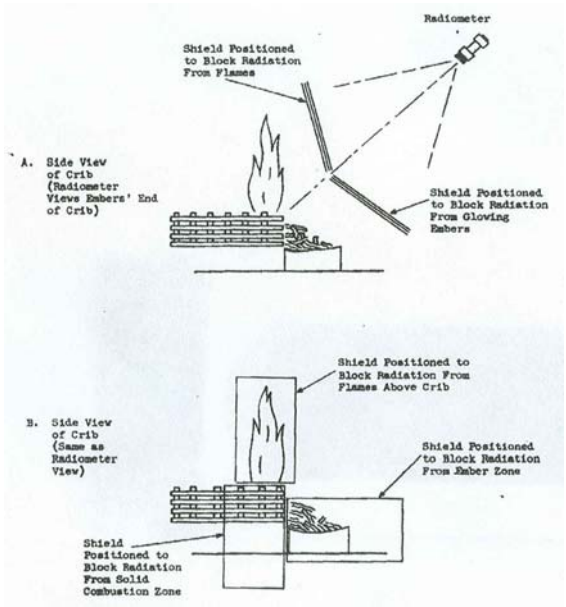

Figure 2.6 : Isolation of Contributing Radiant Sources[9]

The results of these measurements showed a dependence on the location of the radiometer and ranged from a one-third contribution from each source at the side of the

crib to an ember contribution that doubled that of the luminous flame just above the bed of embers.

The analysis for the total rate of radiation measured in a spherical pattern around the crib concluded approximately equal contributions from flaming and glowing modes of combustion. This finding suggests that the burning rate of the crib is influenced not only by energy feedback from the flame but also from the internal and external radiation exchange of the sticks.

In order to further investigate this finding, measurements were taken of the flame propagation rate while the flame above the crib was suppressed. The results of these measurements showed an insignificant drop in the spread of flame throughout the crib structure. Therefore, the internal radiation in the crib was concluded to be more influential than the diffusive flame in determining the steady state burning rate[9].

2.1.6 A Theoretical Model for the Free-Burning Rate

Perhaps the most formative work on free-burning wood crib phenomena was the development of a fundamental theory by a Harvard University researcher names James A. Block. Prior to his efforts, attempts had been made at uncovering empirical relationships between design variables and the mass loss rate of wood cribs. Block recognized that further progress in this field would necessitate the development of a fundamental theory for the burning rate of this three-dimensional fuel structure. His theory focused on the convective flow of gas internal to the structure[10].

The experimental setup was quite similar to that of Gross in that it involved the crib structure placed atop supporting elements lying in a pan filled with starter fuel.

Underneath this arrangement was an insulated weighing system responsible for recording the transient weight of the fuel. The starter fuel used for these tests was acetone. Ponderosa Pine was chosen for use in most of these experiments. Cribs were designed with a range of 2-8 sticks per layer and 4-20 layers. Different designs were achieved by varying the stick cross-section and the length. Table 2.1 lists the designs employed in these tests.

b (cm)	L/b	n	N
0.635	10	2 thru 8	4 thru 20
0.635	20	2 thru 8	4 thru 20
1.270	10	2 thru 8	4 thru 20
1.270	15	2 thru 8	4 thru 20
1.900	10	2 thru 8	4 thru 20

Table 2.1: Block's Crib Design Parameters

The moisture content was standardized by drying the cribs in an oven for 24 hours at 107^{o}C. The cribs were then allowed to cool in a moisture controlled environment prior to beginning a test[10].

In addition to confirming the porosity influenced regions of combustion identified by Gross, Block's testing yielded a few critical design requirements. It was found that the area of the fuel pan must be slightly larger than the base area of the crib so as to avoid a period of flame propagation that influences the mass burning rate of the fuel. As long as this first rule was followed, an arbitrary amount of starter fuel could be used. The preliminary tests also revealed a requirement for the elevation of the wood above the starter fuel. Block found that increasing the elevation of the wood crib corresponded to an increase of as much as 15% in the peak mass loss rate of the fuel. However, he noted that increasing the elevation beyond a value of 1.5 cm yielded no appreciable difference

in the mass loss rate. Although not noted in the literature, this value of 1.5 cm carries meaning when taken into context with Gross' experiments. Gross chose to elevate his wood cribs at a distance equal to the cross section of an individual stick. Note that in Block's tests, his cross sections ranged from 0.635 to 1.90 cm, with an average value of 1.27 cm. Consequently it seems that the value of 1.5 cm carries significance with respect to the sizes of sticks used in these experiments. Therefore, it seems that Gross' design rule should apply to a broader category of crib sizes than Block's.

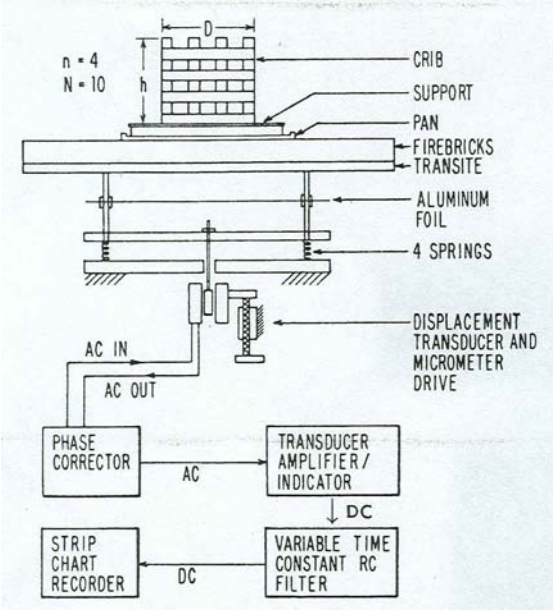

Figure 2.7: Block's Experimental Setup[10]

The determination of mass loss rate as a function of crib porosity or packing density served as a basis for the development of Block's theoretical model. The model was developed with separate considerations for the porosity limited and fuel limited regions of combustion.

The model for the porosity limited regime is derived based on a visualization of a crib comprised of a single vertical shaft that is modeled as a rough-walled porous tube. Air enters the system through the bottom of the vertical shaft as well as the various

openings in its sides. Simultaneously, gaseous fuel is diffusing into the shaft from the burning internal surfaces of the wood sticks. The diffusion flame produced by the fuel and air mixture gives off energy to the system. A portion of this energy is used to pyrolize more fuel and continue the gas phase reactions inside the tube. The flow out of the top of the vertical shaft is comprised of a mixture of unburned gaseous fuel and combustion products[10].

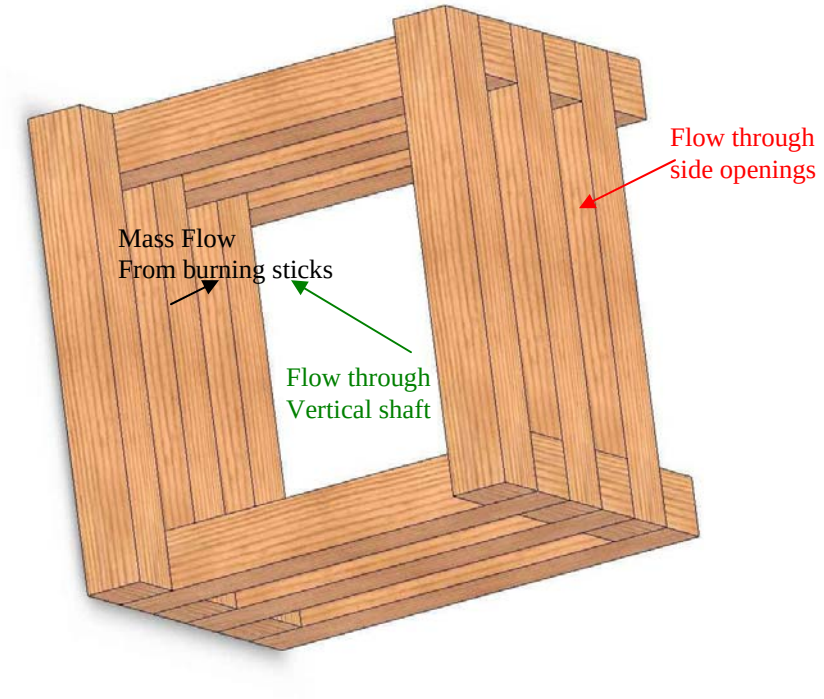

Figure 2.8: Block's Tube Visualization

The governing equations for the flow through this shaft are the conservation of mass, linear momentum, species and energy. Block combines the governing equations in order to arrive at an analytical solution for the burning rate per unit exposed surface area of the tube.

$$\dot{m}_a = \frac{A_v}{2} f\rho\{[(\rho_0 - \rho)/\rho]gh\}^{1/2}[(\lambda - 1)/\lambda](G/\varphi) \qquad (2.8)$$

In the above equation, λ represents a ratio of the mass flux entering and exiting the tube. The variable *f* is simply a friction factor for the walls of the tube. The density of the gas and the supply air are represented as ρ and ρ_0 respectively. The height of the tube is represented by *h*, and the gravitational acceleration is represented by *g*. Thus the first portion of the right hand side of this equation represents a flux of buoyant air traveling through the shaft[10].

The variable φ is a dimensionless variable representing the drag effect of the walls of the shaft. It is derived from the constant-density momentum equation. Its definition is given as a function of the perimeter of the shaft P_s, height of the shaft *h*, friction factor *f* and area of the shaft A_v.

$$\varphi \equiv P_s h\, f / 2A_v \tag{2.9}$$

This definition can now be used to define a porosity function *G* in the following way

$$G(\varphi) = \left\{ \varphi^{-1}\left[\frac{1-e^{-\varphi}}{1-(\rho/\rho_0)^2 \lambda^{-2} e^{-\varphi}} \right] \right\}^{1/2} \tag{2.10}$$

Block claims that the above model can be applied to cribs with multiple shafts by assuming a uniform burning rate per unit exposed surface area of the crib[10].

For a simpler interpretation of this model, assume that the flow of air into the tube from the side openings is negligible. Then, conservation of mass dictates that the right hand side of Block's equation for the mass burning rate is simply the mass flow rate of air into the bottom of the tube. The inclusion of the parameters λ and φ simply accounts for horizontal airflow through the holes in the walls of the tube and the viscous drag of the closely spaced walls.

The empirical models of Gross and Thomas neglected both of the above effects. They arrived at the following expression for the mass flow of air through the crib:

$$\dot{m}_a \cong \rho_a \sqrt{\frac{\Delta\rho}{\rho_a} g h} A_v \propto \sqrt{h} A_v \qquad (2.11)$$

Block's analysis is similar, but more complete in its treatment of flow phenomena. It is important to note that these models do not consider the fact that the outer walls of the tube are burning. These outer wood surfaces are always exposed to ambient air regardless of internal flow restrictions. The concept of these two modes of burning among elements of the same crib becomes less and less significant as the number of sticks per layer is increased. Similarly, as the height of the shaft is increased, the buoyant air entering the bottom will eventually cool and flow out the sides. The height limitation on airflow can also be seen in the link between the Reynolds number and friction factor, which Block relies on for his analysis[10].

Although the majority of the derivation for Block's model in this densely packed regime has been omitted here, the above definitions allow for the presentation of Block's data. The theoretical model for the porosity independent combustion regime is much more pertinent to the current research effort and is therefore discussed in more detail.

As the vertical shafts of the crib are widened and internal airflow is increased, the mass loss rate of the crib can be modeled as a series of turbulent free convection boundary layers each forming on the vertical surface of an individual stick. The limiting factor is no longer the momentum of the internal gas flow, but rather the transfer processes occurring in the boundary layers and in the solid fuel. Here Block invokes a parameter known as Spalding's B number to model the burning rate per unit exposed surface area. This transfer number B can be expressed in the following manner

$$B = \frac{\textit{(Free Stream Enthalpy – Surface Enthalpy)}}{\textit{Energy needed to heat up and pyrolize unit mass of fuel}} \quad (2.12)$$

The mass burning rate of the fuel is said to be proportional to the transfer number

$$\dot{m}'' = \left(h_c / c_p\right) B = \left(h_c' / c_p\right) \ln\left(1 + B\right) \quad (2.13)$$

The heat transfer coefficient h_c' denotes heat transfer in the limit of zero mass flux. It is known that for turbulent free convection boundary layers the heat transfer coefficient for a vertical sheet is independent of the height of the sheet[11]. In this case, the height of the sheet is simply the cross section of the stick. With this in mind, if it is assumed that the specific heat is constant, then the mass burning rate of the fuel can be expressed as a function of the transfer number. Recognizing that the transfer number is a function only of the physical properties of the fuel, Block utilizes an empirical formula to make one final leap. An empirical formula for the relationship between the transfer number and fuel thickness is used[10].

$$\ln\left(1 + B\right) \propto b^{-0.5} \quad (2.14)$$

Combining constants from Equations 2.13 and 2.14 leads to an inverse proportionality relationship between the mass burning rate of the fuel and the fuel thickness for the porosity independent combustion regime. The constant of proportionality is a function of the type of fuel only and varies between wood species[10].

$$\dot{m}'' = Cb^{-0.5} \quad (2.15)$$

The experimental results of Block included the determination of the material constant C for various species of wood as shown in Table 2.2.

Values of C for various species of wood

	C, mg/(sec cm$^{1.5}$)	ρ(dry), g/cm^3	M, %
Ponderosa pine	1.03	0.500	7.9
Ponderosa pine	1.07	0.345	7.7
Birch	1.30	0.630	7.3
Idaho pine	0.87	0.405	8.1
Maple	1.33	0.555	7.6
Oak	1.33	0.700	6.8
Redwood	0.86	0.335	7.7
Sugar pine	0.88	0.330	7.3
Western hemlock	0.96	0.565	7.6
Whitewood	1.11	0.425	6.9

Table 2.2: Block's Data for Mass Burning Rate Material Constant[10]

Block's experimental data is plotted in Figure 2.9 as a series of scattered symbols with the solid line representing the prediction of the theoretical model described above. The burning rate data was taken as a time average of the burning rate during the middle 50-60% of the total weight loss of the crib. Data points shown in Figure 2.9 represent averages of all tests in which the moisture content was varied between 5-10% for a given crib design.

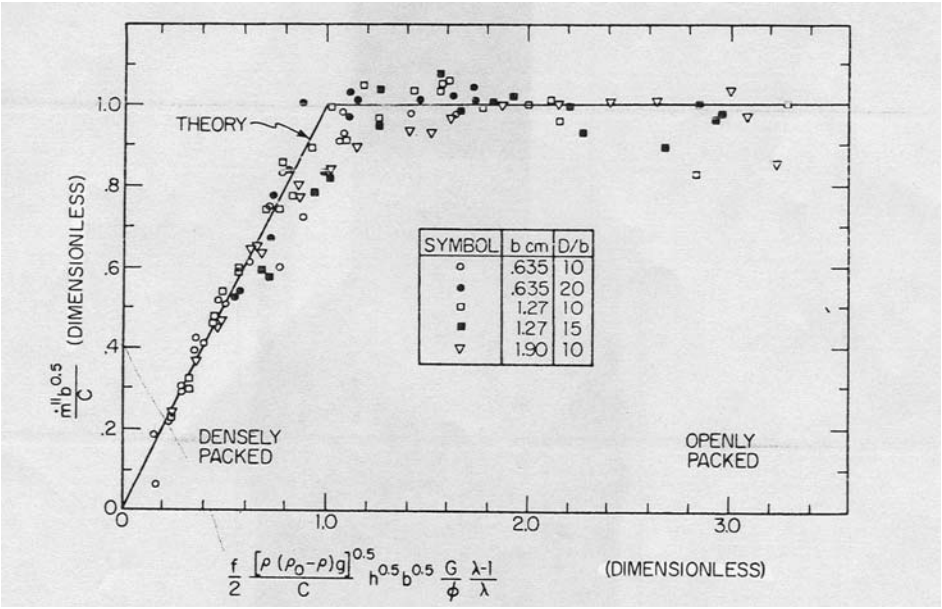

Figure 2.9: Block's Experimental and Theoretical Data[10]

Note that the burning rate in the densely packed region is dependent on the height of the crib and a complex function of its porosity. However, the burning rate in this regime is also independent of the material constant and the cross section of the sticks. The opposite can be said for the openly packed regime. Thus, the two regions of combustion shown above can be thought of as porosity limited and fuel limited[10].

2.1.7 Modeling the Fire Duration

The research of Delichatsios followed the efforts of Block and sought to determine a model for flame propagation within a single crib[12]. The current research effort is not concerned with flame propagation; however, this particular study is mentioned in order to address an important issue. Delichatsios' model for the weight loss rate of the crib due to burning suggests that the quasi-steady burning rate is constant over a period of time equal to the burning time of a single wood stick. He defines the burn time of a single stick based on the quotient of the stick mass and the mass loss rate[12].

$$t_b = \frac{\rho b}{4\dot{m}''} \tag{2.16}$$

The claim that the burn time of a wood crib can be estimated by the burn time of a single fuel element has been an issue of contention in the literature. Delichatsios invokes this estimation claiming that observations made by Gross and Thomas indicated quasi-steady burning conditions in their experiments[3,6]. It is therefore surmised that such steady burning must be analogous to the steady burning period of a single stick.

This claim is contrary to Block's theoretical model as well as the work of McCarter and Broido who investigated the role of internal radiation in the rate of fire growth within the crib. Block correctly points out that for the fuel limited regime, a crib

with large sticks will sustain a constant rate of burning for a longer period of time than an individual stick. Folk was the first to identify the fact that as the porosity of the crib is continuously increased, there exists a limit beyond which burning of the crib is not sustained. Beyond this limit, the burning of the crib can simply be modeled as the burning of so many individual sticks with no significant synergistic heat and mass transfer interactions. Prior to reaching this limit, such interactions do play a role in sustaining combustion and therefore influencing the burn time of the pile. The burning rate of the individual stick is constantly decaying while that of the same stick within a crib is buoyed its neighbors[12].

2.2 Wood Cribs Burning in a Compartment

2.2.1 Standardization

The underlying purpose of studying free-burning wood crib fires is to quantify the behavior of a fire source for use in compartment fire modeling. The purpose of modeling compartment fires dates back to the turn of the century when conflagrations devastated entire cities in various places across the United States. The quest for codes and standardization following these tragedies led to a method of evaluating an appropriate fire severity for a structure. The fire endurance of critical structural members was then evaluated as the duration for which the building element in question could withstand a fire of said severity.

The American Society for Testing of Materials (ASTM) was the first to standardize this process into a test known as *Methods of Fire Tests of Building Construction and Materials* (ASTM E119). The method of testing has remained largely unchanged from the time of Gross and Robertson to the present day. The test dictates that a building element or portion thereof, such as a floor assembly or column, is to be tested against a pre-defined time-temperature curve as controlled by a surrounding furnace. The building element is loaded in a manner representative of its intended use. The length of time for which the element in question maintains pre-defined definitions of structural and thermal integrity is agreed to be its fire endurance[13].

2.2.2 The Importance of Fuel Load

The practice of defining a standard fire exposure was intended to facilitate mass testing of building materials and allow the results to show the attainment of a globally

relevant goal. Engineers have long stated that a major shortfall of this approach is the definition of a globally applicable standard fire. Gross and Robertson's work provides a literature review through the early 1970's of various research efforts conducted by the National Bureau of Standards in this country, as well as several foreign countries, to more appropriately quantify fire severity and fire endurance in structures[14].

2.2.2.1 Classification of Fire Severity by Fire Load

Some of the first efforts to model fire severity and fire endurance were made by the National Bureau of Standards in 1927. Experiments were conducted in two separate brick structures with concrete flooring. The first structure had floor dimensions of 16 ft. x 30 ft. and a height of 9 ft. The fuel was primarily wood furniture and shelving arranged in a manner typical of a contemporary office. The second set of experiments was conducted in a separate brick structure with floor dimensions of 30 ft. x 60 ft. and a height of 9 ft. The fuel loading was very similar; however some of the wood shelving was replaced with steel furniture. In designing these tests, researchers defined a variable known as the fire load, referring to the weight of combustibles per unit surface area of the compartment floor. The fire load was varied over a range of 10-60 pounds of combustible per square foot of floor area (psf) for these tests[14].

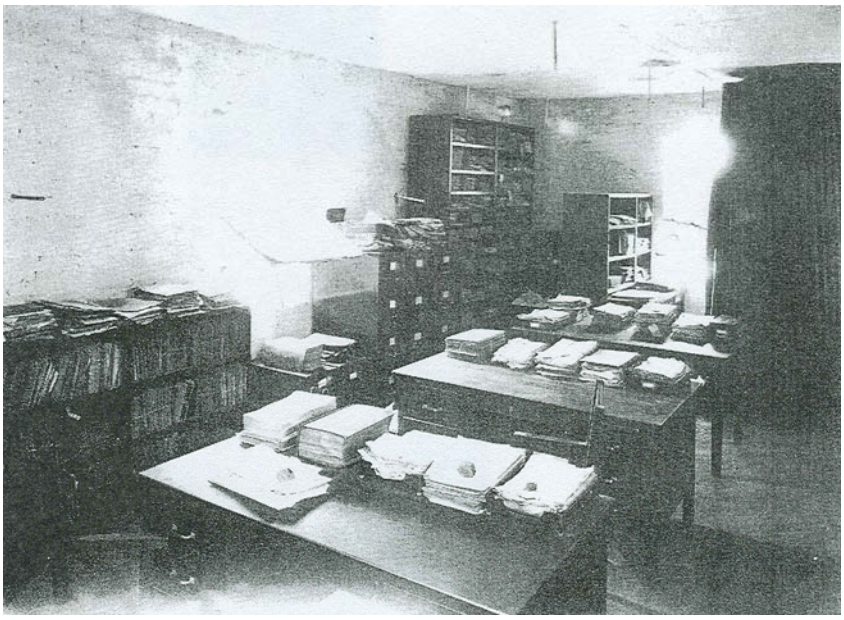

Figure 2.10: Fire Load for NBS Small Test Building[14]

Some windows and doorways were left open during testing and observations regarding the ventilation of these fires were made; however there was no quantification made of the ventilation parameters in the structures. During these experiments, the enclosure fires were allowed to progress freely until the combustibles had been consumed and the structure had cooled. Results were assembled in the form of a relationship between the fire loading and fire endurance of the structure. It is unclear how the fire endurance was defined, but it is assumed that the definition corresponded to that of the standard.

Despite shortcomings in quantifying the role of fire growth within the compartment as well as that of the compartment ventilation, the experimental work took a fundamental step toward a more performance based approach to evaluating fire endurance by defining the fire load of a structure. Following these tests, in 1947, the research community conducted a large survey to determine the fire load for common occupancy categories of the time period. The results are shown in Table 2.3 below. The

data represents the actual weights of all movable combustibles and estimates for immovable ones including compartment boundaries[14].

Occupancy		Number Surveyed	Floor Area, ft²	Combustible Contents: Average, psf	Combustible Contents: Range of Maximum Values for Single Occupied Room, psf	Combustible Contents: Maximum for Any Area, psf
Residence		13	8 165	8.8	8 to 14	49 (linen closet)
Hospital		1	143 780	2.8	3 to 22	19 (service store) 23 (laundry, clothes storage)
School		6	72 385	15.7	7 to 39	228 (textbook storeroom)
Mercantile (department store)		2	1 105 032	10.3	. . .	47 (paint department
Manufacturing	Furniture Factory	2	549 784	15.3	. . .	117 (veneer storage) 104 (paint shop) 167 (paper storage)
	Mattress Factory	2	155 791	16.4		
	Clothing Factory	2	91 701	10.7		
	Printing Plant	2	191 755	34.0		
Warehouse	General	4	518 193	25.0	. . .	256
	Printing	1	135 055	174.4		
Office		82	89 075	18.4 (10.6 excluding heavy files)	7 to 43	86 (heavy files)

Table 2.3: Fire Load Survey for Various Occupancies[14]

2.2.2.2 The Role of Compartment Ventilation

Japanese researchers focused on the spread of fire between buildings in response to the devastation suffered during World War II. The work of Fujita and eventually Kawagoe highlighted the importance of ventilation as a fundamental variable in enclosure fire modeling[14]. Kawagoe asserted that the mass burning rate of fuel was directly determined by a ventilation parameter that he defined as the product of the vent area and the square root of its height

$$Ventilation\ Factor = A_0\sqrt{H_0} \tag{2.17}$$

Through manipulation of this parameter, Kawagoe found that limited ventilation decreases compartment gas and surface temperatures as well as increasing the total duration of the fire. Conversely, an increase in ventilation leads to a reduction in the steady state duration of the fire. Applying these principles to the work of Ingberg, who very likely experimented with limited ventilation fires, it was apparent that the fire endurance relationship to fuel load must be modified to include compartment ventilation[14].

The realization that ventilation plays a significant role in the compartment fire environment was the product of an attempt to balance heat generation and loss from the compartment. This innovative approach further recognized the importance of the enclosure boundaries with respect to heat transfer within the compartment. This recognition led to the consideration of wall surface area, thickness and thermal properties. The role of the fire source in this energy balance included flame emissivity, excess air fraction and the burning rate. One of the beneficial results of this realization was the definition of an opening factor where the compartment surface area is taken as the sum of all interior surface areas of the compartment boundaries.

$$Opening\ Factor = A_0\sqrt{H_0}/A_T \tag{2.18}$$

Through experimentation, Kawagoe was able to show that an increase in the opening factor led to an increase in fire temperatures[14].

One of the main goals of these studies was to utilize the design variable of ventilation to predict the time-temperature curve for a given structure with a specified fuel loading. Although this goal represented a tremendous advancement in modeling, the methods used to achieve it revealed some inaccuracies. For instance, the burning rate of

fuel within the compartment was believed to be controlled solely by ventilation. There was no consideration of rate limitations based on fuel arrangement within the compartment. In addition, the time from ignition to peak burning rate is evaluated as the time over which all of the fuel present in the compartment is consumed. This is certainly not a general truth, as in most compartment fires a decay from peak values can occur during the flaming stage of combustion. Such assumptions lead to significant inaccuracies in temperature and time predictions; however, the goal of prediction was certainly a step in the right direction[14].

2.2.3 A Model for Ventilation Limited Wood Crib Fires in Enclosures

Similar to the work of Gross and Robertson, Harmathy conducted a literature review in an effort to gather many research attempts into a single forum so that a uniform direction could be applied. Harmathy's review is separated into three pertinent categories of interest to the current research effort[15].

2.2.3.1 Free-Burning Wood Crib Fires

To assist in his discussion of free-burning wood crib fires, Harmathy developed a model for the transient mass of a burning wood pile. The regimes commonly referred to as steady state burning and decay are labeled primary and secondary burning. Definition of the mass and time boundaries of these regions in the model is arbitrary although it follows convention (Figure 2.11).

Harmathy correctly asserts that although a decrease in weight of the crib is commonly equated to the burning rate, under certain conditions, some of the solid fuel

may actually sublimate and burn away from the immediate vicinity of the crib. Therefore, he refers to a rate of volatilization throughout his work rather than a burning rate[15].

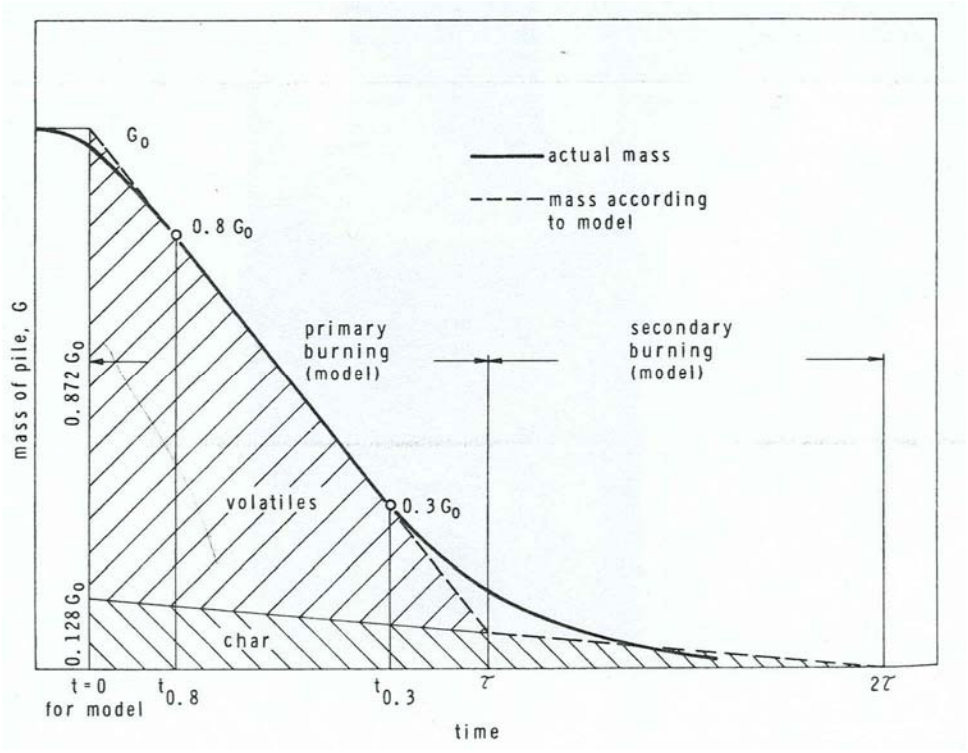

Figure 2.11: Harmathy's Model for Transient Mass of Free-Burning Crib[15]

He defines the rate of volatilization during steady state combustion as

$$\bar{U}_v = 0.932\,\bar{R} \tag{2.19}$$

and the duration of the steady state regime is defined as

$$\tau = 0.936 G_0 \Big/ \bar{R} \tag{2.20}$$

The mass that is consumed during the secondary period of burning is attributed to char oxidation.

A qualitative discussion on the energy flux within the pile notes two key sources. The first is the total area of glowing char surfaces facing the interior of the pile. This

source is directly related to all of the air-flow phenomena occurring in the pile. The second source that is discussed is the external geometry of the pile. This is of particular interest due to the fact that it is not commonly addressed in the literature, particularly in the model developed by Block[10]. Harmathy notes that it is the external surfaces and openings which determine the heat losses from the crib to the surroundings and thus influence the burning rate. The significance of this influence is dependent on the global geometry of the crib structure.

Gross' discovery of a maximum burning rate in a fuel limited region of combustion is sensible when one considers a qualitative energy balance for the system. As the porosity of the crib is continuously increased, the resulting increase in air entrainment is accompanied by an increase in external heat loss. This is the reason for the two sided porosity limit for this region of combustion.

2.2.3.2 Wood Cribs Burning in a Compartment

As seen in the work of Block, the ventilation of the wood crib is critical to determining its burning behavior. The placement of the crib inside a confined space offers modelers a unique advantage in that the airflow allowed to access the fuel can be derived from the known amount of air allowed to flow into the vent. Based on the work of Fujita, Kawagoe and eventually Thomas, Harmathy presents an empirical relationship for the mass flow rate of air entering an arbitrary compartment[15].

$$U_a = \frac{\sqrt{8}}{3} \frac{0.81\left(1 + T_0/T_g\right)^{1/2}}{\left[1 + \left(T_g/T_0\right)^{1/3}\left(1 + R/U_a\right)^{2/3}\right]^{3/2}} \phi \qquad (2.21a)$$

where

$$\phi = \rho_a g^{1/2} A_0 \sqrt{H_0} \tag{2.21b}$$

Treating the above empirical parameter as a constant affords the opportunity to derive a relationship between the mass loss rate of the fuel and the ventilation parameter ϕ. Harmathy asserts insignificant accuracies in the model as long the gas temperature is in excess of 300°C. The airflow through the vent is then simply proportional to ϕ.

$$U_a = 0.145\phi \tag{2.21c}$$

Recognizing that a only a portion of the incoming air will contribute to flaming combustion while the other significant portion will support oxidation of surface char, the following relationship is presented where C_5 is a constant

$$U_{a,c} = C_5 U_a \tag{2.22}$$

Further development of the model relies on two more key assumptions. The first is that the rate of mass loss of the crib is directly proportional to the total char surface area[15].

$$\bar{R} = C_6 A_c \tag{2.23a}$$

where

$$A_c = a C_7 A_s \tag{2.23b}$$

And the parameter a is defined as the fraction of the wood surface area involved in pyrolysis versus the total wood surface area of the crib[15].

$$a = A_{s,involved} / A_s \tag{2.23c}$$

The second assumption is that there exists some critical value for the ratio of the air flow feeding the surface oxidation of char layers to the total surface area of the fuel. Beyond this critical value, the burning rate will not increase with an increase in airflow. This critical value is linked to the definition of a as follows:

$$\frac{U_{a,c}}{A_f} \geq C_8 \qquad a = 1 \tag{2.24}$$

$$\frac{U_{a,c}}{A_f} \leq C_8 \qquad a = \frac{U_{a,c}}{C_8 A_f} \tag{2.25}$$

The above definition is made in order to account for a limited ventilation enclosure fire in which the combination of the vent location and the compartment depth affects the burning rate in a manner that produces non-uniform burning throughout the space. Combination of the above equations allow for a relationship to be developed between the ventilation parameter, surface area of the fuel and the mass loss rate of the fuel. Two linear relationships result. The first is between the ventilation parameter and the fuel surface area. The second is between the mass loss rate of the fuel and the fuel surface area. In order to resolve the constants of proportionality and validate the model, Harmathy utilizes experimental data compiled from 17 laboratories as shown in Figure 2.12.

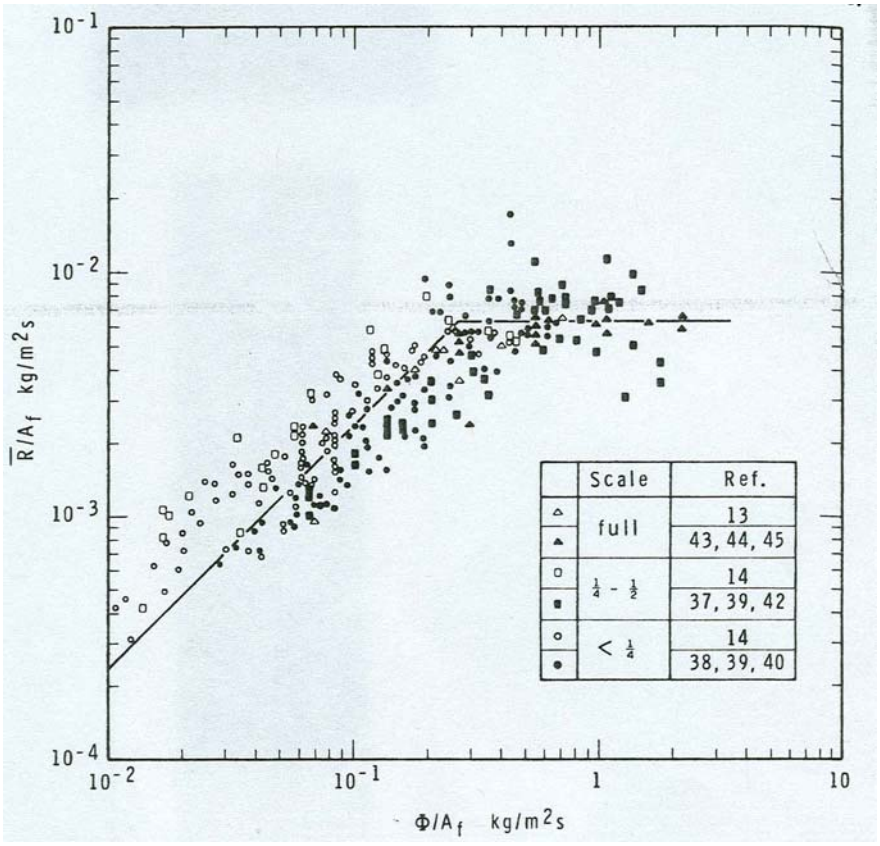

Figure 2.12: Harmathy's Model for Enclosure Ventilation Limited Burning Rate[15]

Analysis of the data confirms Harmathy's assumption of a critical ventilation parameter which he defines based on the best-fit lines shown above.

$$\phi = 0.263 A_f \tag{2.26}$$

In the ventilation controlled combustion region,

$$\frac{\phi}{A_f} < 0.263 \qquad R = 0.0236\phi \tag{2.27a}$$

For the fuel limited region

$$\frac{\phi}{A_f} \geq 0.263 \qquad R = 0.0062 A_f \tag{2.27b}$$

Clearly the eyeball curve-fitting definition of the above constants is open to scrutiny; however the result of deriving a crude relationship between compartment

ventilation and fuel surface area is quite powerful. Note that the one significant omission of the model is the influence of radiation from the enclosure boundaries on the burning rate of the fuel[15].

2.2.3.3 Compartment Fire Duration

Based on the model derived for the fuel mass loss rate, Harmathy presents a model for the duration of the steady state period of a fire based on its time-temperature curve. Based loosely on Figure 2.12 illustrating the transient mass of the burning crib, he defines the steady state period to begin at the end of the growth period and end at the point at which the gas temperature in the upper layer has decayed to 80% of its maximum[15].

For fuel limited combustion

$$\tau = 151\frac{G_0}{A_f} \tag{2.28a}$$

For ventilation limited combustion

$$\tau = 39.7\frac{G_0}{\phi} \tag{2.28b}$$

Note that the former regime is independent of ventilation and the latter independent of total fuel load. It is also important to recognize the similarity of the burning rate's relationship to ventilation in both the confined and unconfined modes of burning. The asymptotic behavior of Figure 2.13 is reminiscent of Block's crib porosity model for the free burning rate of the crib. Although the analogy is more complex, the concept of airflow limitations in each case is critical.

2.2.3 A Worldwide Modeling Effort: *Conseil International du Batiment*

Following the work of Ingberg, Fujita and Kawagoe, a co-operative multi-laboratory effort was designed, under the direction of the Joint Fire Research Organization, in the hopes of producing a more robust database for pertinent enclosure fire variables. Participating laboratories included facilities in Australia, France, Germany, The United Kingdom, The Netherlands, Japan and The United States. The cohesive effort was referred to as the *Conseil International du Batiment Working Party 14*, or C.I.B. as it is commonly known. Laboratories from the above countries conducted over 300 experiments with wood cribs fires in compartments[16].

Consideration was focused on fully developed fires in single compartments. Size constraints of the various facilities necessitated the use of what was referred to as scaled compartments. The term scaling in this particular work refers only to the height of the compartment with respect to the height of a life-sized room. Three heights were used to design the compartments: 0.5 m, 1.0 m, and 1.5 m respectively. The width and depth of the rectangular prism were then set by predefined ratios so as to investigate the effects of compartment shape. Four such ratios (width: depth: height) were used as shown in Figure 2.13.

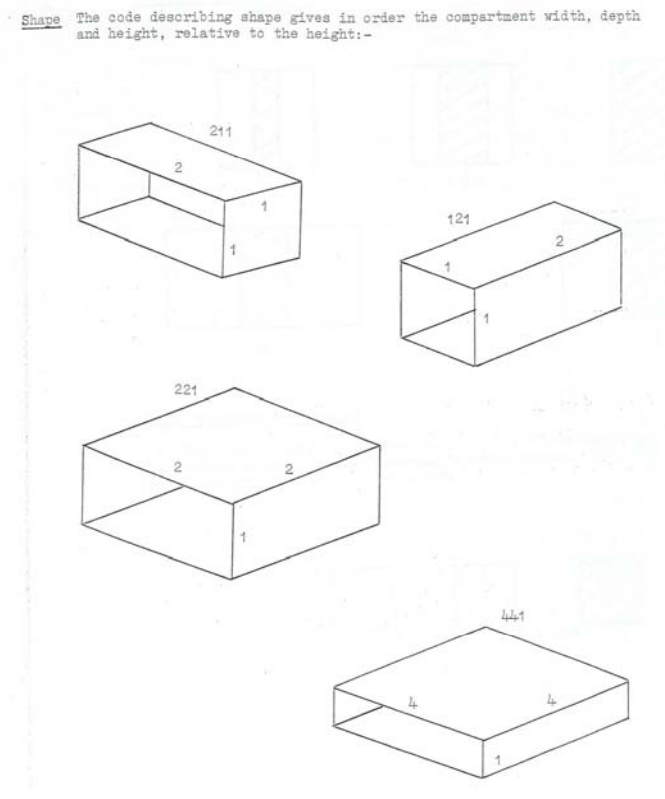

Figure 2.13: C.I.B. Compartment Shape Ratios[16]

Compartment ventilation was achieved with a single rectangular opening extending the full height of the compartment. The vent was centered in the plane of the front face of the compartment. Its width was varied from the full width of the face, one half width and one quarter width. Wood cribs were chosen as the fuel source due to their reputation for producing repeatable data as well as the relative ease of adjusting their design parameters. The size of the fuel load was designed in keeping with Ingberg's definition of fire load. Fire loads of 10, 20, 30 and 40 kg/m^2 were used. A unit conversion corresponds to 2, 4, 6 and 8 psf respectively. Comparison with the survey of occupancy fuel loads presented by Gross and Robertson less than 10 years prior to these studies shows that these fuel loadings correspond to a typical hospital, school or perhaps lightly loaded office or residence[14].

The design requirements for the wood cribs and fire compartments were straightforward. Square cross sections of 1, 2 and 4 cm were used. Spacing between sticks was to be in multiples of 1/3, 1 or 3 of the cross section used. There was no direct requirement for any other design feature of the crib. The species of wood was allowed to vary as was the moisture content. The range of moisture contents reported was 8-13%. The density of the wood species used ranged from 0.37-0.51 g/cm^3. It is stated in the report that the length of the crib sides was 5/6 the length of a side of the compartment wall. This statement suggests that rectangular cribs were permitted since the width and depth of the compartment were not always equal. Therefore, the length of individual sticks within a crib varied between adjacent layers. Compartments were constructed from asbestos millboard with a thickness of 10mm, supported by a framework of angled steel[16].

Measurements were taken with respect to fuel weight loss, temperature inside the compartment and radiant intensity from the interior of the compartment to the ambient through the open plane of the vent.

The wood cribs were distributed across the entire surface of the compartment floors. Ignition was achieved by placing fiber insulation board strips soaked in kerosene into the spaces between sticks in the lowest layer of the wood crib. This method of ignition suggests that the cribs were not elevated, nor was a proper fuel pan used in the manner suggested by Gross and agreed upon by Block. This does not mean that the data produced in these tests was not repeatable; however, comparison of peak mass loss rate values to those of Gross and Block can only be achieved through consideration of this notable discrepancy in combination with the lack of standardization of moisture content.

The method for defining the fully developed stage of the fire, which was of primary interest to the C.I.B. effort, indicates the origins of Harmathy's otherwise arbitrary definition. The fully developed stage of the fire was defined as the period during which the fuel weight had fallen from 80% to 30% of its initial value.

The results of the C.I.B. effort provided the research community with a wealth of tangible data. The current research effort is most interested in the data acquired for compartment gas temperatures and fuel mass loss rate and therefore much attention is paid to these particular results. A proportional relationship of the fuel mass loss rate to Kawagoe's ventilation factor was presented, where K is a constant typically assigned a value of 5-6 kg $min^{-1}m^{-5/2}$.

$$R = KA_o\sqrt{H_0} \tag{2.29}$$

The empirical relationship presented above is dependent on two key assumptions. The first is that the compartment is uniformly heated or in other words a low vertical temperature gradient in the gas phase. The second is obviously that the mass loss rate of the fuel is proportional to the rate of air flow into the compartment. This last concept is empirically found; however, this report will later show a relationship to the law of conservation of mass. Harmathy's model assumes that only minor changes are necessary to account for the distribution of air once it enters the compartment.

Having recognized that variations in compartment ventilation may have produced a split in burning rate behavior between ventilation limited and fuel limited fires, the report contains a caution that the burning rate dependency may well change for cases of low ventilation. Unfortunately, the shape of the best-fit curve presented in Figure 2.14 gives no indication of the change in behavior expected from an inevitable transition to

fuel limitations on the burning rate. It is in this region that one would expect a horizontal asymptote indicating that the data is dependent only on the surface area of the fuel as indicated by the dashed line. It was not until Harmathy's model that a tangible method of predicting such behavior was eventually reached.

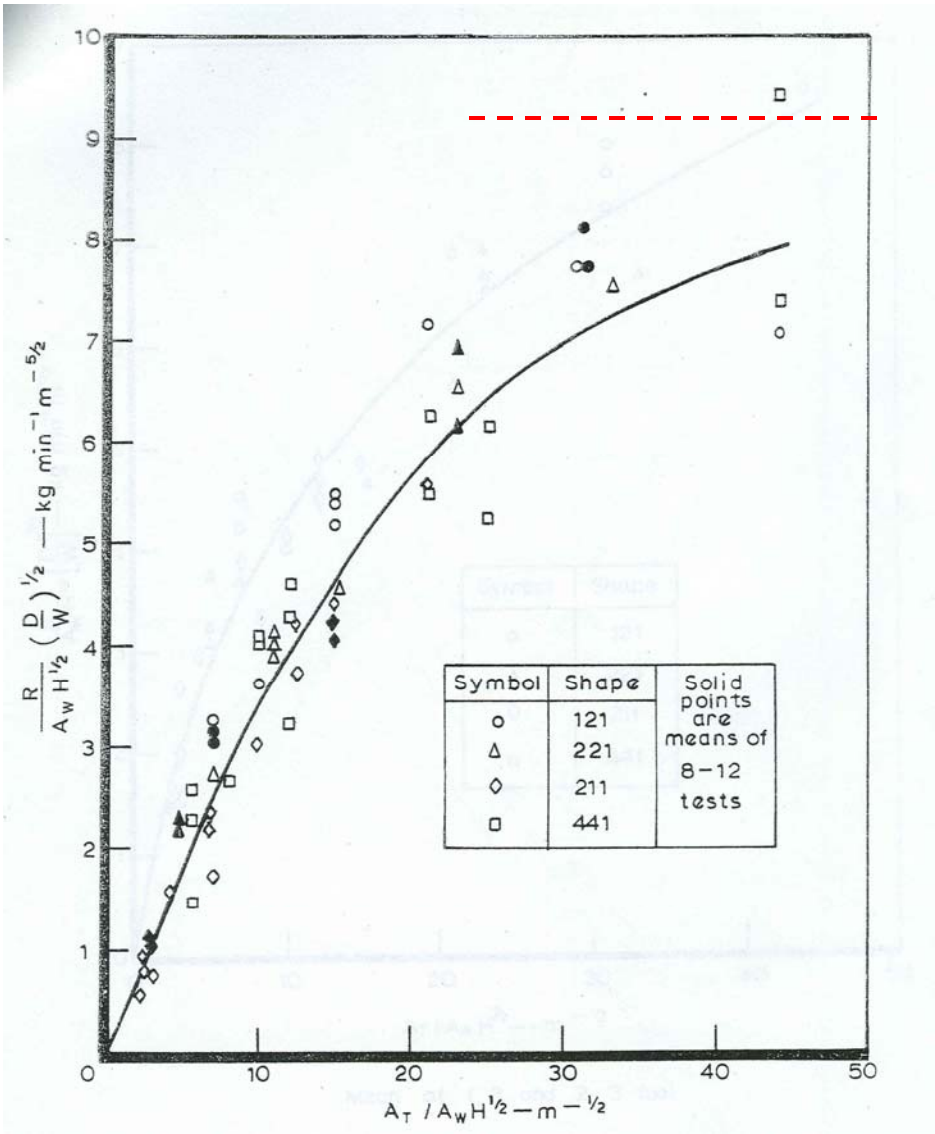

Figure 2.14: C.I.B. Compartment Mass Loss Rates[16]

The results for compartment gas temperatures are compared to a theoretical heat balance within a compartment. This heat balance approximates the heat stored within the compartment as the sum of the sensible enthalpy of the fuel and air combined with both

convective and radiant modes of heat loss as well as the chemical energy generation of the reaction[16].

$$\dot{Q} = (R + U_a)c_p\theta + hA_T\theta + IA_0 + R\Delta H_c \tag{2.30}$$

The equation can be solved for the gas temperature rise. The experimental data is then plotted against the theoretical curve evaluated near the compartment ceiling in Figure 2.15.

Note that the peak compartment temperatures are dependent on the opening factor of the compartment and that there exists an optimal range on the curve. This is indicative of the heat balance phenomenon at work. As the size of the compartment and vent increases, there is a balance that occurs between the heat lost from the vent and the heat generated by pyrolysis of the wood crib. Smaller compartments allow for less heat loss through the vent yet simultaneously limit the rate of energy generation from the fuel by blocking the passage of fresh air into the space. In the case of large compartments with large vents, the fuel may have an adequate supply of air, but the increased heat losses outweigh the increase in the rate of pyrolysis.

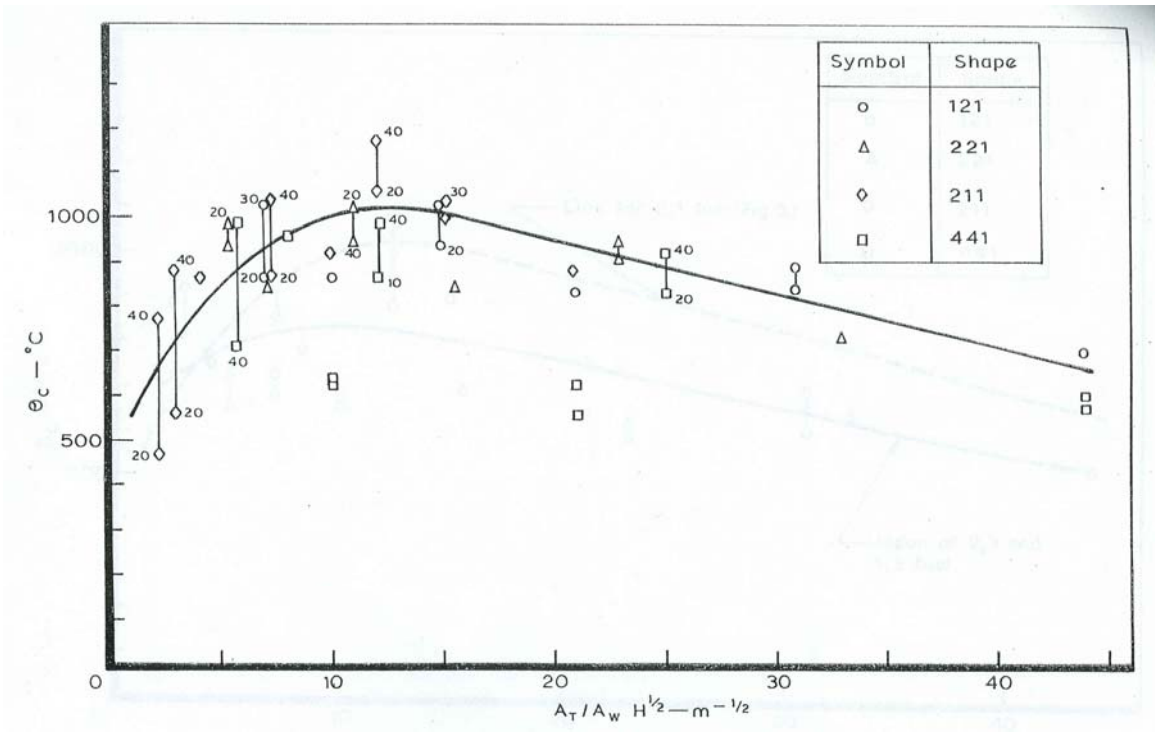

Figure 2.15: C.I.B. Compartment Gas Temperatures[16]

Thomas and Heselden are quick to point out that the data gathered in the C.I.B. effort is time-averaged. Although time-averaged peak values allow for fundamental insights, a firm grasp of transient data will ultimately provide the fire researcher with a powerful analytical tool. Additionally, the variation in shape of the C.I.B. compartments was found to produce slight changes in the data. This observation is made concurrently with the statement that some of the laboratories used wall materials with slightly different thermal properties than the asbestos millboard called for in the agreed design scheme. The significance of the heat balance produced by the C.I.B. researchers was perhaps more critical to successful conclusions than was originally realized. The change in size of a compartment coupled with an arbitrary change in thermal properties of the walls undoubtedly was responsible for much of the scatter observed in the data.

2.2.4 The Role of Gas Species Concentrations

In recognition of the scarcity of data and analysis conducted on gas composition in enclosure fires, Tewarson attempted to develop empirical correlations with respect to compartment ventilation. His efforts were based largely on the assumption that the burning rate inside the compartment is proportional to Kawagoe's ventilation factor.

An analysis was conducted of two separate compartments of dimensional ratios 1:2:1 (width:depth:height) with 2 window vent openings of equal dimensions, centered on opposite faces of the compartment width. The height of the smaller enclosure was 53 cm and the height of the larger enclosure was 98 cm. Thus, the dimensions of the two enclosures were approximately geometrically scaled. Wood cribs were used for the fire source. The wood species selected for use in all tests was Northern White Pine. The crib design for each compartment was geometrically scaled. Moisture content was controlled by drying the wood overnight in an oven prior to testing.

Perhaps the most notable results from Tewarson's research are the relationships developed between gas concentrations of CO and CO_2 versus the ratio of fuel in the compartment to the amount of available air in the confined space. This data is presented in Figure 2.16.

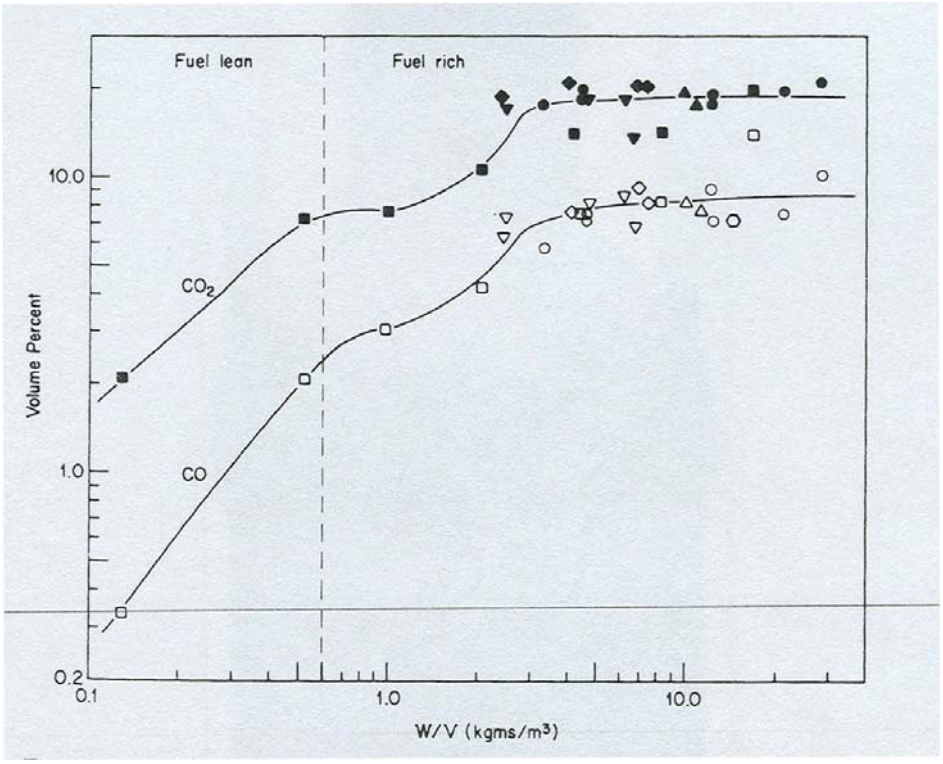

Figure 2.16: Tewarson's Gas Composition Model[17]

The data reveals the effect of an equivalence ratio on the concentration of these two gases. Tewarson has identified both fuel lean and fuel rich regions. Note the horizontal asymptote in the data as it tends far off into the fuel rich region. This is due to the fact that the burning rate in this region is dictated solely by the inflow of oxidizer into the confined space[17].

2.2.5 A Mathematical Model for Enclosure Fire Phenomena

In late 1980, a project was undertaken at the National Bureau of Standards with two major objectives that are relevant to the current research effort. The first of these objectives was to experimentally show the effects of fire size and natural ventilation for wood crib fires in a full scale enclosure. Temperature, heat flux, burning rate and air flow rate into the enclosure were among the variables of interest. In addition to the

experimental work, a second major objective of developing a mathematical model for such room fire conditions was explored[18].

Although both plastic and wood cribs were used in this research, the current effort is concerned only with the wood crib experiments. The species used was Sugar Pine with a density of 370 kg/m^3 and a moisture content ranging between 5 and 8%. The moisture content was controlled by placing the wood cribs in a conditioning room at 20^{o}C and 50% RH for multiple days. The cribs were designed to have sufficient porosity to burn in the fuel surface controlled regime identified by Block[10]. The final design is shown in Table 2.4. It should be noted that experiments were conducted with variations in the number of cribs being burned. The number of cribs was varied between 1, 2, 3 and 4 throughout these experiments. Each crib was identical by design. Wood and plastic cribs were never burned in the same experiment.

Variable	Description	Value
b	Stick Thickness	3.5 cm
L	Stick Length	24.5 cm
n	Number of Sticks per Layer	3
N	Number of Layers	10
s	Stick Spacing	7.0 cm

Table 2.4: Quintiere and McCaffrey Crib Design Parameters

Data from free-burning experiments was collected after burning in the enclosure; however, for the purpose of consistency in this report, the free-burning experimental procedure is presented first. One experiment was conducted to determine the free-burning behavior of a single wood crib. The experimental setup is shown in Figure 2.17.

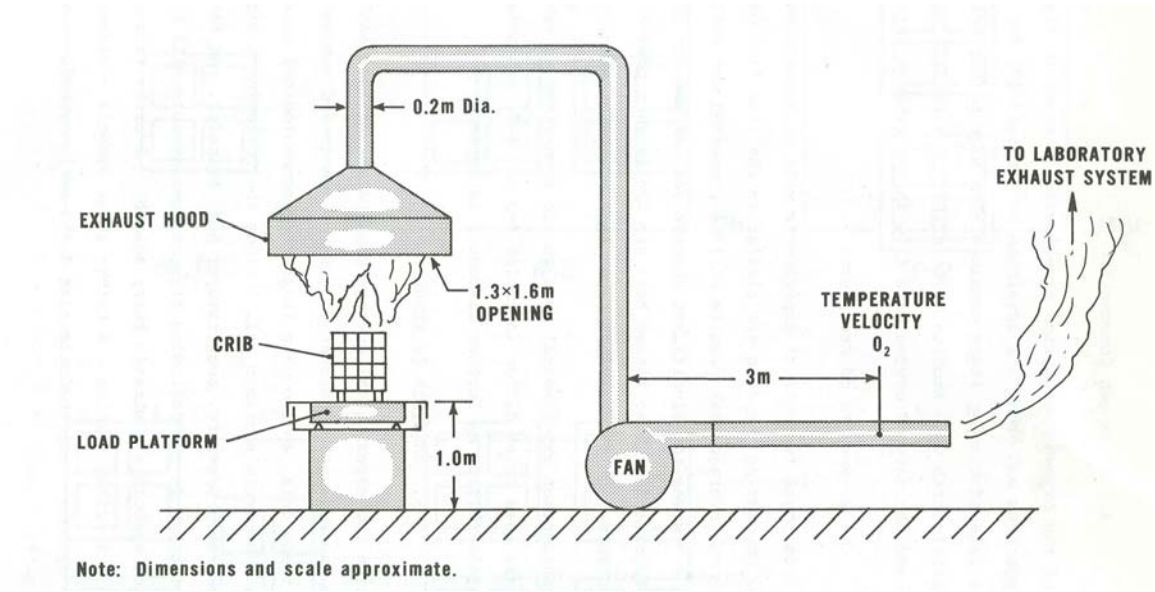

Figure 2.17: Quintiere and McCaffrey Free-burn Experimental Setup[18]

The ignition scheme called for the crib to elevated and centered above a square metal pan with a side dimension of 30 cm. Elevation above the surface of the pan was achieved with the placement of 2 thin Marinite strips of height 2 cm each below the crib. A volume of 40 mL of Heptane was poured into the pan and utilized as the starter fuel for each test.

Measurements were taken of flow velocity, gas temperature, heat flux and fuel mass during the experiment. All data was presented in the form of a single peak value averaged during the time interval corresponding to 95% – 45% of the initial crib mass. This was arbitrarily identified as the steady state period. This duration encompasses 50% of the total crib mass loss, which is similar to Harmathy's model; however, this new definition is more heavily weighted toward fire growth. The current research is interested only in the results for crib mass loss rates, which ranged from 4.40 g/s for a single crib to 25.6 g/s for a four crib layout[18].

The fire enclosure was conducted in a test room with the plan view shown in Figure 2.19. The interior dimensions of the compartment were 2.18 m in long x 2.18 m deep x 2.41 m high, not including the doorway in the corner of the room. The doorway width was varied from its full dimension of 0.79 m to half and quarter widths. The height of the doorway was 1.83 m, measured from the floor surface to the top of the door. The doorway depth extended 0.5 m beyond the otherwise rectangular compartment boundaries. Cribs were centered on the load platform. The top surface of the platform, which insulated a load cell underneath, sat 0.18 m above the surface of the floor. The compartment boundaries were lined with Marinite XL board, a material similar to gypsum board in thermal properties. The thickness of the board was 1.9 cm (Figure 2.18 and Figure 2.19).

Instrumentation was put in place to measure a vertical gas temperature profile outside the flame zone, wall and ceiling surface temperatures, fuel mass loss, gas concentrations, static pressure differences, surface heat fluxes as well as doorway gas temperatures and velocities.

Data for average peak values was used to explore several pertinent phenomena. It should be noted that an approximate 15% increase in the average peak burning rate was observed for a single crib burning inside the compartment versus outside of it. This was thought to be due to both ventilation limitations and thermal feedback from the enclosure boundaries. This reasoning is consistent with the heat balance idea applied in the C.I.B. work. It is also important to note that in the cases where multiple cribs were placed adjacent to each other on the fuel platform, an increase in the burning rate was observed. This was the same effect of internal radiation that is seen inside a single crib structure.

The spacing of these cribs at distances equal to the spacing between individual sticks within a crib ultimately yielded an important insight that will be explored later in the report[18].

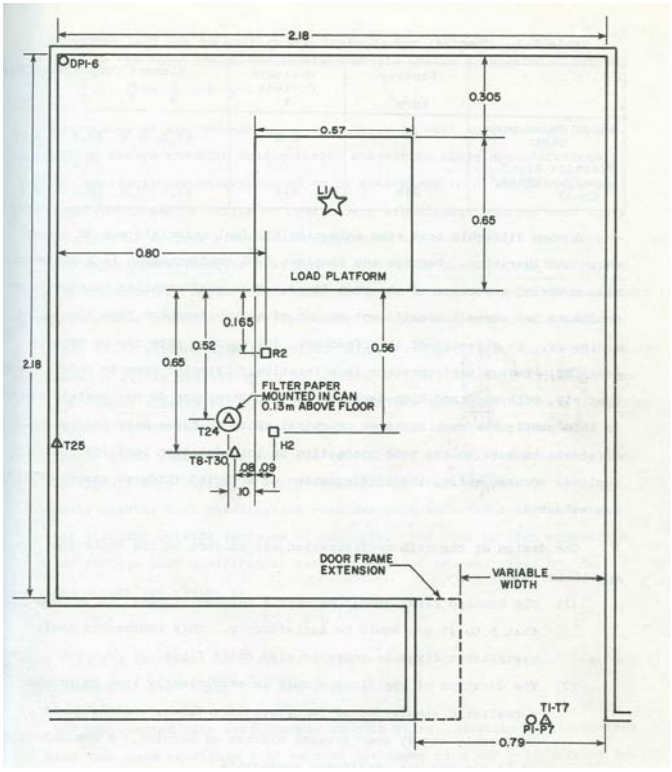

Figure 2.18: Quintiere & McCaffrey Plan View of Test Room[18]

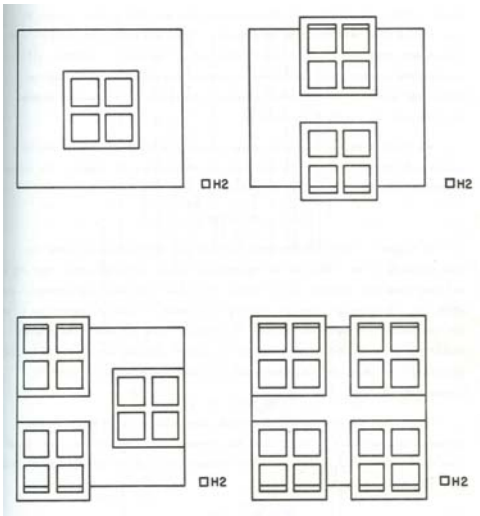

Figure 2.19: Placement of Multiple Cribs on Load Platform[18]

A mass balance is performed to evaluate the mass flow rate of air into the enclosure. It is taken to be a balance between the mass flow generated by the burning wood crib and the net exchange of gas and fresh air in the doorway.

$$\dot{m}_a = \dot{m}_{out} - \dot{m}_v \tag{2.31}$$

The mass loss rate of the fuel is of course measured; however, the mass flows in and out of the compartment are calculated based on the experimentally measured quantities of doorway temperature and velocity.

The calculations assumed a two zone model. An additional assumption was made that temperatures and velocities in the doorway did not vary horizontally across the width. Thus, the values measured near the centerline were used. The location of the neutral plane was taken to be the point at which zero pressure difference was measured. Average peak values were used throughout the calculation.

The results show that the proportionality of the burning rate and the ventilation factor is not fully satisfied. A power-law dependence is suggested by the line drawn through the data[18].

$$\dot{m}_a = \left(\dot{m}_v \right)^{1/4} \left(A_0 / \sqrt{H_0} \right)^{1/2} \tag{2.32}$$

Recall, however, the previously mentioned power dependence of the mass loss rate on the number of cribs placed on the load platform. The power dependence suggested by Figure 2.20 is based on data collected from tests using different numbers of cribs. The close grouping of data points for a certain number of cribs suggests that the power-law line is a function of the number of cribs on the load platform. The proposed ¼

power dependence seems to be a relic of the radiation exchange between cribs enhancing the burning rate. As the burning rate is enhanced, more air is drawn into the enclosure.

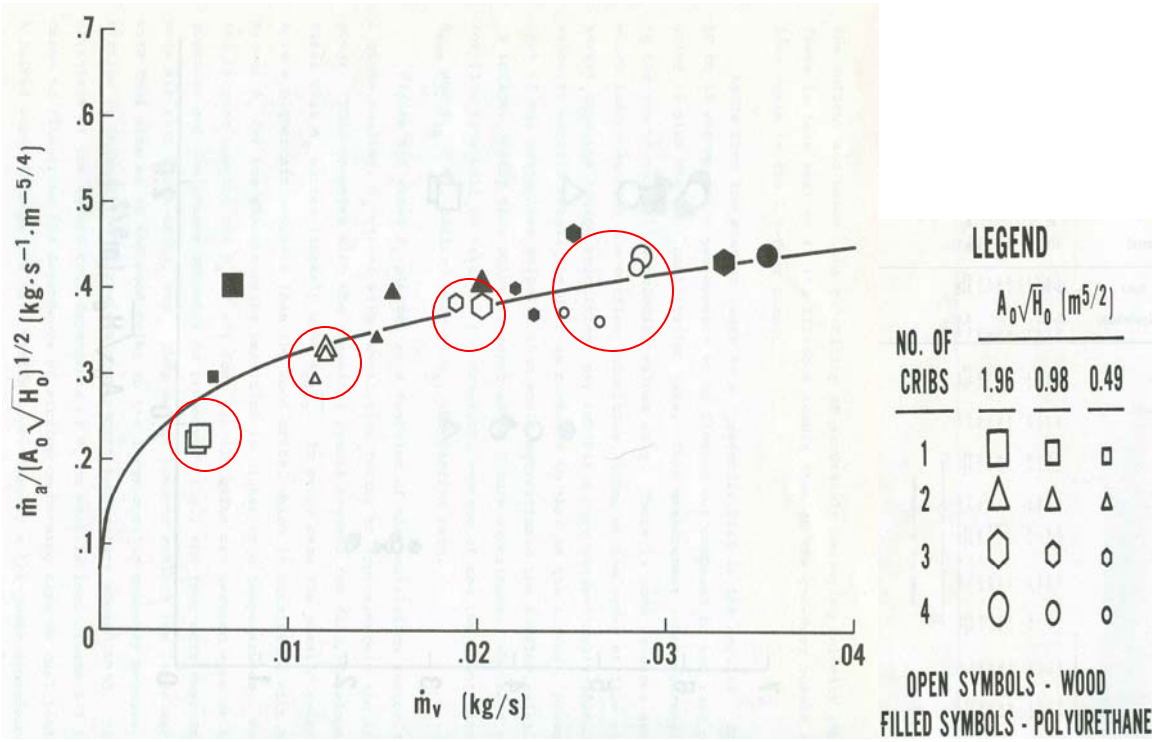

Figure 2.20: Effect of Number of Cribs on Fuel Mass Loss Rate[18]

A steady state, two-zone mathematical model was developed by Quintiere and McCaffrey for comparison with their experimental results. Derivation of the model is accomplished by applying the conservation of energy to the compartment. It should be noted that at steady-state, a constant loss of heat to the enclosure walls via conduction is assumed.

Since the most significant variable affecting the enclosure fire environment is the burning rate of the fuel, the model development for that variable is presented here. The model considers the effects of increased heat flux to the crib and decreased oxygen concentrations present in a confined space. It predicts a burning rate for the crib in the

compartment based on knowledge of the free-burn burning rate and these compartment effects.

$$\dot{m}_{enclosure} = \dot{m}_{free-burn} + \Delta\dot{m}_{thermal} + \Delta\dot{m}_{oxidizer} \tag{2.33}$$

The details of the model are left to be discussed in a later section of this report. Comparison of experimental results obtained by Quintiere and McCaffrey with their model yielded good agreement for all orientations of cribs on the load platform.

A model for the entrainment of air by the crib was also developed. This model considered mass flow contributions from both the airflow through the interior channels and the air flow to the exterior surfaces of the crib. In the case of multiple cribs, the airflow through the contiguous neighboring spaces is also considered[18].

$$\dot{m}_{crib} = \dot{m}_{channel} + \dot{m}_{exterior} + \dot{m}_{contiguous} \tag{2.34}$$

Experimental measurements revealed that 45-50% of the total entrainment is through the interior channels, 30-55% from the exterior and 0-20% through the contiguous surfaces in multiple crib layouts[18]. This suggests that for a single crib of the design used by Quintiere and McCaffrey, the influence of the exterior geometry of the crib is nearly as significant as that of the interior geometry.

2.3 Scaling Attempts

2.3.1 Froude Modeling

Gross and Robertson of the National Bureau of Standards were one of the first to publish experiments conducted solely for the purpose of scaling wood crib fires in enclosures. Their results included correlations for the mass loss rate of the fuel, gas temperatures and gas concentrations inside the enclosure.

Recognizing that the governing flow of the plume was buoyancy driven they decided to scale based on the Froude number, a dimensionless quantity relating length scale to the buoyancy forces driving the flow[3].

$$Fr = \frac{u}{\sqrt{gl}} \tag{2.35}$$

There was an understanding that as the geometric length scale of the compartment decreased, the fundamental buoyancy force driving the flow would change in a proportional manner. Modern knowledge suggests that such modeling can be very successful in an unconfined state.

Three sizes of enclosures were geometrically scaled according to the ratio 1:1:2 (height: depth: width). Ventilation of the enclosures was achieved via a single opening placed in the center of the front wall of the enclosure. The wall material was a cellulose-based fiber board. This same material was used for all three scales. Wood crib design rules were limited to geometric scaling of the cross section and spacing between sticks. Rectangular cribs were used throughout.

Although it was recognized that the length scale present in the Froude number played a role in scaling the fire, the only scaling rules applied in the design phase were simple geometric relationships. This was done in an attempt to scale the burning rate

which was known to be proportional to the ventilation factor. It was thought that geometric scaling would indirectly scale the burning rate by accounting for the airflow allowed through the vent. Several empirical relationships were explored on the basis of average peak values; however, there was poor comparison of fire phenomena between scales[3].

2.3.2 A Hypothesis for Scaling Wood Crib Fires

A more thorough application of scaling to the design phase of wood crib fires in enclosures was undertaken by Heskestad. His hypothesis was the first to suggest that additional scaling rules beyond geometric relationships must be followed in order to observe satisfactory results. The foundation of the hypothesis begins with the research on free-burning wood crib fires performed by Gross, Block and various others. The relationship between the burning rate and stick thickness observed by Gross and derived by Block is used[19].

Heskestad recognized that the relationship between the free burning rate and the mass flow rate of air through the internal structure of the crib could be related with the use of Block's empirical power law.

$$\frac{R_r}{A_s b^{-1/2}} = f\left(\frac{\dot{m}_a}{A_s b^{-1/2}}\right) \tag{2.36}$$

Gross assumed a specific power law relationship of $b^{1.6}$ based on the following assumed relationship of the rate of air flow through the vertical shafts of the crib:

$$\dot{m}_a \propto A_v\sqrt{h_c} = A_v\sqrt{Nb} \tag{2.37}$$

Recall, however, that Gross' power law was based on a stick cross section that possessed subtle design relationships to other parameters of the wood cribs.

Block's more rigorous theoretical model indicates a dependence of the mass flow rate of air through the shafts on the spacing between sticks rather than the height of the shaft.

$$\dot{m}_a \propto A_v \sqrt{s} \tag{2.38}$$

Heskestad recognized that Block's theoretical treatment of the ventilation limited regime for the free-burning cribs was thorough, but the results required some simplification in the interest of practical implementation in the experimental design phase. He therefore surmised that maintaining the above proportionality would suffice. Thus, Heskestad's version of Block's theoretical model became

$$\frac{R_r}{A_s b^{-1/2}} = f\left[\left(\frac{A_v}{A_s}\right) s^{1/2} b^{1/2}\right] \tag{2.39}$$

An effort was made to translate Block's data based on his complex porosity expression to the above simplified model. The result is claimed to be a best-fit curve to Block's data by-eye[19]. The transition region from ventilation to fuel limitations is defined by region I on the plot in Figure 2.21. Heskestad claims that the curve fits Block's data to within ± 20%, which is coincidentally the same level of accuracy claimed by Block for his own best-fit curve[19].

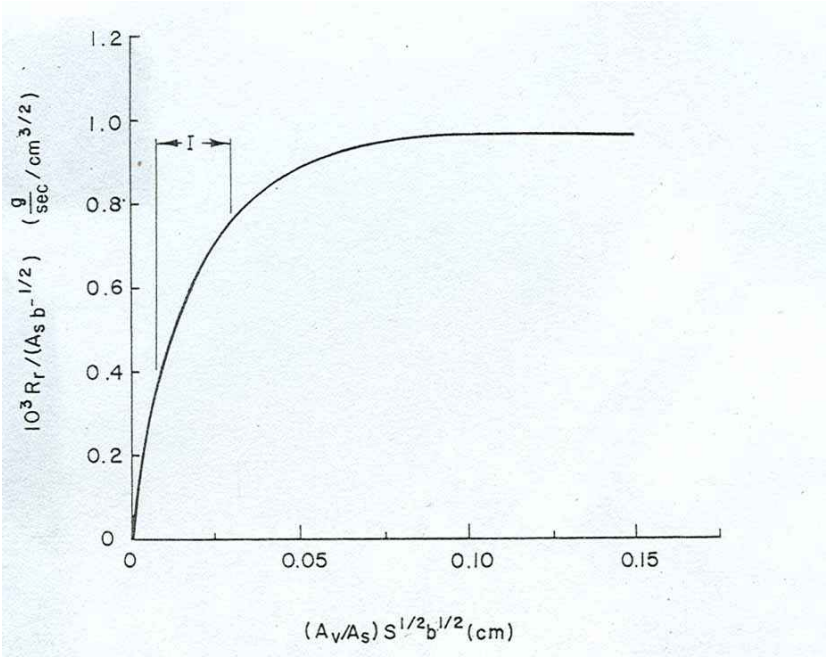

Figure 2.21: Heskestad's Simplified Version of Block's Model[19]

In order to introduce an enclosure to the above model, Heskestad recognized the importance of including additional limiting factors. These factors were identified as the geometry of the enclosure and the air flow rate entering the enclosure. Although not directly stated, conservation of such factors recognizes the importance both an energy and mass balance in the confined space. Thus, the model for wood cribs burning in an enclosure became

$$\frac{R}{A_s b^{-1/2}} = f\left[\left(A_v/A_s\right)s^{1/2}b^{1/2}, G, \left(\dot{m}_a/R_r\right)\left(R_r/R\right)\right] \tag{2.40}$$

The ratio of the free-burning rate to that of the burning rate inside the enclosure is now predicted to be

$$\frac{R}{R_r} = f\left[\left(A_v/A_s\right)s^{1/2}b^{1/2}, G, \left(\dot{m}_a/R_r\right)\right] \tag{2.41}$$

where a porosity factor P is defined as

$$P \equiv \left(A_v / A_s\right) s^{1/2} b^{1/2} \tag{2.42}$$

Kawagoe's empirical determination of the ventilation factor is now used to apply a length scale to the air flow rate entering the enclosure. The characteristic length scale is chosen to be the height of the enclosure *H*. The result suggests that the same length scale must apply to the burning rate[19].

$$\frac{R}{R_r} = f\left[P, G, \left(H^{5/2} / R_r\right)\right] \tag{2.43}$$

Recognizing that the positioning of the crib inside the enclosure will affect temperature and gas concentration distributions, an additional parameter was added to account for this relative geometry

$$\frac{R}{R_r} = f\left[P, G, \left(H^{5/2} / R_r\right), \left(x / H\right)\right] \tag{2.44}$$

The hypothesis is that temperatures and gas concentrations can be predicted for various characteristic enclosure length scales provided the above relationships are maintained.

However, prior to realizing such results, the enhancement of the crib burning rate by the thermal contribution of the enclosure walls must be handled. Thus far, scaling of the airflow into the compartment has only accounted for convective heat and mass transfer through the vent. In order to account for additional heat lost to the vent via radiation and to the enclosure boundaries via conduction, scaling relationships must also be applied to the thermal properties of the walls[19].

Heskestad hypothesizes that the radiation from the source will scale directly with the burning rate and therefore, radiation lost to the vent via radiation should also scale in the same manner. A model for insulated enclosures is presented to arrive at scale

relationships for the heat exchange to the enclosure boundaries. Insulated boundaries are assumed due to the opportunity presented for a simplifying assumption that no heat is lost from the exterior wall surfaces to the ambient[19].

Assuming that the wall is a homogeneous material, the law of conduction is applied across the wall thickness

$$\rho c_p \frac{\partial(T - T_0)}{\partial t} = k \frac{\partial^2(T - T_0)}{\partial x^2} \tag{2.45a}$$

With the following boundary conditions applied at the interior surface ($x = 0$) and the exterior surface ($x = \delta$) of the wall, assuming that all heat transferred to the wall is stored within it

$$\dot{q}'' = k \frac{\partial(T - T_0)}{\partial x}\bigg|_{x=0} \qquad \dot{q}'' = 0 = k \frac{\partial(T - T_0)}{\partial x}\bigg|_{x=\delta} \tag{2.45b}$$

The conduction equation with its boundary conditions is then made dimensionless by introducing a characteristic fire duration time t_r and utilizing the wall thickness δ. The governing equation then becomes

$$\frac{\partial(T - T_0)}{\partial(t/t_r)} = \frac{k t_r}{\delta^2 \rho c} \frac{\partial^2(T - T_0)}{\partial(x/\delta)^2} \tag{2.46a}$$

with the boundary conditions

$$\dot{q}'' \propto \frac{k}{\delta} \frac{\partial(T - T_0)}{\partial(x/\delta)}\bigg|_{x/\delta=0} \qquad 0 = \frac{\partial(T - T_0)}{\partial(x/\delta)}\bigg|_{x/\delta=1} \tag{2.46b}$$

The above relationships suggest that the interior wall temperatures and thus the wall heat exchange can be predicted from one scale to the next if the following relationships are maintained between scales[19]:

$$\frac{kt_r}{\delta^2 \rho c} = const \tag{2.47a}$$

$$\frac{k}{\delta \dot{q}''} = const \tag{2.47b}$$

The last piece of the puzzle is the determination of a characteristic time. Heskestad defines this time as that of the fire duration, which he approximates as the quotient of the crib mass and its quasi-steady state burning rate[19].

$$t_r \propto \frac{m}{R} = \left[\frac{(R_r/R)}{(R_r/m)}\right] \propto \left[\frac{(R_r/R)}{(R_r/A_s b)}\right] = \left[\frac{(R_r/R)}{\left(R_r/A_s b^{-1/2}\right)}\right] b^{3/2} \propto b^{3/2} \tag{2.48}$$

The final step in the above chain of proportionalities is made assuming that free burning rate has been scaled properly with the porosity factor. The result is a characteristic time that is controlled by the stick thickness used in the crib design. Now to further simplify the constant ratios in Equations 2.47a and 2.47b, two steps are required. First, the characteristic time is substituted. Second, the assumption that the heat flux from the source scales directly with the burning rate is made. This assumption results in the following behavior for the heat flux per unit area incident to the wall.

$$\dot{q}'' = \frac{\dot{q}}{A} \propto \frac{H^{5/2}}{H^{4/2}} = H^{1/2} \tag{2.49}$$

The constant ratios then provide the final scaling rules for the thermal properties of the enclosure boundaries[19].

$$\frac{kb^{3/2}}{\delta^2 \rho c} = \frac{k}{\delta}\frac{b^{3/2}}{\delta \rho c} = \frac{H^{1/2} b^{3/2}}{\delta \rho c} = const \tag{2.50a}$$

$$\frac{k}{\delta H^{1/2}} = const \tag{2.50b}$$

The result indicates a strong inter-dependence between the crib and compartment designs between scales. Data from Tewarson[17] was used to explore the hypothesis; however, since Tewarson did not apply these scaling rules to his crib or compartment designs, the validation of the model with his data is inconsequential[19].

2.3.3 Application of Heskestad's Scaling Hypothesis

A more appropriate validation of Heskestad's hypothesis was attempted by Croce not long after it was developed[20]. Croce constructed enclosures at three different geometric scales, with corresponding wood crib fuel sources. The scales chosen were full, half and quarter. The full scale dimensions were 3.66 m x 2.44 m x 2.44 m (length x width x height). Ventilation of the compartments was provided by dual vents spanning the full width dimension of the compartment, centered along with respect to height, on opposite walls. The ratio of the height of the vents to the height of the enclosure was varied over a range of 0.02-1.00 throughout the experiments. Free-burning experiments were conducted to determine the free-burn burning rate prior to experimentation in the enclosures[20].

The thermal properties of the enclosure walls were also scaled in accordance with Heskestad's model[19]. The walls of the full scale enclosure were chosen as gypsum wallboard. The half scale walls were constructed of cement-asbestos board and the quarter scale was made of alumina/silica board. It should be noted that the paper facing was left on the gypsum wallboard during testing, yet not account was made for the effect of its mass or thermal properties on the measured burning rate. The properties of the materials listed above at a temperature of 300^{o}C are presented in Table 2.5.

Scale	Compartment Boundary Material	K (W/m^oC)	ρ (kg/m^3)	c_p (kJ/kg^oC)	δ (mm)
Full	Gypsum Wallboard	0.173	721	1.3	15.9
Half	Cement-Asbestos Board	0.089	368	1.3	12.7
Quarter	Alumina Silica Board	0.065	224	1.3	9.5

Table 2.5: Croce's Thermal Wall Properties

The species chosen for the wood cribs was Sugar Pine. Several wood crib designs were implemented, but the wood species was kept constant for all tests. Designs spanned both the porosity and the fuel limited regimes of burning, with a critical transition region identified as 0.3-0.5 mm from Heskestad's simplification to Block's model. Figure 2.22 shows where these designs fall on the simplified free-burning rate model produced by Heskestad. The term "Reduced Free-Burning Rate" is just the free-burning rate.

The crib moisture content was controlled by drying the wood at 93^{o}C for 24 hours prior to experimentation. The ignition scheme involved the use of asbestos paper wetted with acetone placed below the crib. Although no fuel pan was used, Gross' criteria that the surface area of the pan should be slightly larger than that of the crib, was followed with respect to the surface area of the paper. The crib was elevated above the fuel soaked paper at a distance of 0.026 times the height of the enclosure. The choice of this particular elevation is unclear. It is also unclear why the elevation of the crib was determined by the height of the enclosure rather than the size of the crib itself as suggested by Block[10].

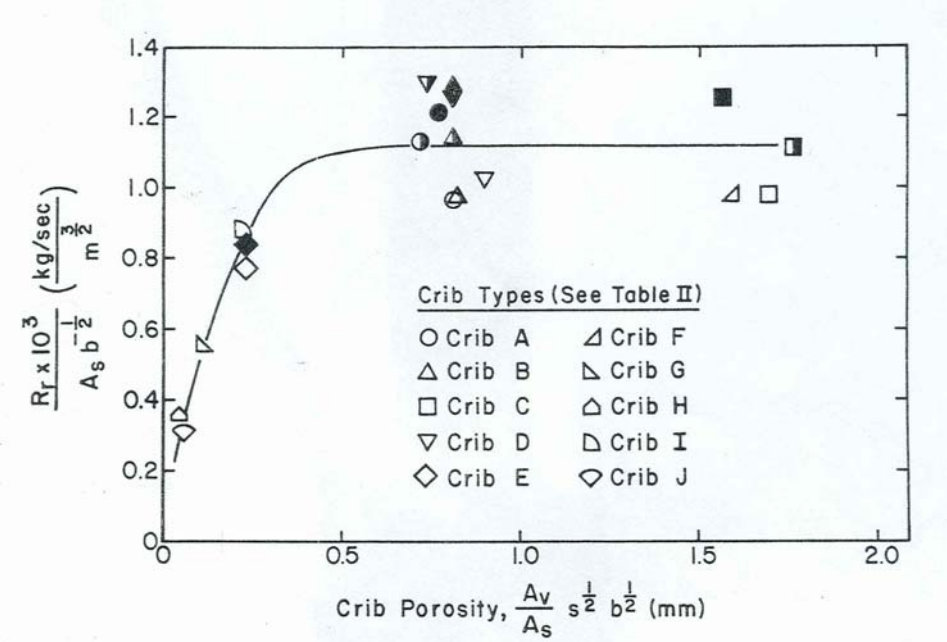

FIGURE 2. REDUCED FREE-BURNING RATE VERSUS CRIB POROSITY: solid points refer to cribs for the large enclosure tests; half-filled points refer to cribs scaled for intermediate enclosure tests; and open points refer to cribs scaled for small enclosure tests.

Figure 2.22: Free-Burn Model for Croce's Wood Crib Designs[20]

Measurements were taken during the quasi-steady period of burning, which was arbitrarily defined by convention as the time interval during which the mass of the crib falls between 80% and 30% of its initial value. Measurements included gas temperatures, surface temperatures, gas concentrations, radiation lost from the compartment and fuel mass loss.

A brief evaluation of the results presented by Croce can be accomplished by evaluating results with respect to the burning rate of the wood cribs. Both Heskestad's hypothesis[19] and the model developed by Quintiere and McCaffrey[18] identify enclosure ventilation and thermal feedback as limiting factors of the confined burning rate. Croce presents his results as a ratio of the confined and unconfined mass loss rates of his wood cribs so that these influences can be more readily appreciated. Figure 2.23 demonstrates

the limiting affect of the enclosure ventilation on the mass loss rate. Note that as the vent area is increased, the peak mass loss rate in the enclosure approaches the same peak value for the free-burning experiment. It is no coincidence that the shape suggested by a best-fit line through this data corresponds to Harmathy's model[15].

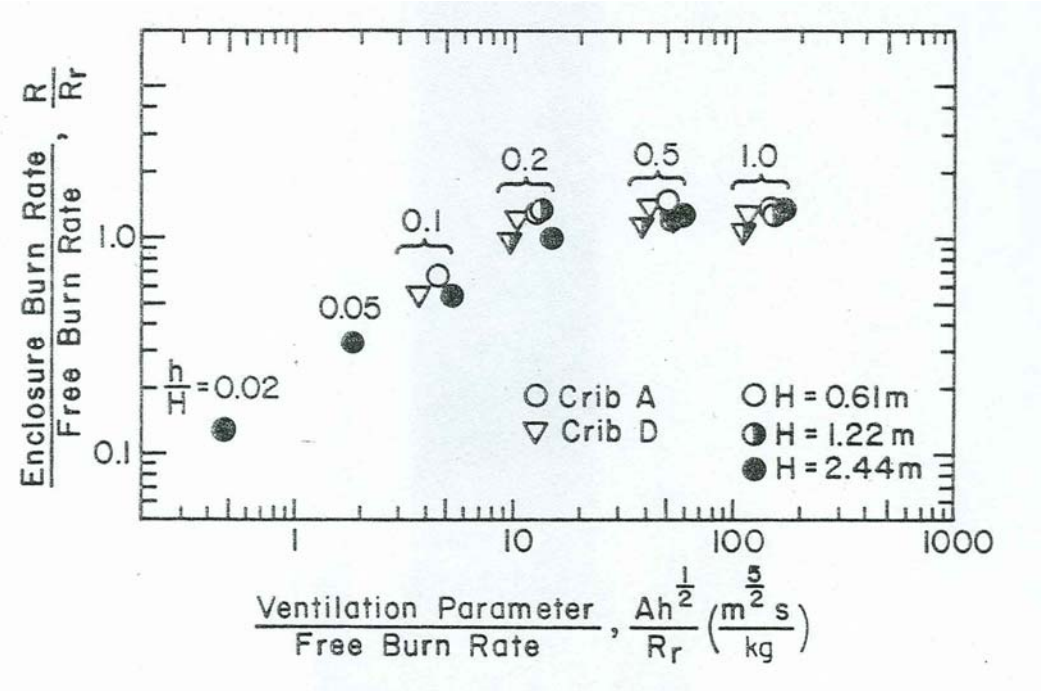

Figure 2.23: Croce's Results for Mass Loss Rate Scaling[20]

Due to a lack of data presented for the small vent sizes, it is unclear whether the scaling accuracy is affected in the limited ventilation region. It appears as though there is very good agreement when there is no ventilation limitation from either the crib or the compartment. However, it is important to note that the data is presented on a logarithmic scale. The same is true throughout much of the report. Therefore, the accuracy portrayed by the overlaying of data is not what it may seem at first glance.

It is also important to consider the effect of crib porosity on the scaling of the burning rate ratio. The results presented in Figure 2.24 correspond to two crib designs in the fuel-limited regime of the porosity curve. In general, it was found that better scaling

agreement is achieved for cribs whose free-burning rates were designed to be independent of porosity. The elimination of this second limitation on airflow undoubtedly simplified the scaling of the system. Results are presented in Figure 2.24 for a single vent opening that was half the compartment height ($h/H = 0.5$). This level of ventilation is shown on Figure 2.23 as not being a rate limiting factor.

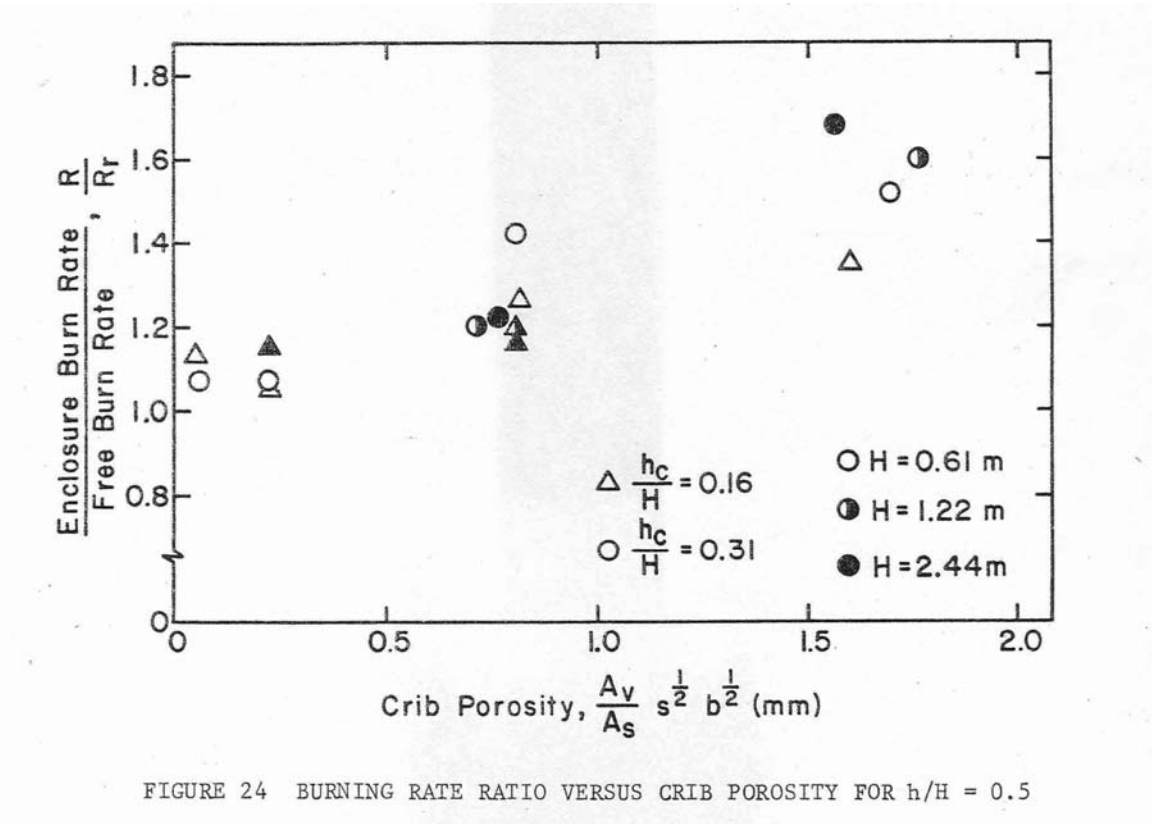

Figure 2.24: Croce's Crib Porosity Effect on Mass Loss Rate Scaling[20]

An energy balance for the enclosure is constructed to reveal a balance between the energy generated by the fire within the space and the heat which is lost through the vent as well as through the boundaries.

$$\dot{Q}_{gen} = \dot{m} c_p \Delta T \Big|_{vent} + \dot{q}_{rad,vent} + \dot{q}_{wall,cond} \tag{2.51}$$

Croce correctly states that the net mass flow through the vent should scale proportionally with the mass loss rate of the fuel. Heskestad's hypothesis does provide for the scaling of the wall conduction during the design phase, and due attention is paid to this term; however, the analysis of the radiation heat loss is sparse. In fact, there are no radiation measurements taken within the model enclosures. Radiation losses through the vents of the enclosures are the only attempt made to quantify the affect of radiation in these fires. It is assumed that radiation travels from the source to the enclosure boundaries based on the definition of the radiant fraction.

$$\chi_r = \frac{\dot{Q}}{\dot{q}} \tag{2.52}$$

It is assumed that the radiation fraction is independent of scale and therefore proper scaling of the energy generation term should force the heat loss term to scale appropriately. No further attempts are made to analyze the net heat flux to the enclosure boundaries. Croce does note the presence of an inconsistency dealing with re-radiation from the enclosure walls. This inconsistency is attributed to emissivities of the boundaries. There is a lack of recognition of the critical role of the emissivity of the gas, which can potentially affect the radiant intensity of the source in a significant way.

Croce's results confirm inconsistencies in the scaling of radiation losses through the vent. It appears as though the scaling relationships are different for different ventilation sizes. This could well be due to the measurement technique. The radiometer is placed outside of the compartment and its view of the compartment is through the vent. As the height of the vent decreases, the radiometer's view of the upper layer is changed. As the ventilation becomes very small, it is likely that some fuel burns outside the

compartment, thus presenting the instrument with a view of the flame at small and large ventilation yet not at intermediate ventilation. It is unclear how this measurement challenge may have been addressed. What is most notable about the data is the lack of measurements taken inside the compartments to attempt to address the apparent inconsistencies in radiation scaling within the enclosure. The thermal affects of this radiation on the mass burning rate are essentially regarded as insignificant.

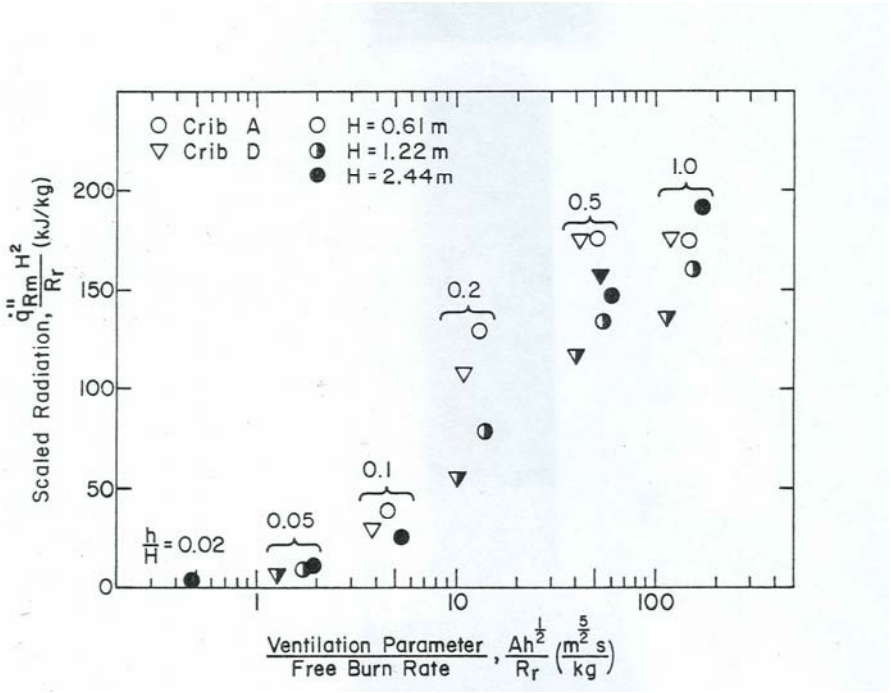

Figure 2.25: Croce's Radiation Scaling Results[20]

To further evaluate the model output, recall Heskestad's hypothesis which stated that the gas temperatures and concentrations measured at homologous locations would be reproduced at different scales. It appears that time and space averaged gas temperatures and concentrations scaled particularly well for vent heights equal to half and full size of the enclosure height. The gas concentrations measured were Oxygen, Carbon Dioxide and Carbon Monoxide in the upper layer. In the absence of ventilation limitations, Carbon Monoxide should appear to scale very well due to the fact that it should be very

near zero concentration. It should be noted that all results from porosity limited cribs produced a considerable degree of scatter between scales (Figure 2.26, Figure 2.27, Figure 2.28).

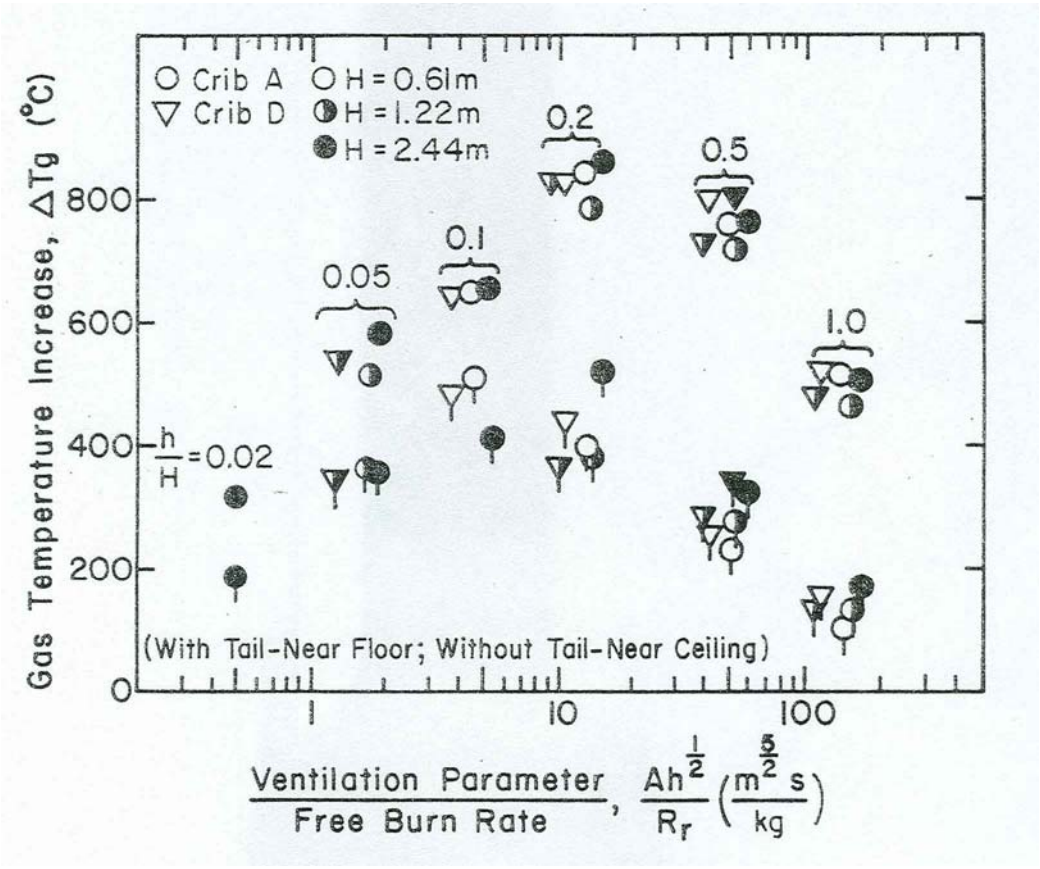

Figure 2.26: Croce's Gas Temperature Scaling[20]

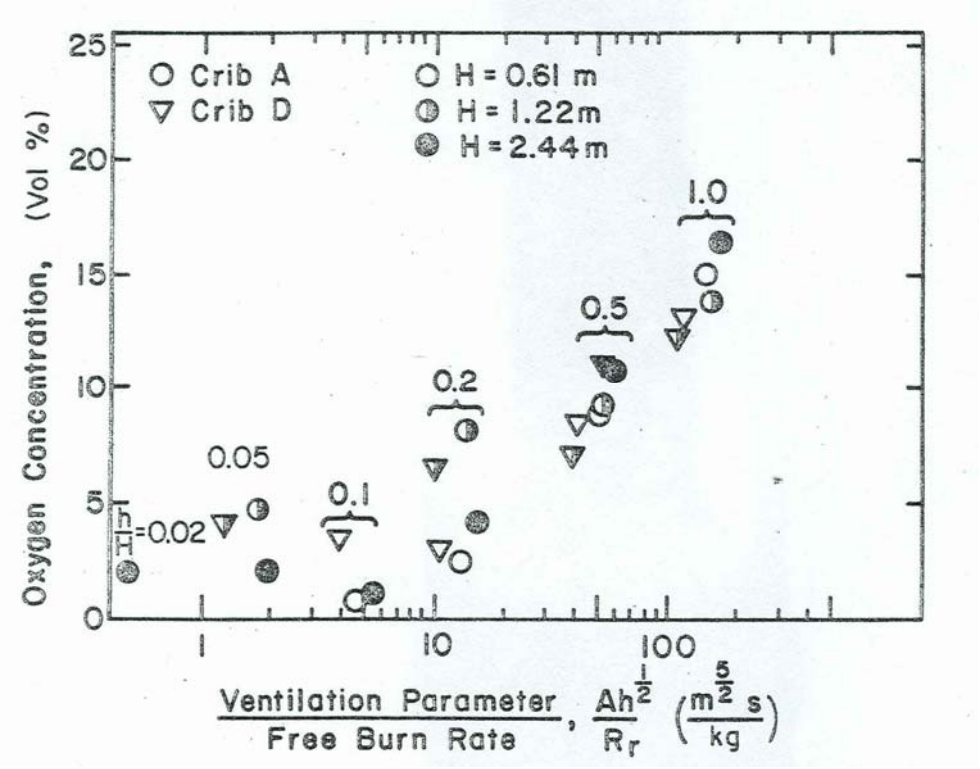

Figure 2.27: Croce's Oxygen Concentration Scaling[20]

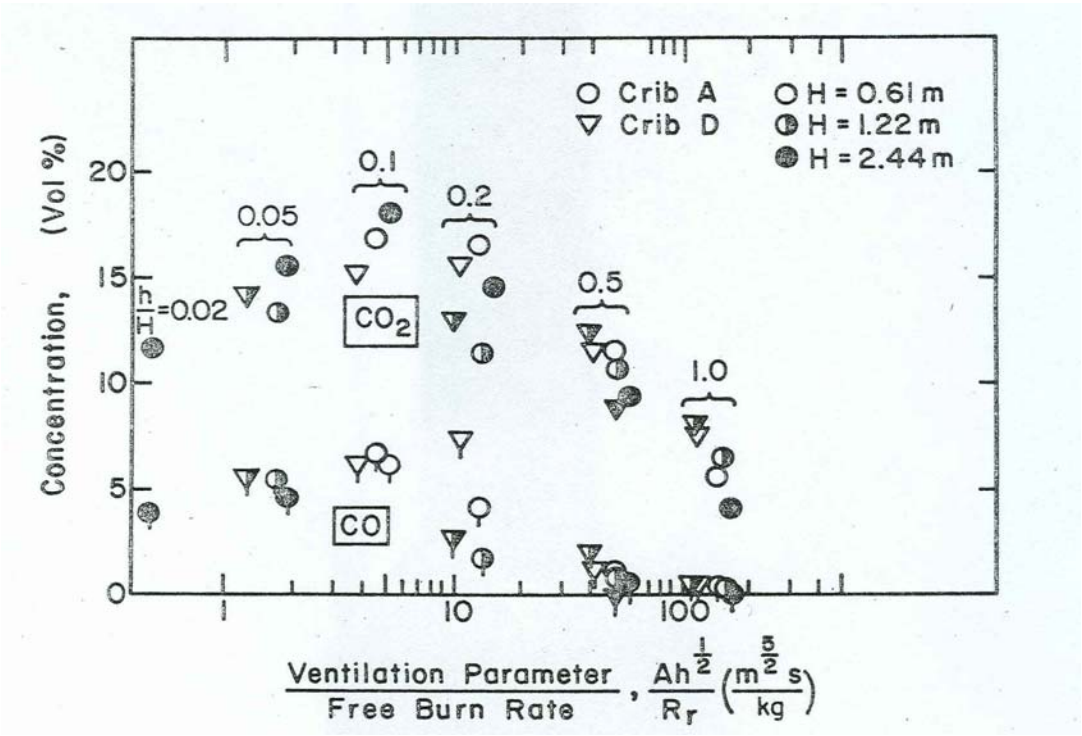

Figure 2.28: Croce's CO and CO_2 Concentration Scaling[20]

3. Theoretical Development and Experimental Design

3.1 Development of a New Scaling Methodology

In pursuit of a fundamental model for the scaling of wood crib fires in an enclosure, a series of dimensionless groups are derived from the conservation equations. The goal is to reveal proportionalities between a set of critical independent variables and the dependent variables of burning rate, heat flux, temperatures and gas composition in the enclosure. These proportional relationships can be quantified without the rigorous use of the three dimensional forms for the equations. Throughout this report, the dimensionless groupings of dependent and independent variables are denoted by the variable π and assigned a descriptive subscript for the purposes of notation. The derivation of these terms is founded on a control volume analysis applied to an arbitrary fluid element of the fire induced flow[21].

3.1.1 The Conservation of Linear Momentum

The conservation of linear momentum applied to a buoyant fluid element is presented. Recognizing that the sum of momentum storage and momentum flux through the element is proportional to the sum of the forces acting on that element, the conservation of momentum in the vertical direction becomes

$$\rho V \frac{du}{dt} + \dot{m} u \sim \Delta\rho g V + pA + \mathrm{TS} \tag{3.1}$$

The result is an ordinary differential equation for the fluid velocity. The proportionality shown indicates relationships between each commutatively linked term in the equation. The length scale present in each term is then revealed.

$$\rho l^3 \frac{du}{dt} + \left(\rho u l^2\right)u \sim \Delta\rho g l^3 + p l^2 + f\left(l^{-2}\right) \tag{3.2}$$

The independent variable in this differential equation is the fluid velocity. As such, an expression for this velocity of the flow is desired. The proportionality between the momentum flux term and the buoyancy term is chosen to be developed in pursuit of this goal. The selection of this relationship will be further explained following its development[21].

$$\rho l^2 u^2 \approx \Delta\rho g l^3 \tag{3.3}$$

$$u \approx \sqrt{\frac{\Delta\rho}{\rho} g l} \tag{3.4}$$

By making the above relationship non-dimensional, the equation can be applied without regard for the physical size of the system. The obvious approach is to normalize both sides of the equation with a characteristic velocity $\tilde{u}$, which is defined in Equation 3.5.

$$\tilde{u} \equiv \sqrt{gl} \tag{3.5}$$

Application of this characteristic velocity to Equation 3.4 yields the following relationship, where the density gradient can be expressed as a temperature gradient under the perfect gas law:

$$\frac{u}{\tilde{u}} \approx \sqrt{\frac{\Delta\rho}{\rho}} = \sqrt{\frac{\Delta T}{T}} \tag{3.6}$$

The pressure term and shear term could also be chosen and different solutions for the characteristic velocity would be obtained. Alpert had some success in a scale modeling attempt that deviated from the current development by making such a choice.

In his scaling, he chose to emphasize flow proportionalities with respect to the pressure force[2].

Support for the selection of the buoyancy term can be found in its relative significance to the flow. The fire plume is a naturally convective flow. While there are influences of pressure and shear force at work, the flow is truly dominated by body forces acting on density gradients, where the density gradients are the product of temperature and mass concentration gradients in the fluid[11]. The choice to emphasize the buoyancy force in the current development gives due regard for the dominant mechanism driving fluid flow for both cases of an enclosure fire and a free-burning wood crib.

We now return to the conservation of momentum equation and utilize the characteristic velocity to identify new critical parameters. Note that the momentum storage term contains the potential to extract a meaningful scaling relationship for the time variable. We therefore develop the following proportionality

$$\rho l^3 \frac{du}{dt} \approx \Delta\rho g l^3 \tag{3.7a}$$

$$\frac{du}{dt} \approx \frac{\Delta\rho g}{\rho} \approx g \tag{3.7b}$$

We now substitute the characteristic velocity to make the proportion dimensionless.

$$\frac{d\left(u/\tilde{u}\right)}{d\left(t/\tilde{t}\right)} \approx \frac{g\tilde{t}}{\tilde{u}} = \tilde{t}\sqrt{\frac{g}{l}} \tag{3.8}$$

The result of this substitution is a solution for a characteristic time as defined below.

$$\tilde{t} \equiv \sqrt{\frac{l}{g}} \tag{3.9}$$

This relationship is an expression of the flow time. Note that in its development we find that the change in flow velocity with respect to time is proportional to a constant. This implies that the flow time is a response time for the fluid. It can be viewed mathematically as a solution based on the integration of the ordinary differential equation over the limits of zero to maximum velocity. This approach takes Heskestad's hypothesis one critical step further by providing a direct relationship between time and length scale based on the driving force of the naturally convective fluid flow. This characteristic therefore functions as a response time rather than a measure of real time. It will later be demonstrated that the current result is critical to the successful scaling of transient fire behavior[21].

Another significant result of the defined characteristic velocity can be found in an analysis of the shear stress proportionality to the buoyancy forces. An application of Newton's law of viscosity followed by substitution of the characteristic velocity yields

$$\mathrm{T} \approx \mu \frac{\partial u}{\partial x} \approx \mu \frac{\tilde{u}}{l} = \mu \frac{\sqrt{gl}}{l} = \frac{\mu}{\tilde{t}} \tag{3.10}$$

The dynamic viscosity of the fluid is known to be dependent on its absolute temperature. It is common practice to model this property for gases by a temperature ratio. The ratio is taken as that of the surface property versus the mixed mean property for confined flows[11].

$$\left(\frac{\mu_0}{\mu_m}\right) \approx \left(\frac{T_0}{T_m}\right)^j \tag{3.11a}$$

In the case of unconfined flows, such as for free-burning wood cribs, this same ratio references ambient properties rather than mixed mean values[11].

$$\left(\frac{\mu_0}{\mu_\infty}\right) \approx \left(\frac{T_0}{T_\infty}\right)^j \tag{3.11b}$$

In both cases, the result of applying the previously defined characteristic flow time is that the shear stress scales with the square root of the characteristic length.

If we now balance the net mass flow with the shear stress acting along the surface area of the fluid element, we obtain an important result.

$$\rho u^2 l^2 \approx \mu \frac{u}{l} l^2 \tag{3.12}$$

The above expression reveals an opportunity to extract the Reynolds number of the flow and examine its dependence on length scale.

$$\frac{\mu}{\rho u l} = \frac{1}{\mathrm{Re}} \propto \frac{\nu}{\sqrt{g} l^{3/2}} \tag{3.13}$$

This result reveals that as the length scale is decreased from prototype to model, the Reynolds number for the flow is also decreased. A practical correction for this inconsistency might be to manipulate the kinematic viscosity of the gas in order to perfectly capture the shear stress influence on the prototype flow. The fires considered in this research will burn in an ambient atmosphere of air. The characteristic length is changed geometrically in each model. Therefore, this change in kinematic viscosity will not be accomplished.

Typically, for natural convection, the length Reynolds number is instead expressed as a Grashof number. Thus, the flow is characterized as a ratio of buoyant to viscous forces as opposed to the ratio of inertial to viscous forces. The relationship between these two dimensionless parameters is shown below with the previous scaling developments implemented.

$$Gr = \frac{g\beta(T - T_\infty) l^3}{\nu^2} = \frac{g\beta(T - T_\infty) l^2}{\nu} \frac{\mathrm{Re}}{u} \propto \mathrm{Re}^2 \tag{3.14a}$$

$$Gr \propto \mathrm{Re}^2 = \frac{u^2 l^2}{\nu^2} \approx \frac{g l^3}{\nu^2} \tag{3.14b}$$

The Reynolds and Grashof numbers are particularly important in that they are used to determine the transition of the flow from laminar to turbulent with turbulence typically occurring at values of $Gr > 10^9$ for gases[11]. The implication is that there is a limiting length scale below which a model for a turbulent full scale fire plume will actually produce a laminar flow. This will alter mixing of the compartment gases and ultimately the heating of the enclosure boundaries. In addition, a transition to laminar flow would increase the size of the boundary layers in the compartment, thus introducing a second characteristic length scale into the system. For turbulent flow, the length scale associated with these boundary layer thicknesses can be assumed insignificant. As long as this potential pitfall is avoided, the scaling inconsistency can be assumed to be small. The magnitude of the inconsistency will be based on the development of the Reynolds number with respect to convective heat transfer. This development is presented with the conservation of energy discussed in section 3.1.3 of this work.

Revisiting the momentum equation, a consideration of the pressure forces acting on the fluid element reveals another inconsistency.

$$\rho V \frac{du}{dt} \approx pA \tag{3.15}$$

$$p \propto \rho g l \tag{3.16}$$

Pressure is most critical in determining the flow of gas through the vent of the enclosure. The pressure difference across a vent given by hydrostatic pressure variations is most strongly influenced by density gradients in the fluid. These density gradients are scaled consistently by the current model. Therefore, the inconsistency presented in Equation

3.16, due to the additional influences of thermodynamic and aerodynamic components, is not deemed critical to the success of the model[21].

3.1.2 The Conservation of Mass

The conservation of mass for the fluid element is now developed. This is certainly the most straightforward of the conservation equations. The integral form for a fluid element is

$$\dot{m} = \rho u A \approx \rho u l^2 \tag{3.17}$$

If we then substitute the characteristic velocity of the flow we are left with an amazing relationship.

$$\dot{m} = \rho \tilde{u} A \approx \left(\rho \sqrt{g}\right) A l^{1/2} \tag{3.18}$$

The above proportionality is the scientific basis, taken from first principles, for Kawagoe's empirically determined ventilation factor in a compartment. Equation 3.18 provides concrete support for this proportionality between the rate of air flow into a compartment and the ventilation factor. Ultimately a coefficient must be included to account for flow through the vent orifice. In Harmathy's model for limited ventilation enclosure fires[15], he chose the ventilation parameter for the compartment to be exactly the mass flow defined above.

3.1.3 The Conservation of Energy

Application of the conservation of energy to the system with the previous developments in mind provides the designer with a set of scaling rules necessary to reproduce transient fire behavior. The form of the energy equation used is

$$\rho_\infty c_p V \frac{dT}{dt} + \dot{m} c_p (T - T_\infty) \approx \dot{Q} - \dot{q} \tag{3.19}$$

The sum of the advected enthalpy and sensible enthalpy rates are balanced with the difference between the heat that is generated in the compartment and that which is lost to the boundaries[21]. The determination of rate of heat generated inside the compartment is dependent on the ventilation conditions.

For fuel controlled combustion

$$\dot{Q} = \dot{m}_f \, \Delta H_c \tag{3.20a}$$

For ventilation limited combustion

$$\dot{Q} = \dot{m}_{o_2} \, \Delta H_{o_2} \tag{3.20b}$$

Utilizing the proportionality between the advected enthalpy rate and the source term

$$\rho_\infty c_p V \frac{dT}{dt} \approx \dot{Q} \tag{3.21}$$

We now move toward a non-dimensional relationship by substituting a characteristic temperature and the familiar flow time. Recognizing again that the flow is buoyancy driven and that the density gradient is the result of temperature gradients, the characteristic temperature is chosen as the ambient temperature.

$$\frac{d\left(T/\tilde{T}\right)}{d\left(t/\tilde{t}\right)} \approx \frac{\dot{Q}\tilde{t}}{\rho_\infty c_p V \tilde{T}} = \frac{\dot{Q}\tilde{t}}{\rho_\infty c_p V T_\infty} \tag{3.22}$$

The right hand side of this proportionality can now be expressed in terms of length scale.

$$\frac{\dot{Q}\sqrt{l}}{\rho_\infty c_p T_\infty \sqrt{g} l^3} = \frac{\dot{Q}}{\rho_\infty c_p T_\infty \sqrt{g} l^{5/2}} \tag{3.23}$$

The result is a dimensionless expression that relates a length scale to the energy output of the fuel source[21].

$$\pi_{source} \equiv \frac{\dot{Q}}{\rho_\infty c_p T_\infty \sqrt{g} l^{5/2}} \tag{3.24}$$

The dimensionless source term is a ratio of the firepower to the fluid enthalpy flow.

The heat loss term in the governing equation can be subdivided into the modes of convection, radiation and conduction. An attempt will be made to balance each of these modes of heat loss in the energy equation. However, prior to showing these balances it is necessary to provide a global context of the energy balance in the fire compartment. Consider an analogy between an electrical circuit and the flow of heat from the source to the ambient through the enclosure boundaries shown in Figure 3.1.

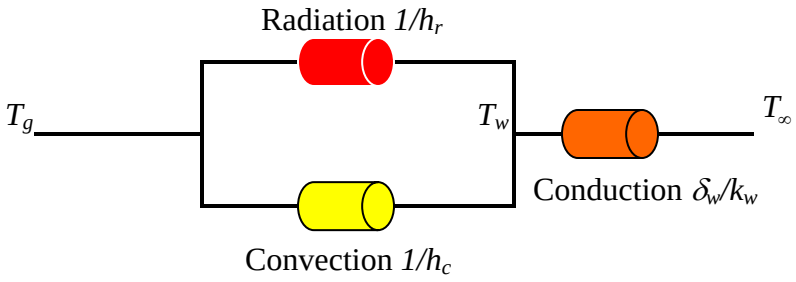

Figure 3.1: Electrical Circuit Analogy to Heat Flow

In the above sketch, the voltage of the circuit is analogous to a temperature difference. The current is analogous to the flow of heat. Each mode of heat transfer presents a resistance to the flow of heat through the circuit as shown. The resistances have been quantified over a wide range of fire conditions by Quintiere[22]. The results are shown in Table 3.1. These results demonstrate that the primary resistor to heat flow is the conduction through the walls of the compartment.

Resistor	Range [m^2K/kW]
Conduction	31-316
Convection	30-100
Radiation	15-150

Table 3.1: Quantification of Heat Flow Resistors[22]

Inconsistencies will be shown in the scaling of radiant and convective heat fluxes within the enclosure; however, it is important to appreciate these inconsistencies in the context of the previous discussion.

The illustration in Figure 3.1 reveals the presence of two dependent dimensionless groups related to the flow of heat through the enclosure boundaries. The first of these groups deals with the heat flux that is incident to the walls. The incident heat flux is comprised of both convective and radiant components. The incident heat flux is therefore an expression of the total heat flux delivered to the wall surfaces.

$$\pi_{incident} \equiv \frac{\dot{q}''_{incident}}{\sigma T_{\infty}^4} \tag{3.25}$$

This total incident heat flux is the same heat flux that was measured by Croce in his investigation of the radiation loss through the vent of his enclosures. Croce's concern for an inconsistency due to wall re-radiation is more succinct in the concept of a total incident flux. The apparent inconsistency is manifested in the concept that $\pi_{incident}$ should be independent of scale, whereas the net heat flux that is absorbed by the boundaries should scale differently.

The heat flux which is absorbed by the boundaries is related to the conduction loss, which will be discussed in more detail as this section of the report develops. For the time being, the dependent dimensionless group of interest is defined.

$$\pi_{absorbed} \equiv \frac{\dot{q}''_{net}\,\delta_w}{k_w T_\infty} \tag{3.26}$$

The net heat flux is a measure of the total heat flow that is absorbed by the surface rather than that which is merely received. In other words, the re-radiation of the boundary is eliminated. In calculating this net heat flux, Kirchoff's law is invoked and the walls again are assumed to behave as blackbodies.

If the walls of the compartment can be assumed to behave as blackbodies, the radiant heat loss can be expressed in the following way:

$$\dot{q}_{rad} = A\sigma\left[\varepsilon_g\left(T^4 - T_\infty^4\right) + \left(1-\varepsilon_g\right)\left(T_w^4 - T_\infty^4\right)\right] \tag{3.27a}$$

where the above form can be simplified further.

$$\dot{q}_{rad} = \varepsilon_g \sigma A\left(T_g^4 - T_w^4\right) \tag{3.27b}$$

A balance between the radiant heat transfer and the advected enthalpy of the flow produces the following results:

$$\rho_\infty V c_p \frac{dT}{dt} \propto \varepsilon_g \sigma A\left(T_g^4 - T_w^4\right) \tag{3.28a}$$

$$\frac{dT}{dt} \propto \frac{\varepsilon_g \sigma A\left(T_g^4 - T_w^4\right)}{\rho_\infty V c_p} \tag{3.28b}$$

Inserting the characteristic time and temperature of the flow in addition to the length scale for the wall surface area and volume reveals a new dimensionless group[21].

$$\frac{d\left(T/\tilde{T}\right)}{d\left(t/\tilde{t}\right)} \propto \frac{\varepsilon_g \sigma A\left(\tilde{T}^4 - T_w^4\right)}{\rho_\infty V c_p} \frac{\tilde{t}}{\tilde{T}} = \frac{\varepsilon_g \sigma T_\infty^3}{\rho_\infty c_p \sqrt{gl}} \tag{3.29}$$

The new group is a ratio of the radiation exchange versus the enthalpy flow.

$$\pi_{radiation} \equiv \frac{\sigma T_\infty^3}{\rho_\infty c_p \sqrt{gl}} \tag{3.30}$$

The physical interpretation of this group is that the radiation exchange at the wall should be proportional to the square root of the characteristic length scale[21]. The challenge of preserving this group lies in the fact that all of its elements are constants with the exception of the changing length scale. Note that the emissivity term has been removed from the expression for $\pi_{radiation}$. The modeling of this emissivity provides an opportunity to balance the radiation loss term in the energy equation despite the inconsistency shown in the $\pi_{radiation}$ term.

The emissivity of the gas must be recognized primarily for its ability to absorb and increase the radiant intensity of the source. The governing equation for the radiant intensity is given by Karlsson and Quintiere[23].

$$\frac{dI}{dr} = -\kappa I + \kappa I_b \tag{3.31}$$

The gray gas assumption is invoked where the properties of the gas are estimated to be independent of wavelength. In addition, the wall surfaces of the compartment are again assumed to behave as blackbodies. Kirchoff's law is used to equate the emissivity and absorptivity of the gas. Assuming a uniform temperature, the radiant transfer equation (3.31) is integrated over a mean radiation length[23].

$$I(l_m) - I_b = [I(0) - I_b] e^{-\kappa_g l_m} \tag{3.32}$$

$$\text{where} \quad I(0) \equiv 0 \qquad \text{and} \qquad I_b = \sigma T^4 / \pi$$

The emissivity of the gas can therefore be modeled as shown below.

$$\varepsilon_g = 1 - e^{-\kappa_g l_m} \tag{3.33}$$

The product of the absorption coefficient and the path length found in the exponential is a dimensionless quantity that contains the key to the scaling of radiant heat transfer.

$$\pi_{emissivity} \equiv \kappa_g l_m \tag{3.34}$$

The dimensionless group is analogous to a ratio of the radiation emitted to the assumed blackbody radiation of the boundaries. If it is assumed that a two-zone model prevails in the compartment, the mean path length corresponds to the depth of the hot upper layer. The absorption coefficient is dependent on the concentration of this upper layer as determined by the fuel and the equivalence ratio for the space. The challenge of maintaining this relationship is therefore a balance between the upper layer height and gas concentration as determined by the choice of fuel and the compartment ventilation.

One useful way of dealing with the layer radiation group is to apply an upper and lower bound. The upper bound applies in the case of an optically thick smoke layer. Such a layer is defined as one in which a significant amount of radiation is absorbed and emitted. Mathematically this is expressed in terms of a large $\kappa_g l_m$ product. In this case, the $\pi_{emissivity}$ group is said to be an uncontrolled or floating independent variable in the model. Conversely, the lower bound occurs for the case where κl_m is small. This corresponds to an optically thin smoke layer, which characteristically absorbs and emits

very little radiation. For such circumstances, the emissivity of the gas is independent of scale. The $\pi_{emissivity}$ group is still uncontrolled; however, the lack of significance in its magnitude produces a known result in this case[21].

If the emissivity of the gas can be forced to change with the square root of the length scale, the wall radiation group will be preserved. Such a relationship can be achieved by manipulating the absorption coefficient and mean path length characteristic of the upper layer. It is perhaps possible to select different fuel species at different characteristic length scales. Given that wood cribs are used for the fuel source throughout, a more practical approach might involve somehow scaling the mean path length while maintaining the composition of the upper layer.

The mathematical model developed by Quintiere and McCaffrey suggests that the mean path length can be modeled as a function of the upper layer geometry[18].

$$l_m \propto \frac{Volume}{Area} \tag{3.35}$$

This model indicates that in a geometrically scaled enclosure, the task of scaling the mean path length reduces to scaling the height of the thermal discontinuity. It is known that the height of the neutral plane at the vent is determined by the pressure difference across it. Therefore, manipulations of this layer height may lie in the preservation of absolute pressure. In the event that the fuel type is unchanged between scales, the layer radiation is expected to scale as dictated by the gas emissivity, somewhere within the range between constant and geometric.

The second mode of heat transfer to the compartment boundaries is that of convection. The rate of convective heat transferred between the gas and the walls is defined below.

$$\dot{q}_{convection} \approx h_c A(T - T_w) \tag{3.36}$$

The proportionality between this rate and the heat capacity term in the energy equation is used to develop a scaling relationship.

$$\rho_\infty V c_p \frac{dT}{dt} \approx h_c A(T - T_w) \tag{3.37a}$$

The characteristic temperature and time is then substituted.

$$\frac{d\left(T/\tilde{T}\right)}{d\left(t/\tilde{t}\right)} \approx \frac{h_c A(T - T_w)}{\rho_\infty V c_p} \frac{\tilde{t}}{\tilde{T}} \tag{3.37b}$$

And the variables are expressed in terms of the characteristic length scale to arrive at a dimensionless group for convective heat transfer[21].

$$\pi_{convection} \equiv \frac{h_c}{\rho_\infty c_p T_\infty \sqrt{gl}} \tag{3.38}$$

Recalling the definition of the characteristic velocity, it is readily apparent that the convective heat transfer coefficient scales in proportion to this velocity. Although the inconsistency for this dimensionless group is acceptable in terms of the magnitude of the convection resistor, there is a more subtle implication that must be considered. A common relationship used to model turbulent flow over a flat plate reveals a relationship between the convective transfer coefficient and the Reynolds number[11].

$$h_c \approx \frac{k}{l} \mathrm{Re}^n \mathrm{Pr}^m \tag{3.39}$$

Recall the notion that there is a limiting length scale below which a turbulent flow in the prototype will be incorrectly modeled by a laminar flow in a scale model. Equation 3.39 demonstrates a link between convective heat transfer in the compartment and that critical

transition. As long as the flow turbulence is maintained in the model, the inconsistency in convective heat transfer scaling is acceptable.

Substitution of the above correlation into the dimensionless group for convective heat transfer yields the following

$$\pi_{convection} \approx \frac{k\,\mathrm{Re}^{n}\,\mathrm{Pr}^{m}}{\rho_{\infty} c_{p} T_{\infty} \sqrt{g} l^{3/2}} \approx \frac{\alpha^{1-m} \nu^{m-n} \left(\sqrt{g} l^{3/2}\right)^{n}}{T_{\infty} \sqrt{g} l^{3/2}} \tag{3.40}$$

Kays and Crawford suggest that for constant free stream flow along a flat plate with an arbitrarily specified surface temperature, the convective heat transfer coefficient can be accurately modeled as shown below[11].

$$h_{c} \approx \frac{k}{l} \mathrm{Re}^{0.8}\,\mathrm{Pr}^{0.6} \tag{3.41}$$

Utilizing these values for the exponents in our method, we obtain the following:

$$\pi_{convection} \approx l^{-1/5} \tag{3.42}$$

It is important to remember that the flow of a fire plume confined by a volume is not exactly analogous to the flow of fluid over a flat plate. The above development shows that the inconsistency produced by the scaling method is potentially very slight. In addition, the dominant mode of heat transfer for enclosure fires at high temperatures is radiation. The above inconsistency will be relatively insignificant.

Once heat has been transferred from the source to the boundary, the scaling method must properly model the conduction of heat through the solid.

$$\dot{q}_{conduction} \approx \frac{k_{w} A \left(T_{w} - T\right)}{\delta_{w}} \tag{3.43}$$

Now the conduction through the wall is balanced with the capacity term.

$$\rho_\infty V c_p \frac{dT}{dt} \approx \frac{k_w A(T_w - T)}{\delta_{thermal}} \tag{3.44}$$

Note the definition of a thermal thickness rather than a physical one. This is done in an attempt to apply the scaling method to walls that are thermally thick or thermally thin. In both cases, the thermal thickness is found to be

$$\delta_{thermal} \approx \left[\left(\frac{k}{\rho c_p} \right)_w t \right]^{1/2} \tag{3.45}$$

Once again, the characteristic values of time and temperature are inserted and length scales are applied to the relevant terms to produce a new dimensionless group[21].

$$\pi_{conduction} \equiv \frac{(k\rho c_p)_{wall}^{1/2}}{\rho_\infty c_p g^{1/4} l^{3/4}} \tag{3.46}$$

The conduction group demonstrates the balance between the enthalpy flow to the wall and the heat lost through the solid by conduction. Due to the fact that the wall materials are chosen during the design phase, this dimensionless group can be preserved successfully. Ultimately, regardless of the scaling inconsistencies surrounding the modes of heat transfer to the wall, if the heat lost from the compartment is properly scaled, a global energy balance is achieved.

A second dimensionless group now arises from the conduction analysis. The purpose of this group is to evaluate the conduction loss in terms of a physical wall thickness[21].

$$\pi_{thickness} \equiv \frac{\delta_{wall}}{\delta_{thermal}} = \frac{\delta_{wall}}{(\alpha_{wall} t)^{1/2}} = \frac{\delta_{wall}}{\left[\left(\frac{k}{\rho c_p} \right)_{wall}^{1/2} \left(\frac{l}{g} \right)^{1/4} \right]} \tag{3.47}$$

The combination of the conduction and thickness dimensionless groups allows for the design of both thermal and geometric properties of the enclosure walls at different scales. In other words, these last two dimensionless groups represent controlled independent variables in the model. The control of these critical heat loss variables ensures the proper scaling of the dominant mode of heat loss in the compartment.

3.1.4 The Conservation of Chemical Species

The final conservation equation to be examined is the conservation of species. It is in this analysis that the preservation of gas concentrations will be accomplished. The conservation of any chemical specie *i* in the compartment is conserved.

$$\rho l^3 \frac{dY_i}{dt} + \dot{m} Y_i = \frac{y_i \dot{Q}}{\Delta H_c} \tag{3.48}$$

The proportionality between the net mass flow through the compartment and the species generation leads to a new dimensionless group[21].

$$\dot{m} Y_i \approx \frac{y_i \dot{Q}}{\Delta H_c} \tag{3.49}$$

$$\pi_{species} \equiv \frac{y_i c_p T_\infty}{\Delta H_c} \tag{3.50}$$

This group expresses a relationship between the species enthalpy and the chemical energy of the reaction. It states that the gas concentrations inside the compartment are determined jointly by the fuel and the compartment ventilation. In the case of a limited ventilation fire, the heat of combustion for oxygen is substituted for the heat of combustion of the fuel.

3.2 Completion of the Theoretical Model: Controlling the Source

3.2.1 Theoretical Application

The theoretical model was applied to wood crib fires. Wood cribs were chosen as the fuel for the model experiments due primarily to their excellent reputation for both repeatability and reproducibility. The proper balance of the energy equation in the fire compartment is dependent on the controlled scaling of both the energy generation and the energy loss. The scaling of the latter has already been discussed. The current section of the report deals with the idea of controlling the source energy of the wood crib fire by applying the scaling theory to the design parameters of this three dimensional fuel. We therefore turn our attention to the dependent variable π_{source}. The goal is to determine a subset of critical independent dimensionless groups that will ensure the proper scaling result for the dependent π_{source}.

Assuming that the gravitational acceleration, density, specific heat and temperature of the air in the compartment are independent of scale, this dimensionless group gives an explicit relationship between the burning rate of the wood crib source and the characteristic length.

$$\dot{Q} \approx l^{5/2} \tag{3.51}$$

In order to relate the energy release rate of the wood crib to tangible design parameters of the pile, an approach similar to Croce[20] was used. First it is assumed that the energy release rate of the pile can be calculated as the product of the mass burning rate of the fuel and the heat of combustion. It is further assumed that the heat of combustion of the pile is independent of the length scale.

$$\dot{m}_f \approx l^{5/2} \tag{3.52}$$

Recall the experimental findings of Gross later supported by Block's model for free-burning wood crib fires. The results show that the mass burning rate of these fires is a function of the crib porosity. Three separate burning regimes were identified based on critical values of this porosity. In the first regime the linear momentum of the air flow through the vertical shafts played a critical role in determining the mass burning rate. The second region belonged to cribs with sufficient porosity such that their burning rate was independent of this parameter. As the porosity was further increased, it was found that the burning rate enhancement provided by internal radiation decreased to a point where the wood cribs burned as so many individual sticks. The scaling theory presented herein applies over the entire range of crib porosities. It was decided that a fundamental design approach to scaling should begin with the design of wood cribs in the second regime where the mass burning rate is independent of porosity.

Block's theoretical model for the burning rate revealed a critical relationship between the design parameters of the crib and its burning rate for all of the regions identified by Gross[5].

$$\dot{m}_f = CA_s b^{-1/2} \tag{3.53}$$

A definition of the surface area of the fuel in terms of common design parameters thus allows for the definition of a set of controlled independent variables to begin.

The burning rate of the wood crib must be fundamentally controlled by the characteristic time derived from the conservation of linear momentum. Control of the total burn time of the wood crib requires that the relationship between this measured time and the characteristic time be preserved.

$$\pi_{duration} \equiv \frac{t_b}{\tilde{t}} \tag{3.54}$$

The total burn time can be estimated as a quotient of the initial fuel mass and Block's model for the burning rate.

$$t_b \approx \frac{m}{\dot{m}_f} = \frac{\rho V}{C A_s b^{-1/2}} \tag{3.55}$$

It is important to note that the above burn time is the expression that was used by Croce[20] to define a characteristic time. The critical difference in this approach is the fact that the characteristic time is now related to length scale. Consequently, the preservation of $\pi_{duration}$ ensures that the total burn time will also be determined by length scale.

The design parameters of interest are the stick cross section, stick length, number of layers, number of sticks per layer and spacing between adjacent sticks. Figure 3.2 provides a visualization of these parameters in a typical wood crib. Note that the number of sticks per layer and the number of layers are not labeled.

The surface area to which Block's model refers can not simply be calculated as the product of the surface area of a single stick and the number of sticks in the crib. The illustration in Figure 3.2 shows that a portion of this area is shielded as successive layers are overlaid. The calculation of interest is therefore the exposed surface area of the wood. It must be taken into account that the top and bottom layers of the crib represent larger exposed surface areas than the interior layers.

$$A_s = 2Nnb^2\left[\left(\frac{2L}{b}\right) + 1 - n\right] + 2n - \frac{L}{b} \tag{3.56}$$

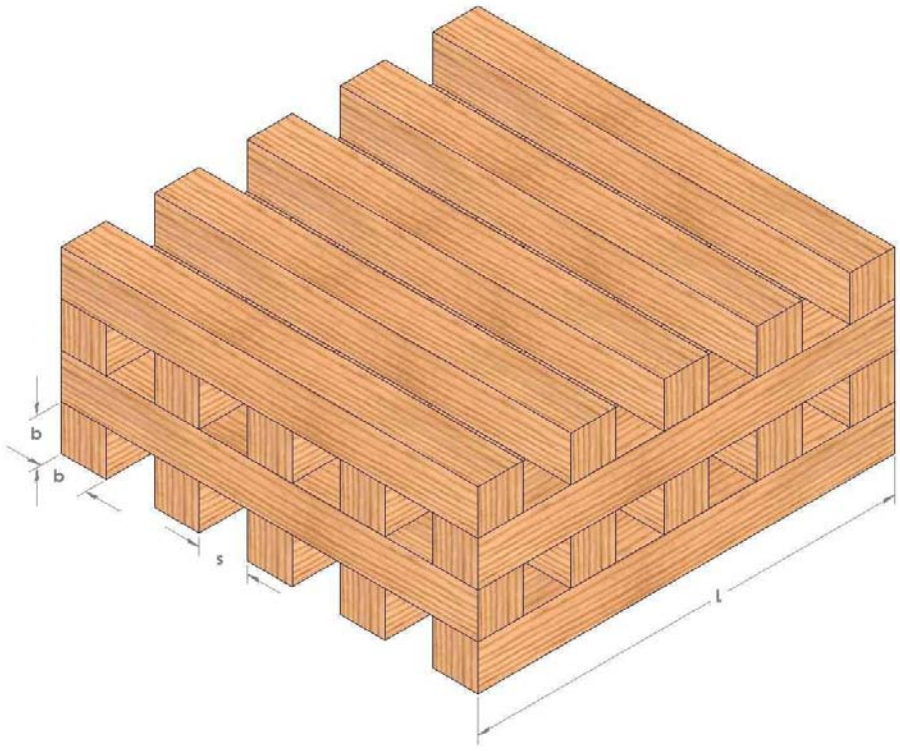

Figure 3.2: Design Parameters for Typical Wood Crib

From the results of the surface area calculation, it is apparent that the first term in the sum contains all of the pertinent design parameters for the crib (the spacing *s* is uniform and therefore dependent on the other primary parameters). The following proportionality can be used as a first approximation.

$$A_s \propto bnNL \tag{3.57}$$

This expression for the exposed surface area can then be substituted into Block's theoretical model to obtain the following relationship between the mass burning rate and the design parameters of the crib:

$$\dot{m}_f \propto C(4bnNL)b^{-1/2} = 4Cb^{1/2}nNL \tag{3.58}$$

The volume of the wood crib can be expressed as the volume of an individual stick multiplied by the total number of sticks in the pile. Utilizing this definition of fuel volume along with the preceding developments for burning rate and fuel surface area, the dimensionless duration group can be simplified.

$$\pi_{duration} \equiv \frac{t_b}{\tilde{t}} = \frac{\rho\left(b^2 LnN\right)}{4Cb^{1/2} LnN}\sqrt{\frac{g}{l}} = \frac{\rho b^{3/2}}{4C}\sqrt{\frac{g}{l}} \tag{3.59}$$

From the simplified relationship in Equation 3.59, it is evident that the cross section of the sticks in the wood crib must scale according to the following proportionality if the experimental burn time is to be properly related to length scale.

$$b \propto l^{1/3} \tag{3.60}$$

Control of the fire duration must now be followed with the control of the fire duration. This task is approached with the identification of a new dimensionless group.

$$\pi_{magnitude} \equiv \frac{\dot{m}_f}{\dot{m}_{net}} \tag{3.61}$$

The above group recognizes that the mass loss rate of fuel in an enclosure may be either fuel limited or ventilation limited. The scaling theory must apply to both cases. The net mass flow into an arbitrary enclosure is taken from the integral form of the continuity equation as discussed earlier in the report. The mass loss rate of the fuel is again estimated by Block's empirical model.

$$\pi_{magnitude} \equiv \frac{CA_s b^{-1/2}}{\rho_\infty \sqrt{g} l^{5/2}} = \frac{4Cb^{1/2} LnN}{\rho_\infty \sqrt{g} l^{5/2}} \tag{3.62}$$

Insertion of the known length scale relationship for the stick cross section results in a second proportionality between a group of crib design parameters and the characteristic length scale.

$$LnN \propto l^{7/3} \tag{3.63}$$

This relationship is held until further developments necessitate its use to arrive at a complete scaling solution.

The second consideration regarding the limiting factor of airflow into the enclosure is related to the air that flows up through the vertical shafts of the internal crib structure. A dimensionless group is defined to preserve this quantity between scales.

$$\pi_{airflow} \equiv \frac{\dot{m}_{a,crib}}{\dot{m}_{net}} \tag{3.64}$$

Block's empirical model is again used to determine the airflow through the vertical shafts. The dimensionless airflow group can then be simplified.

$$\pi_{airflow} \equiv \frac{A_v \sqrt{s}}{\rho_\infty \sqrt{g} l^{5/2}} \tag{3.65}$$

At this point it is important to realize that relationships between mass flow, air flow and duration have been introduced. In order to complete the cycle of logic, the air flow internal to the crib must now be specifically linked to the duration. This is essentially an indirect result of previous scaling manipulations. Nonetheless, it must be controlled for completeness.

$$\pi_{air-duration} \equiv \frac{s}{b} \tag{3.66}$$

The preceding link between the stick spacing and cross section facilitates a simplification to be made to the $\pi_{airflow}$ group.

$$\pi_{airflow} \equiv \frac{A_v \sqrt{b}}{\rho_\infty \sqrt{g} l^{5/2}} \tag{3.67}$$

It is now necessary to define the total area of the vertical shafts in the crib structure.

$$A_v = (L - nb)^2 \tag{3.68}$$

Equation 3.68 reveals a proportion between A_v and the stick length, which will be exploited in order to further simplify the $\pi_{airflow}$ group.

$$\pi_{airflow} \equiv \frac{L\sqrt{b}}{\rho_\infty \sqrt{g} l^{5/2}} \tag{3.69}$$

Substitution of the known length scale relationship for the stick cross section reveals the proper scaling for the stick length.

$$L \propto l^{7/6} \tag{3.70}$$

Along with these considerations for duration, fire magnitude and airflow restrictions, an effort must be made to conserve the relative internal geometry of the crib structure. It is noted that for a wood crib with sticks of uniform length, the internal geometry of each layer can be preserved.

$$\pi_{geometry} \equiv \frac{L}{nb} \tag{3.71}$$

The known length scales associated with the stick length and cross section can be substituted into this dimensionless group to arrive at a scaling relationship for the number of sticks per layer in the crib.

$$n \propto l^{5/6} \tag{3.72}$$

The only remaining design parameter for the wood crib that has yet to be assigned a length scale relationship is the number of layers. Based on the defined relationships for *b*, *L* and *n* along with Equation 3.63, the proper proportion is found.

$$N \propto l^{1/3} \tag{3.73}$$

It is noted that the set of scaling rules presented above does not yield a geometric scaling of the height of the wood crib. It is recognized that the height of the crib can potentially play a limiting role on the peak burning rate in extreme cases of large height to length ratios. The preceding theory expressly scales the magnitude and duration of the fire simultaneously with the airflow internal to the structure. These considerations are far more explicit than the mere assumption that a geometric scaling of the crib height is essential to reproducing the burning rate. This is another major point of contention between the current scaling theory and the one implemented by Croce[20]. Table 3.2 summarizes the relationships between specific crib design parameters and the characteristic length scale. It is noted that the porosity defined by Heskestad is conserved given that it can be expressed as a ratio of $\pi_{airflow}$ and $\pi_{magnitude}$.

Design Parameter	Relationship to Length Scale
Stick Thickness, b	$b \propto l^{1/3}$
Stick Length, L	$L \propto l^{7/6}$
Number of Sticks Per Layer, n	$n \propto l^{5/6}$
Number of Layers, N	$N \propto l^{1/3}$
Spacing Between Adjacent Sticks, s	$s \propto l^{1/3}$

Table 3.2: Applied Wood Crib Design Solutions

Preliminary results, which will be discussed in section 3.2 of this report, will provide an additional dimensionless quantity, $\pi_{elevation}$, related to the ignition of the wood cribs. Prior to summarizing the model, a few new dimensionless quantities must be introduced. The

first of these quantities is a dimensionless temperature. This is simply the ratio of any temperature with that of the constant ambient.

$$\pi_{temperature} \equiv \frac{T}{\tilde{T}} = \frac{T}{T_{\infty}} \tag{3.74}$$

The remaining dimensionless quantities refer to measurements taken in both time and space. This is a critical concept in scale modeling that has yet to be fully appreciated in the literature. All of these dimensionless groups must be measured at dimensionless points in both time and space in order for their harmonization to be appreciated. The dimensionless space is essentially a homologous location in each enclosure. The definition of this dimensionless quantity focuses on the height of the instrument. It is taken for granted that the remaining spatial coordinates will be homologous between scales.

$$\omega \equiv \frac{z}{l} \tag{3.75}$$

Implementation of the dimensionless time is critical to the observance of synchronized data at a given location in the enclosure. Until now, the presentation of transient data in literature has been avoided because of an inability to synchronize results in real time. With the definition of the appropriate characteristic time during the design phase, a dimensionless time can be identified for use in the model.

$$\tau \equiv \frac{t_{real}}{\tilde{t}} = \frac{t_{real}}{\sqrt{l/g}} \tag{3.76}$$

A summary of the model can now be expressed mathematically in the sense that a set of dependent dimensionless groups are determined as a function of a set of independent dimensionless groups.

$$\left\{\pi_{source}, \pi_{temperature}, \pi_{species}, \pi_{incident}, \pi_{absorbed}, \ldots\right\} =$$
$$f\left\{\begin{matrix}\pi_{conduction}, \pi_{thickness}, \pi_{duration}, \pi_{magnitude}, \pi_{airflow}, \pi_{air-duration}, \\ \pi_{geometry}, \pi_{elevation}, \pi_{convection}, \pi_{radiation}, \pi_{emissivity}, Gr\end{matrix}\right\} \tag{3.77}$$

Note that the periods included in the list of dependent variables allude to a continuation of the list. It is recognized that although the five variables listed are the primary focus of the model, the set of independent variables does produce additional fire dynamics, such as absolute pressure affects, that are deemed insignificant to the model success. The mathematical representation can be further clarified by dividing the independent variables into two subsets corresponding to controlled and uncontrolled quantities in the design phase. This is accomplished in Tables 3.3 and 3.4.

$$\pi_{thickness} \equiv \frac{\delta_{wall}}{\delta_{thermal}} \qquad \pi_{fire.duration} \equiv \frac{t_b}{\tilde{t}}$$

$$\pi_{conduction} = \frac{\left(k\rho c_p\right)_{wall}^{1/2}}{\rho_\infty c_p g^{1/4} l^{3/4}} \qquad \pi_{air-duration} \equiv \frac{s}{b}$$

$$\pi_{fire.magnitude} \equiv \frac{\dot{m}_f}{\dot{m}_{net}} = \frac{CA_s b^{-1/2}}{\rho_\infty \sqrt{g} l^{5/2}} \qquad \pi_{geometry} \equiv \frac{L}{nb}$$

$$\pi_{airflow} \equiv \frac{\dot{m}_a}{\dot{m}_{net}} \approx \frac{A_v \sqrt{s}}{\rho_\infty \sqrt{g} l^{5/2}} \qquad \pi_{elevation} \equiv \frac{E}{b}$$

Table 3.3: Controlled Independent Variables

Table 3.3 recalls that control is exerted over energy generation and conduction loss.

$$\pi_{convection} \equiv \frac{h_c}{\rho_\infty c_p T_\infty \sqrt{gl}} \qquad \pi_{radiation} \equiv \frac{\sigma T_\infty^3}{\rho_\infty c_p \sqrt{gl}}$$

$$Gr = \frac{gl^3 \beta \Delta T}{\nu^2} \qquad \pi_{emissivity} \equiv \kappa_g l_m$$

Table 3.4: Uncontrolled Independent Variables

Table 3.4 recalls that the floating independent variables in the design phase are related to convection and radiation inside of the enclosure. Each of these quantities factors into the heat loss term of the energy equation; however, their magnitudes are overshadowed by conduction losses.

3.2.2 Practical Application

In order to test the theory, free-burning experiments must be conducted at a minimum of 2 characteristic length scales. A comparison must then be made between the model and prototype. The experimental work of Quintiere and McCaffrey was chosen as the prototype due to the depth of analysis and availability of the published data[18]. Since the experiments were conducted in a life-size room with a wood crib fuel load sized accordingly, the prototype was referred to as the full scale. The characteristic length

scale associated with the full scale was defined as the height of the enclosure *H*. In choosing the characteristic length, it is important to be mindful of the placement of the crib inside the enclosure. If a different characteristic length is chosen, such as the height of the crib, the geometric scaling of the enclosure is compromised. Regardless of the choice of characteristic length, consistency should ensure a properly scaled free-burning rate in the wood crib.

Recall that the experimental work of Quintiere and McCaffrey[18] utilized both wood and plastic cribs, multiple in number and varying in orientation on the load platform. Due to the desire of the current research to produce a fundamental scaling model, the single wood crib orientation was chosen as the prototype experiment. Table 3.5 lists the design parameters of this wood crib and the proposed ¼ scale model design. The porosity of the wood crib is evaluated using Heskestad's simplified version of Block's theoretical model[15].

Full Scale Prototype	**Quarter Scale Model**
b = 35 mm	b = 22 mm
L = 245 mm	L = 49 mm
s = 70 mm	s = ?
n = 3	n = 1
N = 10	N = 6
P = 1.14 mm	P = ?

Table 3.5: Quarter Scale Model of Quintiere & McCaffrey's Single Crib

The above table illustrates a significant problem in the design of the quarter scale model. The problem is that the model calls for a single stick per layer. The suggested design therefore can not even be classified as a wood crib.

To remedy this design issue it was suggested that a model be constructed based on a multiple crib orientation in the full scale. Figure 2.22 illustrates the various layouts for multiple crib experiments. Note that the open space between adjacent cribs is exactly equal to the spacing between adjacent sticks in a single crib. A hypothesis was therefore put forward that the burning behavior of the 4 crib fire load could be approximated as similar to the burning behavior of a single large crib united through the contiguous openings. Figure 3.3 provides a visualization of this hypothesis.

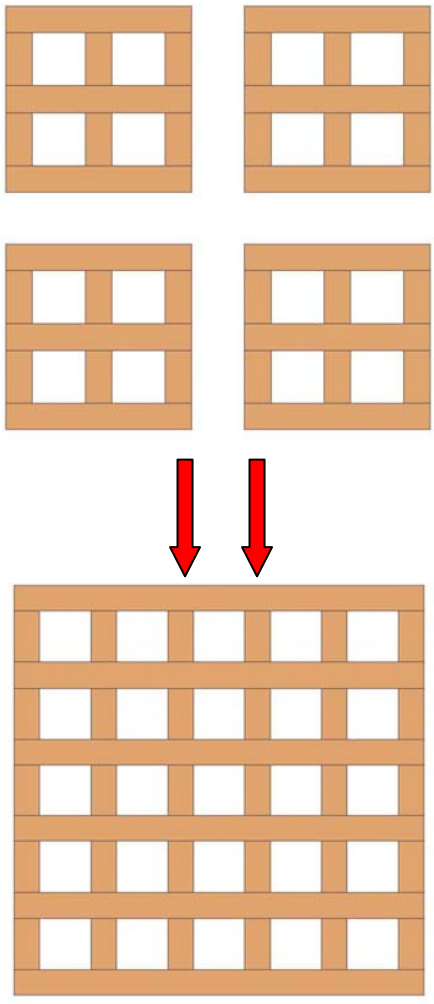

Figure 3.3: Multiple Crib Hypothesis

The notion that four closely spaced cribs can be modeled by a single large crib suggests two things. These assumptions are that neither the air flow through the contiguous spaces between adjacent cribs nor the slight addition of fuel mass and surface area to the system has a significant effect on the burning rate.

The first of these assertions can be addressed by the experimental results of Quintiere and McCaffrey[18]. These results suggest that the rate of airflow through these channels amounts to somewhere in the range of 0-20% of the total air flow entrained by the crib. The remaining air is entrained by the vertical shafts and the exterior surfaces of the crib. Thus, the first assumption for the multiple crib hypothesis has some support despite a maximum 20% uncertainty.

The second assumption regarding the slight addition of fuel mass can be evaluated by calculating the percentage of increased mass and projecting the resulting influence on the burning rate.

$$\frac{m_{1-crib}}{m_{4-crib}} = \frac{V_{1-crib}}{V_{4-crib}} = \frac{\left(b^2 N\right)\left(Ln\right)_{1-crib}}{4\left(b^2 N\right)\left(Ln\right)_{4-crib}} = 1.14 \tag{3.78}$$

The result is a 14% increase in fuel mass. Assuming that the characteristic burn time is the same for both configurations, this increase should translate directly to an approximate 14% increase in the burning rate.

The free-burn experiment for the 4 crib orientation, performed by Quintiere and McCaffrey, listed an average peak burning rate of 25.6 g/s. If the above method is applied to this result, it predicts an average peak burning rate of 29.2 g/s. Therefore, the targeted average peak value for the ¼ scale model is within this range[18].

The design of the new ¼ scale model, based on the multiple crib hypothesis is shown in Table 3.6.

Full Scale Prototype	Quarter Scale Model
b = 35 mm	b = 22 mm
L = 560 mm	L = 111 mm
s = 70 mm	s = 67 mm
n = 6	n = 2
N = 10	N = 6
P = 1.5 mm	P = 1.7 mm

Table 3.6: Quarter Scale Model based on Multiple Crib Hypothesis

The results for the model design reveal a slight change in crib porosity between scales. This is due to the fact that solutions for the number of sticks per layer and the number of layers must be integer values. Strict application of the scaling rules to the model produces decimal values which must be rounded to the nearest integer. This rounding creates a slight change in the porosity. According to Block, such slight changes have no affect on the burning rate for fuel surface controlled burning[10]. However, the magnitude of the porosity in this case places the quarter scale design in a region of un-sustained burning. The combination of the number of sticks per layer and the stick spacing produced a crib structure that burned more like a pile of individual sticks.

A decision was made to modify the model a second time by increasing the number of sticks per layer to 3. This decision was based on the observation that the crib porosity was much higher than the critical value for fuel surface controlled burning. This critical value was identified as 0.5 mm by Heskestad and Croce[15,20]. Therefore, a substantial decrease in crib porosity would still yield a design within the fuel surface controlled burning regime. However, the modification led to a violation of some of the established rules of scaling. Therefore, the model design equations were revisited and a new solution set was calculated based on the substitution of new rule.

A requirement for the number of sticks per layer was put in place of the conservation of internal crib geometry. Table 3.7 compares the modified solution set to the original. Table 3.8 depicts the resulting crib design.

Original Scaling Solution Set	Modified Scaling Solution Set
$b \propto l^{1/3}$	$b \propto l^{1/3}$
$L \propto l^{7/6}$	$L \propto l^{7/6}$
$n \propto l^{5/6}$	$n \propto l^{1/2}$
$N \propto l^{1/3}$	$N \propto l^{1/2}$

Table 3.7: Scaling Relationships Forced by Crib Porosity Modification

Previous Model	**Modified Model**
b = 22 mm	b = 22 mm
L = 111 mm	L = 111 mm
s = 67 mm	s = 22.5 mm
n = 2	n = 3
N = 6	N = 4
P = 1.7 mm	P = 1.0 mm

Table 3.8: Modified Crib Design

The design of the modified model adheres to the proper scaling derived for the mass burning rate of the crib, transient burning behavior. The internal geometric relationships are changed to produce a decrease in the porosity. This decrease in porosity is accompanied by an increase in the internal radiant heat exchange that is commonly observed as a driving mechanism in sustained burning of the crib[22,25]. The new porosity is well above (more than double) the critical value for fuel surface

controlled burning. In addition, the literature suggested that the change in crib height would only play a limiting role on the burning rate for porosity controlled burning[10]. Therefore, it was thought that the burning rate, being independent of crib porosity and driven by internal radiation, would be best modeled by the new set of design rules.

3.2.3 Early Experimental Developments – Lessons Learned

3.2.3.1 Selection of Wood

The next step in the design phase was to select a type of wood for the crib. The specie used by Quintiere & McCaffrey was Sugar Pine with a density of 370 kg/m^3 and an average moisture content of 6.5%. Due to a general lack of availability of Sugar Pine in the Eastern United States, a slightly different specie was chosen from the same family of soft pines. Eastern White Pine was chosen due to the combination of comparative density and good availability. The density of these species was compared based on tabulated values of their specific gravities at 6.5% moisture content. The results showed that the density of Eastern White Pine at this moisture content is approximately 360 kg/m^3. The difference in density at the given moisture content is therefore estimated as 3%.

3.2.3.2 Determining Model Ignition Parameters

Insight provided by the combination of research and preliminary testing revealed that the critical nature of the ignition model in determining the burning rate of the wood crib. The important features of this model are the moisture content of the wood crib, the

elevation of the crib above the fuel pan, the size of the fuel pan and the amount of starter fuel placed in it.

The density of the wood is directly affected by its moisture content. The scaling theory suggests that the density should be independent of length scale. Therefore, the moisture content of the wood used in the model should allow for this criterion to be met. Based on this reasoning, a model crib was conditioned in a dessicator at approximately 20^{o}C and 30% relative humidity overnight, at which point it was assumed that equilibrium was reached. The equilibrium moisture content value at this combination of temperature and relative humidity is known to be 6.2%, very close to the average and well within the range of the prototype values[18].

The elevation of the crib above the starter fuel was accomplished with 2 cm high Marinite support strips in the prototype. This elevation height corresponded to a stick cross section of 3.5 cm. The scaling of the crib elevation was therefore attempted by applying the same length scale relationship for the stick cross section. The result was that the elevation of the crib was scaled according to the $\pi_{elevation}$ group first introduced in Equation 3.77.

$$\pi_{elevation} \equiv \frac{E}{b} \tag{3.79}$$

The result suggests that the elevation of the model should be 1.25 cm above the pan surface.

Gross' experimental findings with respect to the size of the fuel pan indicated that the size has no significant effect on the burning rate as long as it is slightly larger than the base area of the crib[5]. In other words, a starter pan with a much smaller base area would ignite a smaller portion of the structure and the burning rate would be influenced by the

propagation of the flame. Due to its availability in the laboratory, a circular glass dish of 14 cm diameter was chosen as the starter fuel pan. This base area of 17671 mm^2 proved to be 25% larger than the base area of the crib. Despite the fact that the dish was circular and the crib base was square, it was thought that this combination should satisfy Gross' rule.

Another finding of Gross suggested that the type and amount of starter fuel used should have no effect on the peak burning rate of the crib[5]. Therefore an arbitrary decision was made to use 10 mL of heptane as the starter fuel. All sticks within the wood cribs were assembled using wood glue on adjoining surfaces.

3.2.3.3 Free-Burn Experimental Setup

The quarter scale model wood crib and ignition model were constructed and placed atop an insulated load cell. It so happened that the size of the free-burning model permitted placement inside of a cone calorimeter device in the laboratory. Unfortunately, at the time of testing, much of the calorimetry instrumentation was undergoing modifications and therefore only the load cell device was used. Figure 3.4 illustrates the experimental setup. A load cell is positioned underneath the fuel pan to record transient mass. The type of load cell used was an *ATC Series 6005D* transducer. This Linear Variable Differential Transformer (LVDT) outputs an electrical voltage proportional to the weight applied based on vertical displacement of a spring mounted platform. The range of this particular load cell was 0-8 lbs.

Data was collected from the load cell with the use of a data acquisition system from National Instruments. *LabVIEW* version 5.1 data acquisition software was installed

on a desktop PC. This PC was equipped with a *PCI-MIO-16-E-4* DAQ card and connected to a model *SCXI-1100* chassis from *National Instruments*. Connected to this chassis was a single *SCXI-1300* terminal block module with 32 analog channels to convert transducer signals. A single channel was used to collect data from the load cell at a frequency of 1 Hz for all free-burning experiments.

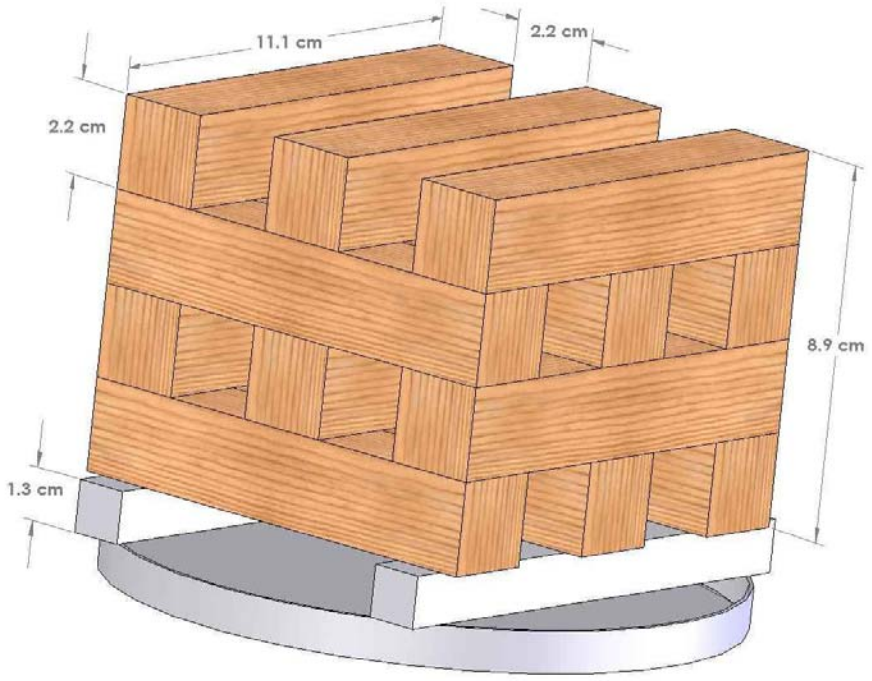

Figure 3.4: Free-Burn Wood Crib and Ignition Model

3.2.3.4 Initial Results: Ignition Model Modifications

The transient mass data for the free-burning wood crib was used to calculate an instantaneous mass loss rate. Fluctuations in the voltage during testing suggest the application of a mathematical tool to smooth the data. The method of calculation for the

transient mass loss rate suggested by Quintiere and McCaffrey is the slope of a least square linear fit of the transient mass data given by the following formula[18]:

$$\dot{m}(t_i)\Big|_{i=5} = \frac{\sum_{i=1}^{10} t_i m_i - \frac{\sum_{i=1}^{10} t_i \sum_{i=1}^{10} m_i}{10}}{\sum_{i=1}^{10}\left(t_i^2\right) - \frac{\left(\sum_{i=1}^{10} t_i\right)^2}{10}} \tag{3.80}$$

There are a few things to note about the smoothing tool used above. The first is that the tool takes a moving average over a ten second period. Therefore, boundary conditions must be applied to the first and last 5 data points taken. In this analysis where the first five seconds of data are of little importance to the global picture, the boundaries are simply ignored. Along with this feature of the formula it is also important to recognize that fluctuations in the measured voltage sometimes produce illogical instantaneous values suggesting a slight mass gain. The smoothing tool simply differentiates between discrete data points without eliminating the influence of this infrequent occurrence.

Clearly, the magnitude of the mass loss rate and burn time will not remain constant between scales. The scaling theory suggests a method for presenting the data in a manner by which all length scales can be analyzed simultaneously. Although these preliminary results are taken from the same length scale, they must be compared to the average peak value of the full scale in a meaningful way. The transient mass loss rate for all scales is presented as π_{source} as a function of dimensionless time. Since these free-burning wood cribs were designed based on the selected length scale of the compartment height, this length scale must be maintained in the calculations for consistency.
The dimensionless source term is restated for quick reference.

$$\pi_{source} \equiv \frac{\dot{m}_f \Delta H_c}{\rho_\infty c_p T_\infty \sqrt{g} H^{5/2}} \tag{3.24}$$

Where the following values are used

$$\rho_\infty = 1.2 \frac{kg}{m^3}$$

$$c_p = 1 \frac{kJ}{kgK}$$

$$T_\infty = 300K$$

$$g = 9.81 \frac{m}{s^2}$$

$$\Delta H_{c,Model} = 15 \frac{kJ}{g}$$

$$\Delta H_{c,prototype} = 13.4 \frac{kJ}{g}$$

The thermal properties of the ambient air are not listed in the data presented for the ambient experiments. These properties are therefore applied consistently to both scales such that the mass burning rate is the defining characteristic of the dimensionless group. The heat of combustion of the Eastern White Pine is taken form a suggested value for general wood in the literature[24]. In the case of the prototype, the average measured value was applied.

Due to the fact that an average peak value is the only data listed, a comparison of average peak values is the only meaningful result available.

$$\pi_{source,prototype,APV} = 0.038 \qquad \pi_{source,model,APV} = 0.022$$

The result is an inconsistency of approximately 42% in the dimensionless group. Such a discrepancy is not due to slight differences in the ambient thermal properties of

air, nor slight differences in the heat of combustion for these closely related wood species. Block's theoretical model, which contributes in part to the development of this dimensionless group, suggests that the mass burning rate is proportional to a material dependent constant; however, only slight changes are expected in this material constant. Porosity, or internal ventilation, should not be an issue because the crib is burning well within the fuel surface controlled regime. Such a large inconsistency in the dimensionless group suggests a more fundamental oversight in the design phase. The multiple crib hypothesis could certainly account for an inconsistency approaching this magnitude, but prior to examining this possibility it was decided to more thoroughly explore the ignition model.

Another equally motivating factor for exploring the ignition model was the transient data provided by Quintiere and McCaffrey for the wood cribs burning inside an enclosure[18]. Although the burning behavior in the enclosure must not be compared directly with the free-burn due to thermal enhancements and oxidizer deficiency influences, the relative shapes of the two curves indicated a much more rapid climb to the quasi-steady state in the prototype. This difference in shape is most clearly illustrated by comparison in Figure 3.5. The data from Quintiere and McCaffrey has been digitized to fit into the plot. Dimensionless quantities are used to compare the data from the prototype and the model.

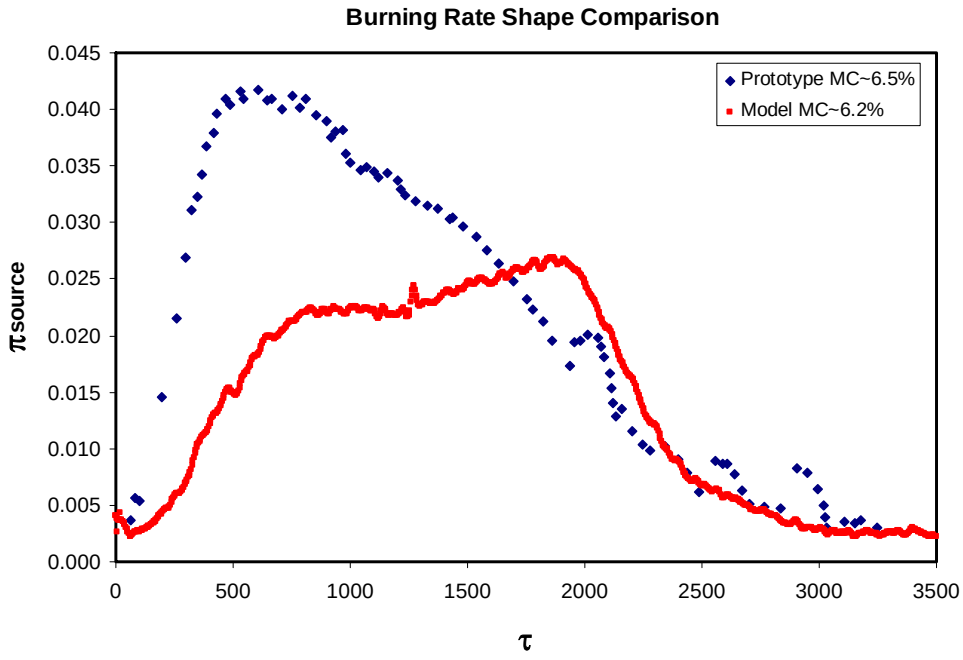

Figure 3.5: Transient Mass Loss Rate, Shape Comparison Only

Clearly, the magnitudes of these burning rate curves can not be accurately compared due to the burning rate enhancement of the thermal feedback from the enclosure. However, it is interesting to note that the total burn time appears to be similar. The free-burning prototype wood cribs certainly would have burned for a longer duration than the time scale presented above. Therefore, it appeared that the time scaling may also have been inconsistent.

The delayed development of peak burning was thought to a flame propagation issue. Ignition of the wood crib was achieved uniformly along its internal geometry, but the flames took slightly less than a minute longer to spread to the exterior surfaces of the crib. It was decided that the ignition model should be investigated in order to shift the area under the burning rate curve to more closely resemble the shape of the prototype enclosure fire curve.

The first variable that was altered was the moisture content of the crib. The moisture content has a direct influence on the density of the wood. The density in turn determines the mass of the fuel. The practical application of the scaling method to the crib design incorporates an estimate of the burning rate utilizing the total crib mass. A decrease in the moisture content of the wood should result in an increase in the burning rate accompanied by a more rapid development of the quasi-steady state burning period. A second free-burning experiment was conducted in which the wood crib was placed inside an oven at 105^{o}C for 48 hours. The intent of this preparation was to lower the moisture content to 0% and investigate the effect on the burning rate. All other testing parameters were kept constant. Figure 3.6 illustrates the results.

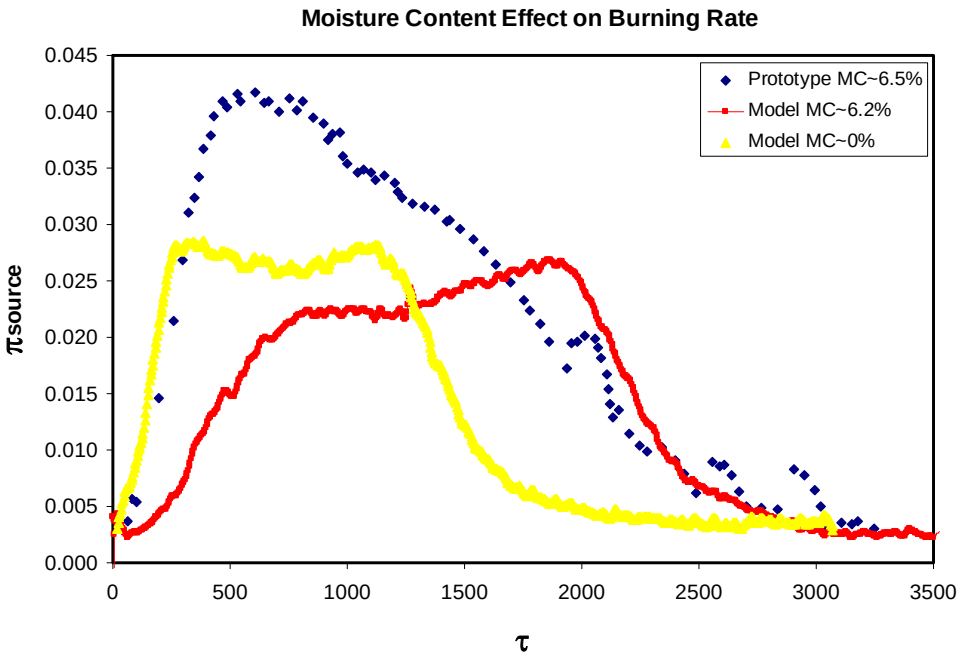

Figure 3.6: Effect of Moisture Content on Burning Rate

The decrease in moisture content seems to be accompanied by a decrease in the area under the burning rate curve. The area under this curve represents a dimensionless

energy that is directly proportional to the mass of the crib. The second effect of decreasing the moisture content is the achievement of the desired rapid rise to quasi-steady burning. Conversely, the total burn time has decreased significantly as a result of the decrease in mass. The general shape of the curve compares more favorably with that of the prototype fire than does the moisture laden curve.

In terms of average peak values, the result for the dry wood crib was an increase of 18% above the peak value reported for the moist crib and 29% shy of the peak value reported for the prototype free-burn.

$$\pi_{source,dry,APV} = 0.027$$

Herein lay an example of the deceptive nature of the average peak value comparison. It is the inability to distinguish magnitude from duration. The previous comparison shows that the duration of the prototype fire is perhaps better modeled by the moist crib, while the magnitude is better represented by the dry one. To date, this discrepancy has not been appreciated in the literature, which has yet to focus on transient burning behavior for such fires.

In an attempt to further transform the shape of this curve and also increase the average peak value for the burning rate, the elevation of the crib above the fuel pan was increased. The results of Gross and Block suggest that an increase in crib elevation, to a certain limit, increases the peak burning rate[5,10]. Initial attempts to scale this parameter recognized these findings, which stated the elevation limit to be a distance equal to the cross section of an individual stick[10]. Beyond this elevation, no increase in the peak burning rate was observed. When applied to the prototype, whose elevation was less than this dimension, Gross' conclusion was taken to mean that the elevation should follow the

same scaling relationship as the stick cross section. A modification was made such that the elevation of the crib above the fuel pan was doubled. The moisture content of the wood crib was once again set to 0%. The results are shown in Figure 3.7.

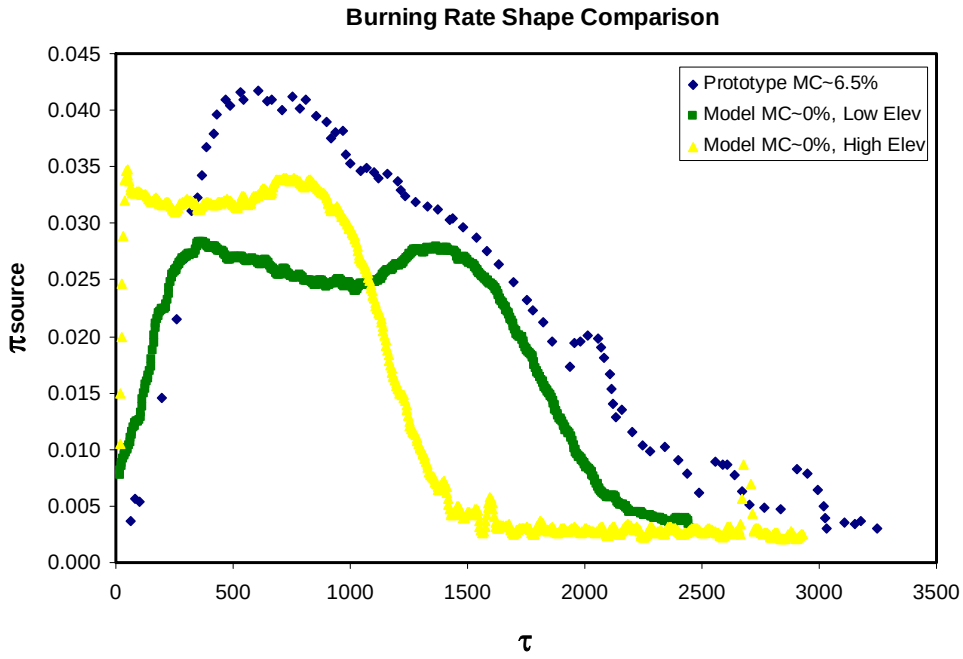

Figure 3.7: Crib Elevation Effect on Burning Rate

The model behavior shows a fairly significant increase in the peak burning rate and a dramatic change in the growth period. This result suggests that sufficient elevation of the crib had already been achieved by the scaling. The most important result of this model fire is found in the comparison between time averaged and transient behavior. The average peak value result for the dry crib at double elevation was

$$\pi_{source,elev,APV} = 0.015$$

This value is 40% below the value for the crib at the scaled elevation. This is the result of a much steeper slope during fire growth and decay. The conventional practice of using average peak values based on an arbitrary time interval thus has the potential to lead to

incomplete conclusions. The former method of averaging essentially combines the magnitude and duration of the fire into a single measurement of severity. In this particular case, the increase in the peak energy release of the fire was masked by transient averaging.

One possible reason for the difference in peak duration between the cribs with different moisture content is the issue of repeatability in the data. Wood cribs have traditionally been used in compartment fire experiments in large part for their high degree of repeatability. Nonetheless, 3 repeat tests were conducted for the dry wood cribs at the scaled elevation to determine the extent of repeatability in the transient data. The results are shown in Figure 3.8. The scale of the plot axes is consistent with previous plots in order to avoid artificial distortion of the shape of the curves.

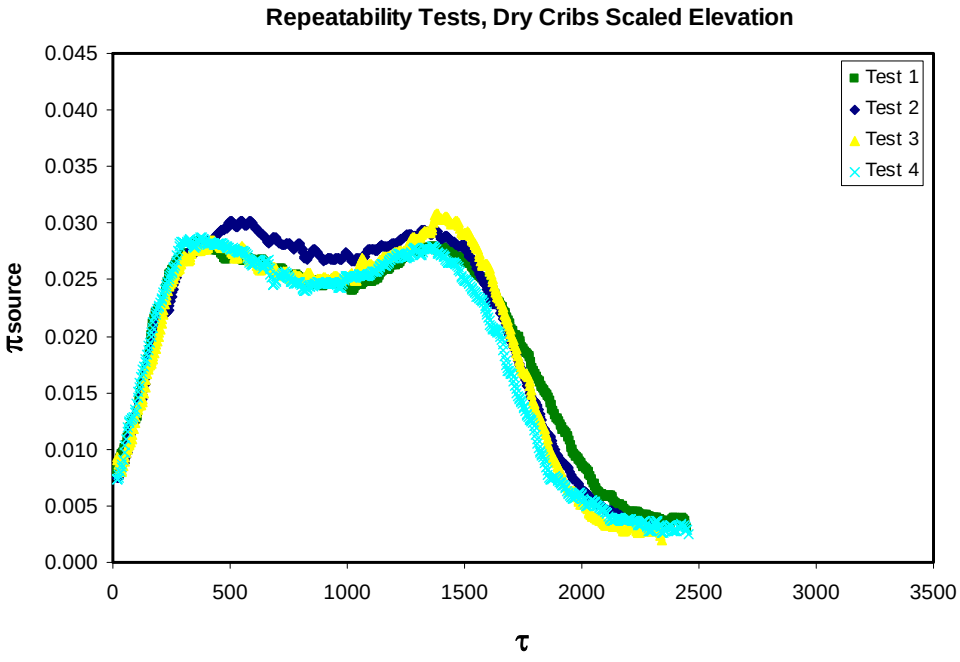

Figure 3.8: Repeatability of Dry Model Cribs, Scaled Elevation

Clearly, there is a high degree of repeatability with respect to fire growth and duration in the model. It is for this reason that the repeatability can be illustrated in a plot of average peak values. Had there been similarity in growth and dissimilarity in duration, the use of average peak values would have been an incomplete approach to determining repeatability (Figure 3.9).

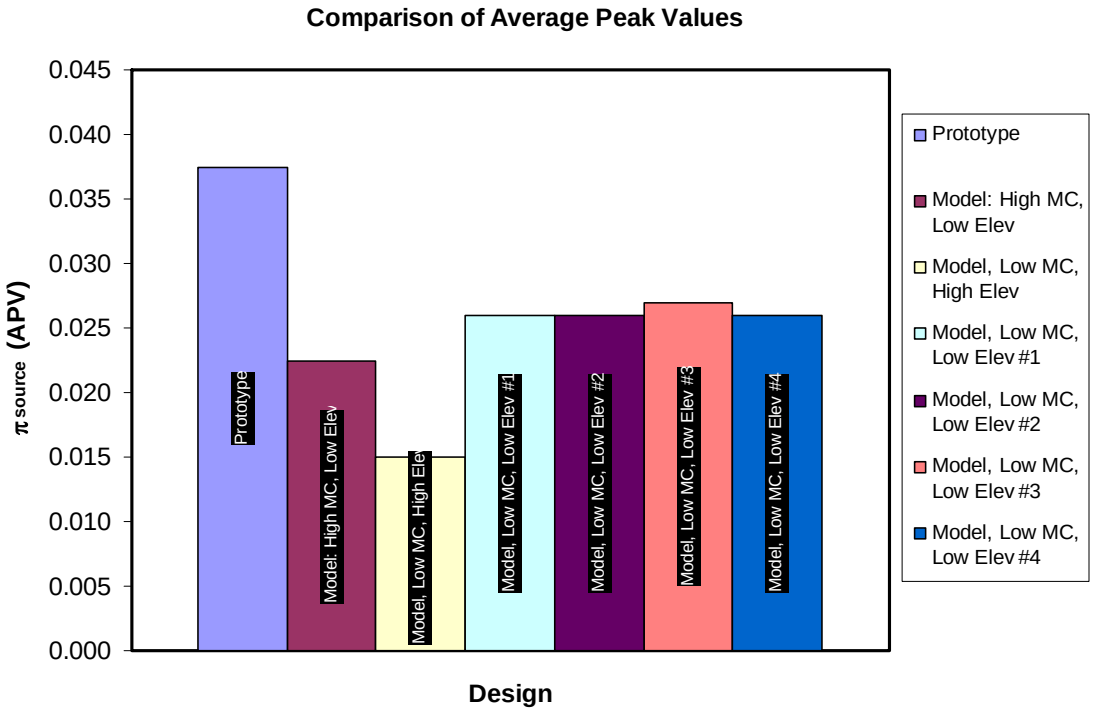

Figure 3.9: Average Peak Values

The four tests tasked with determining repeatability show a maximum difference in average peak values of 3.8%. The twin peak behavior of these curves was thought to have been due to flame propagation from the core to the external surfaces of the crib. The repeatability demonstrated in Figure 3.8 suggests a search for a different explanation as it is unlikely that the flame would have propagated in such a repeatable fashion in each of these tests.

It is recognized that neither the increase in elevation, nor the decrease in the moisture content of the wood, followed an explicit relationship determined by the theoretical model. In the case of the crib elevation, it was found that the scaling relationship to the prototype must be maintained. However, the excellent repeatability already demonstrated by the low moisture content led to the continuation of its use as the ignition model was explored one step further.

Although the size of the fuel pan and the amount of heptane used to ignite the wood was within the parameters suggested by Gross, in the interest of completeness, it was decided to explore this piece of the ignition model. The area of the fuel pan previously used was slightly larger than the base of the crib; however, the pan was circular while the base of the crib was square. Figure 3.10 illustrates a top view of the model, emphasizing the lack of exposure of the 4 corners to the burning heptane.

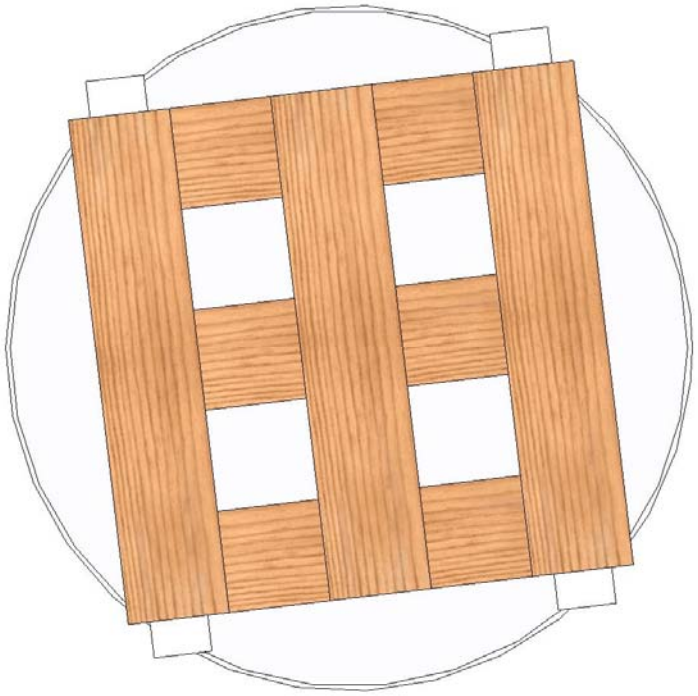

Figure 3.10: Circular Fuel Pan vs. Square Crib Base

The issue of propagation did not seem to be related to a critical ignition flux for the wood because the crib successfully ignited in each of the previous experiments. Rather, the issue was though to be the blockage of the crib corners from the exposure to flame.

Thus, one final attempt to determine whether the twin peaks of the burning rates were due to a propagation issue must necessarily involve a change in fuel pans and the amount of heptane used. A new fuel pan with a rectangular surface area much larger than the base of the crib was used. The new fuel pan had dimensions 18 cm x 28 cm, yielding an area 75% larger than the base of the wood crib. The pan was filled with 30 mL of heptane, three times the volume used in previous experiments. This combination also supplied a depth of heptane that was approximately equal to that used in the initial attempts. This is important in that the depth of the pool is directly related to the total burn time of this starter fire. These extreme values ensured uniform ignition of the wood crib from the heptane fire. The result of the modifications to the fuel pan size and heptane volume is shown in Figure 3.11. The curve representing the small pool fire is the same as repeatability test #1.

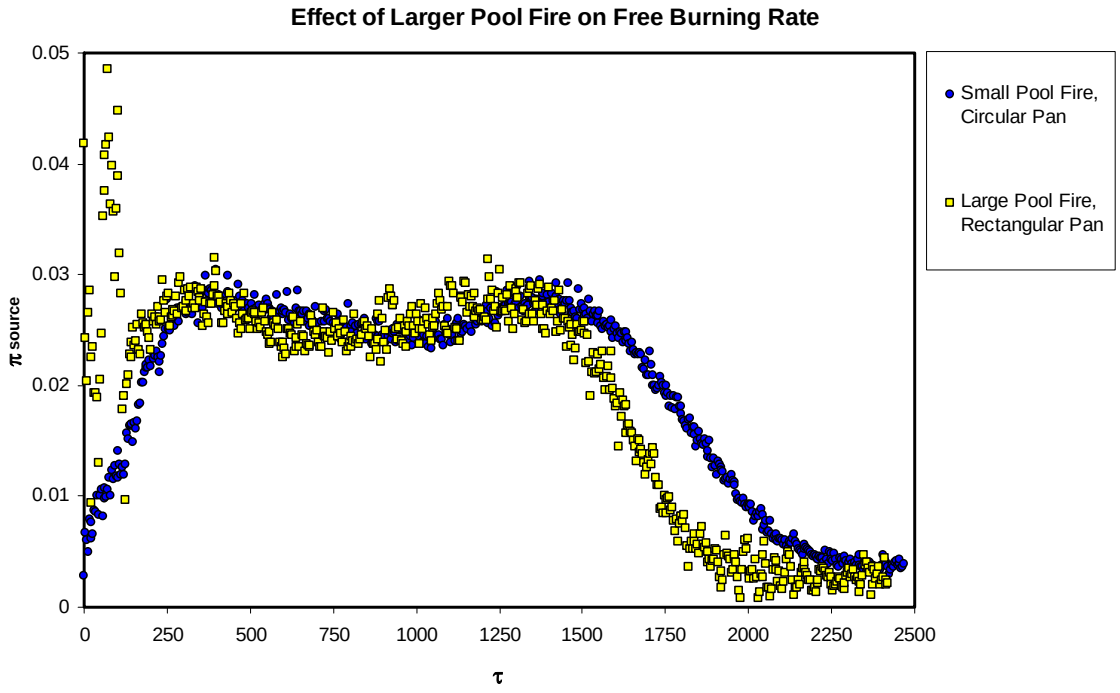

Figure 3.11: Modifications to Fuel Pan Area and Heptane Volume

The large fluctuations at the beginning of the curve are due to the dramatic increase in the heat release rate of the heptane pool fire caused by the much larger pan area. Observations made during the experiment revealed that the crib was ignited uniformly during this period. After the cessation of the heptane fire, it is clear that the transient behavior of the crib very closely follows the model behavior with the smaller pool fire. The decrease in the total burn time is due to the increased consumption of fuel during the burning of the larger pool fire. From this result, it can be inferred that the shape of the burning rate curve is not the product of flame propagation to the corners of the crib.

An examination of the prototype data from Quintiere and McCaffrey revealed a different explanation altogether. The same prototype crib design was used throughout this experimentation. However, recall that multiple cribs were placed on the load

platform for various tests. The prototype crib that the current research was trying to emulate was based on a 4 crib layout, where the spacing between cribs was the same as the spacing between individual sticks within a single crib. The multiple crib hypothesis equated the burning behavior of this multiple crib layout to that of a single large crib. The key to examining the validity of this hypothesis with respect to burning rate shape is a closer look at the burning rates produced a variation in the number of cribs in the prototype experiments. In other words, the shape of the single crib must be compared to the shape of all other multiple crib orientations. The data from these full scale experiments was digitized and is presented in Figure 3.12 to illustrate this comparison.

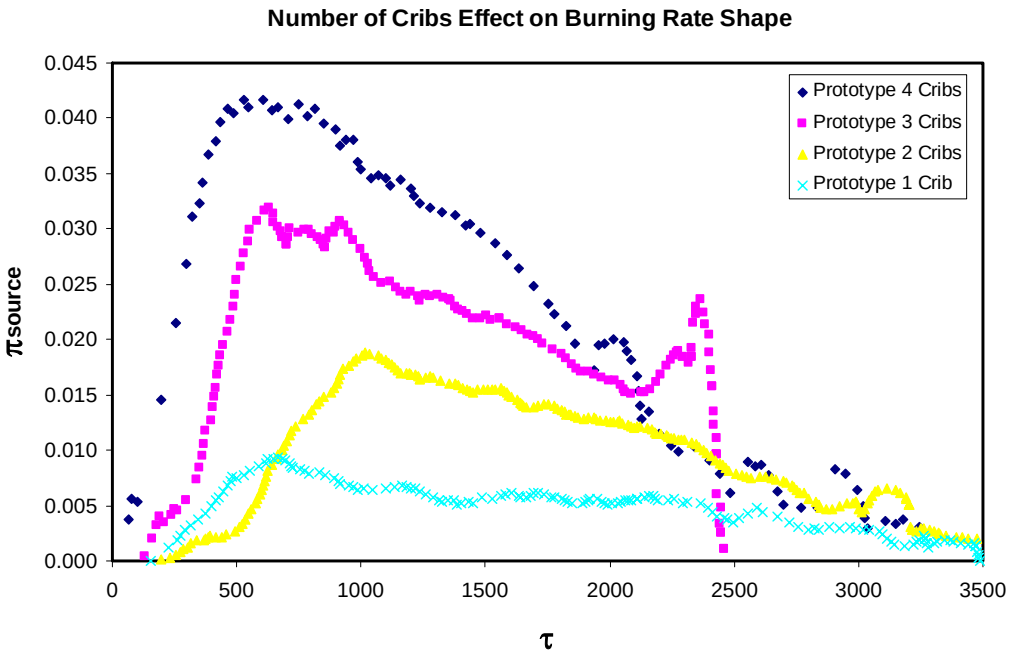

Figure 3.12: Effect of Multiple Cribs on the Transient Burning Rate Shape[18]

The data reveals a significant difference in shape that gradually develops as the number of cribs on the load platform is increased. This effect on shape is likely revealed by the power law relationship suggested by the authors between the average peak burning

rate and the number of cribs. It appears that the shape of the single crib burning rate most closely resembles that of the model. If these combinations of cribs are all viewed as a single crib increasing in size, then the cause of the change in shape must be due to an increase in the number of sticks within the crib.

The contribution of the number of sticks is found in the internal radiation mechanism of the crib. The glowing sticks within the pile are undergoing heterogeneous combustion in which reactions are occurring at both the surface and the gas phase. The outer surfaces of the crib which are exposed to the ambient atmosphere are also undergoing heterogeneous combustion. However, these surfaces are not observed to be glowing during any part of the experiment. The reason for the lack of glowing is that the burning of these outer surfaces is not enhanced by internal radiation. Heat is lost to the ambient from these external surfaces. Consideration of the internal surfaces reveals an altogether different phenomenon. The flame convectively heats the internal and external surfaces in a similar manner. The difference between the two is that the synergistic feedback of the internal surfaces prevents a loss of heat from the core. In other words, it acts as a near perfect resistor. To better appreciate this behavior, the following simplified model for the burning rate is presented for two parallel internal surfaces:

$$\dot{m}_f'' = h\left(T_{flame} - T_{surface}\right) + \sum_{j=1}^{N} F_{ij}\sigma\left(T_i^4 - T_j^4\right) \tag{3.81}$$

The first term represents a combination of convective and radiant heating from the flame, while the second dictates the radiation exchange between surfaces. In the case where both surfaces are glowing, the surface temperatures can be assumed equal. In this case, there is no net heat transfer via radiation between these surfaces. As the fire progresses, heat transfers from the flame to the surfaces, but it is not lost from the surfaces. The

surface temperatures gradually increase toward the limit of the flame temperature. Such is not the case for exterior surfaces, where there is some degree of heat loss to the ambient. If one appreciates the structure of the crib as a whole with respect to these two simple models of heat transfer, an intuitive conclusion is reached. As the number of interior surfaces in the crib is increased, the burning rate model for the interior surfaces dominates the combustion process.

A traditional argument in the literature suggests that the surface temperature of the glowing wood surface is higher than that of the flame[15,23,25]. The consequence of such behavior would be that heat is transferred from the surface to the flame rather than the flame to the surface. The implications of this argument must be considered from the standpoint of simple heat transfer through a typical wood stick found in the crib. At the beginning stages of the fire, the surface of the stick is heated by the flame emanating from the heptane pool fire below. There comes a point when the surface reaches its ignition temperature. Heat must be transferred from the flame to the surface in order for this to occur (Figure 3.13).

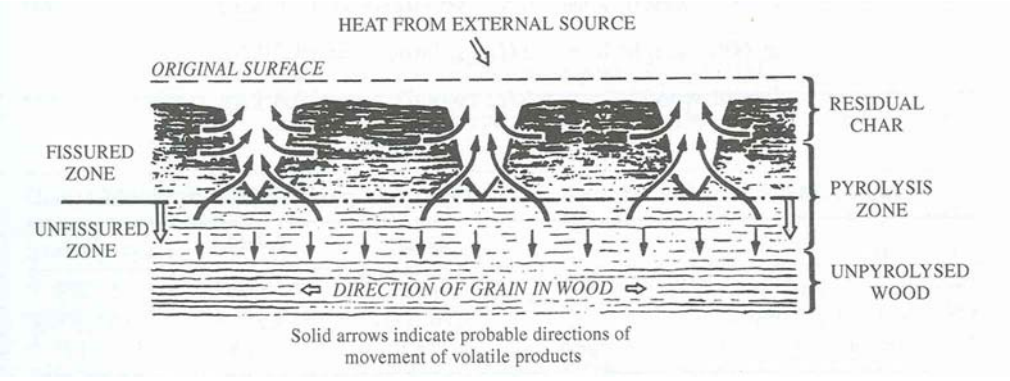

Figure 3.13: Heat Transfer in Wood Slab[25]

Now consider the same stick at a much later time. The surface of the stick is glowing as it undergoes heterogeneous combustion. The thermally thick solid must

necessarily have some thermal penetration depth $\delta_{thermal,}$ which must increase in time in order for the wood to be consumed. For this to happen, heat must be conducted from the hot surface facing the flame to the cool interior of the stick at a depth greater than $\delta_{thermal}$. Heat will diffuse in the direction of the steepest gradient. Either it feeds the flame at the surface or it conducts into the solid leading to consumption of the fuel. From this reasoning alone, a surface temperature that is higher than the flame temperature would result in the cessation of fuel consumption. Experimental evidence to the contrary is likely due to a flaw in the measuring technique.

There is merit to the observation of McCarter and Broido[9] that the brief extinguishment of flames above the crib does not markedly affect the magnitude of the burning rate[23]. This observation was made during the quasi-steady period of burning when the surface temperatures of the wood had reached their maximum. The model for the burning rate offered above must be considered. During this stage of the fire, the surface temperatures of adjacent sticks are assumed to be equal and therefore there is no net exchange of radiant heat. The only remaining heat transfer mechanism in the model is that from the flame to the surface. At this point in the development of the fire, the difference between the flame and the surface temperatures should be small. If this were not the case, the burning rate would continue to grow beyond this quasi-steady state to higher peak values. As long as the surface temperatures of the adjacent sticks are at equal peak values, the heating from the flame will be small and no heat will be lost from the internal structure. Thus a brief elimination of this small contribution to the burning rate yields little affect on its peak value.

Prior to proceeding it is important to note the data of Folk in Figure 2.2. The burning rate curve represents a wood crib with 3 sticks per layer and 6 layers. The porosity of the wood crib evaluated with Heskestad's model is 0.8 mm, which is well within the fuel surface controlled burning rate regime. The shape of Folk's transient burning rate curve, shown in Figure 2.3, illustrates the same twin peak affect observed in the current research. The shape of the curve does not seem to be due to any limiting design parameter other than the number of sticks per layer in the crib.

With these concepts in mind, the next step in the free-burning analysis was to reproduce this effect in the laboratory by burning multiple cribs spaced closely together to give the effect of a single large crib with many sticks. It should be noted that there exist no scaling relationships between the following experiment and any of the prototype experiments. The utility of this experiment instead lies in the shape of the transient burning rate curve that is produced. The experimental setup of the 4 crib orientation was used as a guide. Four cribs, of the same design used thus far as a quarter scale model, were elevated above a large square fuel pan. The spacing between cribs was made equal to the spacing between sticks in an individual crib. Four equally sized square fuel pans, one underneath each crib, were used. The base area of each pan was 20% larger than the base area of each crib. The pan was constructed of ½ inch thick insulation board wrapped in aluminum foil to create a lip and prevent spillage. All 4 cribs were dried to approximately 0% moisture content prior to testing. Elevation of the cribs was consistent with previous experiments at approximately 1.25 cm. Figure 3.14 illustrates the experimental setup for this test. The depth of heptane poured into the fuel pans was 0.5 mm. The placement of the crib over its respective fuel pan was slightly off-center in

order to allow for perfect spacing between cribs. Figure 3.15 shows the results of the experiment.

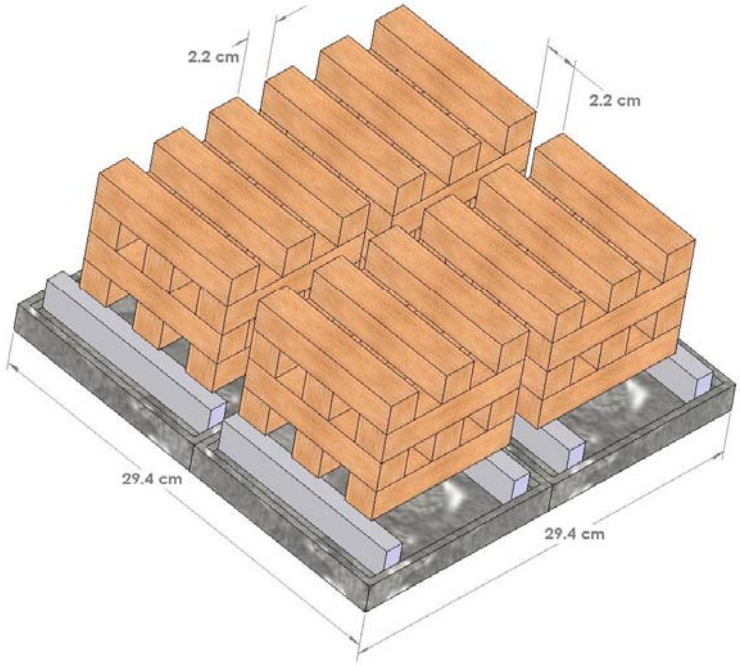

Figure 3.14: Experimental Setup, 4 Crib Test

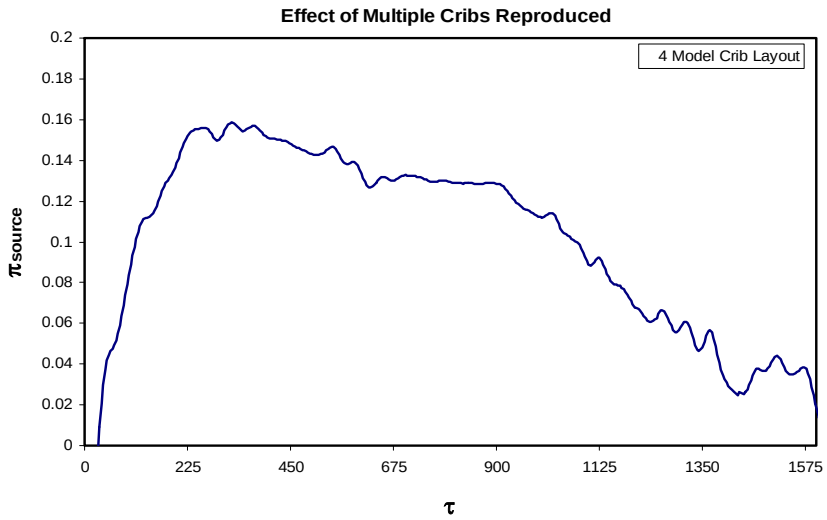

Figure 3.15: Reproduced Effect of Multiple Cribs on Burning Rate Shape

An analysis of the previous results utilizing a large pool fire beneath the crib seems to suggest that the twin peaks of the burning rate curve are not due to flame propagation outward from the core. In fact it appears that the cause of the twin peaks is not due to flame propagation, but rather is a relic of the heat transfer process described above. The rate of temperature rise in the core of the crib exceeds that of the outer surfaces. The first peak signifies the rapid growth of the core to a quasi-steady state. The second peak represents the more delayed rise of the exterior surfaces to peak values. The burning of the sticks is simply unsynchronized.

3.3 A New Practical Approach to Validation of the Theory

3.3.1 Wood Crib Design

3.3.1.1 Determination of Minimum Number of Sticks

The results of the initial free-burn experiments indicated that further attempts to utilize the crib design of Quintiere and McCaffrey[18] as a full scale prototype would require excessive manipulation of the scaling theory. It was therefore decided that the modeling of this prototype at reasonable laboratory length scales was not feasible. A new practical and more feasible approach was adopted. The experimental plan was to first find the minimum number of sticks necessary for the internal radiation mechanism to dominate free-burning wood crib combustion. Based on these results, wood crib compartment fires would be tested at three geometric scales in the laboratory. The wood crib designed at the smallest scale would have a minimum number of sticks in the structure.

The number of sticks in a wood crib is determined both by the number of sticks per layer and the number of layers. Experiments were conducted to determine the minimum number of each parameter required to achieve the desired results in the burning rate. The previous model and prototype indicated that the critical number of sticks per layer was either 4 or 5. A simple approach to selecting one over the other is to visualize a wood crib. In the case of 3 sticks per layer, only 1 of those 3 sticks is entirely internal to the crib. Thus, the number of sticks whose burning rate is influenced by the ambient is greater than those that are influence only by internal processes. With this logic, the minimum number of sticks per layer should be 5. This ensures that the burning rate of 3 sticks is governed by purely internal processes, while only 2 are influenced by external

heat loss. This simple but logical approach was used to set a minimum number of sticks per layer at 5.

The problem now reduced to the determination of the minimum number of layers. Recall also that the porosity of the crib must also be above a critical value of 0.5 mm. Two free-burning experiments were conducted where the number of sticks per layer was varied from 3 to 4. The porosity, number of sticks per layer and stick cross section were all kept constant. An otherwise arbitrary set of design parameters was used (Table 3.9). Eastern White Pine was again used for these tests. The cribs were both elevated 4 cm above the base of the fuel pan and a 0.5 mm depth of heptane was used for each test. Figure 3.16 shows the results.

Test 1	**Test 2**
b = 25.4 mm	b = 25.4 mm
L = 206.4 mm	L = 222.3 mm
s = 19.9 mm	s = 23.9 mm
n = 5	n = 5
N = 3	N = 4
P = 0.6 mm	P = 0.6 mm

Table 3.9: Minimum Number of Layers Experimental Parameters

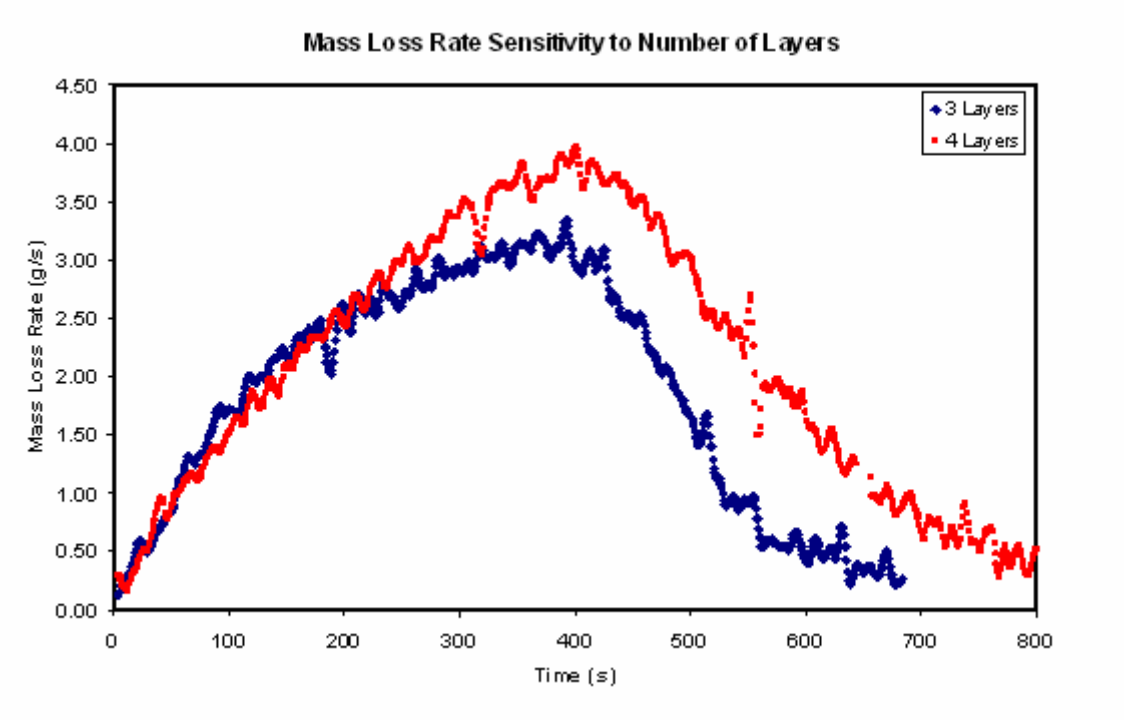

Figure 3.16: Results of Minimum Number of Layers Experiments

The above results are not represented with dimensionless variables for two reasons. The time scale is not dimensionless because the stick cross sections are equal for both cribs. Therefore, the measured times are comparable. The mass loss rate is not represented as a dimensionless source energy parameter because the designs are not based on any characteristic length. The only significant difference in the two crib designs is the number of layers in the crib. It is evident that as the number of layers is decreased, the quadratic shape of the curve for 4 layers begins to level at the peak. Based on this observation, it was deduced that 4 was the minimum number of layers necessary to yield a mass loss rate that was reproducible with increasing length scale. It is important to note that the approximate minimum value for the number of sticks per layer is larger than that for the number of layers. The scaling method shows that the number of sticks per layer is more dependent on length scale then the number of layers.

3.3.1.2 New Design Requirements

A new practical approach involved designing, constructing and testing of both confined and unconfined wood crib fires at three length scales. A list of desired model features was added to those suggested by previous experimental results to produce the following list of design requirements for the models:

1) Models must be constructed at three workable geometric scales
2) Must follow the scaling laws set forth in the theory
3) Cribs must burn in the fuel surface controlled region of the Porosity curve
4) Full Scale crib must have a 1 hour total burn time in its enclosure
5) The full scale fuel loading must be representative of a realistic occupancy
6) The minimum number of sticks per layer at the smallest scale is 5
7) The minimum number of layers at the smallest scale is 4
8) Design for 1 large fire and 1 small fire

The length scales chosen for the models had to be representative of the size of a fictional life-sized prototype enclosure. The dimensions of this enclosure were arbitrarily chosen to be 0.376 m wide x 0.376 m deep x 0.254 m high. At first glance, the basis for the choice of these dimensions appears ambiguous. Translated to English units, the dimensions are 12.3 ft wide by 12.3 ft. deep x 8.3 ft high. The extra third of a foot is added to each dimension in recognition of the desire to eventually place a steel frame inside the models. The dimensions of the steel frame and its connections required this slight addition. Based on these dimensions, it was decided that three manageable scales with which to conduct testing in the laboratory were 1/8, 2/8 and 3/8 of the full scale prototype.

The bases for the next two requirements have already been addressed. The desire for a 1 hour burn time in the full scale enclosure is related to the implementation of a steel structure in the compartment. The ASTM E119 Standard rates the fire resistance of building assemblies on the basis of their ability to withstand exposure to the testing furnace conditions for a certain period of time. This period of time is referred to as the fire resistance of the assembly[13]. Ratings are typically given on the order of hours. Based on this conventional view of fire exposure, a 1 hour burn time is desired for the full-scale wood crib in the compartment[13]. Figure 3.17 illustrates the standard time vs. temperature curve for the ASTM E119 test.

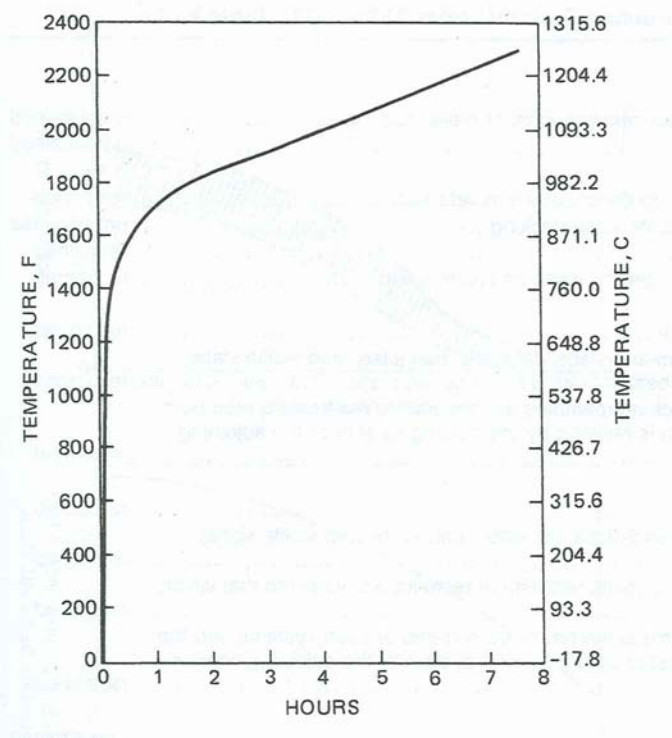

Figure 3.17: ASTM E119 Standard Exposure[13]

The ability of a single crib to burn for 1 hour is not a common design criterion. The standard exposure is accomplished with a gas burner fuel source. The advantage of using a wood crib in the scale model is that the cross section of its members can represent

an equivalent solid fuel thickness. Attempts could be made to correlate the burning rate of a wood crib to various pieces of actual furniture with different characteristic thicknesses. Although the current effort is focused on examining the scaling in a more fundamental comparison between a model and prototype crib, the ability to correlate the wood crib data to that of actual furniture would be extremely useful in future applications.

Other design criteria must be considered simultaneously with the burn time requirement. The combination of design requirements for minimum crib porosity and a minimum number of sticks per layer indirectly affect the base area of the crib. It is critical to recognize that while the compartment boundaries are subject to geometric scaling, the length of the sticks in the crib must scale with the 7/6 power of the characteristic length. This means that as the geometric scale of the model is increased, the base area of the crib will occupy a larger portion of the compartment floor surface area. Recognizing that the wood crib must fit inside the compartment for every geometric scale between 1/8 and full, some reasonable ratio of crib base area to compartment floor area at the full scale must be set. The lesser dependency on length scale for the number of layers in the crib means that the crib base area will grow with scale much faster than the crib height. Therefore, the base area is the critical design consideration.

The burn time of the crib is directly proportional to the fuel mass. The design parameters of the crib that play the most critical role in determining the duration of the burn are the wood density and the stick cross section.

$$t_{burn} = \frac{m_f}{\dot{m}_f} = \frac{\rho V}{C A_s b^{-1/2}} \propto \rho b^{3/2} \tag{3.82}$$

In order to provide the greatest amount of flexibility for crib geometry relative to the enclosure, White Oak was chosen for use in the models due to its high density and availability. An approximate range for oven-dry density of common domestic wood species is 320-720 kg/m^3. The density listed for Eastern White Pine[26] is 370 kg/m^3. In comparison, that which is listed for White Oak[26] is 720 kg/m^3. This suggests that the burn time for a crib constructed of White Oak is nearly twice that of Eastern White Pine. Now that the density of the wood has been dramatically increased, care must be taken to ensure that the fire load in the compartment corresponds to a reasonable value.

There are now 3 simultaneous design considerations that have been added to theoretical scaling laws. These are the geometry of the crib relative to the enclosure, the total burn time and the fire load. The global set of design rules revolves around the concept of a certain mass of fuel burning for 1 hour in the full scale compartment. Until this point, the burn time for the wood crib has been approximated as the quotient of the crib mass and the burning rate model developed by Block for free-burning wood cribs[10]. It is recognized that the burning rate of the wood crib inside the enclosure must be estimated in a different way than for the free-burning scenario.

The enclosure burning rate is affected by both the thermal feedback from the boundaries and a possible decrease in the flow of oxidizer to the fuel bed. To date, the only known model, supported by experimental data, that is capable of providing a relationship between the mass of a wood crib, its burning rate and the ventilation of the compartment was developed by Harmathy[15]. Figure 2.14 presents his results for the burning rate of wood cribs in an enclosure. The data explicitly recognizes the influence of compartment ventilation and implicitly recognizes that of thermal feedback from the

boundaries. However, the fact that this influence was not directly addressed by the model suggests that it was not well considered.

The application of Harmathy's model to the current design begins with Figure 2.14, which graphically presents the following relationship:

$$\frac{\dot{m}_f}{A_s} = f\left(\frac{\dot{m}_a}{A_s}\right) \tag{3.83}$$

where the burning rate can be found with knowledge of the fuel surface area and the size of the compartment vent. Recall that the burning rate in this model is an average peak value. As such, the model can not be used to predict a burn time from ignition to extinction. Nonetheless, it is a powerful tool that can provide a reasonable estimate for the steady state duration. The mass flow rate of air through the vent is determined via Equation 2.19c and the surface area of the fuel is found from Equation 3.56. Harmathy indicates that the duration of the steady state regime can be determined from knowledge of the initial fuel mass and the peak burning rate in Equation 2.18. These equations are restated for quick reference[15].

$$t_{ss} = 0.936\, m_{0,f} \Big/ \dot{m}_f \tag{2.20}$$

$$\dot{m}_a = 0.145 \rho_a g^{1/2} A_w H^{1/2} \tag{2.21b}$$

$$A_s = 2Nnb^2\left[\left(2\frac{L}{b} + n - 1\right)\right] + 2n - \frac{L}{b} \tag{3.56}$$

The unknown independent variables in this analysis are the design parameters of the crib and the dimensions of the vent. Selection of a set of crib design variables yields a result for both the surface area and mass of the fuel. Selection of vent dimensions allows for the calculation of the mass flow rate of air. Once both selections are made, the

corresponding burning rate can be approximated from the best-fit line shown in Figure 2.14 and presented in Equations 2.27a and 2.27b.

For ventilation controlled combustion

$$\frac{\phi}{A_s} \leq 0.263 \qquad \dot{m}_f = 0.0236\phi \tag{2.27a}$$

For fuel surface controlled combustion

$$\frac{\phi}{A_s} \geq 0.263 \qquad \dot{m}_f = 0.0062 A_f \tag{2.27b}$$

The result can then be substituted into Equation 2.18 to arrive at a prediction for the steady state duration of the fire.

The first step in this process is to set the minimum requirements for *n* and *N* in the 1/8 scale crib. Now, the only two parameters to be determined for this crib are the cross section and the length of the sticks. One must be chosen and the other adjusted so as to meet the minimum porosity requirement. In the interest of ensuring that porosity is not a factor in these designs, the design value for porosity was set to 0.7 mm. In order to make the optimal choice for the smallest scale, one must first ensure that the full scale crib fits reasonably well within the full scale compartment. Applying the scaling rules in Table 3.2 to the parameters *n* and *N*, we arrive at values for the full scale crib of 28 sticks per layer and 8 layers. An arbitrary selection of the stick cross section is made and the length of the sticks adjusted so as to keep the porosity constant between scales. The resulting full scale crib design must be evaluated with respect to relative geometry and fire load. The final design for the full scale used a cross section of 4.45 cm (1.75 in). In order to maintain the porosity of the crib at 0.7 mm, the resulting base area of the crib occupied almost 40% of the total floor area of the compartment. The resulting fire load was 11.8

psf. According to the results of the survey conducted by Gross and Robertson[14] in Table 2.12, this fire loading corresponds most closely to an educational occupancy. Thus, all of the full scale parameters are indicative of a model that emulates a feasible fire scenario.

Now that a full scale wood crib has been designed, the vent geometry must be selected. If the height of the vent is fixed as the full height of the compartment, then the width of the vent is the only variable left to be determined. Harmathy's data can now be applied and a solution to the fire duration can be obtained. It is now clear that the two somewhat arbitrary selections to be made in this design process are the stick cross section and the vent width. Therefore, the duration of the full scale fire can be plotted as a function of the vent width for different possible values of the full scale stick cross section. Figure 3.18 shows the results for various cross sections. Based on this Figure, a full scale stick cross section was chosen as 0.045 m (1.75 in), with a vent width of 0.5 m.

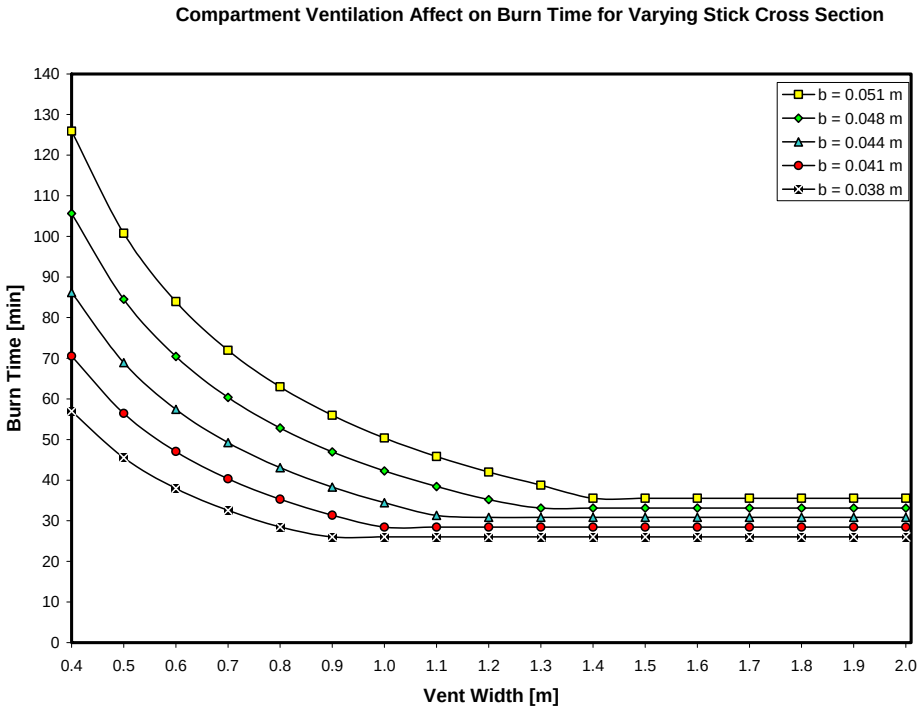

Figure 3.18: Prediction of Full Scale Fire Duration

The full scale wood crib design can now be translated to various length scales with the application of the scaling rules in Table 3.2. The model wood crib parameters are shown in Table 3.10. Note that the number of sticks per layer and the number of layers must be rounded to integer values. This causes slight differences in the porosity of the crib between scales.

Scale	b (mm)	L (mm)	n	N	P (mm)	Fire Load (kg/m^2)
Full	44.5	2334.9	28	8	0.73	57.6
3/8	32.1	743.5	12	6	0.79	21.8
2/8	28	463.3	9	5	0.68	14.6
1/8	22.2	206.4	5	4	0.72	7.3

Table 3.10: Large Wood Crib Design Parameters

The desire for a second smaller design is based on the eventual placement of a steel frame in the compartment. Experimentation with an approximate maximum and minimum fire exposure will ultimately provide a sense for a realistic range of conditions. The same design process is followed to produce a smaller crib design at each of the above scales. The only added specification is that the fire load for the small design should be approximately 1/10 of the fire load for the large design. This number was selected to correspond to approximately the lowest fire load listed on the survey by Gross and Robertson[14]. Consultation with this survey in Figure 2.12 suggests that this fire load is just shy of a typical hospital. It is important to remember that this survey was conducted nearly 50 years ago. Typical occupancy loading conditions have certainly changed since then; however, this experimental work was considered a satisfactory approximation. The results for the small crib design are shown in Table 3.11.

Scale	b (mm)	L (mm)	n	N	P (mm)	Fire Load (kg/m^2)
Full	19.1	1257.2	28	8	0.70	5.7
3/8	13.7	400.4	12	6	0.75	2.2
2/8	12.0	249.5	9	5	0.68	1.4
1/8	9.5	111.1	5	4	0.71	0.7

Table 3.11: Small Wood Crib Design Parameters

The ignition model for the wood cribs was designed based on the results of the previous experiments. The fuel pan design was square to correspond to shape of the crib base. The scaling of the pan length followed that of the crib length so that the surface area of the pan was approximately 20% larger than the surface area of the crib at all scales. Cribs were elevated above the fuel pan at a height equal to the cross section of the sticks plus an additional height equal to the lip of the pan. Therefore, the total clear height underneath the crib was equal to *b*. The amount of heptane used in each experiment was standardized at a 0.5 mm depth. This depth was chosen based on simple experiments measuring the time of uniform burning of the pool fire across the entire surface of the pan. The duration of the burn was short enough not to interfere with the mass loss rate data for the crib, but long enough to uniformly expose the interior and exterior surfaces of the crib.

3.3.1.3 New Approach: Free-Burn Experimental Setup

The new experimental approach began with conducting free-burning experiments for each of the model scales for both the large and small crib designs. The full scale prototype represented a fictional experiment whose design was critical to determining model parameters. For the sake of demonstrating repeatability, two free-burning tests were specified for each experimental configuration. The proposed testing matrix is

shown in Table 3.12. The naming convention adopted for these tests utilizes a 4 character sequence. The first character denotes the length scale of the model by identifying the numerator of the scale factor in increments of 1/8. The second distinguishes between the large and small crib design. The third character identifies the experiment as either free-burning of confined. The last character identifies the number of that test with respect to repeatability. For example, test 2-L-F-2 refers to the 2/8 scale, large design, free-burning test, test number 2.

Test ID	Description
1-L-F-1	1/8 Scale, Large Design, Free Burn, Test #1
1-L-F-2	1/8 Scale, Large Design, Free Burn, Test #2
1-S-F-1	1/8 Scale, Small Design, Free Burn, Test #1
1-S-F-2	1/8 Scale, Small Design, Free Burn, Test #2
2-L-F-1	2/8 Scale, Large Design, Free Burn, Test #1
2-L-F-2	2/8 Scale, Large Design, Free Burn, Test #2
2-S-F-1	2/8 Scale, Small Design, Free Burn, Test #1
2-S-F-2	2/8 Scale, Small Design, Free Burn, Test #2
3-L-F-1	3/8 Scale, Large Design, Free Burn, Test #1
3-L-F-2	3/8 Scale, Large Design, Free Burn, Test #2
3-S-F-1	3/8 Scale, Small Design, Free Burn, Test #1
3-S-F-2	3/8 Scale, Small Design, Free Burn, Test #2

Table 3.12: List of Free-Burning Experiments

The setup for these experiments was dependent on the scale of the model. In all cases, the wood crib was elevated above a fuel pan filled with heptane. A load cell was positioned underneath the ignition model to record the transient mass of the burning crib. The weight of the new models far exceeded that of the previously designed models and as such, different load cells were used in these experiments. The two smaller model scale tests utilized a *Futek* model *LRF400* In-Line Tension and Compression Load Cell with overload protection. The device was calibrated for compression so that measurements

could be taken from underneath the wood crib. The rated capacity of the load cell was 222 N (50 lbs). The rated output was 2 mV/V. The device had a nonlinearity of $\pm 0.05\%$ of the rated output. The data acquisition system described in the previous experiments was also used for the 1/8 and 2/8 scale model free-burns.

Once the free-burn experiments for the two smaller scales had been conducted in the laboratory, their results were implemented with the scaling theory to predict the energy release rate of the 3/8 scale model large crib design. This calculation suggested a peak fire size that would be too large for the laboratory facilities. Based on this prediction, all of the 3/8 scale model tests were conducted at the Bureau of Alcohol, Tobacco and Firearms (ATF) Fire Research Laboratory in Beltsville, MD, where more appropriate facilities for the given fire size could be used. The change of venue for the 3/8 scale model tests necessitated the use of a portable data acquisition system. A *Fluke NetDAQ*, Model *2640A*, was selected for use in these tests. The system was equipped with a terminal block consisting of 20 analog channels to convert transducer signals and relay them to a laptop PC equipped with an Ethernet connection and the *Fluke NetDAQ Logger* software. A single channel was used to collect data from the load cell at a frequency of 1 Hz. The load cell used for the 3/8 scale model tests was a 1332 N (300 lb) capacity flat bed instrument. The device was borrowed from the ATF laboratory and calibrated prior to testing.

The size of the model cribs was much larger than that which could be accommodated in the available cone calorimeter. Therefore, the free-burning experiments were conducted on a make-shift platform constructed underneath a large exhaust hood in the center of the laboratory. Figure 3.19a shows this platform in which

threaded connections in the top and bottom of the load cell are used to attach a support base and an aluminum platform to provide stability. Figure 3.19b illustrates the load cell setup for the free burning experiments conducted at the 3/8 scale. The wood crib designs are illustrated in Figures 3.20 through 3.25.

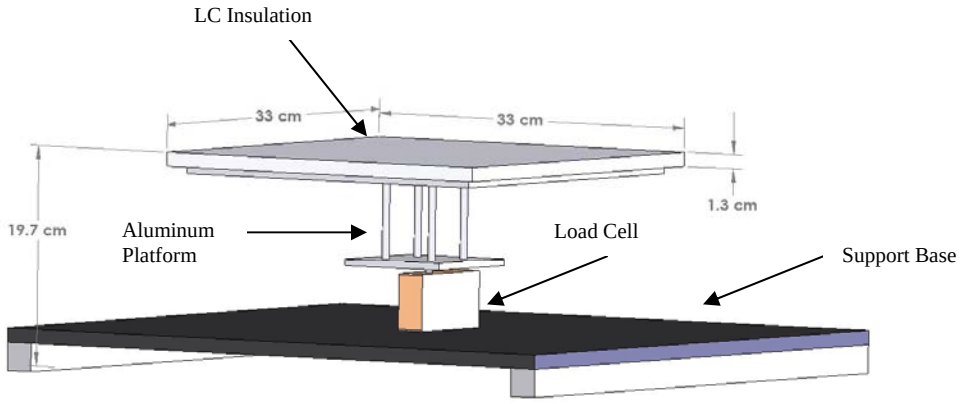

Figure 3.19a: Free-Burn Load Cell Platform for Small Model Scales

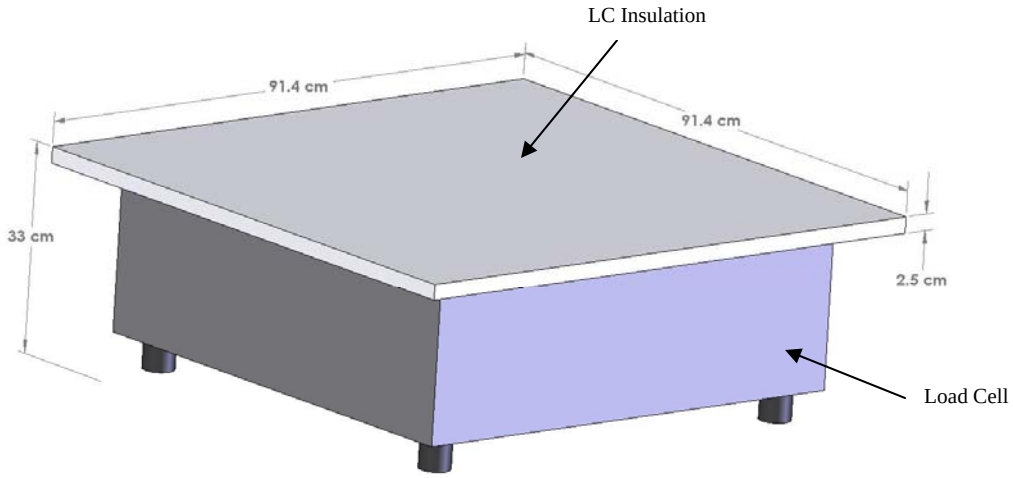

Figure 3.19b: Free-Burn Load Cell Platform for 3/8 Scale

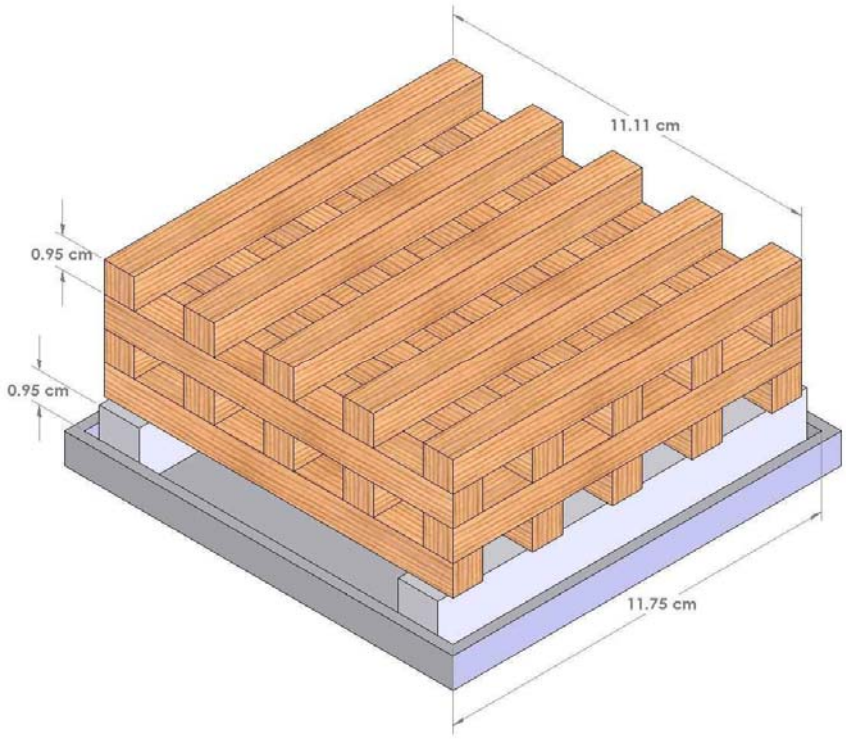

Figure 3.20: 1/8 Scale, Small Design Wood Crib & Ignition Model

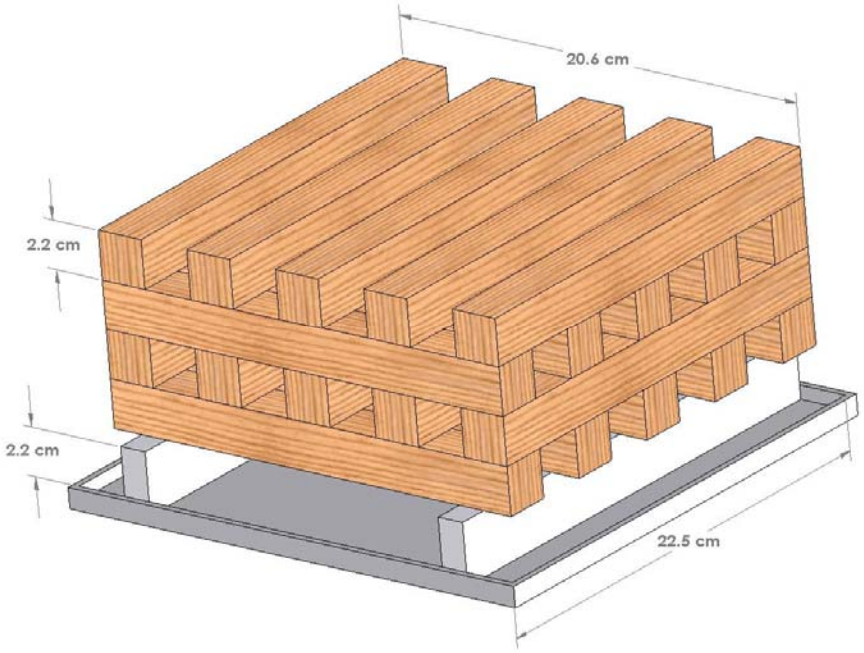

Figure 3.21: 1/8 Scale, Large Design Wood Crib & Ignition Model

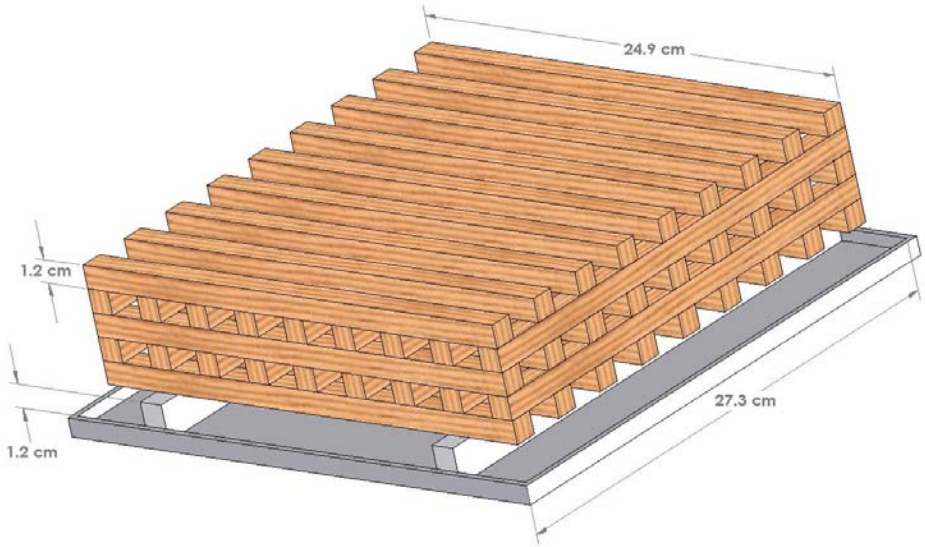

Figure 3.22: 2/8 Scale, Small Design Wood Crib & Ignition Model

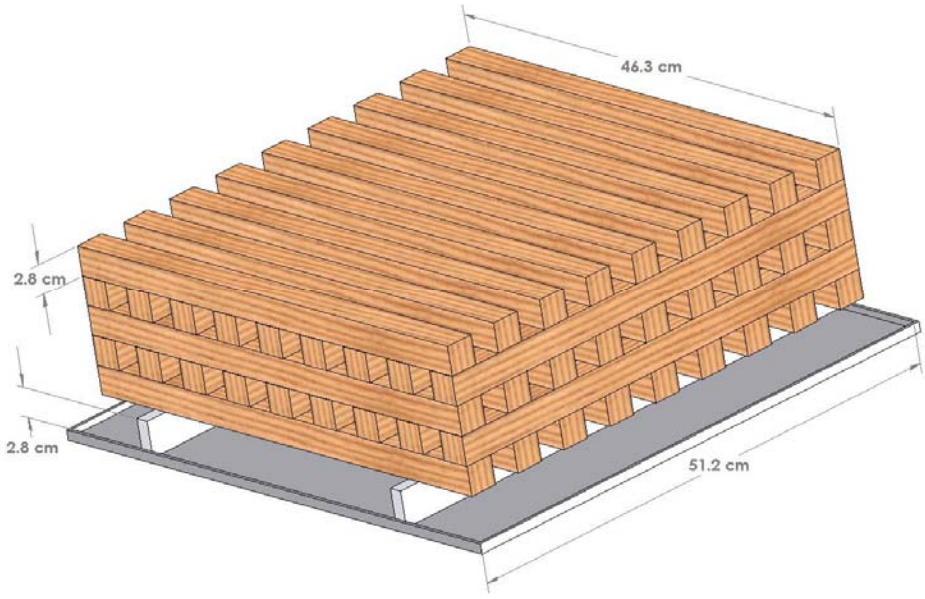

Figure 3.23: 2/8 Scale, Large Design Wood Crib & Ignition Model

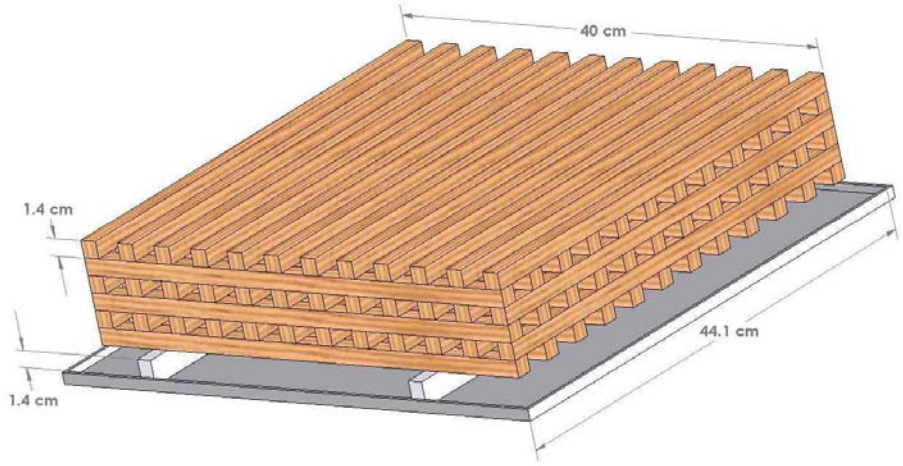

Figure 3.24: 3/8 Scale, Small Design Wood Crib & Ignition Model

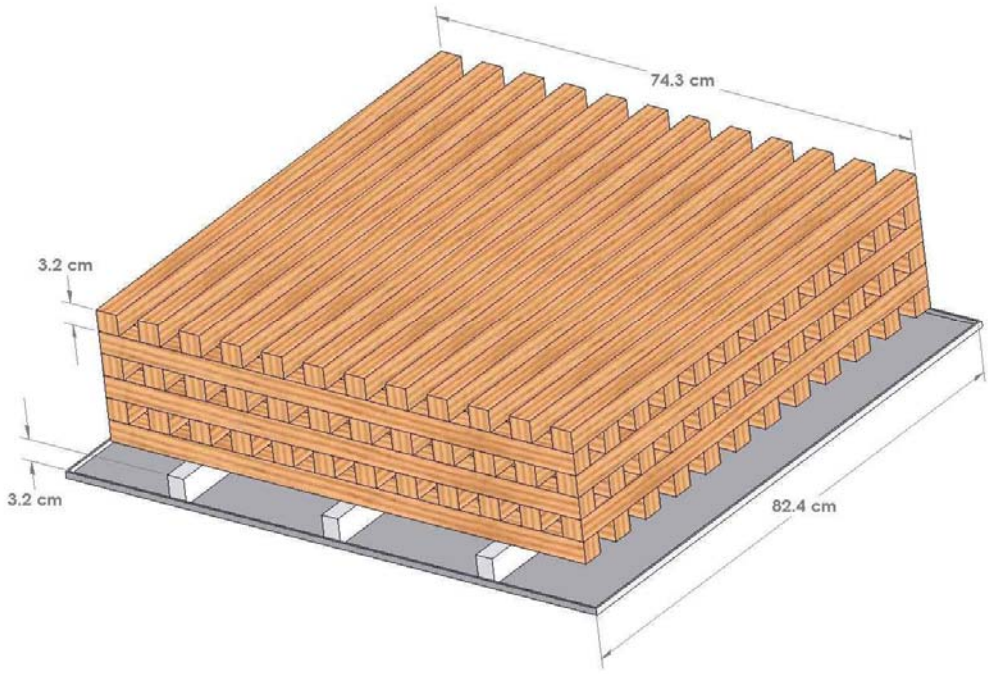

Figure 3.25: 3/8 Scale, Large Design Wood Crib & Ignition Model

A third elevation strip had to be used in the large crib design for the 3/8 scale model in order to support the large weight of the fuel. The use of this strip did block some airflow underneath the crib; however, the effect was not appreciable in the results.

3.3.2 Compartment Design

3.3.2.1 Application of Scaling Theory

The scaling theory had been applied to the fire source and an attempt had been made to scale the ventilation influence of the compartment on the burning rate. The final step in the design phase was to scale the thermal feedback from the enclosure boundaries. As a result of these design measures, the most significant influences on the burning rate were given proper attention in the model.

Heat generated by the wood crib fire travels from the source to the compartment boundaries via convection and radiation. The heat that is lost from the compartment is either conducted through these solid boundaries, or lost through the vent opening. It is assumed that geometric scaling of the enclosure accompanied by the proper scaling laws outlined for the wood crib source will regulate the heat losses through the vent. It is possible that some inconsistencies will arise in the scaling of heat transport to the wall; however, if both the energy generation and the wall's thermal response are scaled, then the global energy equation should properly balance.

The scaling of the thermal response of the wall is accomplished by ensuring two critical balances in the flow. The first is the enthalpy flow to the wall versus the conduction loss through it. This balance is symbolized by the dimensionless group $\pi_{conduction}$.

$$\pi_{conduction} \equiv \frac{\left(k\rho c_p\right)_{wall}^{1/2}}{\rho_\infty c_p g^{1/4} l^{3/4}} \tag{3.46}$$

The ambient design fluid that will be used throughout experimentation is air. The thermal properties of air along with the gravitational constant are all assumed to be independent of scale. Therefore, the theory suggests that the practical balance of these flow properties reduces to a change in the thermal inertia of the wall material.

$$\left(k\rho c_p\right)_{wall} \approx H^{3/2} \tag{3.84}$$

A second wall property balance must be considered simultaneously with the thermal inertia. This is the balance between the thermal and physical thickness of the solid boundary.

$$\pi_{thickness} \equiv \frac{\delta_{wall}}{\left[\left(\frac{k}{\rho c_p}\right)_{wall}^{1/2}\left(\frac{l}{g}\right)^{1/4}\right]} \tag{3.47}$$

Once again, the gravitational acceleration is assumed independent of scale. The balance then reduces to the following length scale dependency:

$$\frac{\delta_{wall}}{\alpha_{wall}^{1/2}} \approx H^{1/4} \tag{3.85}$$

Initial attempts to perform these two balances by selecting various sets of materials assumed that the thermal conductivity and density of the wall follow the same length scale relationship. In addition, the specific heat of the material was assumed to be independent of scale. This simplification dictates that the thermal diffusivity of the solid is independent of scale and the relationship between the wall thickness and length scale can be determined in a straightforward manner from Equation 3.85.

This approach to scaling the wall materials may be sufficient for an analysis of thermal properties at a single ambient temperature. However, the subtlety in this selection process that is missing in previous scaling attempts is the recognition that the operating temperature of these boundaries is not ambient during experimentation[20]. The thermal properties of the solid are strongly influenced by temperature. This is especially true for the thermal conductivity of the solid which may change as much as 300% over the range of temperatures encountered in an enclosure fire[27]. Such a drastic change in thermal properties at elevated temperatures can lead to considerable scaling inconsistencies[28]. Consideration of this simple but undoubtedly critical piece of applied materials science has been entirely lacking in all previously published scaling attempts. This lack of consideration is the product of a simple lack of available data for such materials in the

temperature ranges of interest. Luckily, the current research was equipped with a materials database capable of taking this transient factor into consideration. This critical design resource led to a different approach in the selection of materials. Rather than selecting a thermal conductivity, density, specific heat and thickness separately, the entire quotients presented in Equations 3.84 and 3.85 were scaled as functions of a wide range of possible exposure temperatures.

Just as with the design of the wood cribs, the fictitious full scale prototype must be designed to provide a reference for the models. In this case, this means selecting a boundary material for the full scale enclosure. Obviously, in the construction of an actual life-sized room, composite materials are used for walls which are likely different than the materials used for the floor and ceiling. The current research is focused on producing a fundamental experimental validation of the scaling theory. Therefore, a simplifying assumption was made. This assumption was that all of the compartment boundaries in the full scale prototype were constructed of the same material.

Gypsum board, or drywall as it is also called, is very commonly used as an interior lining in both residential and commercial occupancies. In fact, it is the most common interior lining used to provide fire resistance to light frame structures[13]. The fact that gypsum board is used as an interior lining means that it is the first line of fire resistance for the walls and ceiling.

Fire resistant gypsum wallboard is generically referred to in the United States and Canada under the designation Type X. This category of drywall is specified by a fire resistance rating. In order to be designated as Type X board, a sample of the material must be fixed to a wall stud assembly and exposed to the furnace conditions of ASTM

E119. A Type X board will maintain its own internal structural and thermal integrity for a period between 45 minutes and 1 hour for either a 12.7 mm or 15.9 mm thickness respectively[13]. Based on the above discussion, a full scale thickness of 15.9 mm was chosen for the prototype walls. It was recognized that this thickness did not equate to the fire resistance of the assembly above. The thickness was chosen to represent a basic design for a single layer of commonly used material.

A review of available data for the thermal properties of gypsum wallboard lead to research performed by the National Research Council of Canada on special purpose Type C Gypsum Board. The difference between Type X and Type C is minimal. Type C is a special purpose board that typically contains some additives to slightly increase fire resistance[13]. Due to this similarity and the readily available data for Type C, the full scale prototype compartment material was designated as Type C with a thickness of 15.9 mm. The available data for specific heat, density and thermal conductivity is for an exposed sample with a square cross section of 13 mm and a length of 76.2 mm. The data is shown in Figure 3.26.

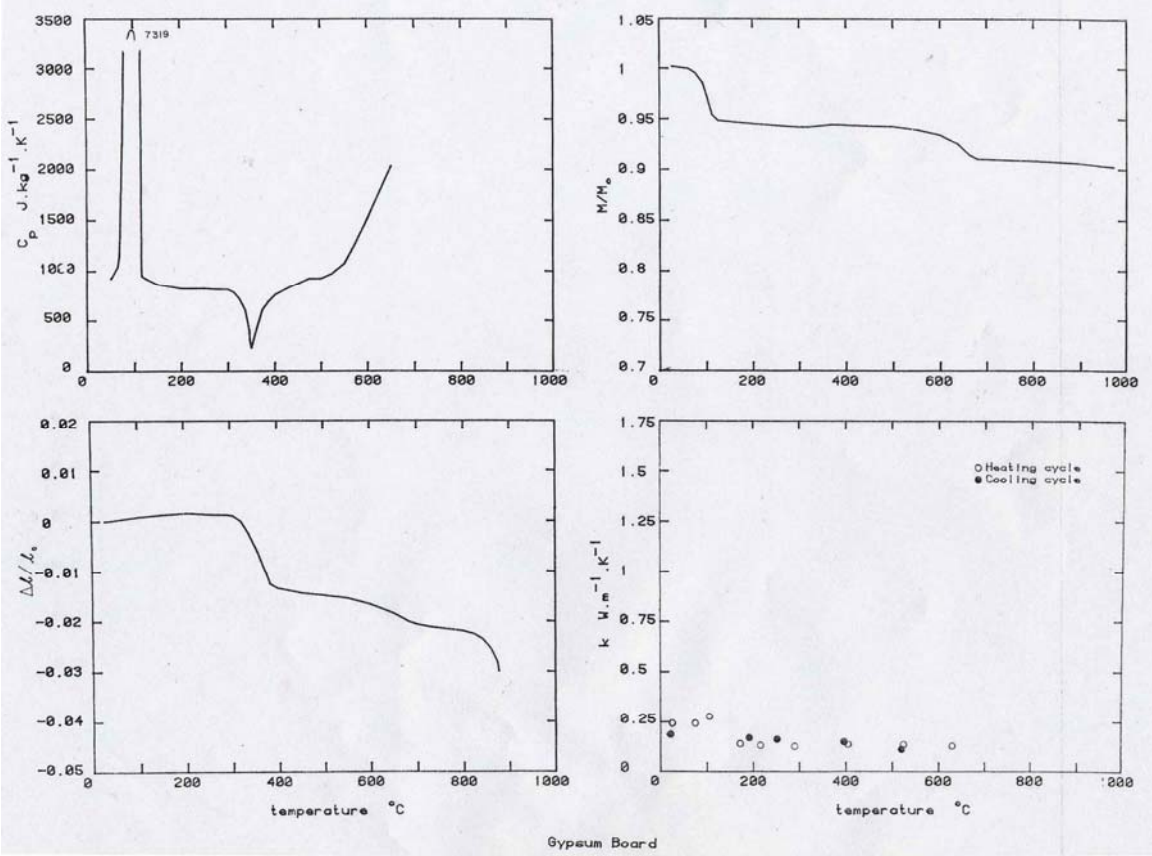

Figure 3.26: Thermal Properties of Type C Gypsum Board at Elevated Temperatures[28]

There are a few critical things to note about the data presented in Figure 3.26. The specific heat at constant pressure of the gypsum board shows a dramatic spike in the range of 100°C – 120°C. This is evidence of what is known as a calcination reaction. The dramatic increase in specific heat indicates an endothermic reaction as water present in the material changes phase. The result of this dehydration is a loss in structural integrity. This process is completed at approximately 700°C, where a second endothermic reaction is apparent and the data in Figure 3.26 abruptly ends. The abrupt dip in the specific heat curve at approximately 400°C is accompanied by a significant shrinkage in the sample marking a loss of strength in the binder[13,28].

In order to obtain density values for the sample by processing the change in mass and volume with respect to temperature, the data in Figure 3.26 was digitized. The initial density of the sample was listed as 678 kg/m^3. The result of digitizing the data was a set of discrete data points for thermal conductivity, specific heat and density. These discrete points did not correspond to exactly the same temperature values. Therefore, in order to obtain the thermal inertia of the sample as a function of temperature, an averaging scheme was used. The available data in Figure 3.26 spanned a domain of 20^{o}C-700^{o}C. Data for each of these properties was therefore averaged over seven sub-domains of 100^{o}C. The average values of thermal inertia for these sub-domains were then plotted at the midpoint of the temperature sub-domain. For example, the average thermal inertia between 100^{o}C and 200^{o}C was plotted at a temperature of 150^{o}C. The results of this data extraction were then scaled according to the relationships presented in Equations 3.84 and 3.85.

Material for the models was selected with the intent of scaling to a primary and secondary target. The primary scaling target was a comparison of thermal properties between the various model scales. The secondary scaling target was the comparison of the model thermal properties to those of gypsum wallboard at the fictitious full scale. Clearly, the primary target holds greater importance in demonstrating the validity of the scaling theory. The data for the gypsum wallboard merely offers a realistic perspective of the potential full scale applicability of these models. The results for the enclosure material selection are shown in Figures 3.27 and 3.28.

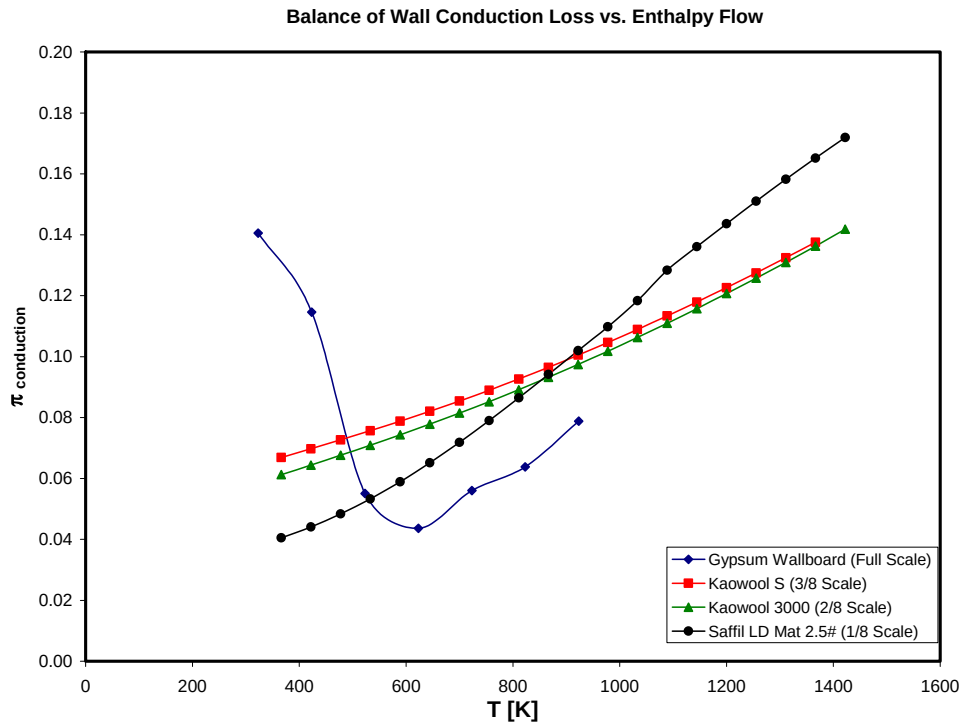

Figure 3.27: Balance of Conduction Loss and Enthalpy Flow

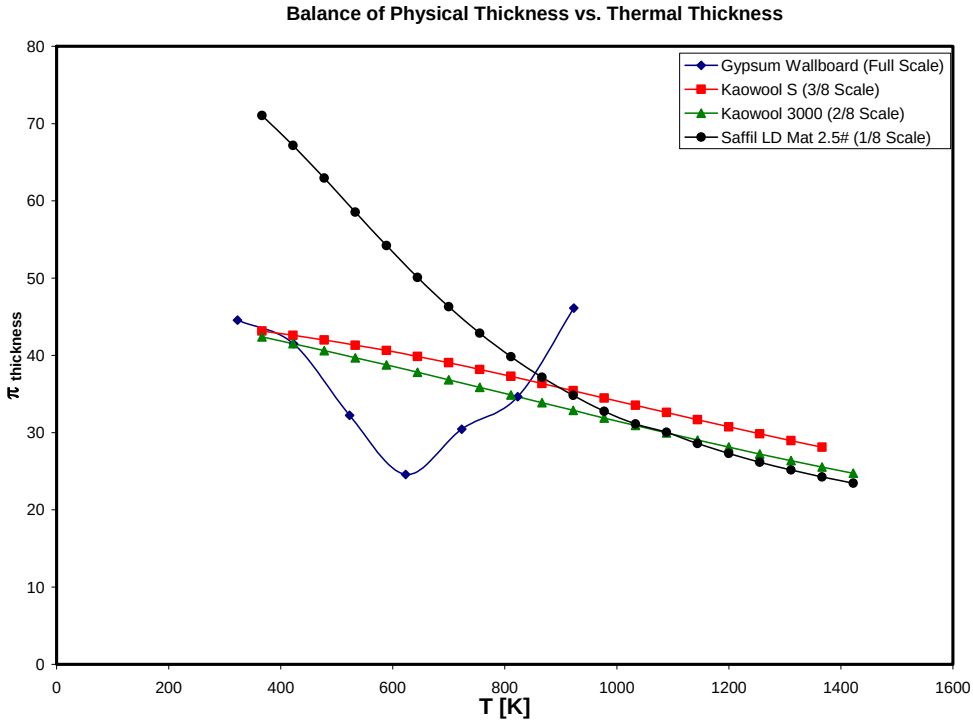

Figure 3.28: Balance of Physical and Thermal Wall Thickness

The result of the balance shown in Figure 3.28 was the selection of specific wall thicknesses for the various materials. The thickness chosen for the 1/8 scale model Saffil material was 34 mm. The remaining model scales were both constructed with an identical wall thickness of 13 mm. The difference in the thermal thickness of the materials allowed for the proper balance to be achieved in Figure 3.28.

The choice of materials illustrated in the above plots incorporates the use of trade names. In order to appreciate the type of materials chosen, their chemical properties are presented in Table 3.13. The density of the materials is decreasing with length scale. Note that the 1/8 scale model is constructed of a blanket material.

Product Trade Name	Chemical Composition	Material Type
Gypsum Wallboard	$CaSO_4 \cdot 2H_20$	Rigid Board
Kaowool S	46% Alumina, 53% Silica, Trace	Rigid Board
Kaowool 3000	66% Alumina, 34% Silica	Rigid Board
Saffil LD Mat 2.5#	~96% Aluminum Oxide, ~4% Silica	Blanket

Table 3.13: Chemical and Physical Properties of Enclosure Materials[27]

The balance of wall thermal properties as a function of exposure temperature gives rise to an important question. What average peak gas temperatures are expected to be produced in these model compartments? To answer this question, the results of the C.I.B. research were utilized[16]. This research compiled over 300 wood crib fires in compartments of various sizes. All of the fires were fully developed. The fires in the current research are expected to be fully developed as well, based on the amount of fuel and the size of the compartments. Figure 2.16 shows the results of the C.I.B. tests in the form of an average peak gas temperature prediction as a function of the compartment

opening factor. The opening factor is not itself a dimensionless quantity. Therefore, it is not independent of length scale. The data in Figure 2.16 predicts a range of peak temperatures between 600^{o}C and 700^{o}C for the current models. This translates to a range of approximately 900 – 1000 K as applied to the wall thermal properties shown in Figures 3.27 and 3.28. The advantage of applying the C.I.B. data is the ability to focus on a specific temperature domain in Figures 3.27 and 3.28. It is recognized that the correlation used to fit the data in the C.I.B. analysis is lacking in its consideration of ventilation limitations; however, the comparison to this research provides a baseline perspective.

3.3.2.2 Measurement and Instrumentation

Measurements were taken at homologous locations in each of the model compartments. These measurements included gas temperatures, solid surface temperatures, gas composition, surface heat flux and fuel mass. The instruments used to make these measurements are described in the following section of the report. The exact locations of the instruments will be shown in the section dealing with construction.

3.3.2.2.1 Gas and Solid Surface Temperatures

Type K chromel-alumel thermocouples were used to measure both gas and solid surface temperatures throughout the compartment. The instruments were equipped with 15.2 cm long Inconnel 600 probe sheathing leading from the connector assembly to the base of the bead. The diameter of the bead was 0.035 mm. Following experimentation with the 1/8 scale model enclosure, it was found that connectors for thermocouples

placed in the doorway had to be properly protected from exposure to flame. For this reason, different thermocouples were substituted for use in the doorway. These thermocouples were once again Type K chromel-alumel. The wire was shielded over a distance of 30.5 cm by a ceramic tube. The beads for these thermocouples were approximately 0.1 mm in diameter.

The desired locations were vertically aligned in the plane of the vent, vertically aligned inside the compartment, on the inner surface of the ceiling and the inner upper surface of an arbitrary wall. These locations will be shown in much greater detail in the next section on compartment construction.

3.3.2.2.2 Gas Composition

Gas composition was measured at a representative location in both the upper and lower layers of the compartment. This was accomplished with the use of 4 separate analyzers for each of the gases of interest. The mole fraction of oxygen was the only gas to be measured in both the upper and lower layer. Two *Servomex Oxygen Analyzers, Model 540A*, were used to collect this data. The sampling tube positioned in the upper layer of the compartment also fed the compartment gases to two separate *Horiba PIR-2000* gas analyzers. The first of these analyzers measured the mole fraction of Carbon Dioxide. The second measured the mole fraction of Carbon Monoxide.

The path of the gas from the compartment to the analyzer contained several important features. It is known that water vapor and Carbon Dioxide both affect the accuracy of the oxygen analysis. The gas tubing was passed through a 50 cm x 30 cm x

30 cm cooler filled with ice in order to condense the water vapor and thus remove it from the gas inside the tube.

After passing through this cold trap, soot was filtered from the gas with the use of a *Type-304 Fisher Scientific* soot filter with an *Advantest Glass Sheet Filter Model 934-AH*. Once the gas had passed through the soot filter, it was pumped to the various analyzers. An electric vacuum pump with a flow rate of 60 mL/min and a bypass flow rate of 1.01 mL/min was used. Just prior to reaching the oxygen analyzers, the gas was passed through a Drierite® (Anhydrous Calcium Sulfate) filter to further absorb moisture and an Ascarite® (Sodium Hydroxide coated non-fibrous Silicate) filter to remove Carbon Dioxide. All filters were changed and replenished after each experiment.

3.3.2.2.3 Heat Flux

Two Schmidt-Boelter type Heat Flux Transducers were used to measure the incident heat flux to the floor and ceiling of the compartment respectively. The devices were both Medtherm Model 64-10-20 with water cooling provisions. The gauges were supplied with cooling water at a laminar flow rate on the order of 10 mL/s during testing.

3.3.2.2.4 Fuel Mass

The fuel mass was recorded with the use of the same load cells used for the free-burning wood crib experiments.

3.3.2.2.5 Data Acquisition

The data acquisition systems used in the compartment experiments were the same as those used for the free-burns. For the 3/8 scale model, two *NetDAQ* data acquisition systems were used in order to provide the necessary number of data channels.

3.3.2.3 1/8 Scale Model Compartment Construction

Table 3.13 notes that the material used to construct the 1/8 scale model compartment was a blanket fabric. This presented two major challenges in constructing a rigid compartment. The first of these challenges was to produce semi-rigid boundaries that would not collapse during testing. The second was to ensure that the flexibility of the material would not result in inconstancies in the physical thickness of the wall.

Selection of a different kind of material for this scale model was a desirable alternative solution. A broad survey of ceramic materials from multiple manufacturers was conducted prior to selecting the Saffil material. The results of this survey were used to make the comparisons shown in Figures 3.27 and 3.28. Clearly, this process involves a delicate balance between thermal and physical properties that are theoretically desired and those that are practically manufactured. Generally speaking, the density of the wall material decreases with the length scale of the model. The design of the 1/8 scale model called either for the use of a low density blanket material or an unrealistic compensation in the physical thickness of a rigid board.

Thus, to meet the challenges outlined above, an aluminum frame was constructed to serve as a supporting outer boundary for the enclosure. The frame was welded together from individual pieces of 0.6 cm thick aluminum angle with a 6.4 cm flange.

The welding produced two separate sections of the frame such that the attached ceiling and columns could be removed from the floor piece. This was done to accommodate future work with the experimental structural steel frame mounted inside of the fire compartment. The ability to remove all but the floor of the compartment provides the necessary large degree of access to the experimental frame.

Two methods were used to attach the blanket to the supportive frame. The first was the application of furnace cement along its flanges. The second method was the insertion of 10 all thread rods approximately 0.3 cm in diameter. With the exception of the front face of the enclosure, 2 rods were used for each face. The rods were inserted along the plane of the surface, dividing its area approximately into thirds. The position of insertion with respect to the wall thickness was at the desired thickness of the material. Thus, the function of the rods was to prevent the material from bulging and causing inconsistencies in the wall thickness. Once inserted through the aluminum angles, the rods were held in place with wing nuts fastened to the aluminum surface. The rods ultimately served an additional purpose of joining together the two separate sections of the frame.

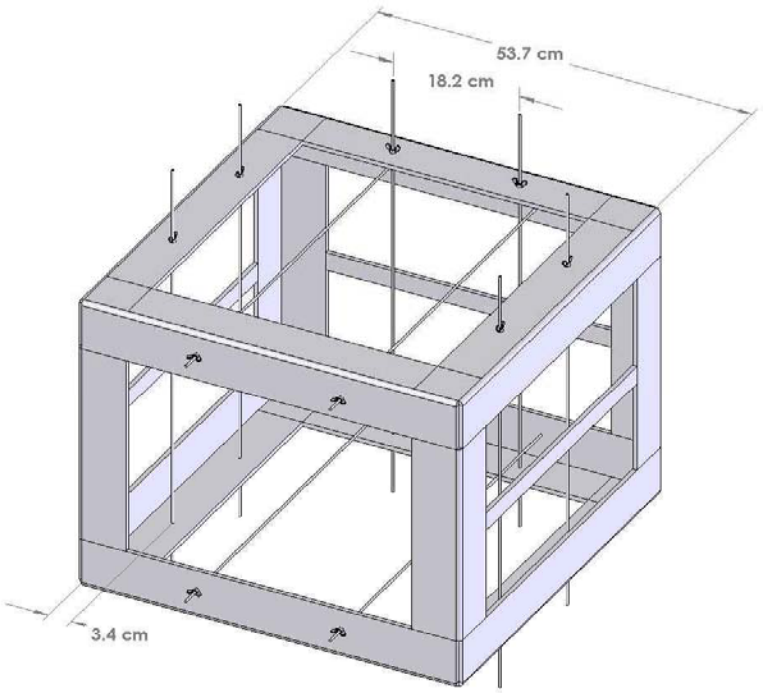

Figure 3.29: 1/8 Scale Model Compartment Frame

The compartment had to be elevated off of the floor for two reasons. The first was a desire to measure the mass loss rate of the fuel from underneath the compartment with the use of a load cell. The second was the obvious protrusion of the supporting rods through the bottom plane of the enclosure shown in Figure 3.29. The compartment was thus elevated by simply placing 4 cement blocks underneath the frame, one at each corner. The height of the compartment above the floor thus required the construction of a simple platform for the load cell.

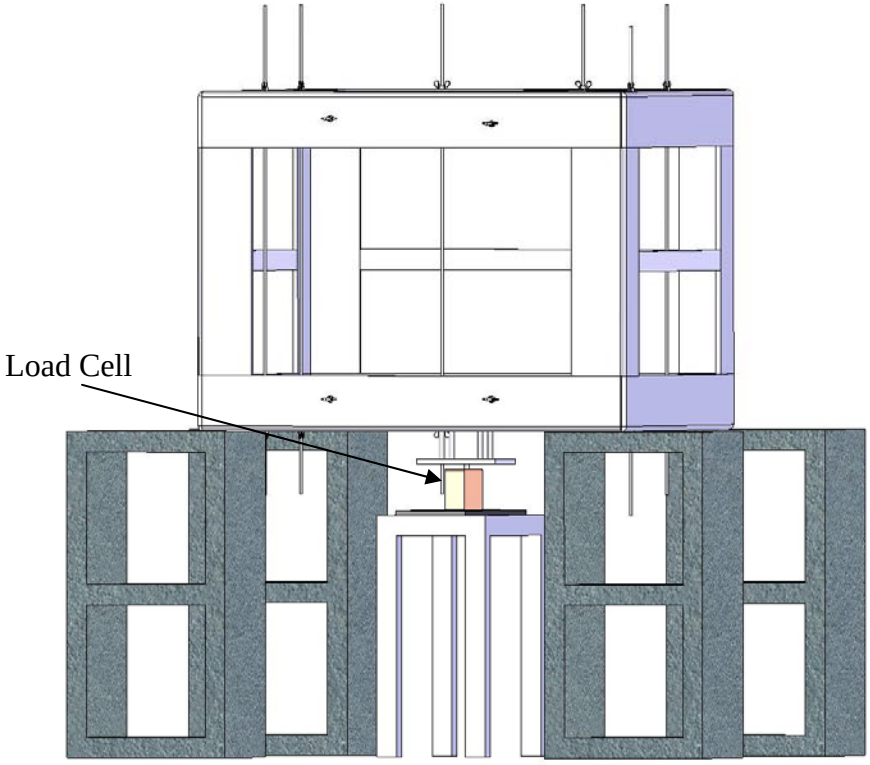

Figure 3.30a: 1/8 Scale Model Load Cell Positioning – Front View

The aluminum platform attached to the top of the load cell during the free-burning experiments was also used for the compartment fires. The top plate of this platform was detached in order to allow the legs of the platform to penetrate the compartment floor as shown in Figure 3.30b. The plate was then reattached to the legs and insulation was placed over top of it to protect it from heat.

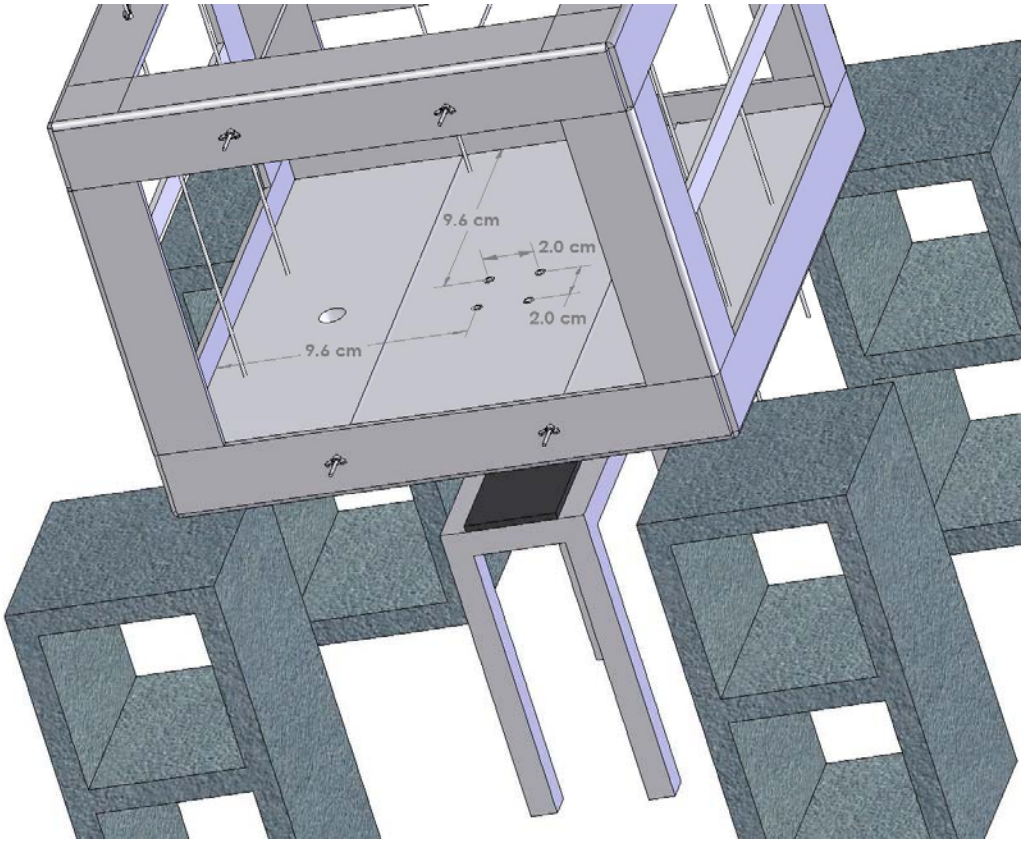

Figure 3.30b: 1/8 Scale Model Load Cell Floor Penetration

Gas sampling tubes were both inserted in the right wall of the compartment at the midpoint of the compartment depth dimension. The copper ends of these tubes are shown in the design drawings. Certain pieces of the supporting frame have been removed for the sake of presentation clarity.

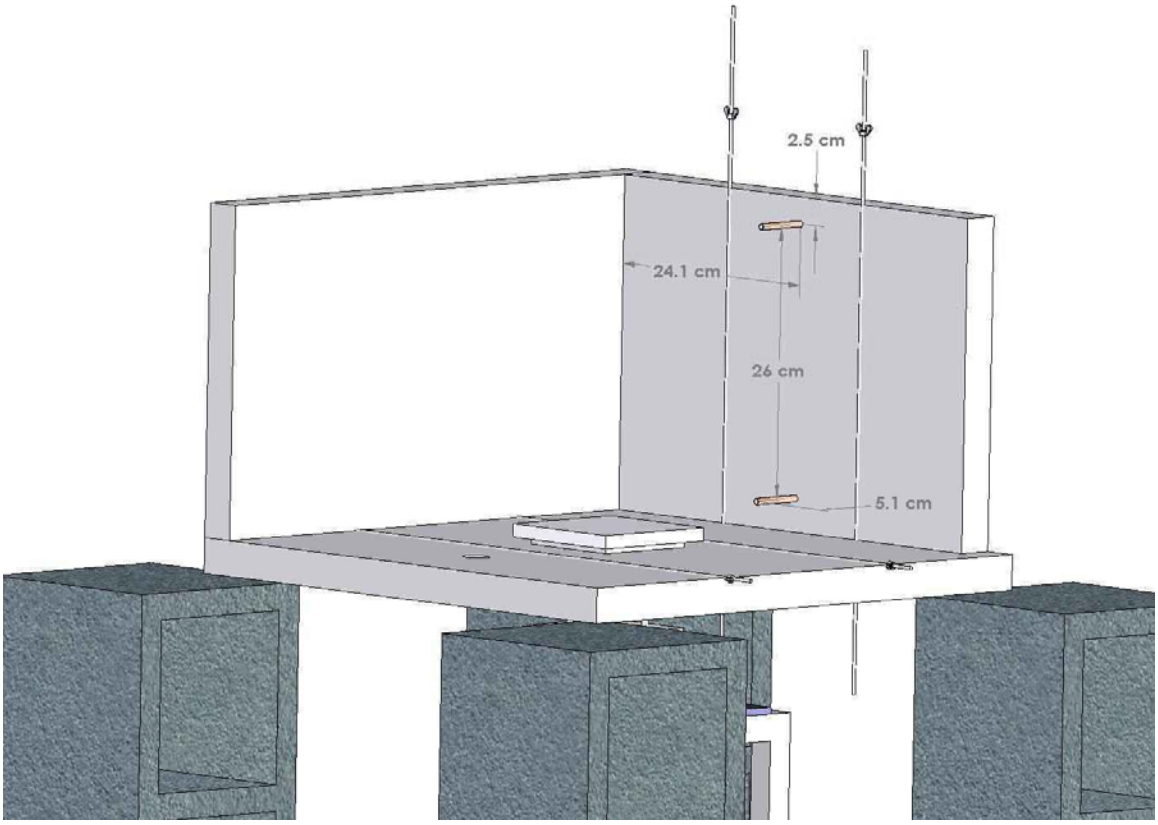

Figure 3.31: 1/8 Scale Model Gas Sampling Tube Locations

Heat flux gauges were inserted through circular holes made in the floor and ceiling. The top surface of the meter was aligned in the plane of the compartment boundary surface. Figures 3.32a and 3.32b depict the placement of these gauges.

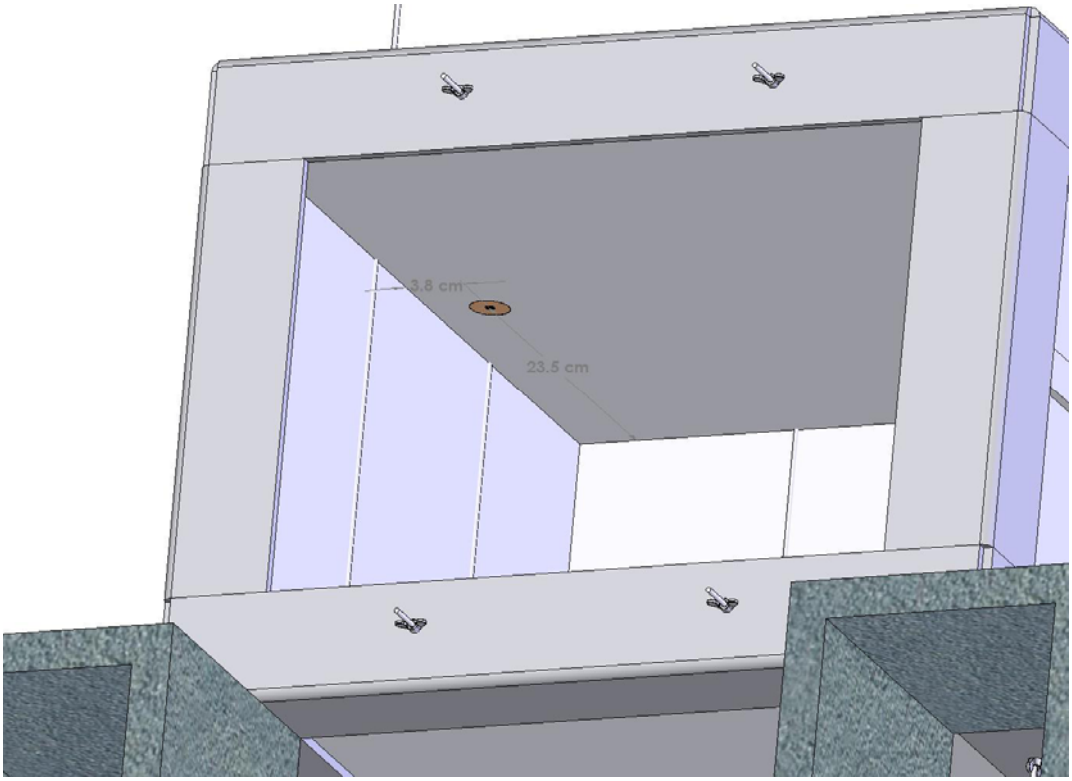

Figure 3.32a: 1/8 Scale Model Ceiling Heat Flux Location

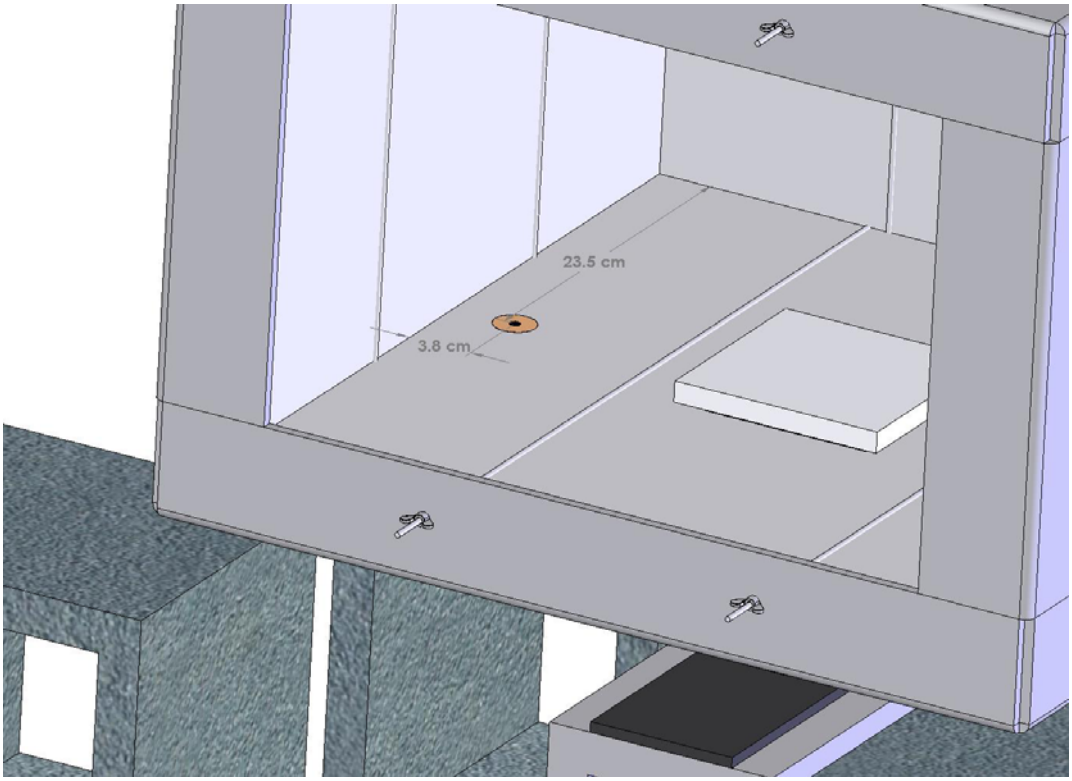

Figure 3.32b: 1/8 Scale Model Floor Heat Flux Location

Thermocouples were used to provide a vertical profile of gas temperatures inside the compartment. Eight thermocouples were used in this profile, located in approximately the same vertical plane as the heat flux gauges.

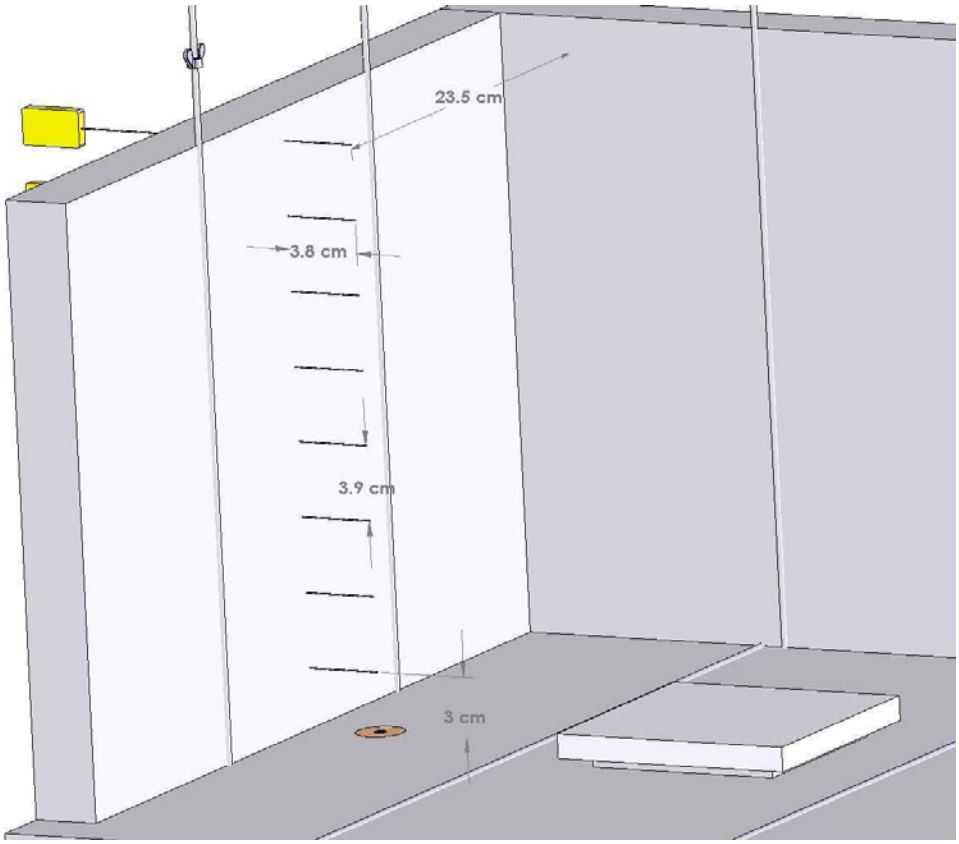

Figure 3.33: 1/8 Scale Model Interior Gas Temperature Measurements

The temperature of the ceiling surface is taken by placing a thermocouple bead on the surface of the ceiling more towards the center of the surface. The upper wall surface temperature is taken with the placement of a thermocouple bead on the surface of the right compartment wall. The height of the bead is identical to the height of the upper layer gas sampling tube. The thermocouple is positioned approximately 3 cm closer to the front wall of the compartment than the gas tubes. The only remaining

instrumentation is found in the plane of the vent. The placement of these thermocouples is shown in Figure 3.34.

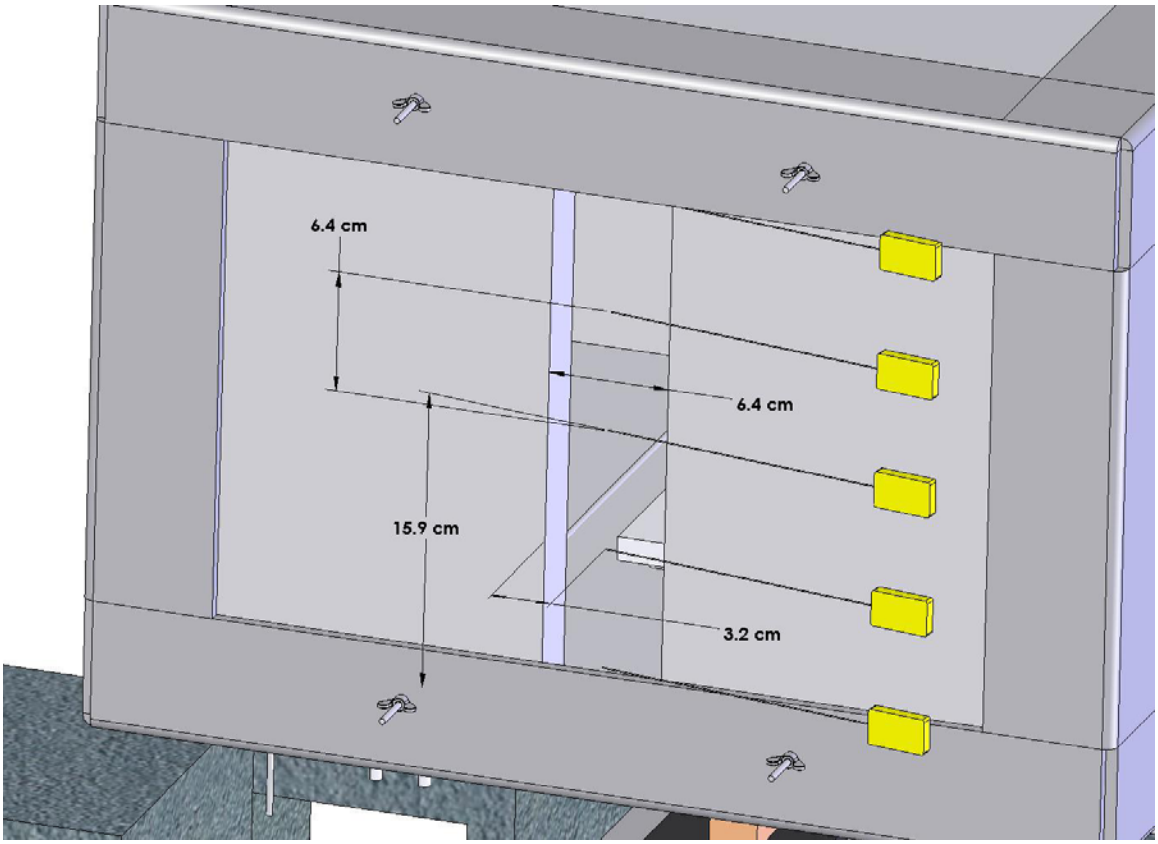

Figure 3.34: 1/8 Scale Model Vent Thermocouple Placement

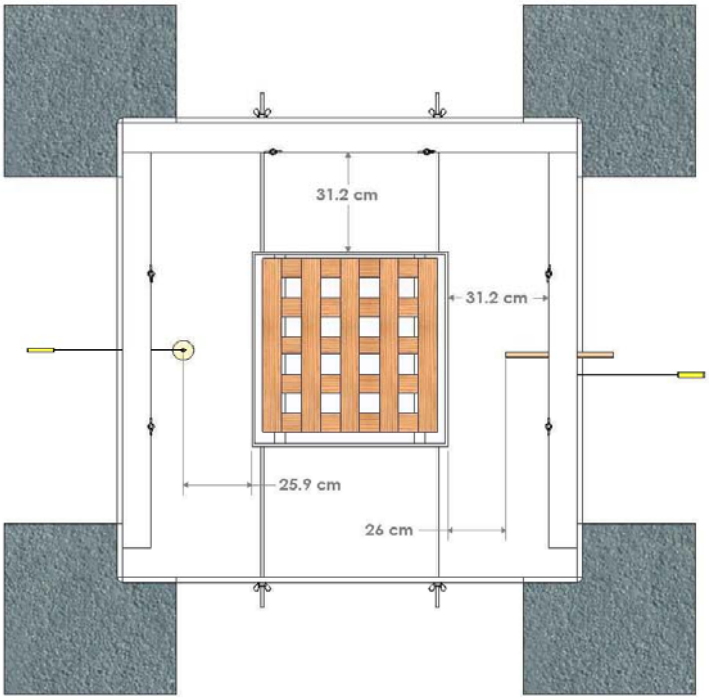

Figure 3.35: 1/8 Scale Model with Large Crib Design: Top View

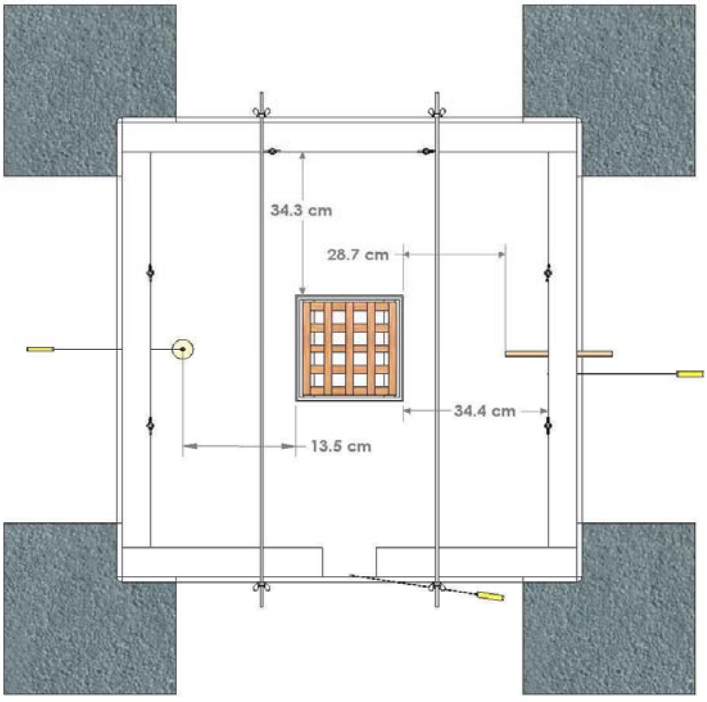

Figure 3.36: 1/8 Scale Model with Small Crib Design

The finished compartment contains the wood crib and ignition model placed centrally atop the load platform. No changes are made in the placement of instrumentation between the small and large design fires.

3.3.2.4 2/8 Scale Compartment Construction

The material selected for the intermediate enclosure was *Kaowool 3000*. Material flexibility was not a concern for this rigid board. The compartment was geometrically scaled and therefore was double the size of the 1/8 scale model. Instrumentation was placed in homologous locations within the compartment. The lone exception was the depth of the gas sampling tubes in the compartment. Testing with the 1/8 scale model revealed the possibility of a blockage in the tubing perhaps due to close proximity of the tube to the crib. For this reason, it was decided to keep the gas sampling tubes at the same depth into the compartment at all scales. The scaling suggests that the depth should have been doubled for the intermediate enclosure and tripled for the large enclosure. However, the assumption of uniform gas composition across a horizontal layer of the compartment is already being made by the designation of only two instruments to account for a lower and an upper layer respectively.

The insulation board for the intermediate compartment came in rectangular boards of 91.4 cm length, 121.9 cm width and 1.3 cm depth. Once again, a supporting frame was constructed for the material; however, in this case, there was no need for additional supporting rods in the frame. The fact that the dimensions of the compartment boundaries exceeded the dimensions of the available board meant that multiple boards were used to construct a single wall. In anticipation of this design parameter, the

supporting frame was equipped with additional horizontal supports along its outer boundaries. Boards were joined together at the seams with *CeraKote-Mod* high temperature cement. The supports further ensured that seams between boards would not bow out of place.

The supporting frame was once again welded together into two separate pieces. The material used for this frame was stainless steel angles with a 2.5 cm flange and a 0.3 cm thickness. Unlike the smaller compartment, the columns attached to the floor rather than the ceiling. The ceiling was therefore the removable piece for access between testing. This larger compartment was of sufficient physical dimensions to allow for eventual work with a frame inside the enclosure by simply removing the ceiling.

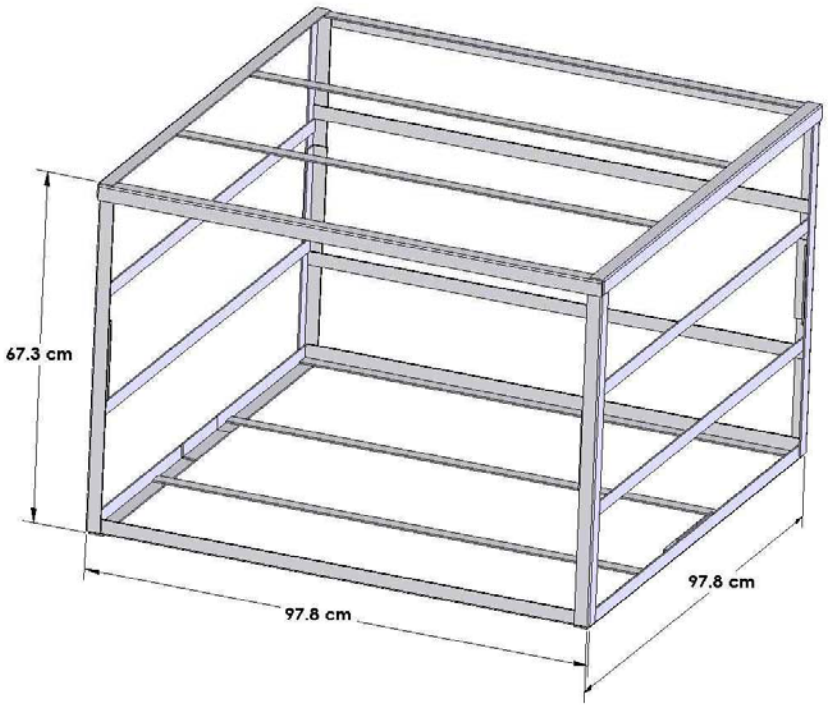

Figure 3.37: 2/8 Scale Model Supporting Frame

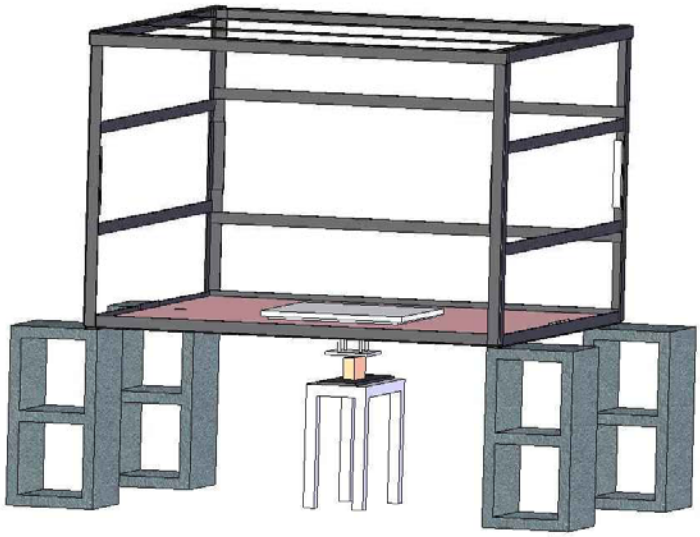

Figure 3.38: 2/8 Scale Model Load Cell Positioning – Front View

The size of the top plate of the load cell platform for the two larger enclosures was increased from 10.2 cm x 10.2 cm to 30.5 cm x 30.5 cm. This was done to ensure that the larger cribs would balance properly on the platform.

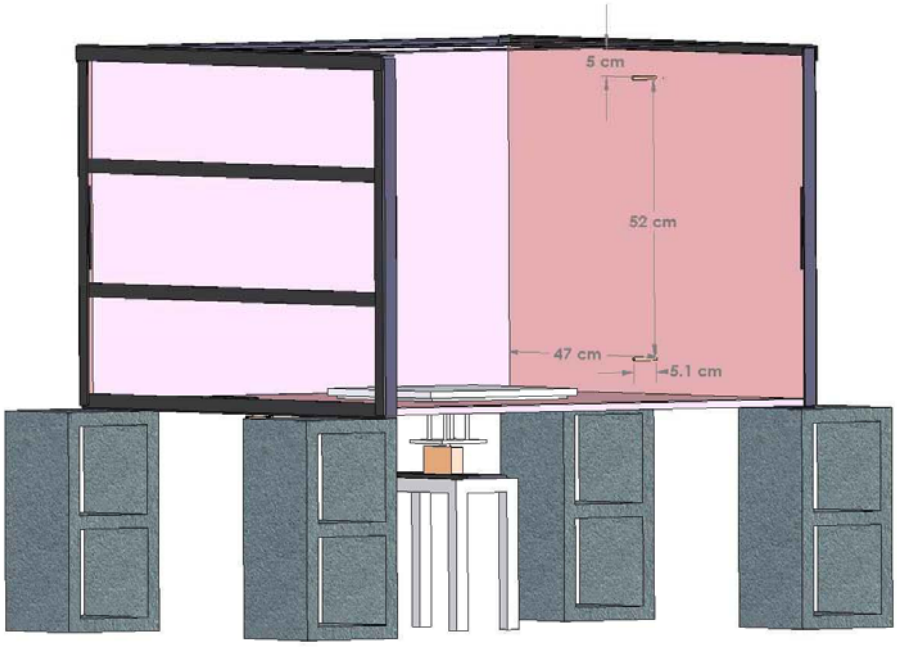

Figure 3.39: 2/8 Scale Model Gas Sampling Tube Locations

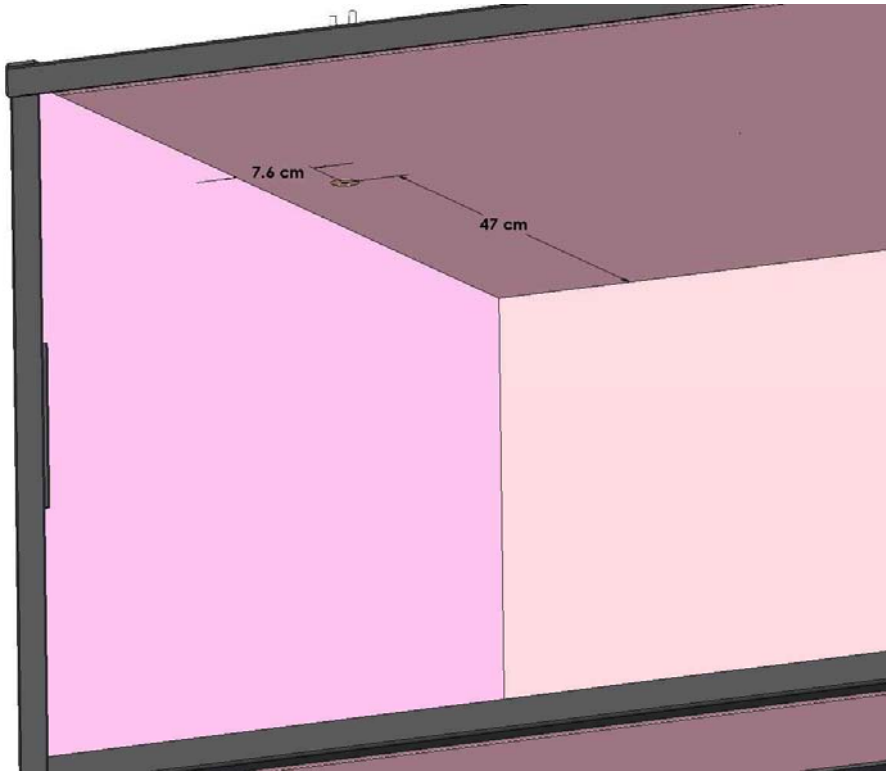

Figure 3.40: 2/8 Scale Model Ceiling Heat Flux Meter Location

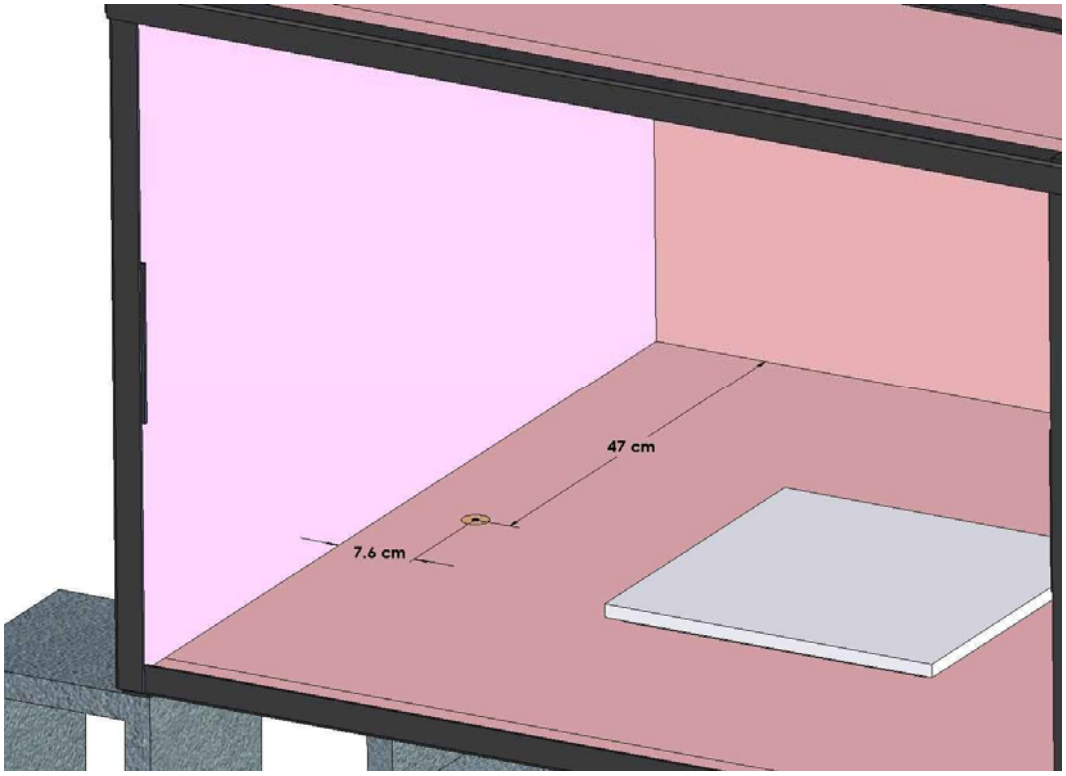

Figure 3.41: 2/8 Scale Model Floor Heat Flux Meter Location

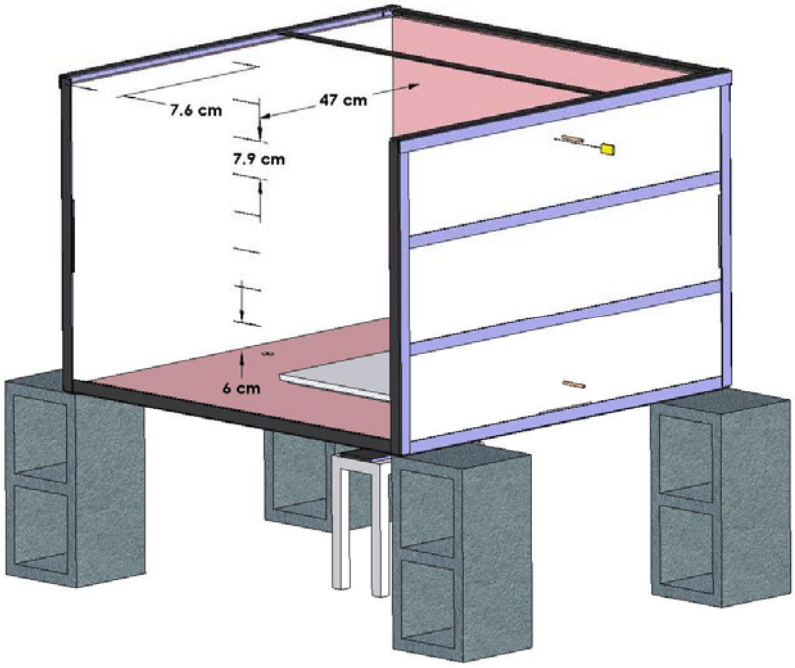

Figure 3.42: 2/8 Scale Model Interior Gas Temperature Measurements

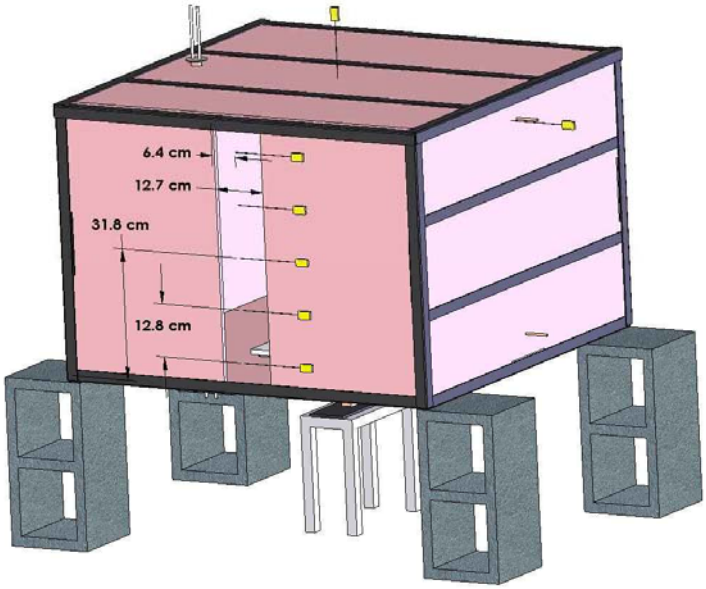

Figure 3.43: 2/8 Scale Model Vent Thermocouple Placement

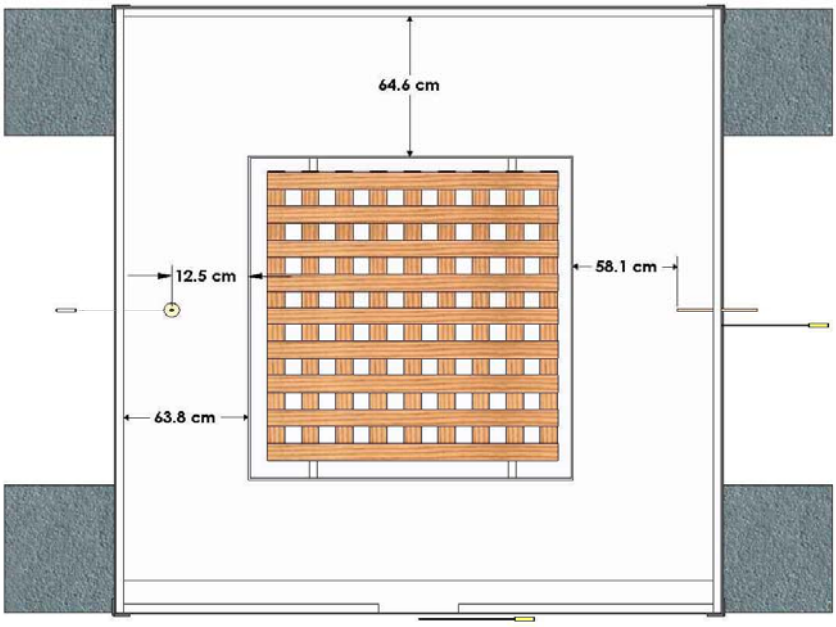

Figure 3.44: 2/8 Scale Model with Large Crib – Top View

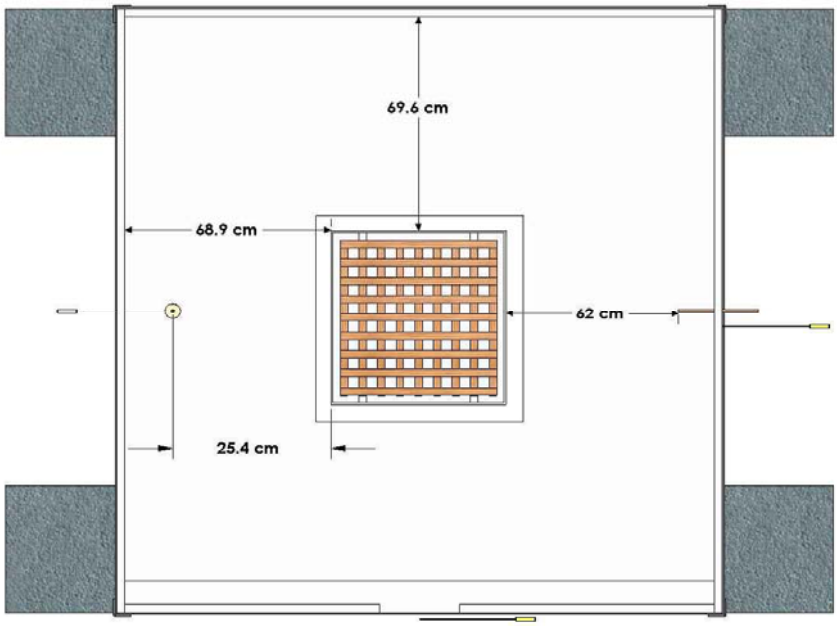

Figure 3.45: 2/8 Scale Model with Small Crib – Top View

3.3.2.5 3/8 Scale Compartment Construction

The 3/8 Scale model enclosure was constructed from *Kaowool S* rigid board insulation. Once again multiple boards were used for each of the compartment boundaries. In the case of the 2/8 Scale model, an addition fraction of a board was used to complete the floor and ceiling. For the 3/8 Scale model, the overall size of the compartment is increased in all directions. Unfortunately, the standard board size for the *Kaowool S* material was 61 cm wide and 91.4 cm long. The result was as many as 5 seams in a single boundary of the compartment. It was found that at this size, the furnace cement typically used to bond the board together lacked sufficient strength to hold the boards in place at the seams. Therefore, the supporting frame of the compartment was

used extensively for the support of the floor and walls. The frame was once again constructed of angle steel with a 2.5 cm flange and a thickness of 0.3 cm.

Recall that all 3/8 Scale model testing was to be conducted at the ATF Laboratory. The load cell used for these experiments was a 1000-lb capacity *Sterling Scale, Model 810-N4*. Rather than use a platform to penetrate the floor of the compartment as in the smaller models, this particular load cell was used to weigh the entire 3/8 scale compartment. The decision to weigh the fuel in this manner meant that the compartment itself had to be elevated above the floor during testing. This meant that the floor of the compartment had to be capable of supporting not only its own weight, but that of a 41 kg (90 lb) wood crib as well. The insulation material is not meant to be load bearing. Therefore, in order to support this weight, a series of additional 2.5 cm wide, 0.6 cm thick steel bar stock was welded to the floor section of the supporting frame. The ceiling part of the frame was once again removable; however, its construction is presented separately.

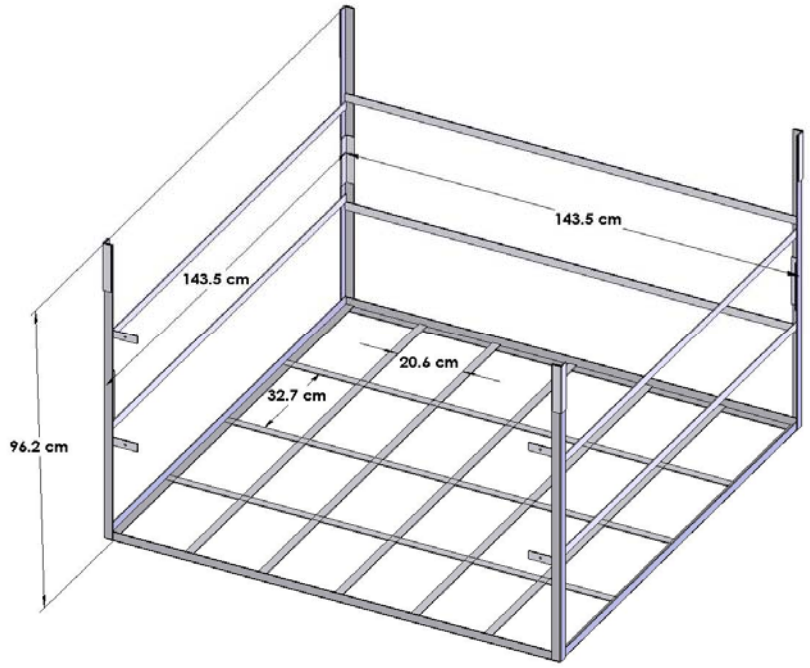

Figure 3.46: 3/8 Scale Model Supporting Frame, Walls and Floor

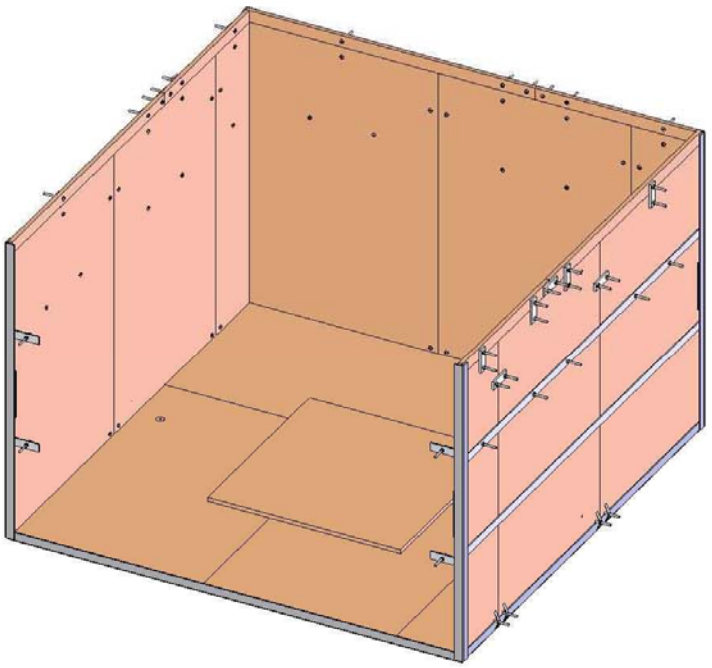

Figure 3.47: 3/8 Scale Model Construction of Walls and Floor

As is shown in Figure 3.47, the method of attaching boards together utilized a combination of nuts, bolts and channel plates. The head of the bolt was always facing inside the compartment so that this smaller area could be more easily covered with furnace cement. The alternative would have been to allow multiple channel plates or long ends of bolts to heat up during an experiment and act not only as a heat sink, but also perhaps threaten the integrity of the assembly.

As the size of the model increases, it becomes clear why larger structures utilize more than just a membrane for structural stability. This was not an option during the current testing. As a result, the removable ceiling was the most challenging piece of the compartment to construct. This large composite element had to resist bowing induced by gravity while being carried to and from the compartment before and after testing. In order to overcome this problem, 3 pieces of steel bar stock were added to the ceiling frame as shown in Figure 3.48. In order to protect these steel supports from flame during testing, they were covered with long strips of 1.3 cm thick *Kaowool S* insulation, the same as was used for the compartment boundaries. In addition to these insulated steel supports, a series of small channel plates was used to hold together the seams between boards. In this application, the channel plates faced the inside of the compartment and were insulated with small strips of *Kaowool S*. A small gap was left between the ceiling boundary and the steel angle so that the wall columns could be snugly inserted.

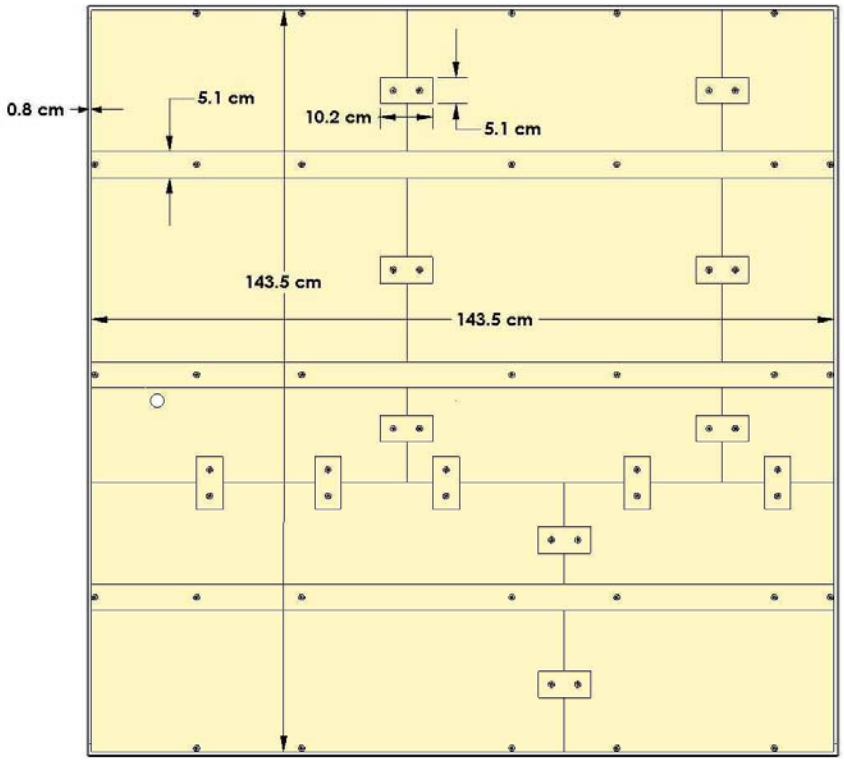

Figure 3.48a: Underside of Ceiling Support System

The top side of the ceiling was equipped with toggle nuts to complement the bolts. One common application for these toggle bolt combinations is for hanging heavy shelves from drywall, the very material being modeled at the full scale. The claw form of the bolt increases the area over which the gravity force is resisted, thus giving the material the best opportunity to maintain the integrity of the assembly. The large number of bolts used indicates the fragile nature of the material.

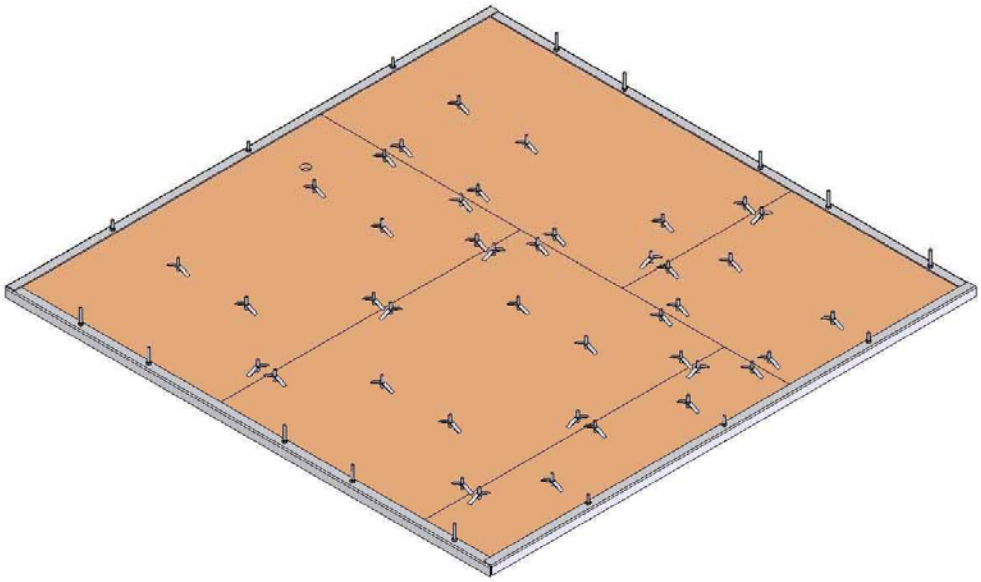

Figure 3.48b: Top Side of Ceiling Support System

The load cell used for these experiments was equipped with a large steel frame extension atop which the compartment was placed.

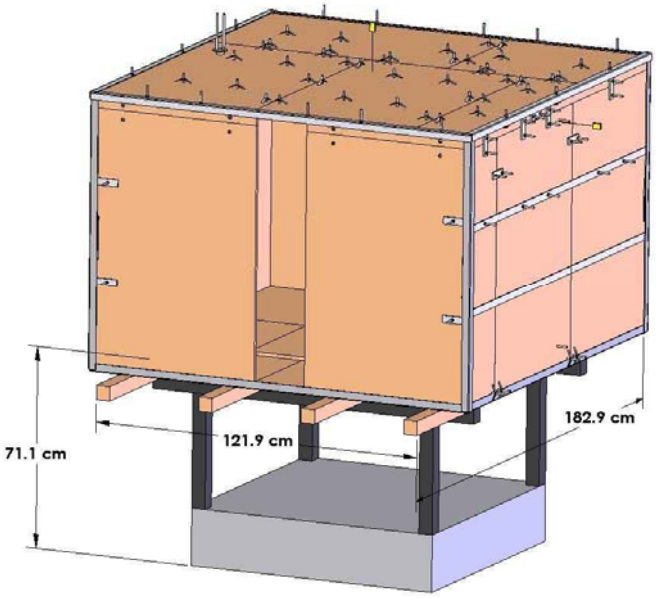

Figure 3.49: 3/8 Scale Model Load Cell Positioning

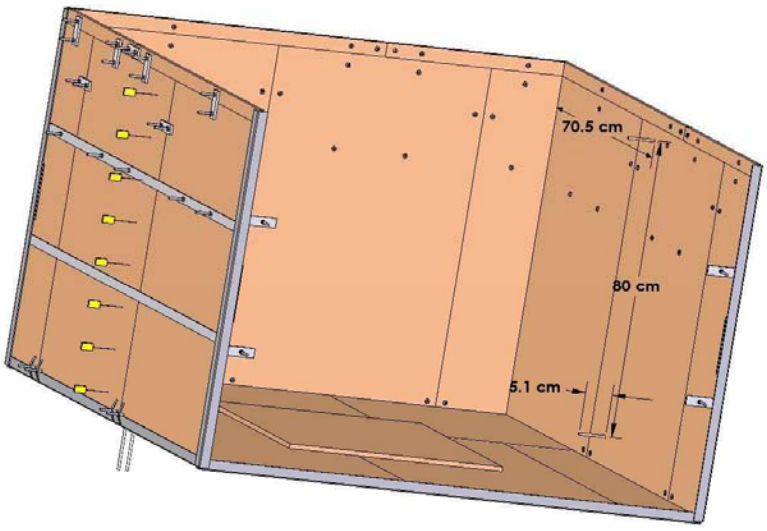

Figure 3.50: 3/8 Scale Model Gas Sampling Tube Locations

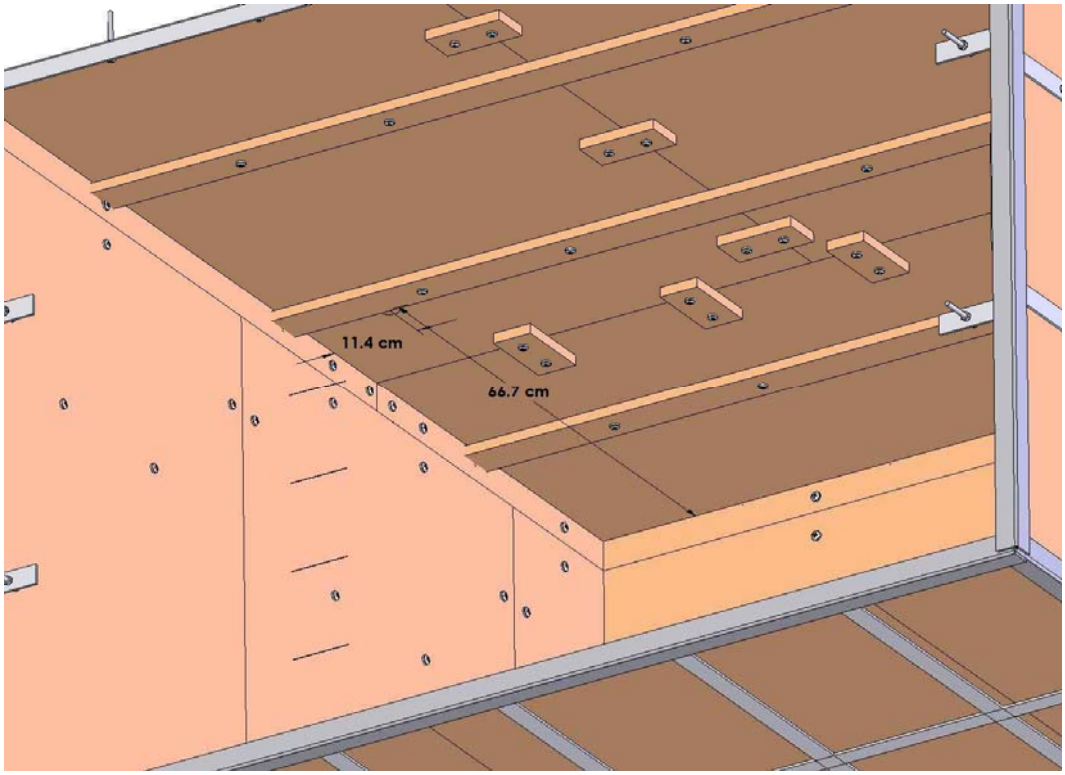

Figure 3.51: 3/8 Scale Model Ceiling Heat Flux Meter Location

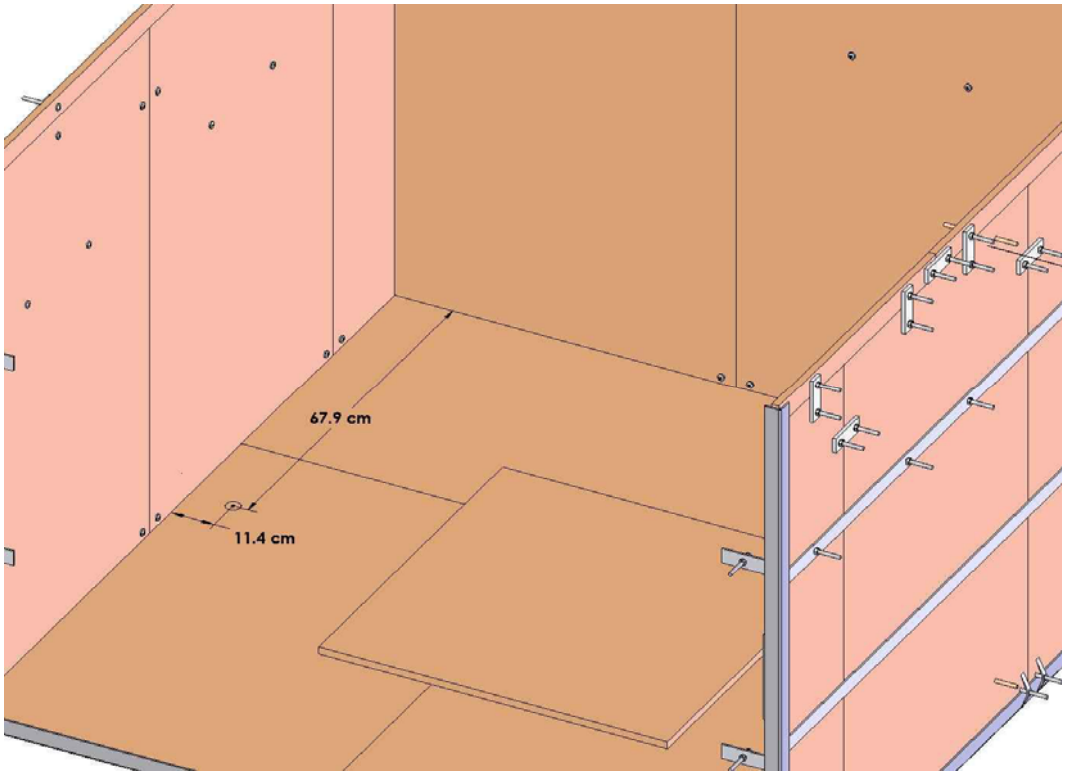

Figure 3.52: 3/8 Scale Model Floor Heat Flux Meter Location

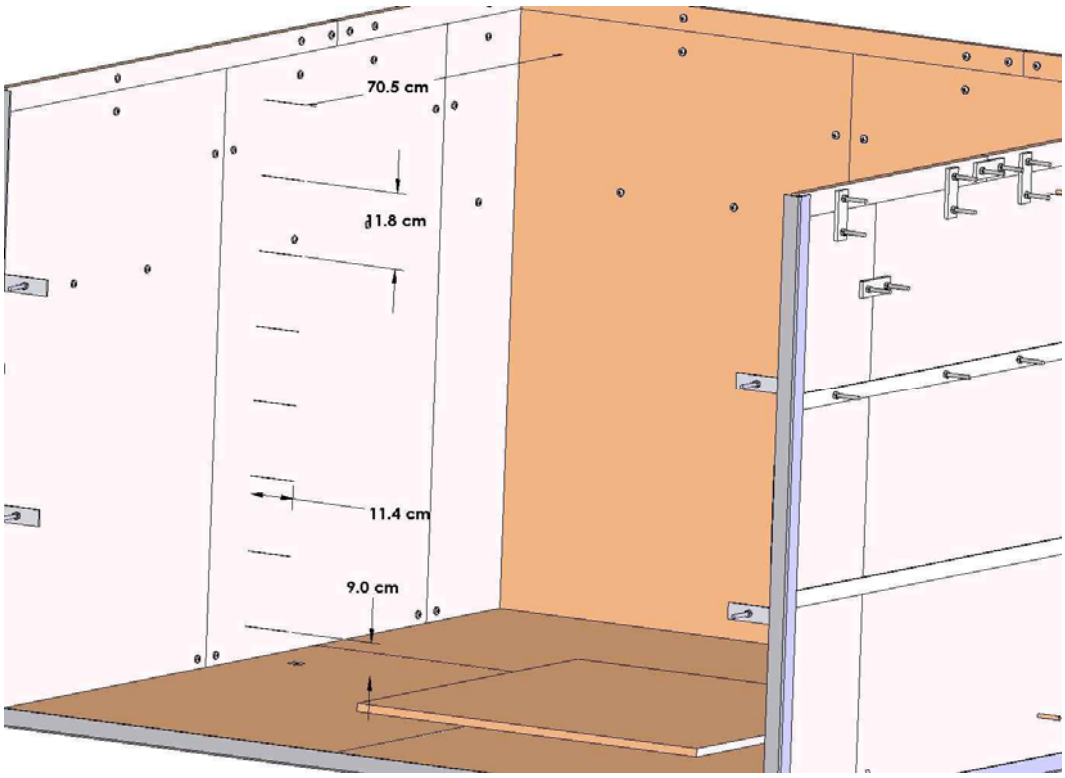

Figure 3.53: 3/8 Scale Model Interior Gas Temperature Measurements

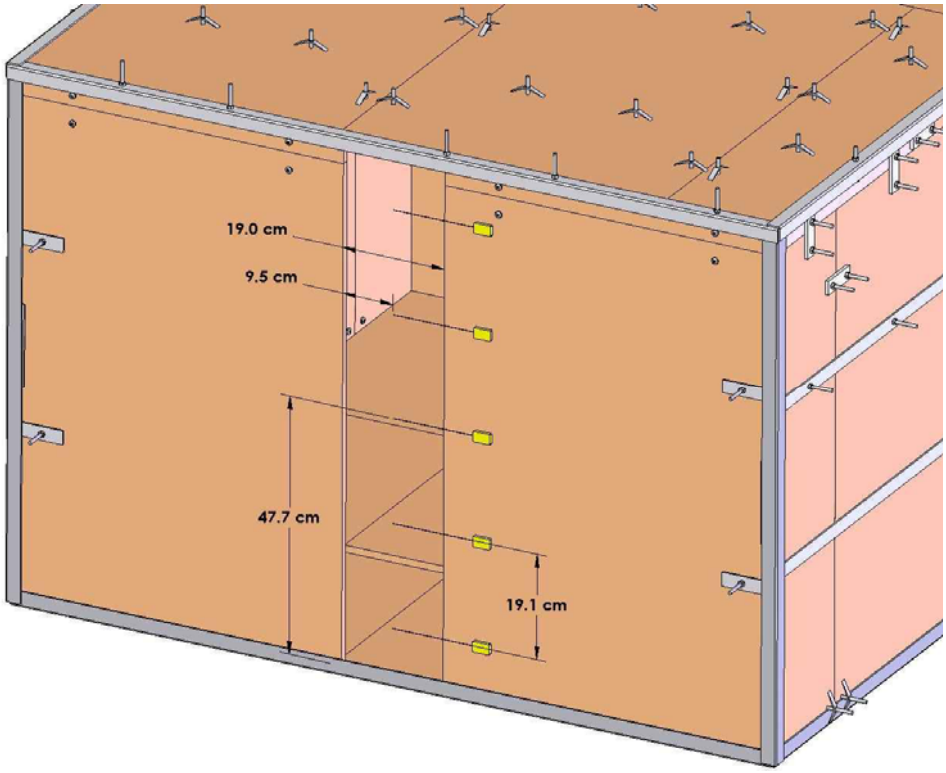

Figure 3.54: 3/8 Scale Model Vent Thermocouple Placement

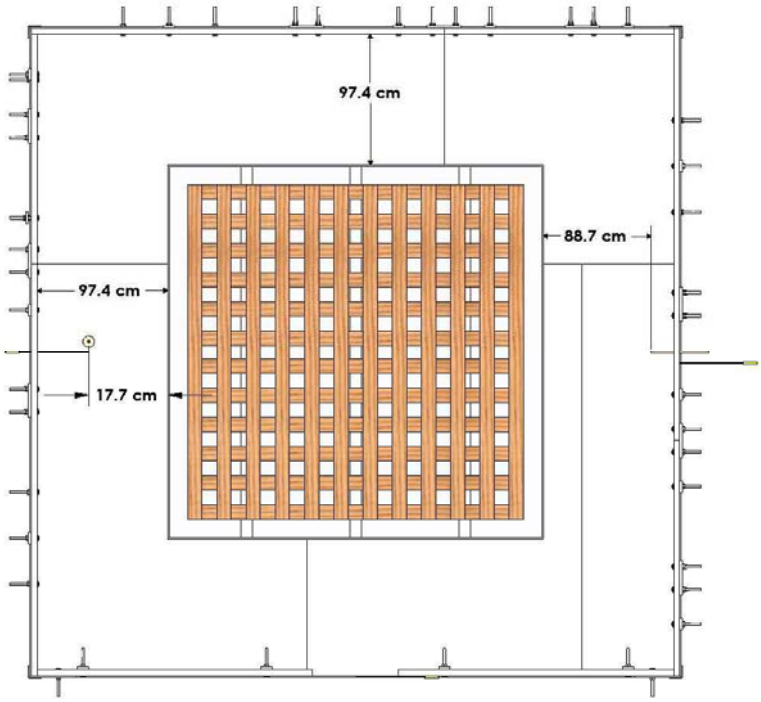

Figure 3.55: 3/8 Scale Model with Large Crib – Top View

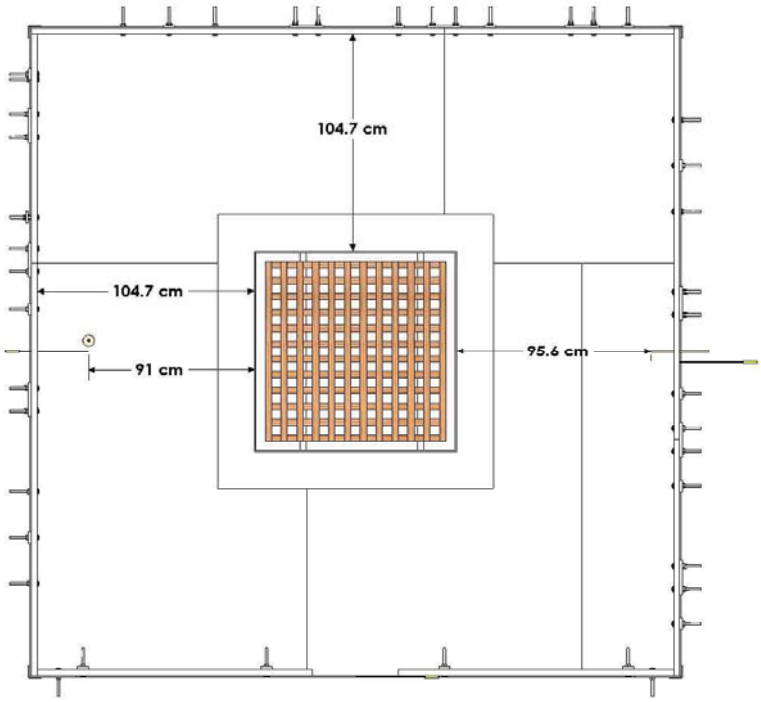

Figure 3.56: 3/8 Scale Model with Small Crib – Top View

Note the location of the heat flux meters in Figure 3.51. The floor heat flux meter was moved slightly closer to the front of the compartment in order to avoid an obstruction from the steel support frame underneath the compartment.

4. Experimental Results and Discussion

4.1 Free-Burning Wood Cribs

4.1.1 Experimental Results

The free-burning wood crib experiments were conducted prior to experimentation in the enclosures. This was done to ensure that the results of scaling the energy source were amenable to proceeding with the more complicated experiments. Twelve experiments are listed in Table 3.11. These experiments include repeat tests for both the large and small crib designs, at each of three model scales. The ignition model for these tests involved the use of a 0.5 mm deep pool of heptane as a starter fire. This pool was poured into a square fuel pan with base area approximately 20% larger than the footprint of the crib being tested. The wood crib was elevated above the lip of the pan at a distance equal to the cross section of the sticks. Recall that the ignition models are shown in detail in Figures 3.20 thru 3.25.

Prior to testing, the cribs were dried in an oven at 105^{o}C for 48 hours. It was desired that the wood be allowed to cool before testing, but not regain significant moisture. For the 1/8 and 2/8 scale models, this was accomplished by placing the wood crib in a sealed glass container with sufficient Drierite® to keep the relative humidity at approximately 15%. This cooling process was very brief, typically on the order of 15 minutes. Special considerations had to made for the 3/8 scale model. Its size precluded it from being placed inside the previously mentioned cooling container. Therefore, the sample was wrapped in several layers of clear plastic wrap immediately upon removal from the oven. The wrap was kept in place during transport to the ATF laboratory and only removed seconds prior to ignition. In order to ensure that significant moisture was

not regained during the cooling process, cribs were weighed immediately after removal from the oven and also just prior to ignition. The results of this weighing consistently showed no significant increase in crib weight. The moisture content for the cribs was approximately 0% for all testing. The raw results for the large crib design are shown in Figure 4.1a. Note the difference in both magnitude and duration of the raw data for each of the model scales. If these same results are plotted as a function of dimensionless parameters in Figure 4.1b, the predictive power of the scaling method becomes apparent.

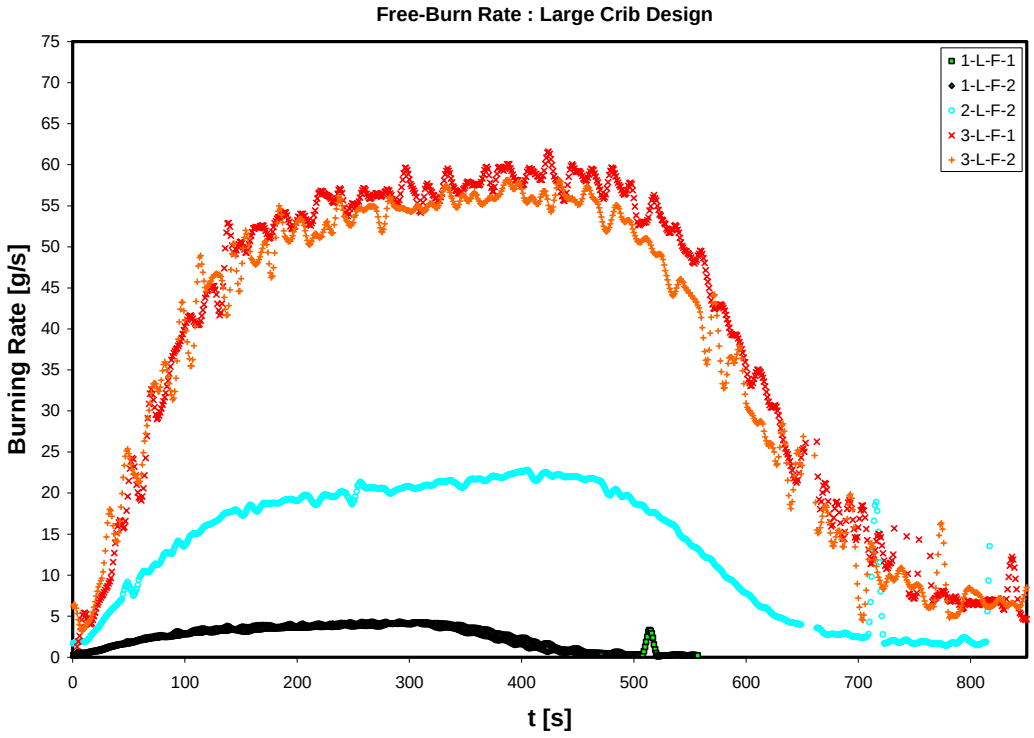

Figure 4.1a: Raw Free Burning Rate Results – Large Crib Design

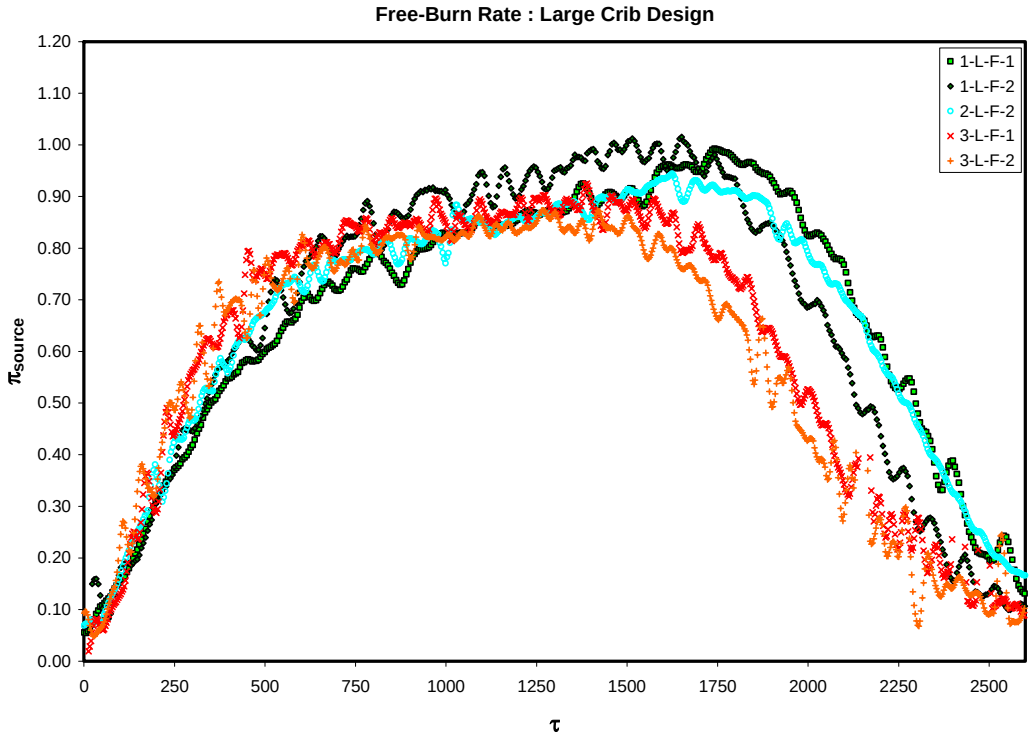

Figure 4.1b: Dimensionless Free Burning Rate Results – Large Crib Design

The results indicate that the twin maxima effect due to unsynchronized burning of the crib core and exterior is now masked at all scales. This is despite the common observation of a lag in ignition of portions of the crib exterior in many of these tests as shown in Figure 4.2. Thus, the dominant mechanism of core radiation is masking this lack of synchronization.

Figure 4.2: Observation of Flame Spread to Crib Exterior, Test 3-L-F-1

There is evidence of a very slight difference in the duration of the quasi-steady state between the 3/8 scale model and the other two scales. The most probable cause of this difference is the rather substantial increase in the size of the crib core and consequently its radiant influence between scales. Another explanation may lie in the fact that the number of sticks per layer and the number of layers in the crib must be integer values. The scaling method dictates a precise relationship for these variables with respect to length scale. Comparison of the current model designs reveals that the greatest rounding occurs in the 3/8 Scale model. The loss of a fraction of a stick per layer or layer in the crib affects the burning rate in two ways. The first is the absence of a fraction of an additional radiating surface in the structure. This affect, however should not be of great

significance given that the minimum number of sticks to avoid adverse affects on the burning rate has already been considered in the design. The second affect is that of a possible decrease in the total mass of the crib. Table 4.1 shows the difference in crib mass produced by the rounding of theoretical design parameters at each model scale. The theoretical design mass is simply the product of the wood density and crib volume without significantly rounding any design parameters. The actual design mass reflects the change in crib volume due to rounding.

Model Scale	Theoretical Design Mass (kg)	Actual Design Mass (kg)	Test 1 (kg)	Test 2 (kg)
3/8	41.1	40.3	38.5	36.8
2/8	12.2	12.2	X	11.6
1/8	1.5	1.5	1.7	1.4

Table 4.1: Affect of Rounding Crib Design Parameters – Large Crib Design

This table takes into account the rounding of all design parameters. The difference in design mass and actual mass is consistently slight; however, so is the difference in the duration and magnitude of the quasi-steady state between model scales.

In order to evaluate the accuracy of the scaling in a global approximation, an analysis of the average peak values can be used. Such an analysis takes into account the combination of magnitude and duration. The average peak duration was chosen to correspond to the time range during which the crib attains 95%-45% of its initial mass. This selection was meant to coincide with the experimental work of Quintiere and McCaffrey[18]. Figure 4.3 shows a maximum difference of 5.9% in the average peak

values among the three scales. It is important to note that the maximum difference between scales is within the range of values for the same scale.

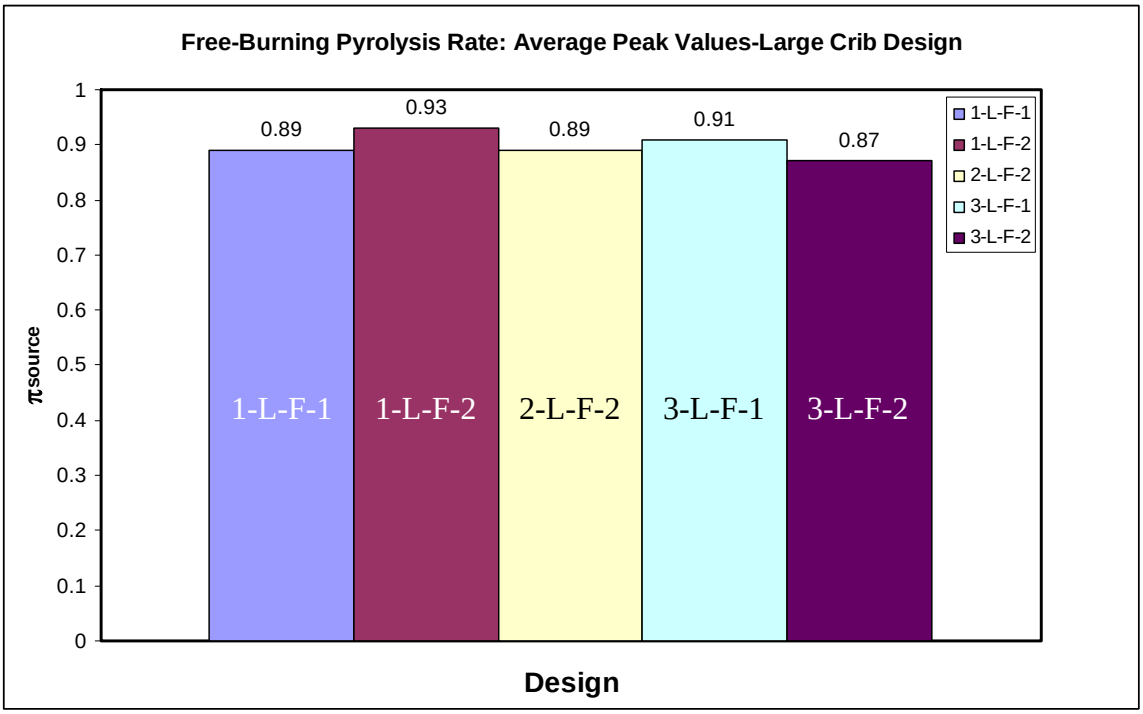

Figure 4.3: Free-Burning Rate: Average Peak Values - Large Crib Design

Such precise agreement in time-averaged results has not yet been attained in the literature. However, clearly the more impressive result is the ability to scale the instantaneous rate of burning.

The results of the experiments conducted for the small crib design are shown in Figure 4.4. It is important to note that a change in the fuel pan material was made during the testing cycle. Originally, the fuel pan was constructed from *Kaowool* insulation board wrapped in aluminum foil. After some tests had been completed and the supply of *Kaowool* began to dwindle, square metal pans were instead used. The dimensions of the pans remained consistent, but the material changed. All of the original free-burning experiments labeled X-X-X-1 were conducted using the insulated pan lined with foil. All

other tests were conducted with the use of a metal pan. The only significant difference in the burning rate appeared to be in the 1/8 scale model of the small crib design. Figure 4.4a illustrates the transient results in raw form. Figure 4.4b plots the results as a relationship between dimensionless groups.

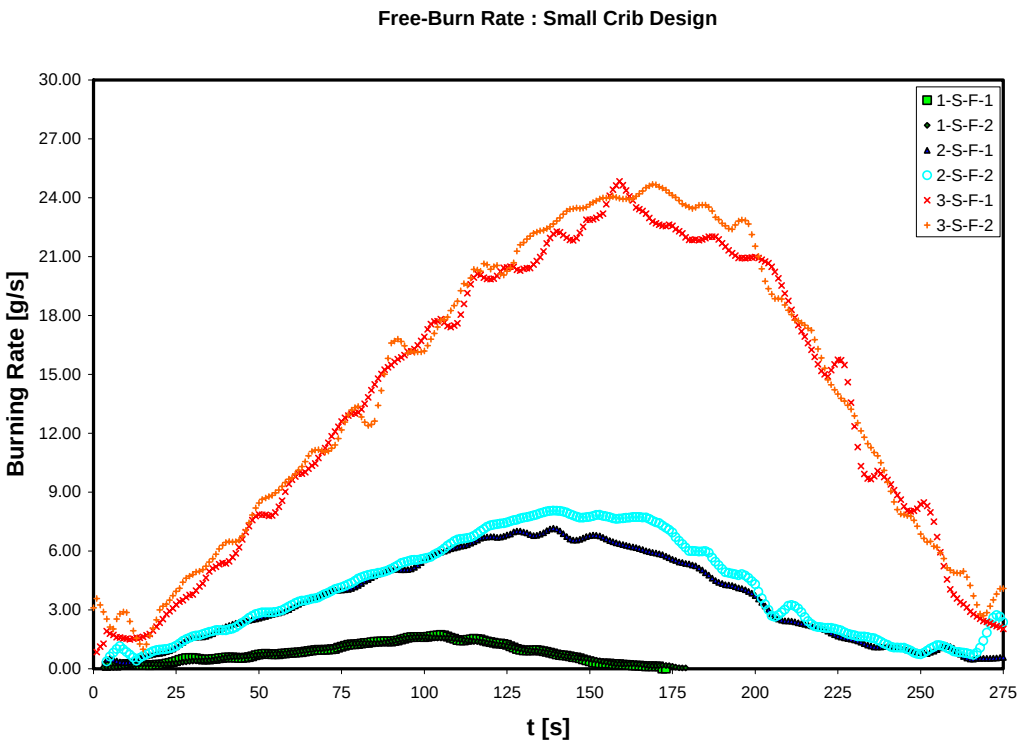

Figure 4.4a: Raw Free Burning Rate Results – Small Crib Design

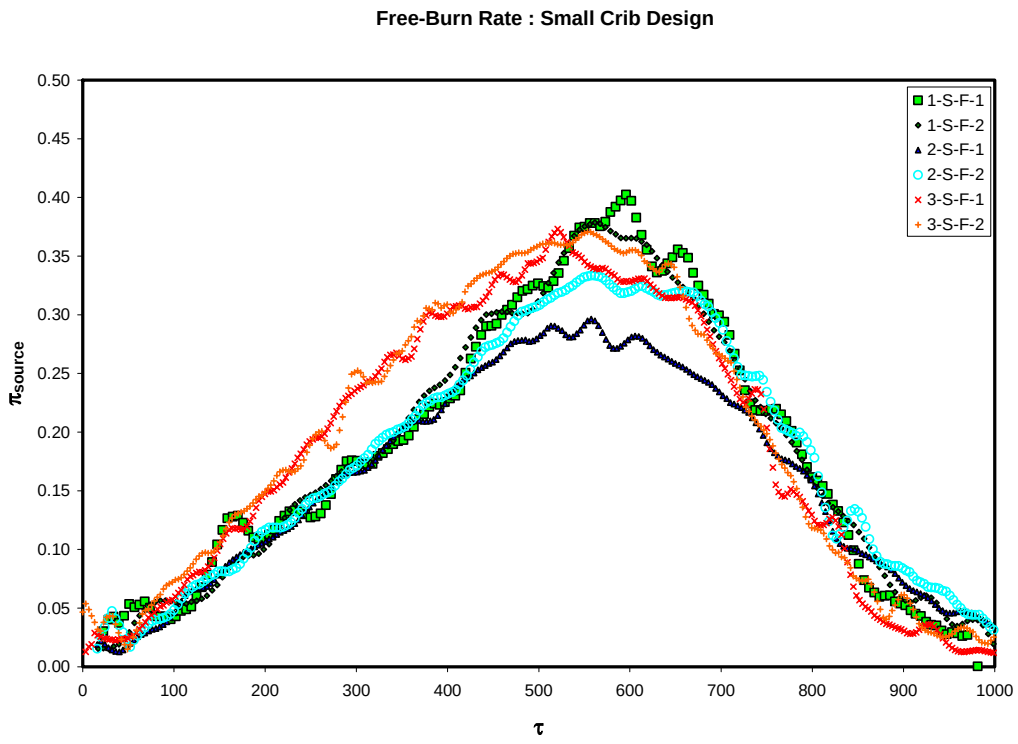

Figure 4.4b: Dimensionless Free Burning Rate Results – Small Crib Design

The result for test 2-S-F-2 is clearly lower than its counterparts with the metal fuel pans. If this result was the product of a change in fuel pans, one would expect a decrease in the burning rate due to the increased heat loss from the metal pan to the surface beneath it. As it so happens, the surface directly beneath the fuel pan was the same *Kaowool* insulation board used to construct the original fuel pans. Therefore, the heat transferred through the metal pan was simply stored in this insulation in a manner similar to the original pan. The change in fuel pans should therefore cause only a slight difference in the burning rate of the wood crib.

A more appropriate explanation lies in the initial mass of the cribs. The maximum expected variation of density within a given domestic wood species is approximately 10% [26]. This fact illustrates the importance of the wood density in

determining the burning rate of the crib. The density variation for dry wood merely confirms the prudence of conducting tests at nearly 0% moisture content.

A comparison of the average peak values for the small crib design reveals particularly good agreement between the 1/8 and 2/8 scale models.

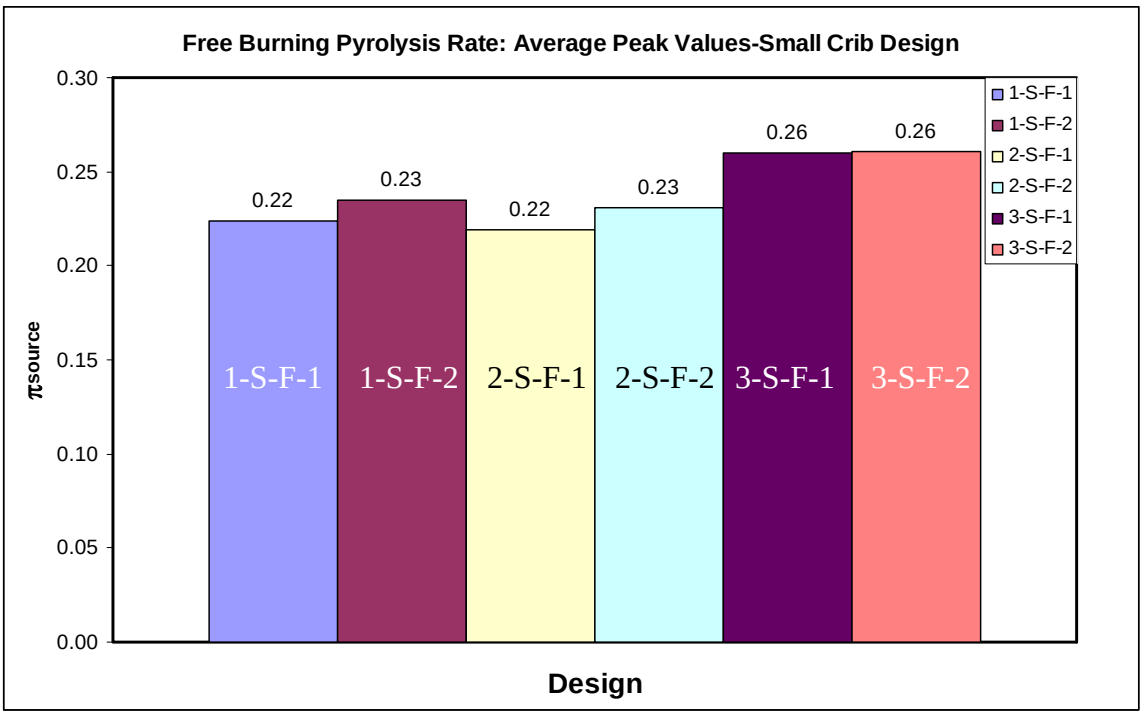

Figure 4.5: Free-Burning Rate: Average Peak Values - Small Crib Design

A comparison of the results for the transient and time-averaged values shows a slight change in the fire growth period as the length scale of the model is increased. This result appears to be more significant for the small crib design than it is for the larger one. It is important to note that the burning rate for the 1/8 scale model (with the exception of test 1-S-F-1 with very low mass) is slightly higher than that of the 2/8 scale model in both the transient and the time-averaged data. This suggests that the initial mass of the wood cribs was slightly above target for the 3/8 scale model.

Model Scale	Theoretical Design Mass (kg)	Actual Design Mass (kg)	Test 1 (kg)	Test 2 (kg)
3/8	4.06	4.21	4.15	4.14
2/8	1.20	1.21	1.13	1.14
1/8	0.15	0.15	0.14	0.14

Table 4.2: Initial Crib Mass: Small Crib Design

Table 4.2 shows that indeed the mass of the 1/8 and 2/8 scale cribs were on the low end of the design range, while the opposite was true for the 3/8 scale model. This data suggests that the difference in average peak values is likely due to variations in the density of the wood.

The transient scaling accuracy thus far achieved is certainly a desirable result. Ultimately, the results demonstrate the ability to accurately scale both the magnitude and duration of the energy source. Recall that the 3/8 scale model testing for the large crib design was conducted at the ATF Fire Research Laboratory. This decision was made based on knowledge of the data in Figure 4.1b for the two smaller scales. This data provided the necessary insight to accurately estimate a transient heat release rate for the 3/8 scale model prior to conducting the test. This is the ultimate value of scale modeling. Such a result forms a formidable foundation for experimentation in the model enclosures.

4.1.2 Comparison of Results to Published Research

Research on free burning wood crib fires has been discussed in Chapter 2 of this report. There are a few particularly noteworthy results in the literature which provide deeper insight into the experimental results presented thus far. The mass loss rate data presented by Folk was unique in that it was presented as a function of time[4]. The transient data exhibited a brief peak at the end of the quasi-steady state. When applied to the current research, this peak is of great significance because of the design of the wood crib. The wood crib contained 3 sticks per layer and 6 layers. The porosity, according to Heskestad's model, was well within the fuel surface controlled burning rate regime[19]. The experimental results presented herein illustrate a characteristic shape for the transient burning rate. The scale model of Quintiere and McCaffrey's multiple crib fire load revealed twin peak behavior for a crib with 3 sticks per layer and 4 layers[18]. Folk's data shows that as the number of layers is increased to 6, there is still some evidence of a second peak[4]. However, it is important to recognize that the crude method of measuring transient mass may have masked the presence of a more pronounced peak. Thus, the phenomenon first observed by Folk is likely unsynchronized burning of the interior and exterior portions of his wood crib.

The efforts of Thomas and Smith[6] to statistically determine the crib design parameters that played the most significant role in determining the burning rate produced the correlation shown in Equation 2.6.

$$\frac{\dot{m}}{\sqrt{A_v A_s N b}} = \frac{0.0017}{\left(A_v A_s\right)^{0.052}} \tag{2.6}$$

The surface area and interior ventilation area are calculated consistent with Gross' estimates[5]. The correlation is intended to be applied to cribs with a square footprint between 0.9 m^2 and 4 m^2. This criteria applies to the 3/8 scale models in both the large and small crib designs as well as the 2/8 scale model for the large crib design. Table 4.3 compares the measured value of the time averaged quasi-steady state burning rates to those predicted by Thomas and Smith[6]. The averaged values are taken during the period corresponding to a crib mass of 80 – 30% of the initial mass.

Design	Measured (g/s)	Thomas & Smith (g/s)
3-S-F-1	17.309	5.6
3-S-F-2	17.369	5.6
3-L-F-1	54.692	23.53
3-L-F-2	52.529	23.53
2-L-F-2	19.411	7.88

Table 4.3: Comparison of Free Burn Data to Thomas and Smith[6]

The results of this comparison show that the burning rate prediction underestimates the measured burning rate by a substantial margin. A change in the constant of proportionality could improve the comparison, but there seems to be no basis for such a change. It seems that this correlation was not derived from a statistical analysis of a wide enough sample of data to accurately predict the burning rate in the current research. Nonetheless, the relationship between the burning rate and the surface and vent areas is a step toward Heskestad's simplified version of Block's porosity function[10,19].

One of the most important comparisons to be made is with Block's burning rate relationship derived for the porosity independent burning rate regime. This relationship states that the burning rate per unit area of the crib is a function of the stick cross section .

$$\dot{m}'' = Cb^{-0.5} \tag{2.15}$$

It is this relationship on which much of the current design is based. The comparison of the data to Equation 2.15 found in Figure 4.6 is therefore significant.

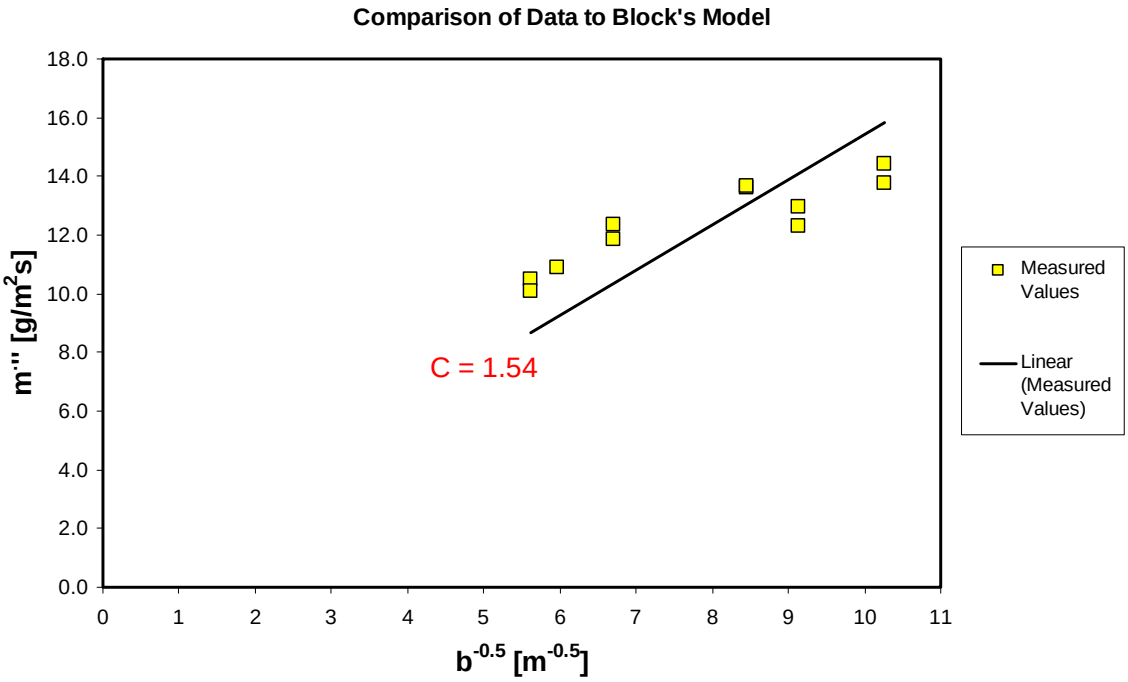

Figure 4.6: Comparison of Data to Block's Model[10]

The results of this comparison show good agreement with Block's model for the free burning rate of the wood cribs. The constant of proportionality of 1.54 is larger than the recommended value of 1.33 for Oak. This is likely due to Block's use of a moisture content of 6.8% for this particular species. A steeper slope is expected for dry wood.

The results support the use of the model in deriving relationships between critical design parameters of the crib and the characteristic length scale.

In order to address a topic of debate in the literature, the burn time for the wood cribs is compared against the predicted burn time of an individual stick. Delichatsios gives the burn time of an individual stick as listed in Equation 2.14 of this report[12].

$$t_b = \frac{\rho b}{4\dot{m}''} \tag{2.14}$$

Block's relationship for the burning rate and stick cross section can be substituted above.

$$t_b = \frac{\rho b^{3/2}}{4C} \tag{4.1}$$

A prediction can therefore be made for the duration of the quasi-steady state with knowledge of the average peak burning rate. This estimation is compared with the measured duration in Figure 4.7. The value of 1.54 m^2s^2/g is used for C and the density of the dry wood is 720 kg/m^3.

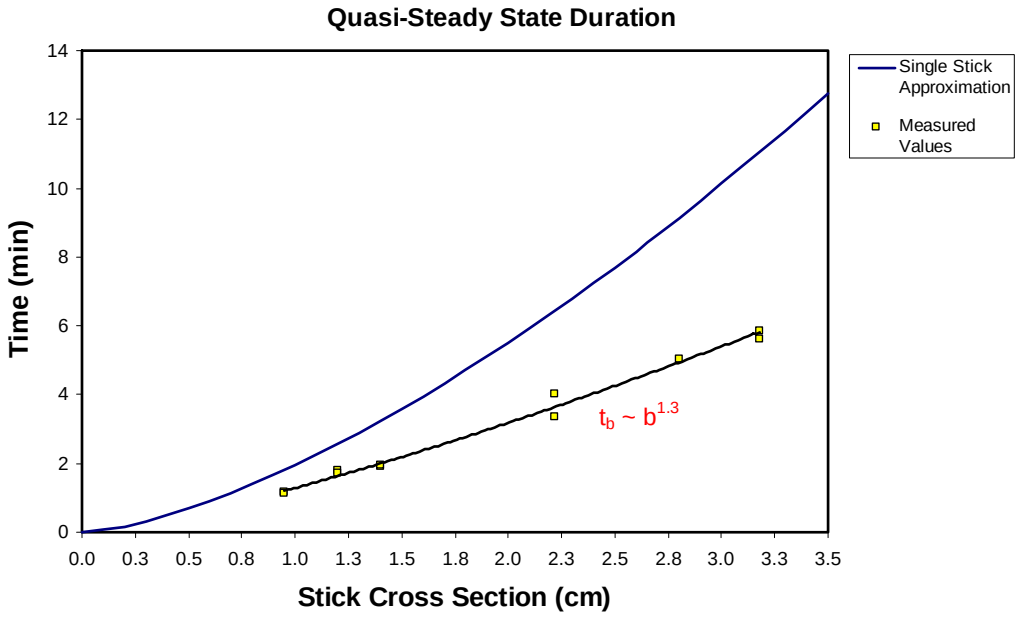

Figure 4.6: Duration of Quasi-Steady State

A best-fit power law approximates the measured values obeying a slightly different power law relationship with the stick cross section. This difference appears to be more noticeable as the size of the cross section is increased. The wood crib burns for a slightly shorter period than an individual stick due to the burning rate increase produced by the internal radiation interaction in the core. For relatively small cross sections, the magnitude of the radiation fluxes is small and therefore, the burn time is not significantly changed. Clearly, the transient results presented in Figures 4.1b and 4.3 show agreement with the total burn time between scales. Another reason behind the slightly different dependence of the quasi-steady state duration on the stick thickness is likely due to the fact that previous research attempts have not dealt with dry wood. The burning rate is prolonged by the presence of moisture. This suggests a modification to Block's model for the free burning rate[10].

$$\dot{m}'' = Cb^{-f(density)} \tag{4.2}$$

At first glance it seems that this modification should warrant reconsideration of the scaling theory. However, this does not seem to be necessary as long as the characteristic length scale is consistently applied to determine each of the design parameters.

4.1 Wood Crib Fires in Enclosures

4.2.1 Experimental Procedure

The testing matrix used for the enclosure fires was similar to the free-burns in that 2 tests were conducted for each crib design corresponding to its respective scale model compartment. Unfortunately, due to time constraints at the ATF Laboratory, tests 3-L-C-2 and 3-S-C-2 had to be eliminated from the test plan.

Test ID	Description
1-L-C-1	1/8 Scale, Large Crib, Compartment, Test #1
1-L-C-2	1/8 Scale, Large Crib, Compartment, Test #2
1-S-C-1	1/8 Scale, Small Crib, Compartment, Test #1
1-S-C-2	1/8 Scale, Small Crib, Compartment, Test #2
2-L-C-1	2/8 Scale, Large Crib, Compartment, Test #1
2-L-C-2	2/8 Scale, Large Crib, Compartment, Test #2
2-S-C-1	2/8 Scale, Small Crib, Compartment, Test #1
2-S-C-2	2/8 Scale, Small Crib, Compartment, Test #2
3-L-C-1	3/8 Scale, Large Crib, Compartment, Test #1
3-S-C-1	3/8 Scale, Small Crib, Compartment, Test #1

Table 4.4: List of Enclosure Fire Experiments

All of the preparation for the enclosure experiments was identical to the preparation for the free burns. All instrumentation positions and calibrations were checked prior to each test. Data acquisition systems were set to record prior to ignition. Each test officially began with ignition of the heptane pool beneath the wood crib.

4.1.2 General Observations

Although the size of the vent was quite small, particularly at the 1/8 scale, some general observations were made for these experiments. Each of the ten experiments

outlined in Table 4.4 produced signs of limited ventilation. Ignition of the heptane was followed by a period of growth within the newly ignited crib. It was difficult to determine visually whether uniform ignition was achieved. The reuse of the thin metal fuel pans eventually produced a concave warping, which likely caused the heptane pool to be more concentrated in the center of the pan. This phenomenon likely produced slow growth within the crib (Figure 4.8).

Figure 4.8: Example of Non-Uniform Ignition, Test 3-S-C-1

From the point of ignition through the period of propagation in the crib, flames impinged upon the ceiling above. It was not long before these flames protruded from the

vent and towered high above the roof of the compartment. As the fire progressed toward its peak burning rate, the height of the flame above the compartment grew (Figures 4.9 and 4.10).

Figure 4.9: Example of Flame Towering Above Compartment, Test 3-L-C-1

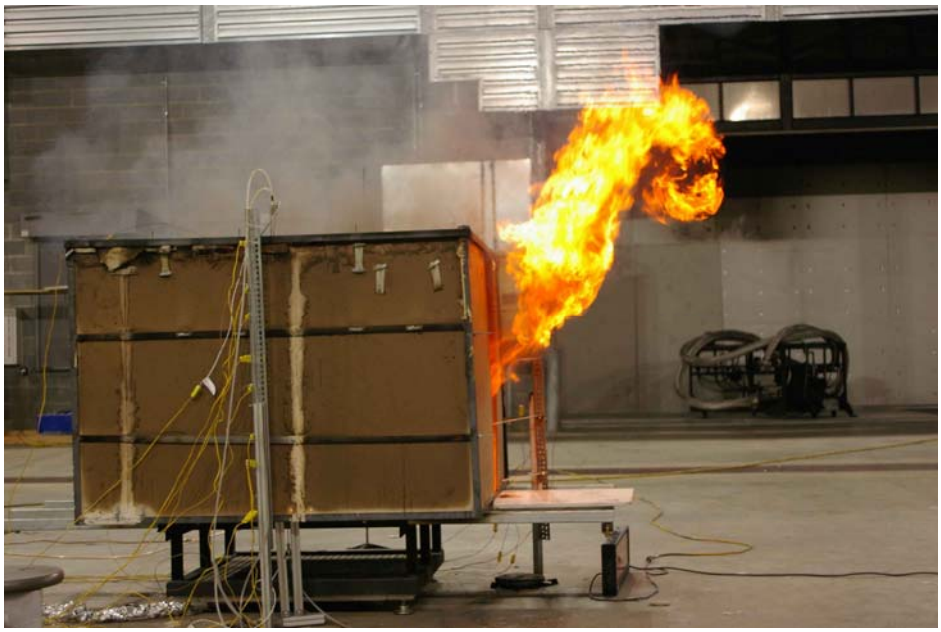

Figure 4.10: Example of Tall Flame and Turbulent Eddy, Test 3-L-C-1

It is also important to note the presence of a thin smoke layer emanating through the ceiling of the compartment in the above pictures. The *Kaowool S* material used to construct the 3/8 scale model compartment was prone to minor cracking and shrinkage. The result was the escape of some hot gases in the upper layer early in testing. As the fire progressed, tiny flames eventually appeared through these cracks in the ceiling (Figure 4.11). These flames were periodically suppressed with the use of a fine water mist. This occurrence was unique to Test 3-L-C-1.

Figure 4.11: Flame Protrusion through Ceiling, Test 3-L-C-1

Perhaps the most intriguing observation which proved to be consistent between scales was the absence any trace of soot inside the compartment following the fire. This clean burn fire pattern[29], was first observed in the 1/8 scale model at the conclusion of

Test 1-L-C-1. In order to examine its reoccurrence, a small pool of toluene was burned in the compartment prior to test 1-L-C-2 (Figures 4.12a and 4.12b).

Figure 4.12a: Dirty 1/8 Scale Compartment, After Toluene Fire, Before Test 1-L-C-2

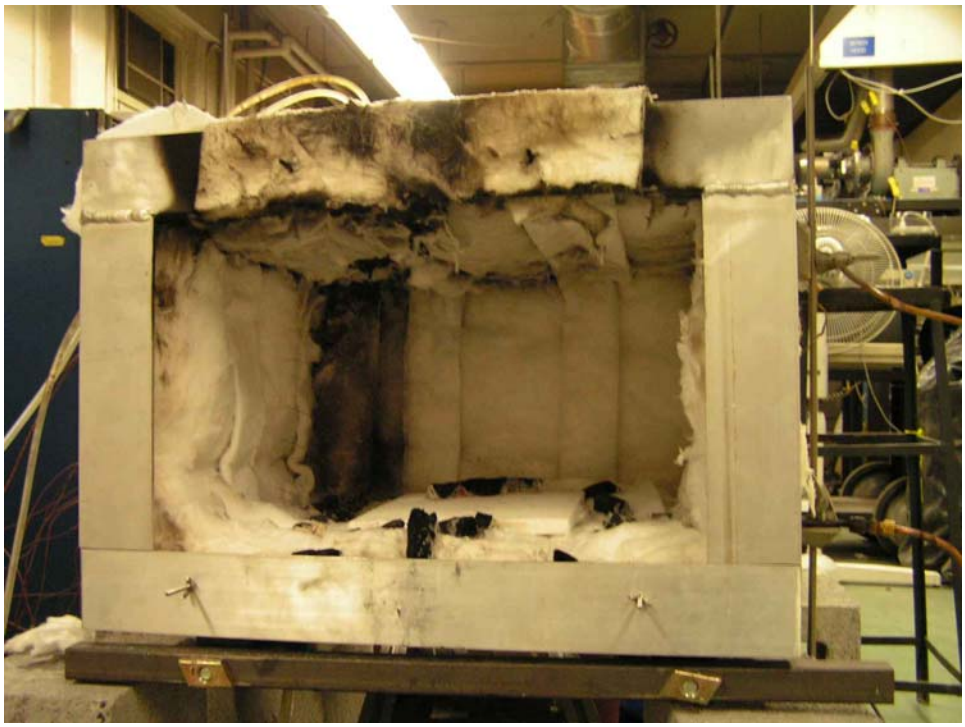

Figure 4.12b: Clean 1/8 Scale Compartment, After Test 1-L-C-2

The phenomenon was observed again in each of the two larger scale model compartments. In these larger compartments, not only were the walls free of soot, but the pigment of the insulation also was consumed, leaving a color gradient through the material thickness. The interior of the compartment was completely white and the exterior a dark brown (Figures 4.13a and 4.13b).

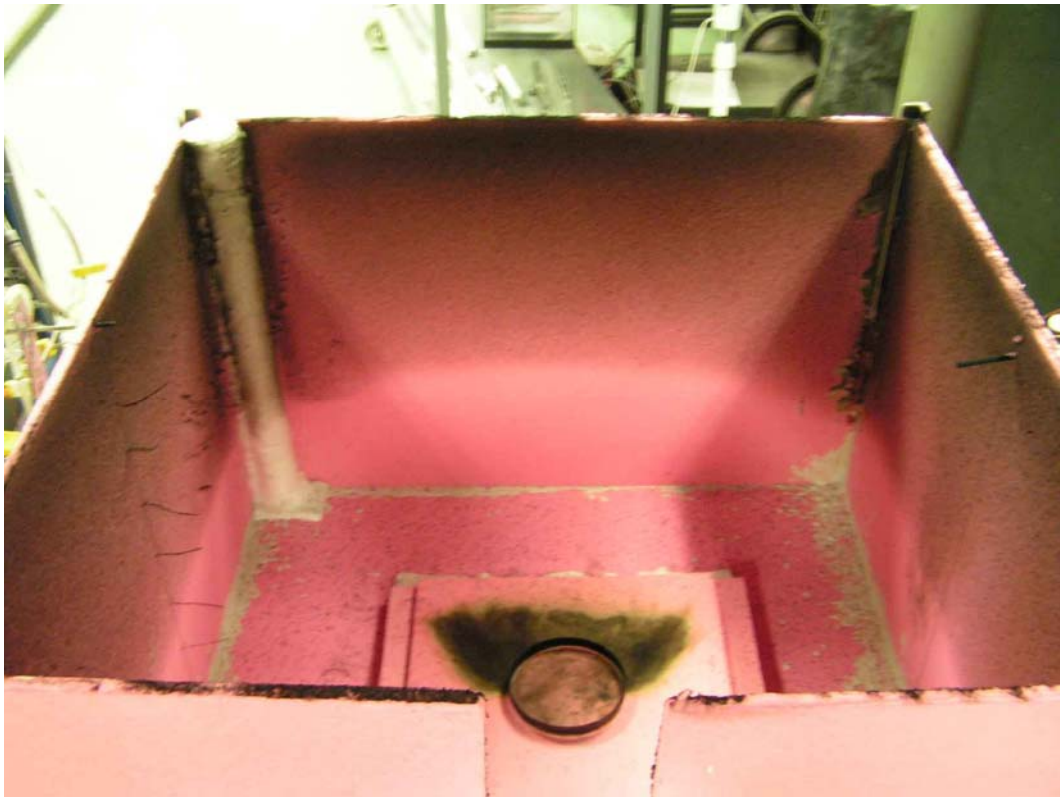

Figure 4.13a: Dirty 2/8 Scale Compartment, After Toluene Fire, Before Test 2-S-C-1

The clean burning phenomenon will be discussed in more detail in the next sections of this report.

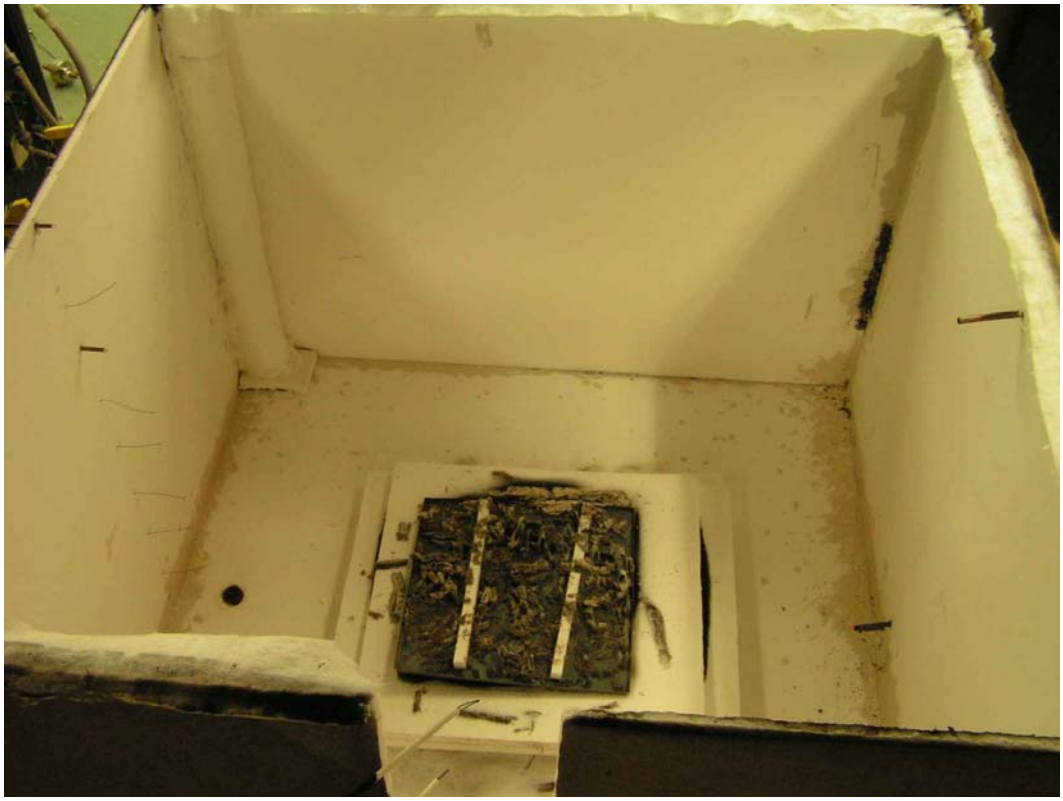

Figure 4.13b: Clean 2/8 Scale Compartment, After Test 2-S-C-1

4.1.3 Fuel Supply Rate and Burning Rate Results

A distinction is made between the terminology of burning rate and fuel supply rate. The enclosure fires studied herein are consistently ventilation limited. As such, a certain amount of fuel is vaporized within the compartment but does not ignite until it reaches sufficient oxygen at the enclosure exit. The rate measurement is taken by a load cell which records the mass of the fuel over time. Therefore, this data corresponds precisely to a rate of mass loss or fuel supply due to vaporization rather than a rate of burning within the enclosure. The dimensionless source group must be altered to reflect this change in physical meaning.

$$\pi_{fuel,supply} \equiv \frac{\dot{m}_f}{\rho_\infty \sqrt{g} H^{5/2}} \tag{4.3}$$

The results of the dimensionless fuel supply group are presented in Figure 4.14 for each of the three length scales for the large crib design. The same presentation of data is made in Figure 4.15 for the small crib design.

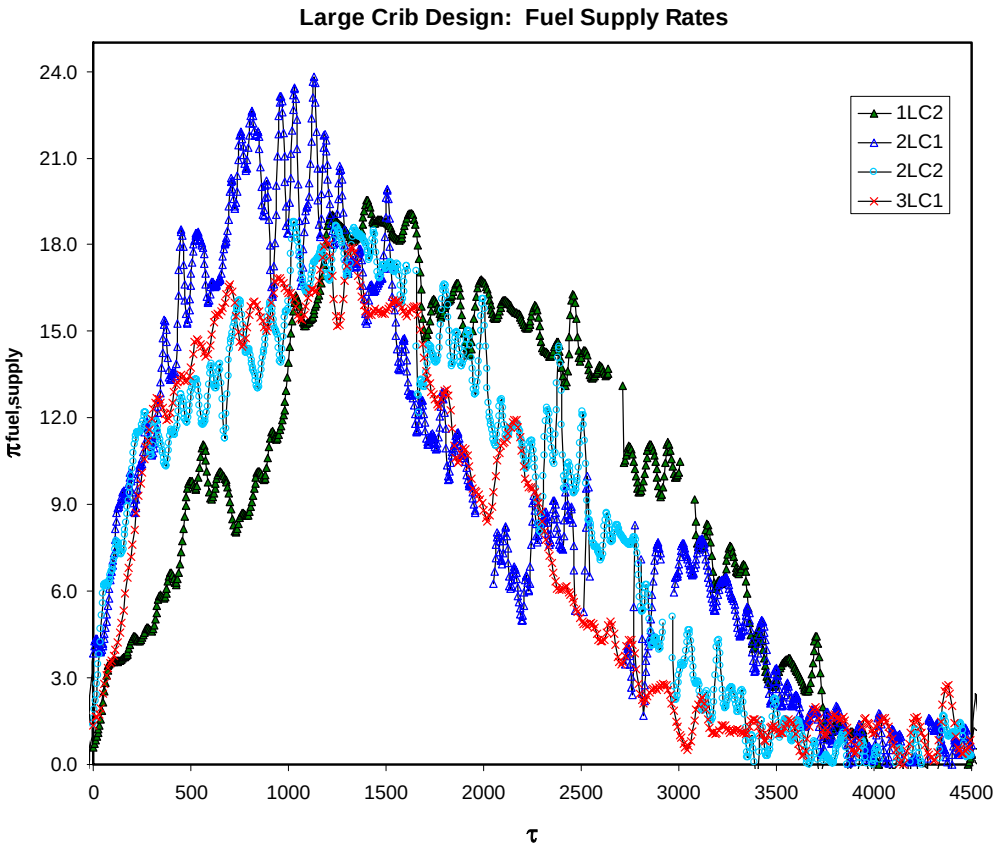

Figure 4.14: Dimensionless Fuel Supply Rate – Large Crib Design

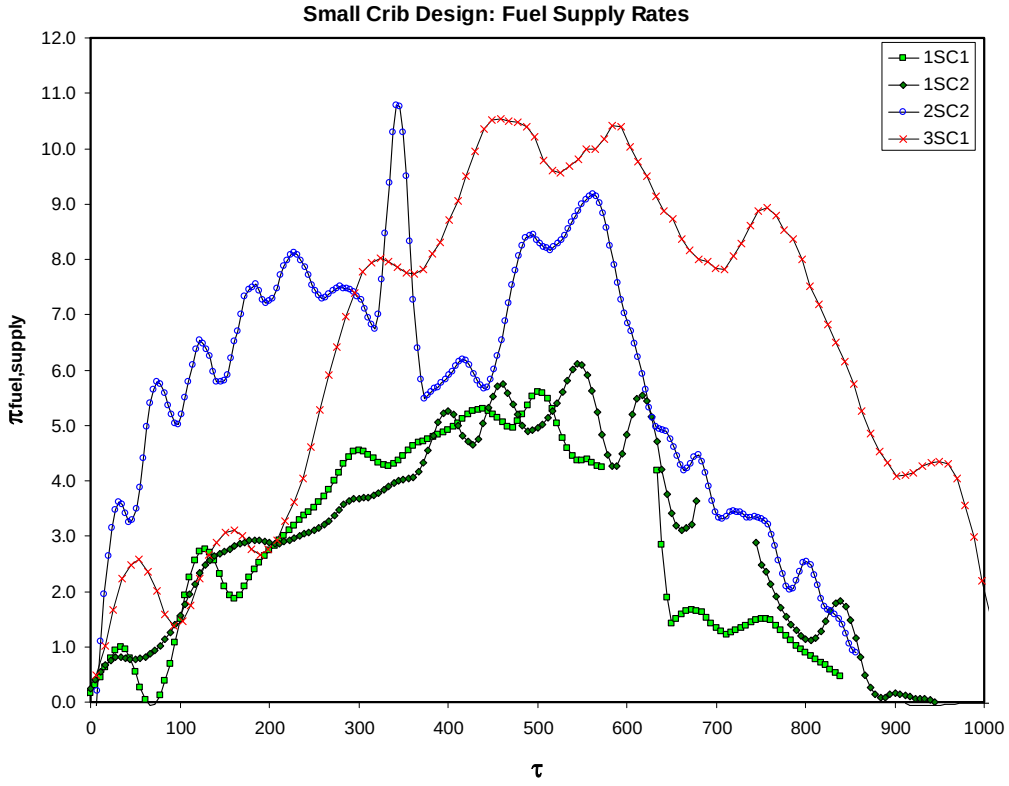

Figure 4.15: Dimensionless Fuel Supply Rate – Small Crib Design

The results presented in Figures 4.14 and 4.15 reveal that the magnitude of the mass loss rate for the 1/8 scale model is consistently smaller than those recorded at the higher scales. Unfortunately, the reason for this result is a simple inconsistency in the scaling. Recall that each of the scale model compartments utilized a supporting frame of either steel or aluminum angle. The vent height was designed to be the full height of the enclosure. The inconsistency is that for each compartment, a portion of the supporting frame covers the very bottom and very top of the vent opening. This inconsistency is quite small for the 2/8 and 3/8 scales. However, in the case of the 1/8 scale model, where the blanket material required extensive support, the supporting angles had 6.4 cm flanges. This left a total vent height approximately 19% below the design value. The height inconsistency was only 4% and 3% at the 2/8 and 3/8 scale models respectively.

It is known that the fuel supply rate must scale in proportion to the ventilation factor first identified by Kawagoe[14]. The power dependence of the vent height further magnifies the inconsistency with respect to the fuel supply rate. Table 4.5 reveals the significance of the ventilation inconsistency at each model scale.

Model Scale	Design Ventilation Factor [$m^{5/2}$]	Actual Ventilation Factor [$m^{5/2}$]	% Difference
3/8	0.177	0.170	4.1
2/8	0.064	0.060	6.3
1/8	0.011	0.008	36.5

Table 4.5: Significance of Compartment Ventilation Inconsistency

The vent height will be corrected for future testing. The results obtained thus far provide encouraging evidence of the potential accuracy of the scale models.

A simple correction scheme for the data involves simply adjusting the magnitude of the dimensionless fuel supply term measured at each time step in accordance with the ventilation factor % differences presented in Table 4.5. These results with adjusted magnitudes are presented in Figures 4.16 and 4.17.

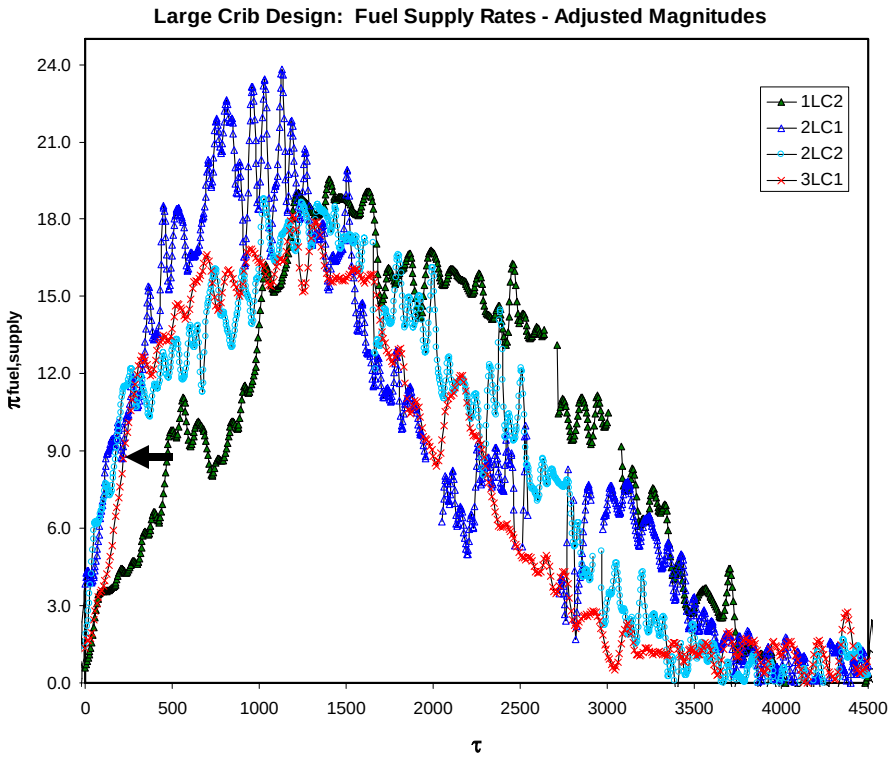

Figure 4.16: Large Crib Design: Fuel Supply Rates – Adjusted Magnitudes

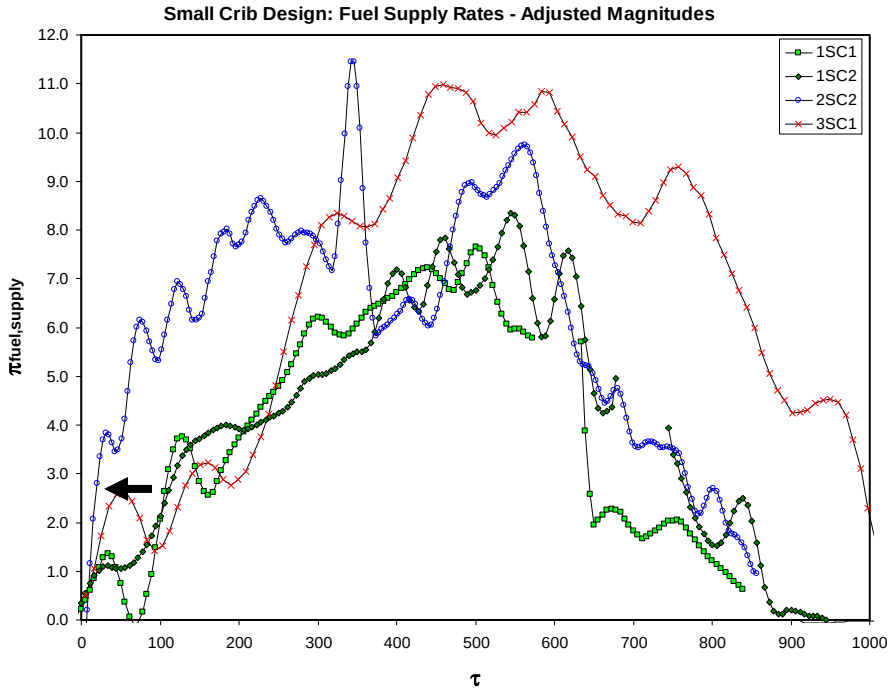

Figure 4.17: Small Crib Design: Fuel Supply Rates – Adjusted Magnitudes

Further adjustment can be accomplished with the recognition of slowed growth to steady state in tests 1-L-C-2, 1-S-C-1, 1-S-C-2, and 3-S-C-1. The reason for this slowed growth is perhaps due to slight warping of the reused metal fuel pans. The concavity of the pan resulted in a tendency for heptane to pool in a more central location. The result of such pooling was ignition of the crib core followed by a period of propagation to the external sticks. This period of propagation can be appreciated visually in Figures 4.14 thru 4.17, and is identified explicitly by black arrows in Figures 4.16 and 4.17. An adjustment of the data is accomplished by merely shifting the measured time so that the identified curve segments overlap. The final result indicates the potential accuracy of the model given consistency in vent height and uniform crib ignition (Figures 4.18 and 4.19).

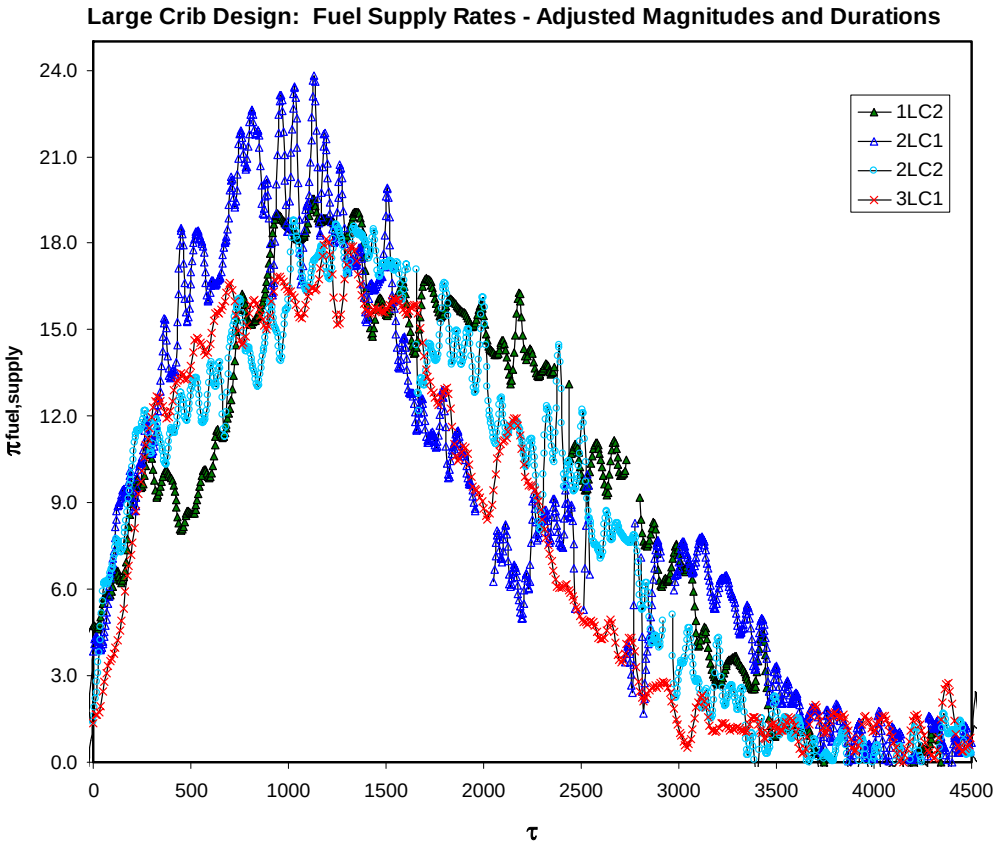

Figure 4.18: Large Crib Design: Fuel Supply Rates – Adjusted Magnitudes & Times

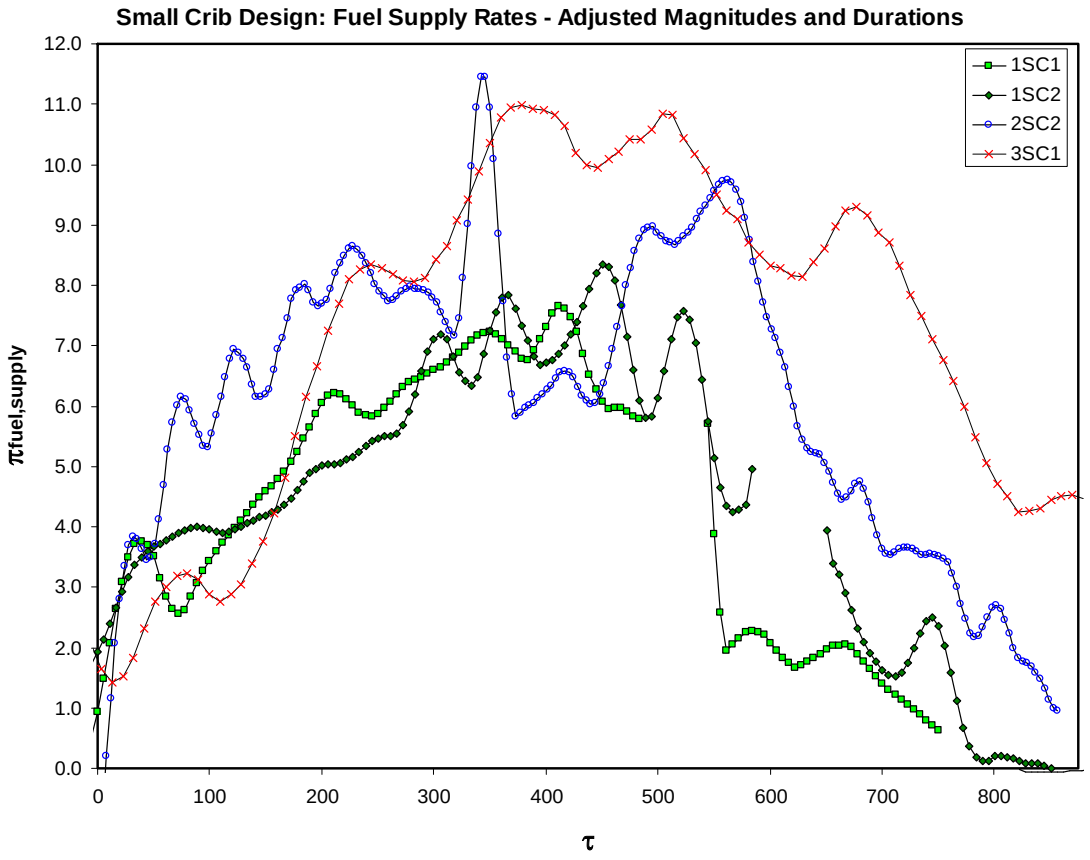

Figure 4.19: Small Crib Design: Fuel Supply Rates – Adjusted Magnitudes & Times

These modifications to the magnitude of the fuel supply rate were accomplished with the help of a very simple but fundamental proportionality for the burning rate. Recall that the size of the vents was determined based on Harmathy's limited ventilation model for the fuel supply rate presented in Section 2.2.3 of this report. Harmathy's ventilation factor presented in Equation 2.21b is in perfect agreement with the scaling relationship derived for the mass flow rate of air into the compartment[15].

$$\phi = \rho_a \sqrt{g} A_v \sqrt{H} \qquad (2.21b)$$

Comparison of the mass flow rate of air into the compartment with the surface area of fuel inside dictates his predictions for the quasi-steady state fuel supply rate. Figure 4.20 illustrates these predictions in comparison to the measured experimental data.

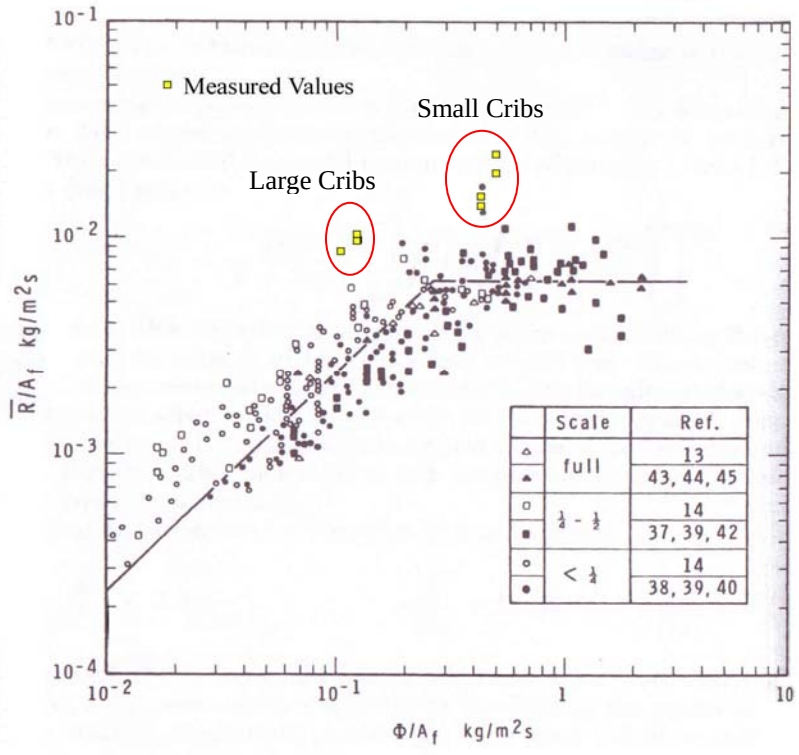

Figure 4.20: Harmathy's Fuel Supply Rate Predictions[15]

The inconsistency in the vent height is inconsequential to the predictions for these compartments. Calculations were made based on the as-built dimensions of the compartment and the fuel. The average peak values were taken during the time interval in which the crib reached 80%-30% of its initial mass in accordance with Harmathy's model specification.

The results show a consistent and significant under-prediction of the average peak fuel supply rate in the compartments. The issue of its accuracy with respect to this data is somewhat subtle. The model is presented on a log-log plot. The scatter of the data on

this plot is therefore greatly reduced. It appears that the maximum scatter shown in this Figure is $\pm 100\%$. This figure is calculated based on a single data for an experiment conducted in a well ventilated small scale compartment. The estimate of the uncertainty is not uncharacteristic of the model. Harmathy himself noted a "very significant scatter of data points" [15]. This large degree of scatter is very likely a product of radiation in the compartment. This is particularly true for the fires conducted in this research where high temperatures prevailed. The dominant influence of radiation actually increases the burning rate significantly above the limitation predicted by ventilation alone. In order to quantify this effect, one could assess the ratio of the total surface area of the compartment and the exposed surface area of the fuel. Table 4.6 presents this calculation for each of the scale model cribs.

Crib Design	Area Ratio: A_T/A_s
1-S-C-X	14.73
2-S-C-X	9.37
3-S-C-X	7.49
1-L-C-X	3.53
2-L-C-X	2.27
3-L-C-X	1.83

Table 4.6: Consideration of Thermal Feedback in Harmathy's Model

Applying the calculation to Harmathy's model suggests that the lower the magnitude of the Area Ratio, the higher the influence of radiation. If both the ordinate and the abscissa of Harmathy's plot are normalized with the free burning mass loss rate, the affect of this radiation can be best appreciated. Figure 4.21 groups the cribs into distinct categories based on this area ratio. Note that the affect of radiation pulls the

magnitude of the fuel supply rate above that which is predicted by the model. Furthermore, the plot reveals the competing forces of ventilation and radiation by showing that in the fuel limited regime, much less thermal feedback is required to increase the fuel supply rate. This plot is a representation of how Harmathy's model could be modified to include this affect.

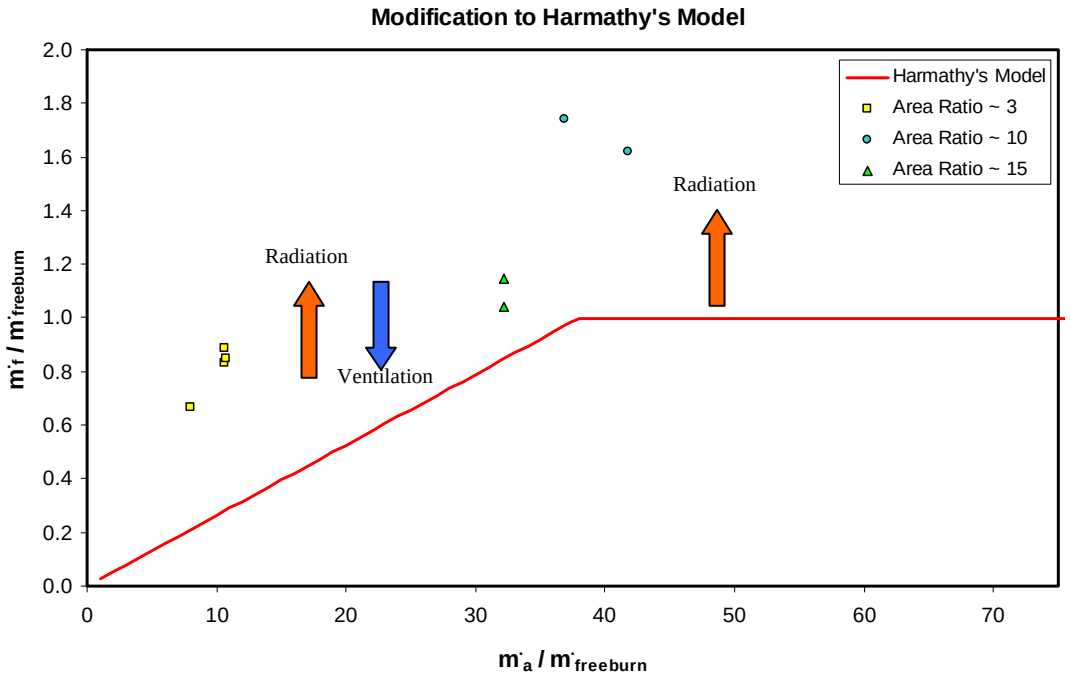

Figure 4.21: Possible Representation of Radiation Influence for Harmathy's Model

Recall that Harmathy's model was used in the design phase to predict the necessary stick size and vent width to satisfy the requirement of a full scale fire duration of 1 hour for the large crib design. The results of the large crib fires X-L-C-X as presented in Figure 4.14 show that the scaling of the fire duration is consistent, corresponding to a dimensionless time of approximately 3750. This dimensionless time equates to a full scale measured fire duration of approximately 30 minutes. Thus, the

desired limitation on fire duration has not been achieved. This is undoubtedly due to the degree of scatter in the model.

A substantial increase in the size or density of the wood crib may be necessary to achieve a full scale fire duration of 1 hour. However, such changes in the design are impractical for this size compartment. The wood density is already at the maximum for the common range of domestic woods[26]. An increase in the cross section would necessitate an increase in the overall footprint area of the crib so that the porosity could be maintained. Therefore, a much larger compartment floor area would be required to satisfy the 1 hour burn time requirement. A dramatic decrease in the size of the vent may well lead to extinction rather than a substantially prolonged duration.

Aside from the model presented above, it should be noted that although the burning rate within the enclosure is being limited by the small vent, the fuel vaporization rate is still very high. The result is an inability to slow the rate of fuel exiting the compartment and thus prolong the duration of the fire. If one extends a control volume outside of the compartment boundaries, there is a burning rate outside of the compartment that must be considered. By conservation of mass for this larger control volume, although the rate of burning inside the compartment is limited, the rate of burning outside of the compartment compensates for the limitation.

The distinction between the fuel supply rate and the burning rate in these fires can be further substantiated with a transient comparison of the dimensionless fuel supply rates in the free burning and confined compartments for each of the various scales. In the case of the large crib design, the ventilation is certainly limited and has a decreasing effect on the enclosure fuel supply rate. The opposite is true for the thermal feedback

contribution. Results are shown in Figures 4.22 a-f. Note that all enclosure data has been modified to correct the vent height inconsistency.

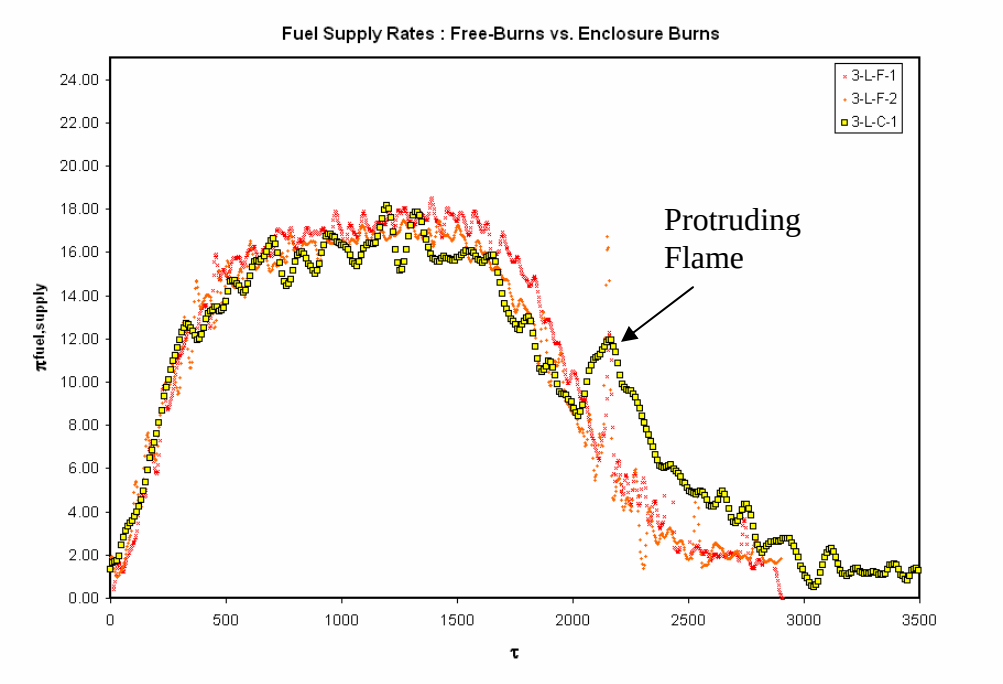

Figure 4.22a: Fuel Supply Rates – Free Burns vs. Enclosure Burns, 3-L-X-X

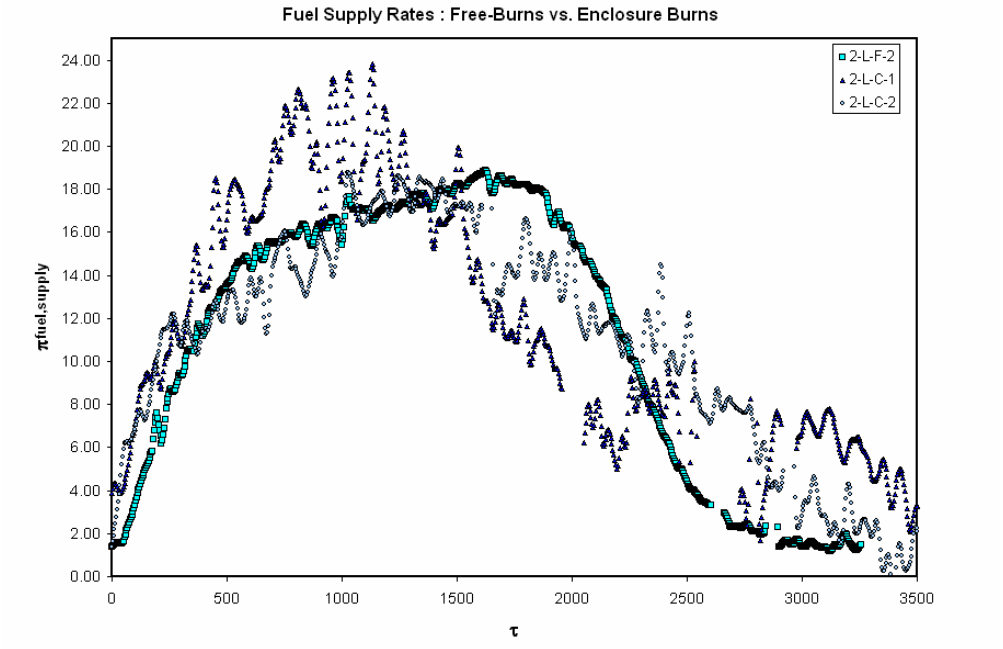

Figure 4.22b: Fuel Supply Rates – Free Burns vs. Enclosure Burns, 2-L-X-X

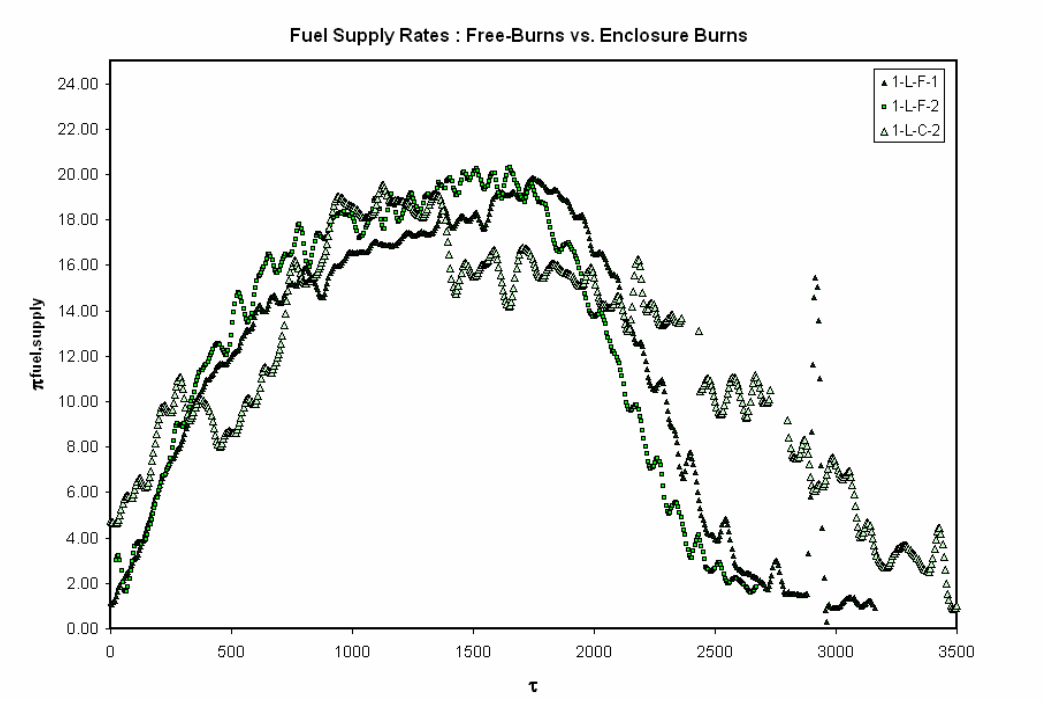

Figure 4.22c: Fuel Supply Rates – Free Burns vs. Enclosure Burns, 1-L-X-X

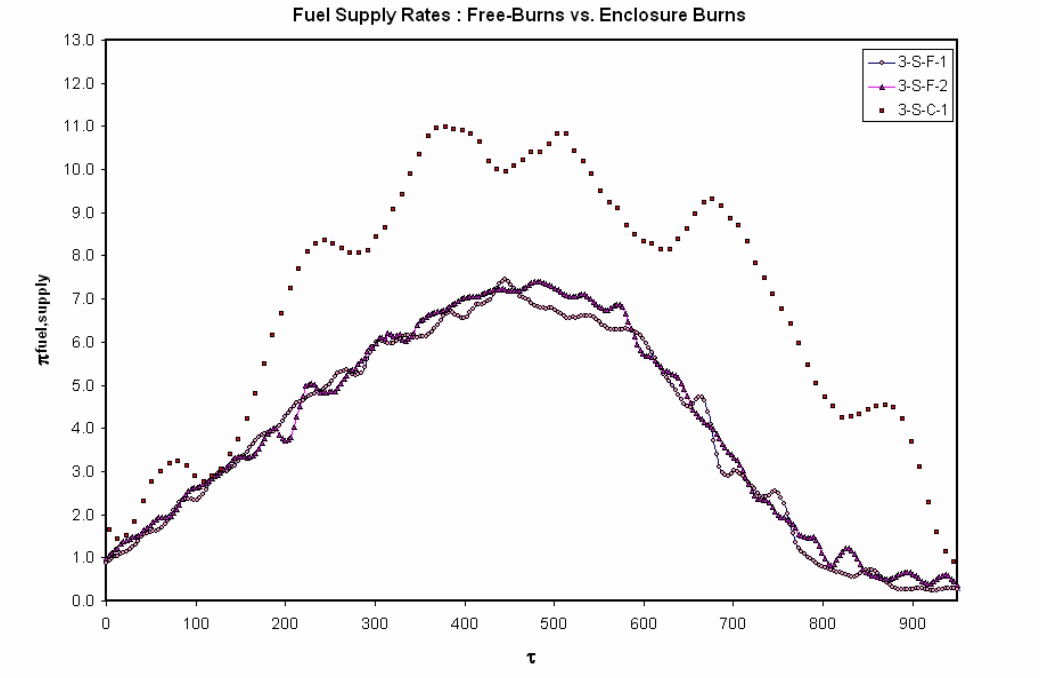

Figure 4.22d: Fuel Supply Rates – Free Burns vs. Enclosure Burns, 3-S-X-X

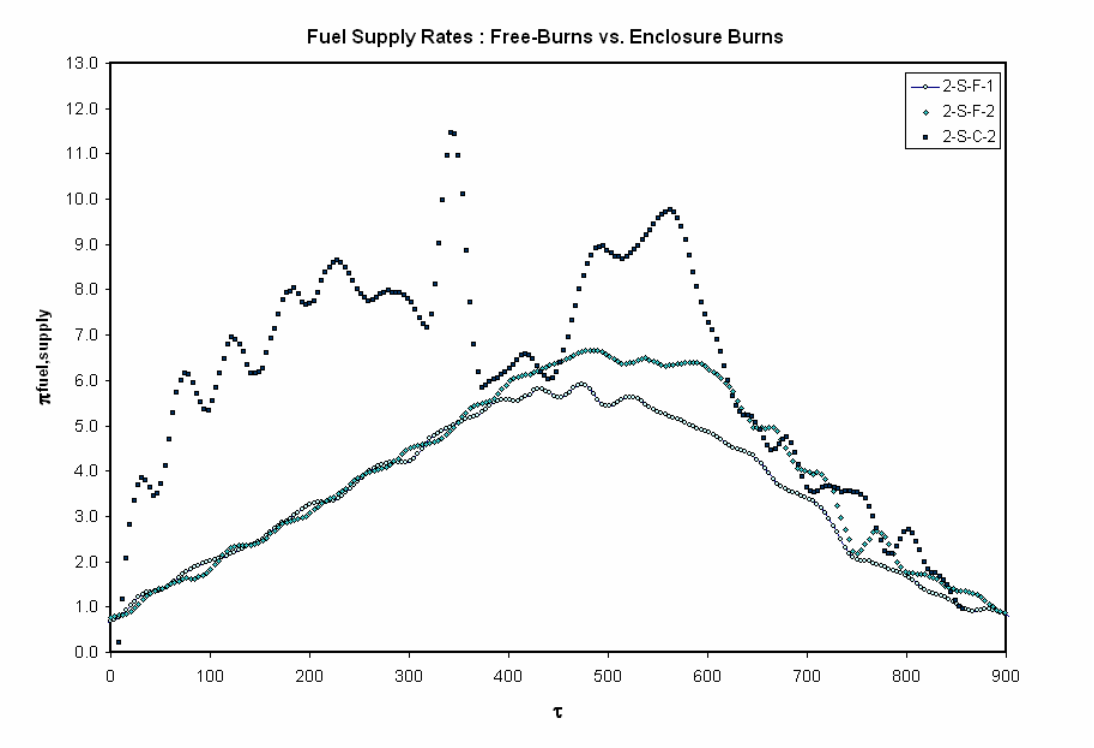

Figure 4.22e: Fuel Supply Rates – Free Burns vs. Enclosure Burns, 2-S-X-X

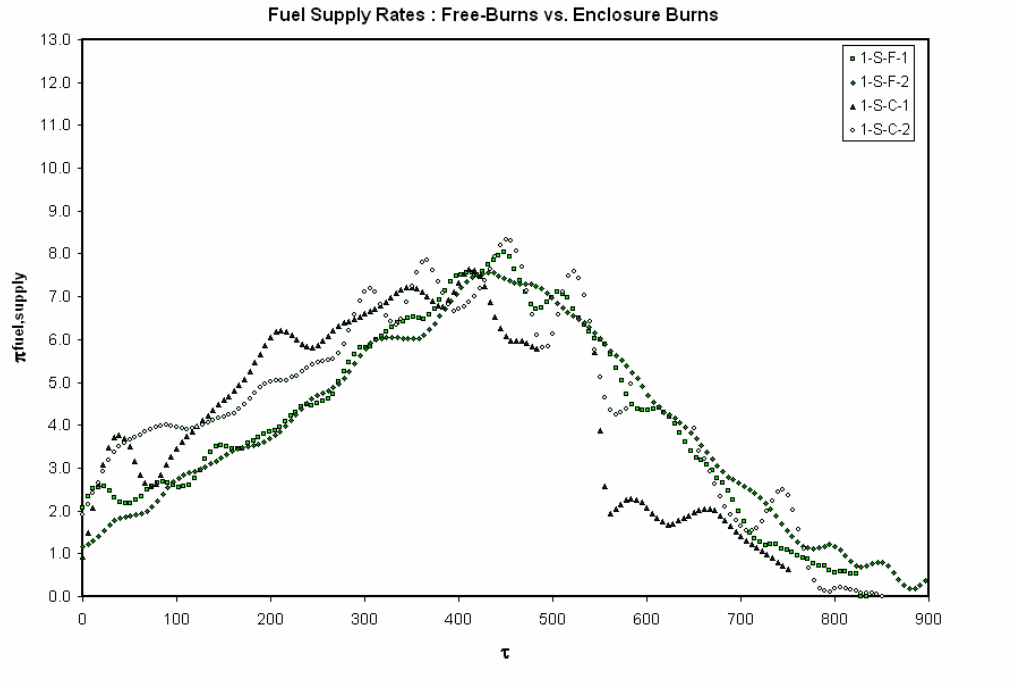

Figure 4.22f: Fuel Supply Rates – Free Burns vs. Enclosure Burns, 1-S-X-X

The results shown in Figures 4.22a through 4.22f illustrate two sets of crib designs generally burning under ventilation limited conditions. The small cribs produced ventilation limited fires, but were very near the transition point. The data presented in Figures 4.22a, b, c and f demonstrate that the rate of fuel vaporization in the compartment is equal to the rate of vaporization observed in the free burning state. In the case of Figures 4.22d and e, the ventilation limitation is not so severe and the radiation influence prevails. Note that these last two cases correspond to the Area Ratio of 10 on Harmathy's modified model in Figure 4.21. This plot shows that perhaps these fires have crossed the transition point into the fuel limited regime.

For the limited ventilation fires, the fuel is not being burned at the same rate that it is vaporized because of the lack of available oxygen in the compartment. In order to determine the scaling relationship for the ventilation limitation on the burning rate, the mass flow rate of air into the compartment must be determined. This can be estimated from the vertical temperature profile in the doorway. The data for this temperature profile has not yet been presented, but will be used to calculate flow density in the following calculation for each of the wood crib fires[23]:

$$\dot{m}_{air} = \frac{2}{3} C_d A_v \sqrt{H_v} \sqrt{2g} \rho_\infty \sqrt{\frac{\left(\rho_\infty - \rho_g\right)/\rho_\infty}{\left[1 + \left(\rho_\infty / \rho_g\right)^{1/3}\right]^3}} \tag{4.4}$$

where 0.7 is used to approximate the flow discharge coefficient.

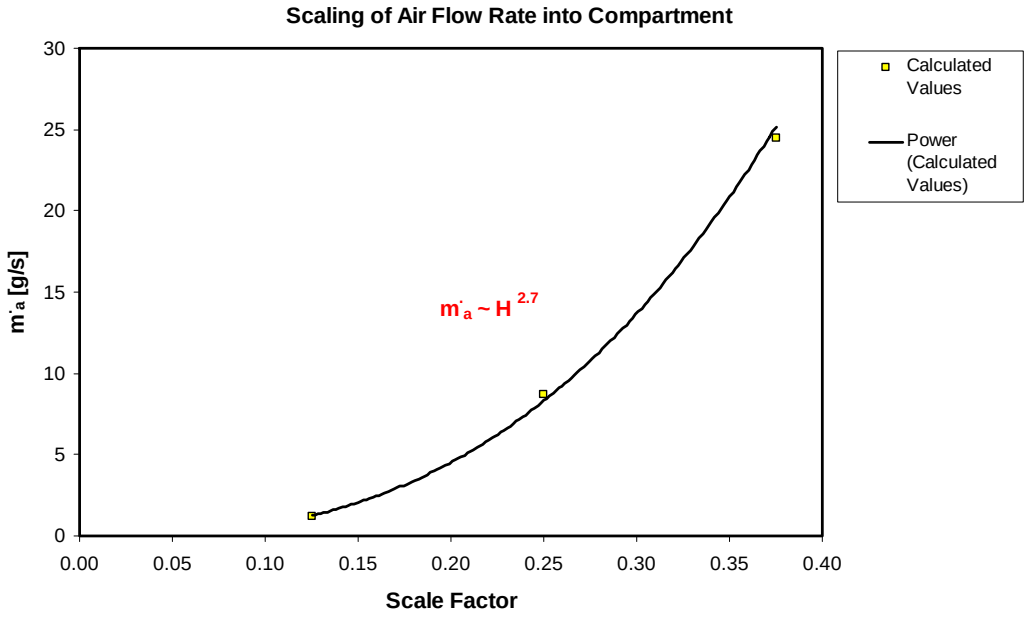

Figure 4.23: Calculated Scaling of Airflow into Compartments

The calculation used to determine the airflow rate is based on both transient and spatial averaging of the temperature profiles in the doorway. This is the reason why the mass flow rate of air does not appear to scale exactly as $H^{2.5}$. The calculation shown in Figure 4.23 is simply a crude estimation. Note that the term scale factor is simply another way of referring to the ratio of the model to prototype enclosure heights.

While Harmathy's model values ventilation over thermal feedback, the opposite is true for a burning rate model presented by the C.I.B. research. Data from the C.I.B. tests is taken from Figure 2.14 and compared with the scaling theory. By normalizing the data with respect to the ventilation factor, the scaling relationship between the enclosure burning rate, ventilation and interior surface area is shown in Figure 4.24.

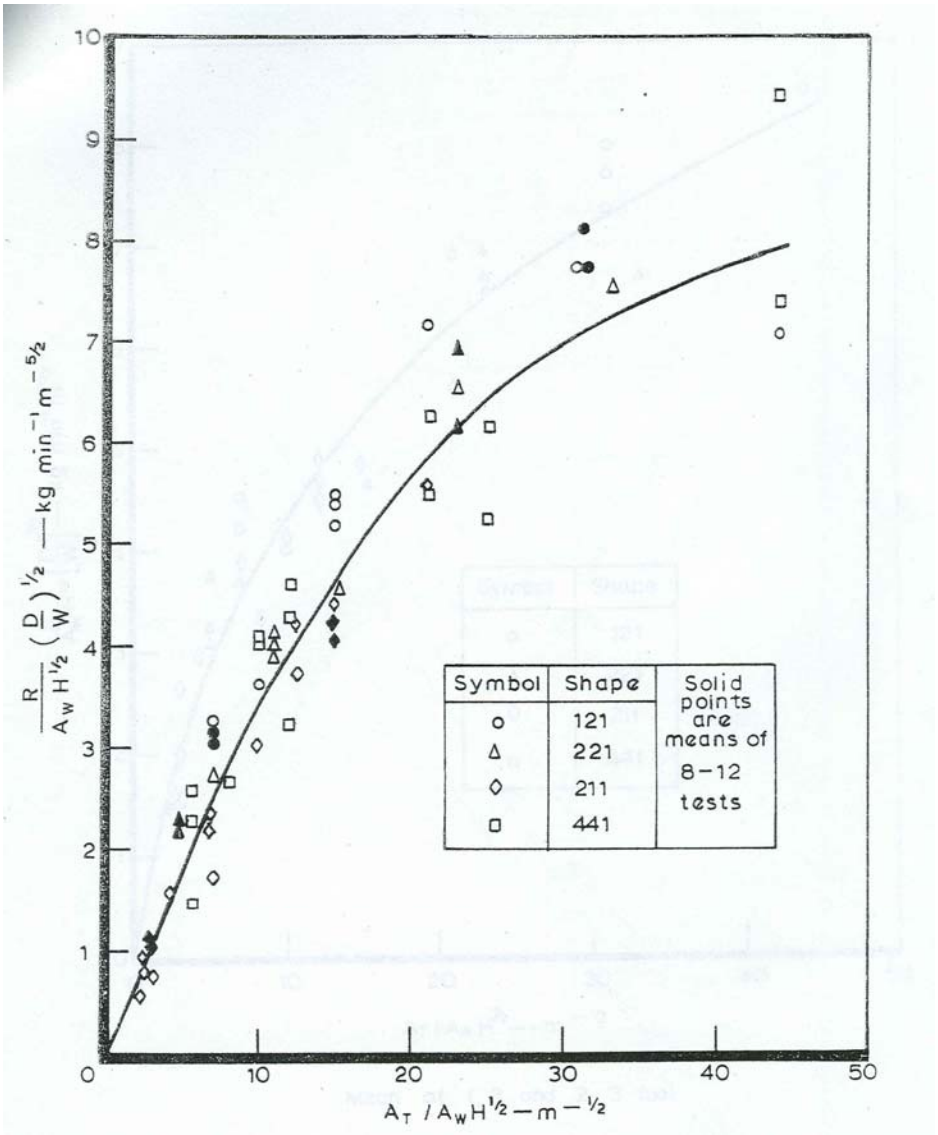

Figure 2.14: CIB Burning Rate Model[16]

The above plot shows essentially a relationship between the burning rate and the interior area of the enclosure. The influence of this area on the burning rate is thermal feedback due to a net heat flux at the boundaries. However in order to fully appreciate this influence on the burning rate, the ventilation limitation and fuel surface area should be included in the model. Applied to the current research, the burning rate must scale directly with the mass flow rate of air into the compartment as estimated by the

ventilation factor. Therefore, the burning rate expressed in this model should be independent of the opening factor in the current research. Figure 4.25 confirms this reasoning.

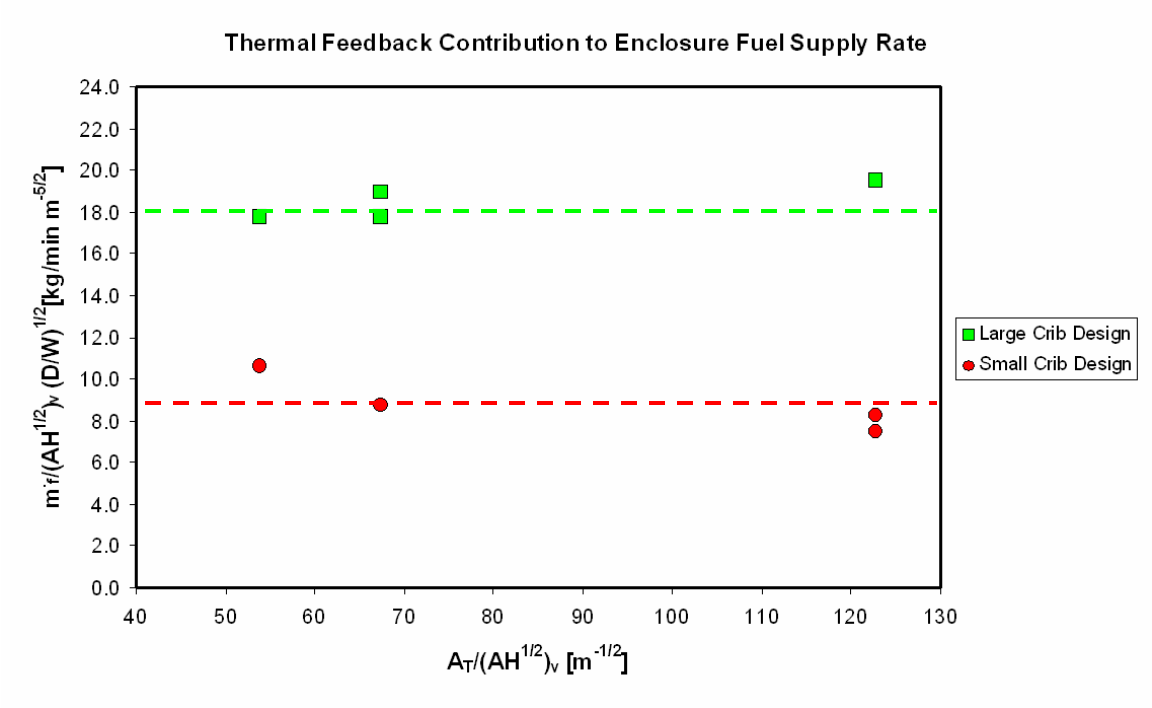

Figure 4.24: Scaling of Thermal Feedback Contribution to Fuel Supply Rate

Croce's scaling attempt for the burning rate relied on Heskestad's hypothesis for the quasi-steady period of burning. The hypothesis chose the duration of the steady state as the characteristic time and as such, many of the model inputs were different than those used in this report. The importance of scaling the thermal properties of the boundaries was recognized; however, the assumption that the walls act as perfect insulators essentially negates this consideration. The results for the scaling of the boundaries contained two primary differences. The first was the absence of a dimensionless group for transient wall conduction. This is because it was assumed that heat would only be

stored in the walls, not lost through conduction. The second was a modified relationship between the wall thickness group and the characteristic time. In addition to these changes, the application of the theory to the compartment design did not recognize the change of thermal properties with respect to temperature. Thermal properties were evaluated at a reference temperature of 300^{o}C.

The results for the burning rate of the wood cribs inside the enclosures are plotted as a function of compartment ventilation in Figure 2.28. The time averaged data are presented in log-log fashion. This combination coupled with a lack of published values makes it difficult for one to appreciate the true accuracy of the results. The data suggests that for well ventilated compartments, the burning rate inside the enclosure is approximately equal to the free burning rate. Therefore, the thermal feedback from the walls of the compartment is said to have a negligible influence on the burning rate.

4.2.4 Temperature Results

Transient gas and surface temperatures were recorded during each experiment. The change in these temperatures with time reflects the growth of the fuel supply rate from the wood crib. The scaling theory dictates that all such temperatures, measured at homologous locations, are independent of length scale. The temperature results are therefore presented for individual locations in Figures 4.25a through 4.25h. In order to provide a consistent definition of spatial location, the dimensionless height is

$$\omega \equiv \frac{z}{H} \tag{4.5}$$

where z is the height of the thermocouple above the floor surface. Note that inconsistency in the vent height at the 1/8 scale should create generally lower

temperatures due to decreased ventilation. This effect is not so well appreciated in the small crib design; whose burning rates were not significantly influenced by ventilation.

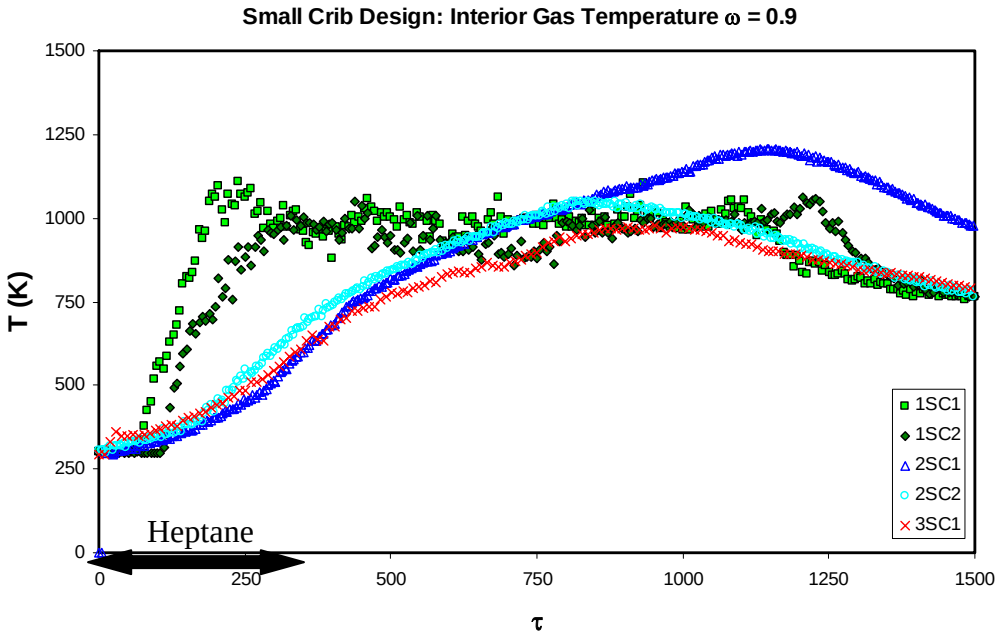

Figure 4.25a: Small Crib Design, Interior Gas Temperatures ω = 0.9

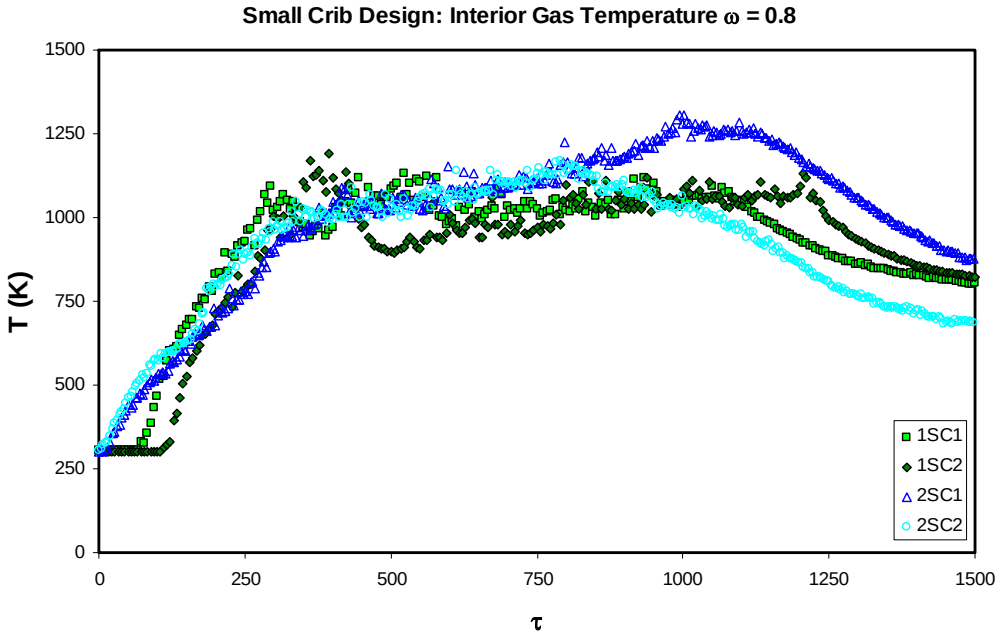

Figure 4.25b: Small Crib Design, Interior Gas Temperatures ω = 0.8

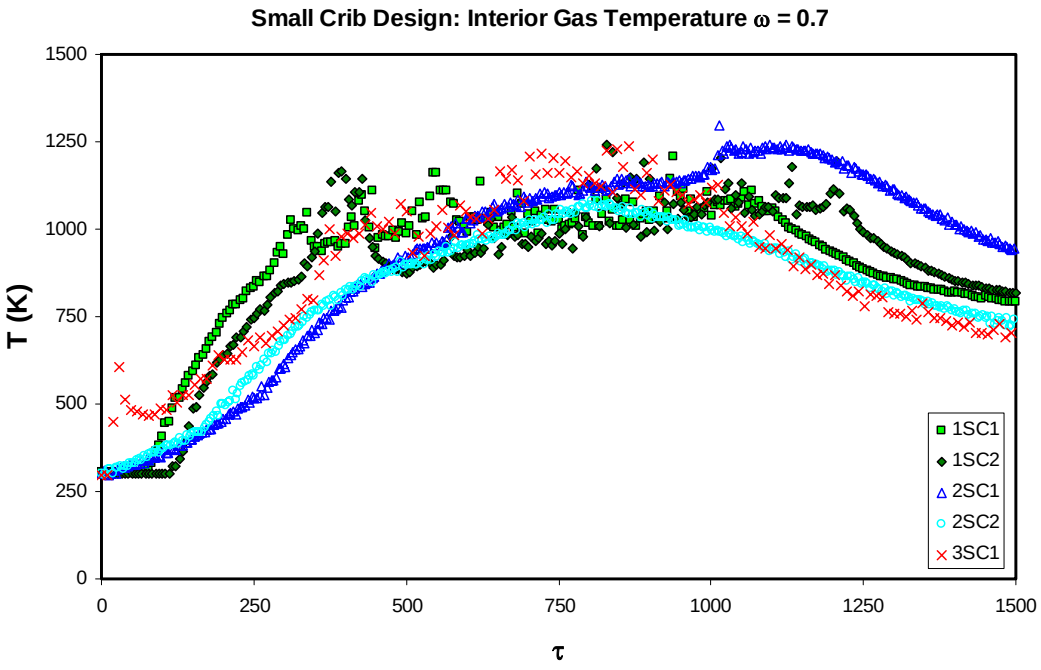

Figure 4.25c: Small Crib Design, Interior Gas Temperatures ω = 0.7

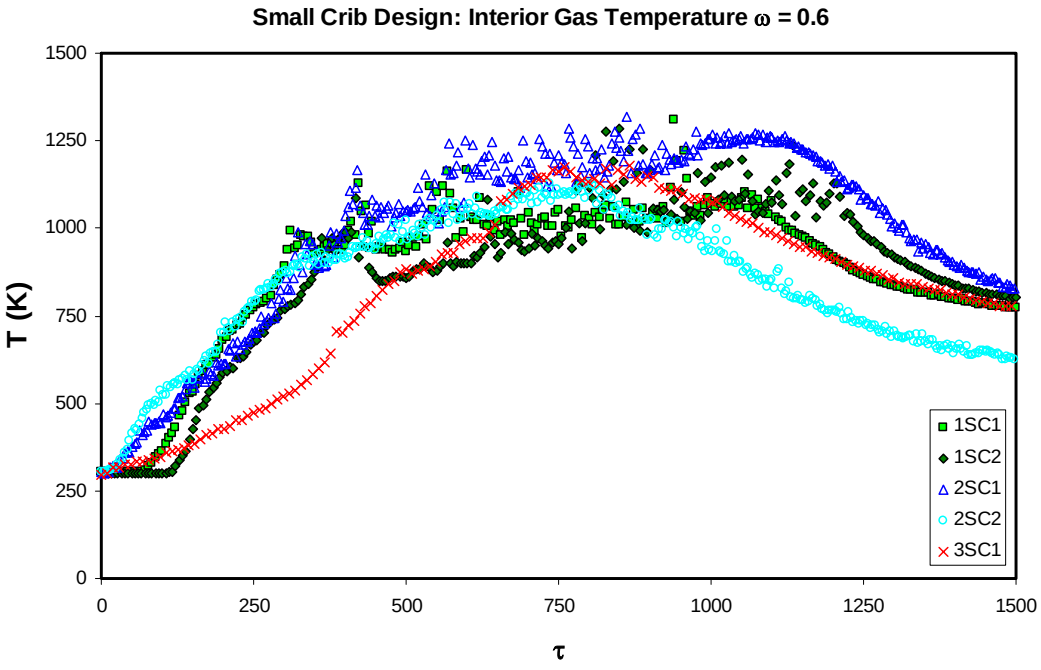

Figure 4.25d: Small Crib Design, Interior Gas Temperatures ω = 0.6

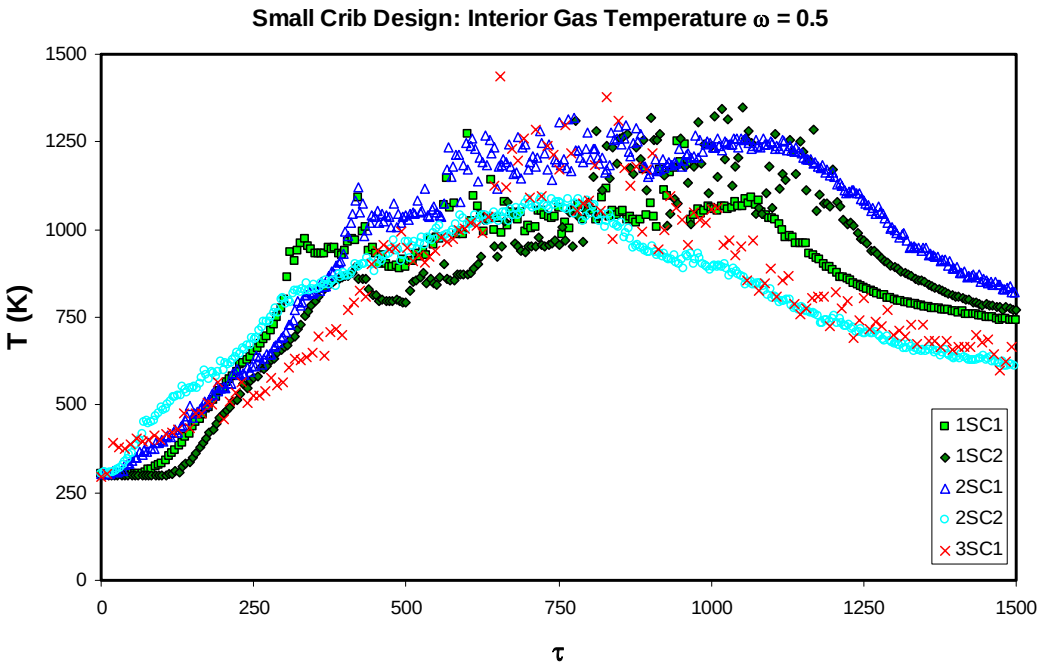

Figure 4.25e: Small Crib Design, Interior Gas Temperatures ω = 0.5

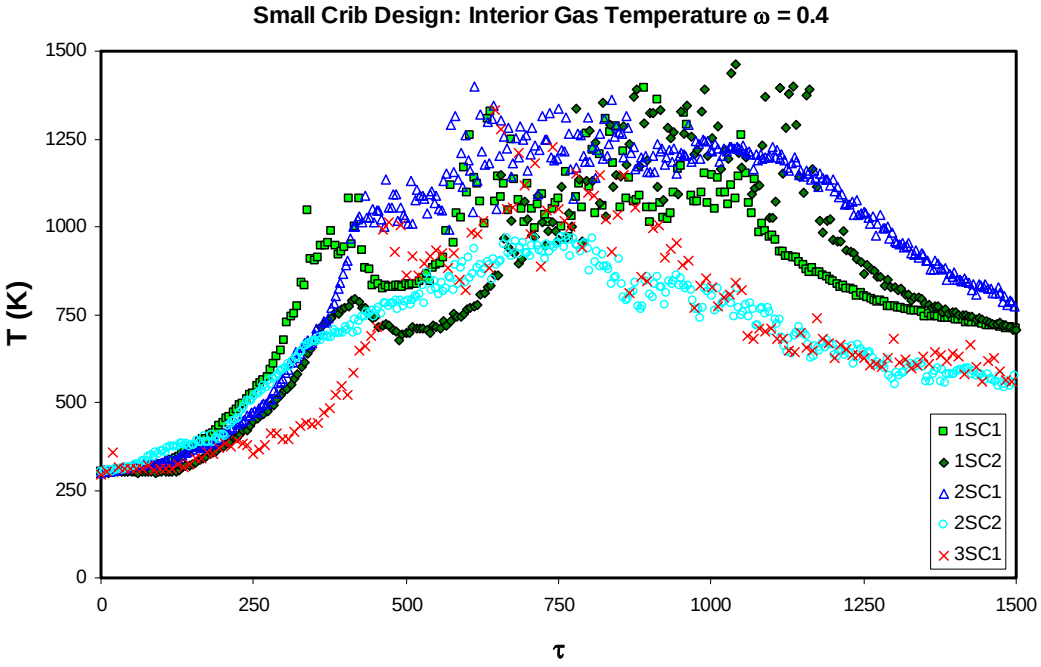

Figure 4.25f: Small Crib Design, Interior Gas Temperatures ω = 0.4

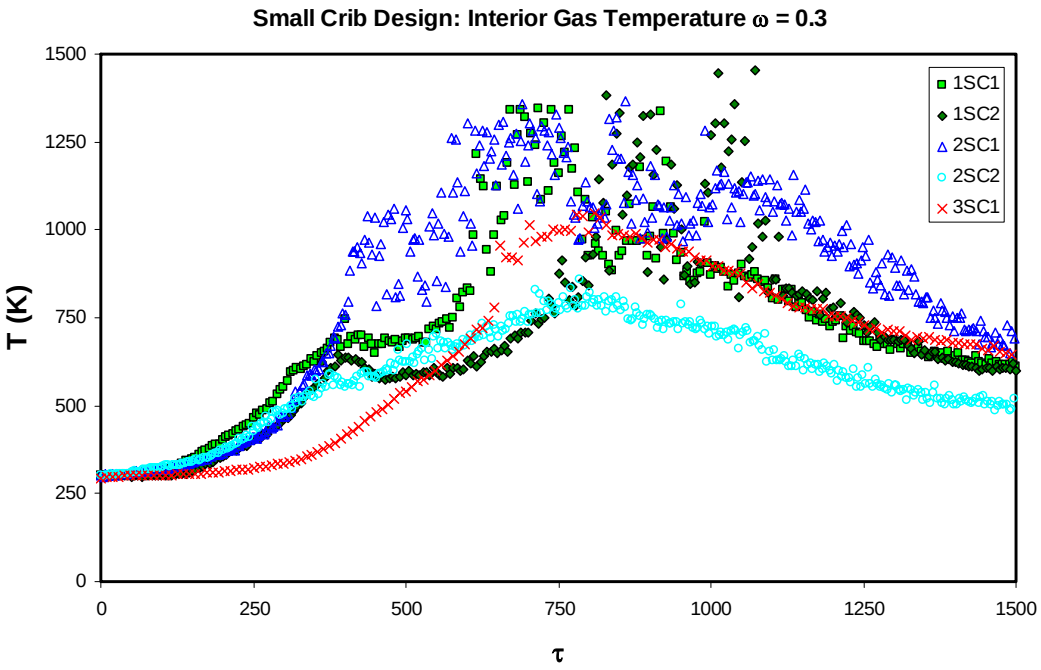

Figure 4.25g: Small Crib Design, Interior Gas Temperatures ω = 0.3

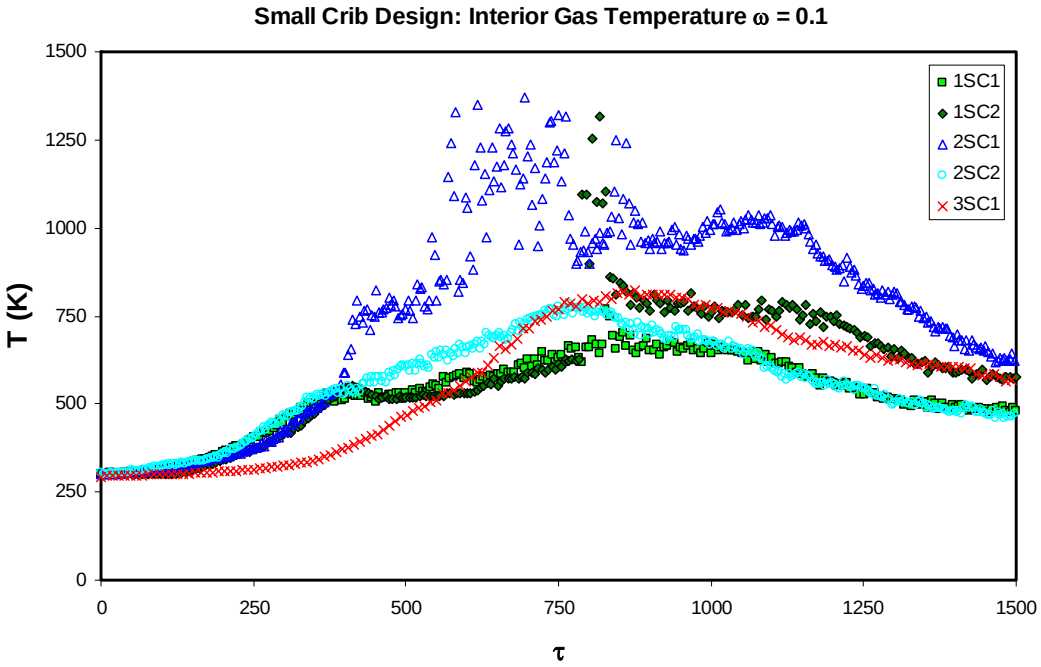

Figure 4.25h: Small Crib Design, Interior Gas Temperatures ω = 0.1

The interior homologous transient temperatures are generally in good agreement for the small crib design. It is clear that there is a time lag in temperature rise for the uppermost thermocouple in the profile. This time lag is due to a lag in ignition of the wood. Figure 4.25a denotes the duration of the heptane pool fire. The same time lag is not present for thermocouples at lower locations due to their proximity to the heptane flame. The largest difference in temperatures between experiments seems to occur in the transition region between the hot upper and cool lower layers of the compartment corresponding to the two zone concept.

In recognition of the scale independence of gas temperatures, the same independence should be found for the location of this transition region. In order to more clearly present this region, an instantaneous temperature profile is presented in Figure 4.26 for a representative steady state dimensionless time.

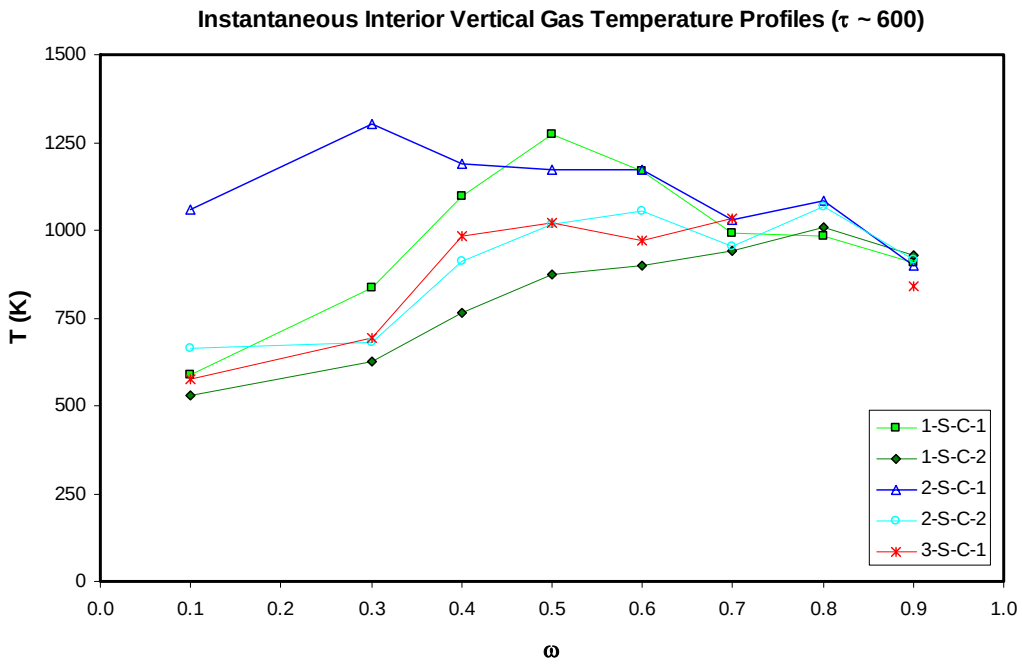

Figure 4.26: Small Crib Design, Interior Vertical Temperature Profiles, $\tau = 600$

Figure 4.26 shows much more clearly how the temperature profile variation is quite small in the clearly defined regions of the upper and lower layers. The middle three thermocouple locations measuring the transition region show the largest variation.

The best agreement between experiments is found with 3-S-C-1 and 2-S-C-2. Recall that the same can be said for the fuel supply rate results. This indicates the influence of the latter on gas temperatures in the compartment. Based on visual observation of Figure 4.26, with the exception of test 2-S-C-1, it appears that the transition from upper to lower layers consistently occurs at ω of approximately 0.35. This approximation is based simply on the steepest gradient between temperature measurements.

The temperature profile observed for experiment 2-S-C-1 is approximately uniform throughout the compartment. This instantaneous snapshot of the profile is representative of the steady state temperatures achieved during that test. It is not readily apparent why the lower layer temperatures achieved in this test are so much higher than those in its counterpart experiment 2-S-C-2. One possible explanation would be more effective sealing at the ceiling-wall connections during test 2-S-C-1, allowing for a more well developed hot upper layer. However, no significant leakage of smoke from the compartment was observed during either test. This inconsistency points to the need for further testing in this experimental configuration. Such testing will be accomplished as the research effort continues.

The same presentation of temperatures is given for the vertical profile at the vent is given in Figures 4.27a through 4.27e. These temperatures can be used with a mass balance to calculate the airflow into the compartment.

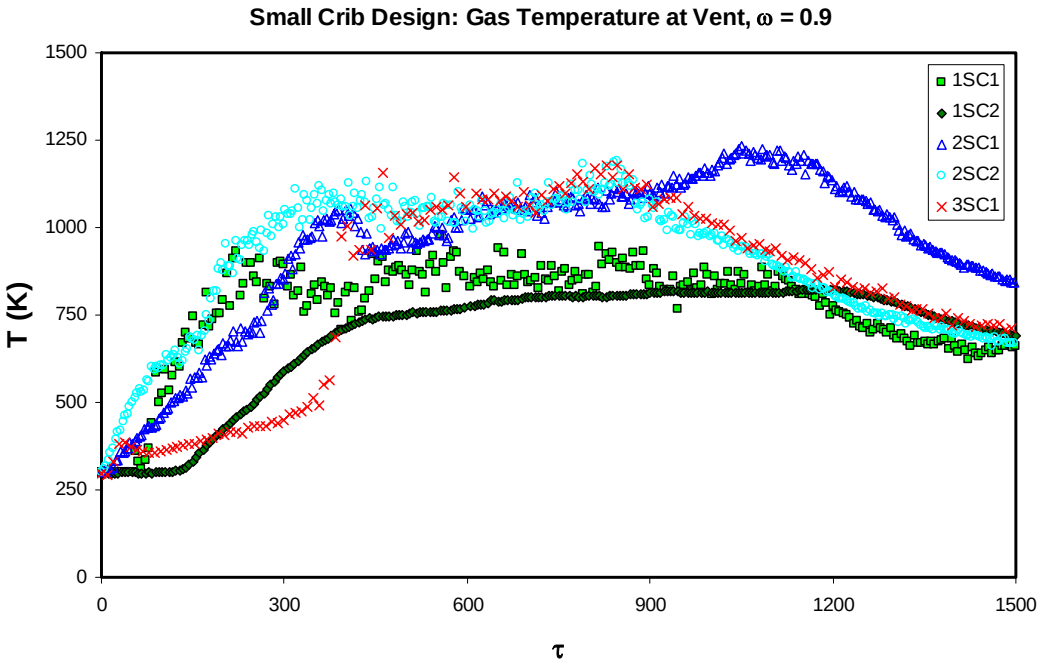

Figure 4.27a: Small Crib Design, Gas Temperature Profiles at the Vent ω = 0.9

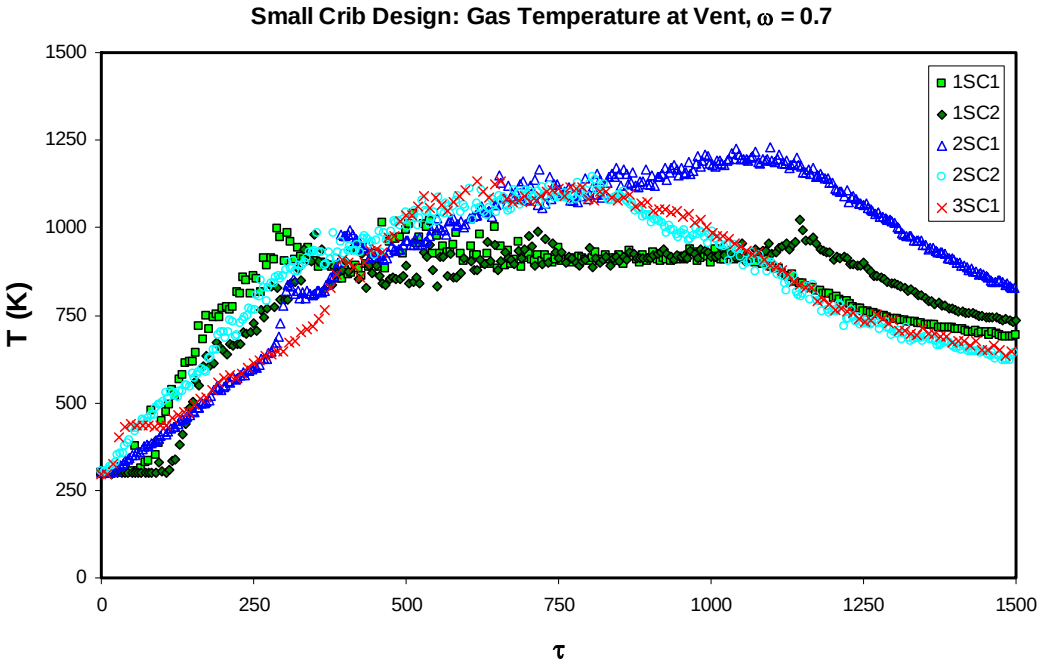

Figure 4.27b: Small Crib Design, Gas Temperature Profiles at the Vent ω = 0.7

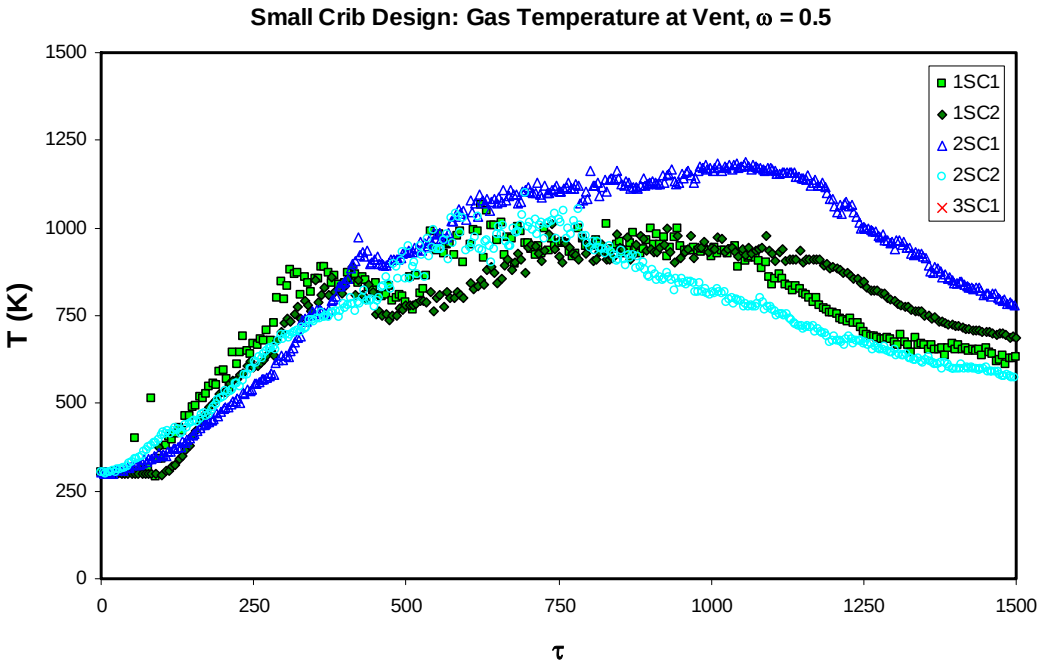

Figure 4.27c: Small Crib Design, Gas Temperature Profiles at the Vent ω = 0.5

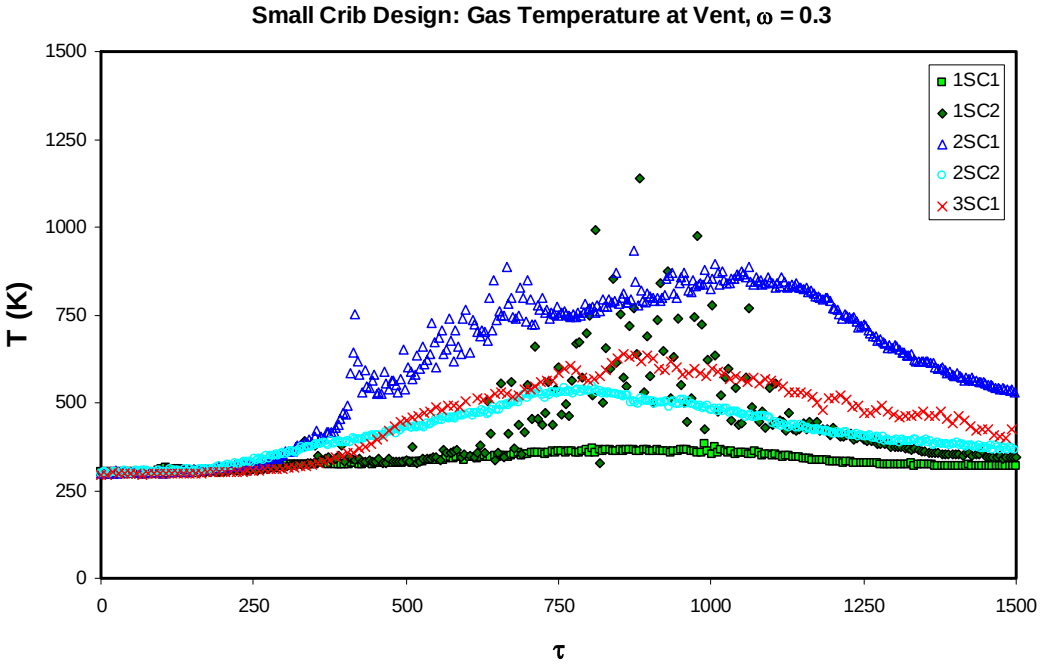

Figure 4.27d: Small Crib Design, Gas Temperature Profiles at the Vent ω = 0.3

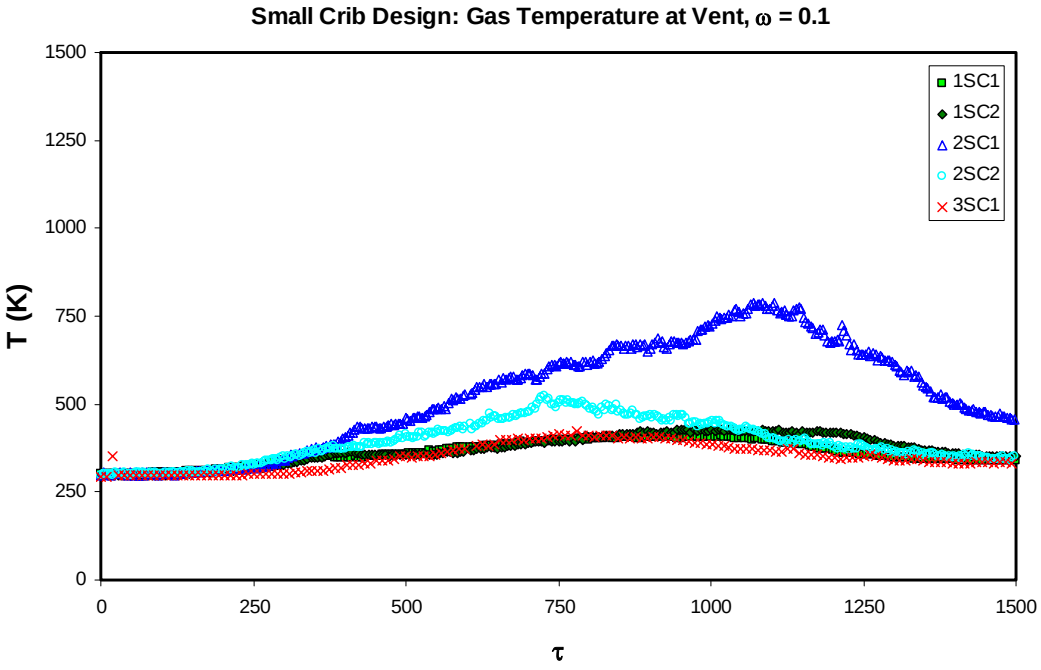

Figure 4.27e: Small Crib Design, Gas Temperature Profiles at the Vent ω = 0.1

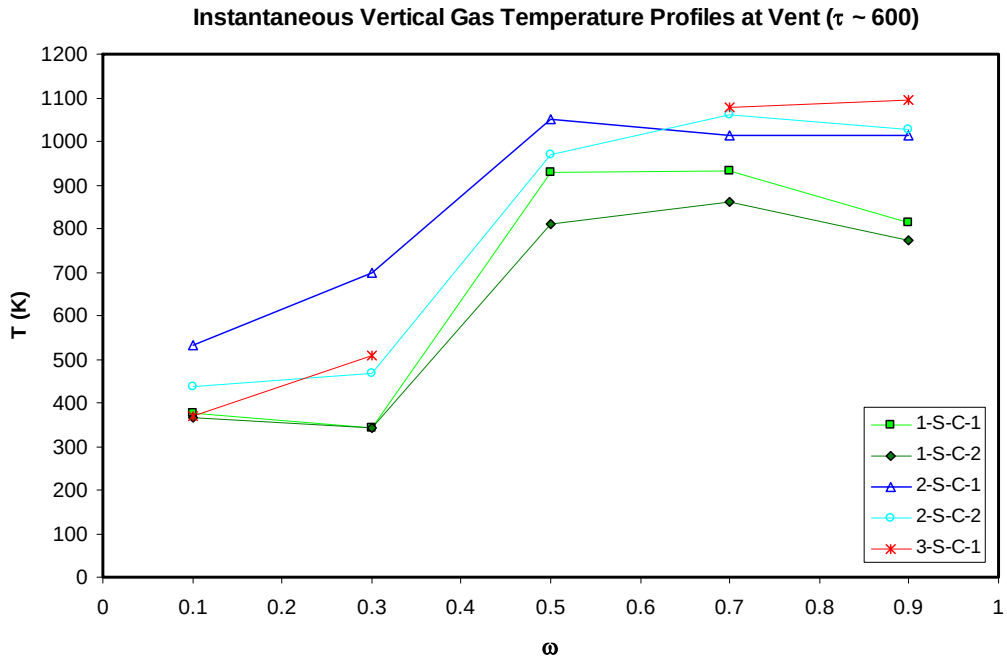

Figure 4.27f: Small Crib Design, Vertical Temperature Profile at Vent (τ~600)

The gas temperatures at the vent confirm that test 2-S-C-1 produced a higher than anticipated range of temperatures in the lower portion of the compartment. Visual comparison of temperatures in the interior portion of the compartment with those at the vent suggests horizontal layer uniformity, a common assumption in zone modeling. The final temperatures presented for the small crib design are the surface temperatures of the upper wall and ceiling in Figures 4.28a and 4.28b. Note the time lag between the rise of the previously presented gas temperatures and that of the surface temperatures. Unfortunately, the ceiling surface temperature measurements were found to be questionable for both sets of crib designs as the values consistently indicate movement of the bead off of the surface and into the gas stream. This result for the ceiling surface temperatures has consequences in calculating net heat fluxes in section 4.2.6 of this report.

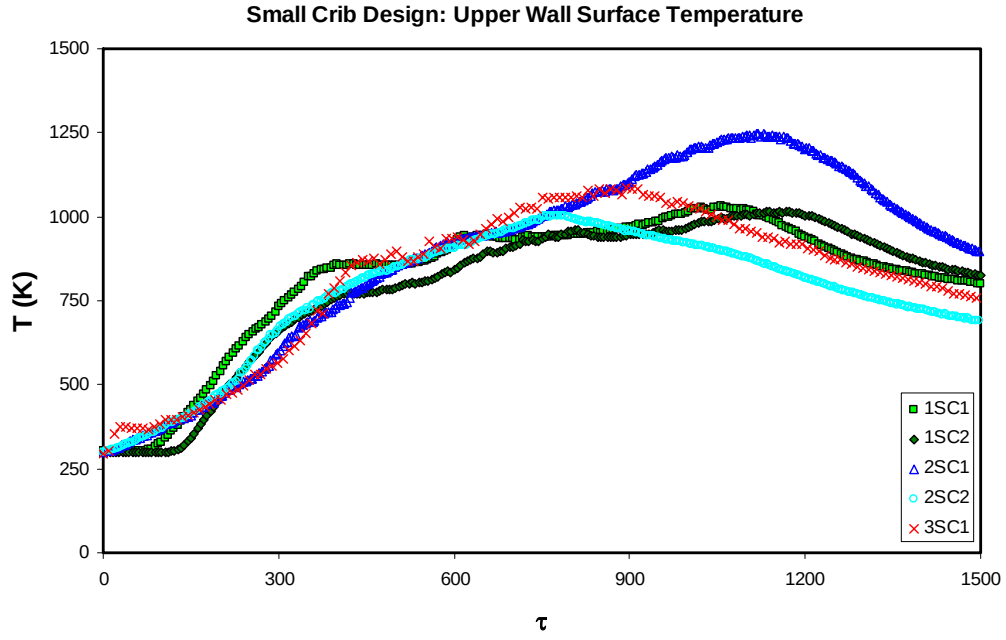

Figure 4.28a: Small Crib Design, Upper Wall Surface Temperatures

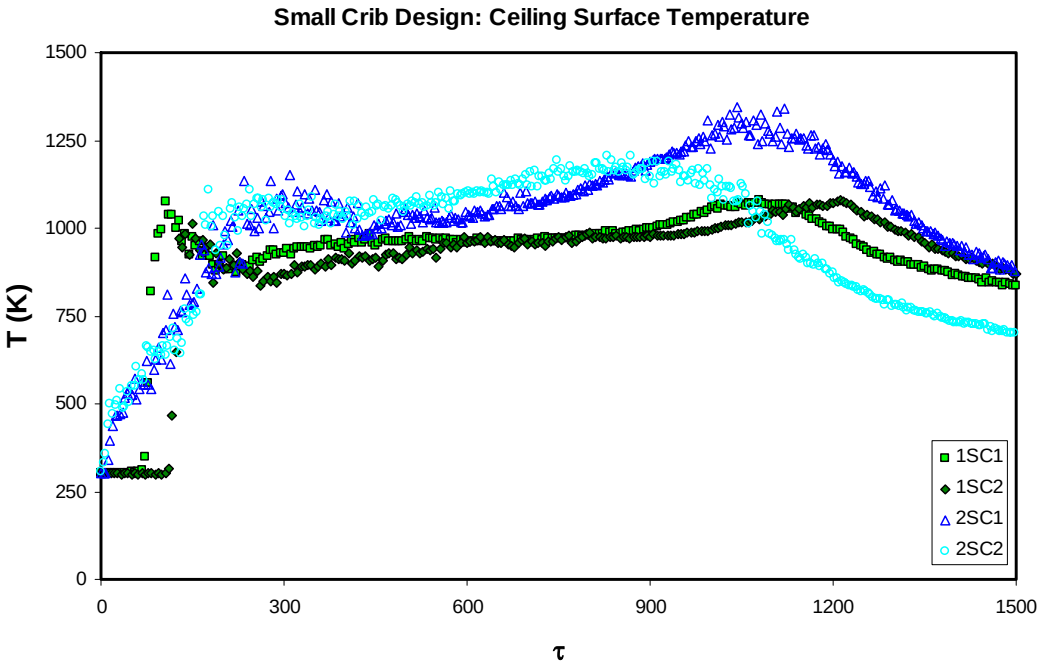

Figure 4.28b: Small Crib Design, Ceiling Surface Temperatures

The same presentation of temperature data is made for the large crib design.

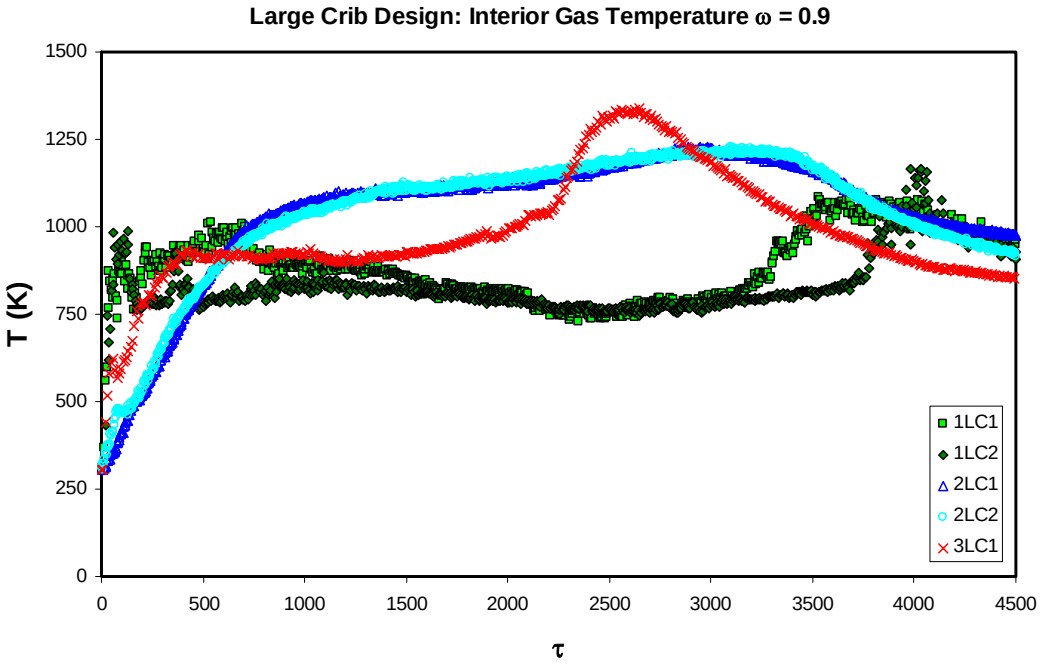

Figure 4.29a: Large Crib Design, Interior Gas Temperatures, ω = 0.9

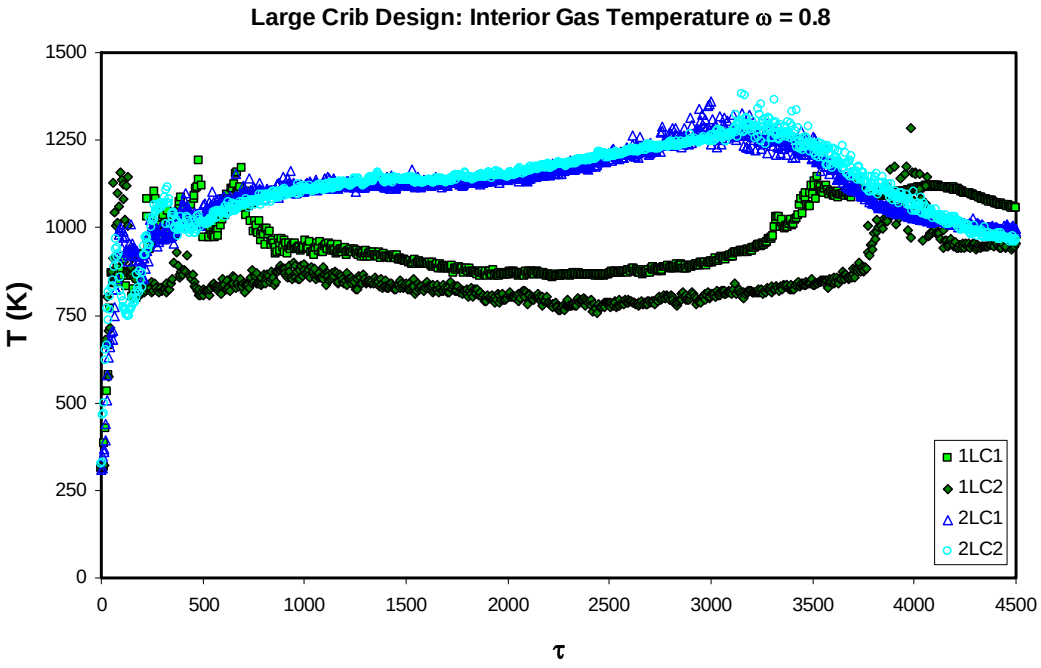

Figure 4.29b: Large Crib Design, Interior Gas Temperatures, ω = 0.8

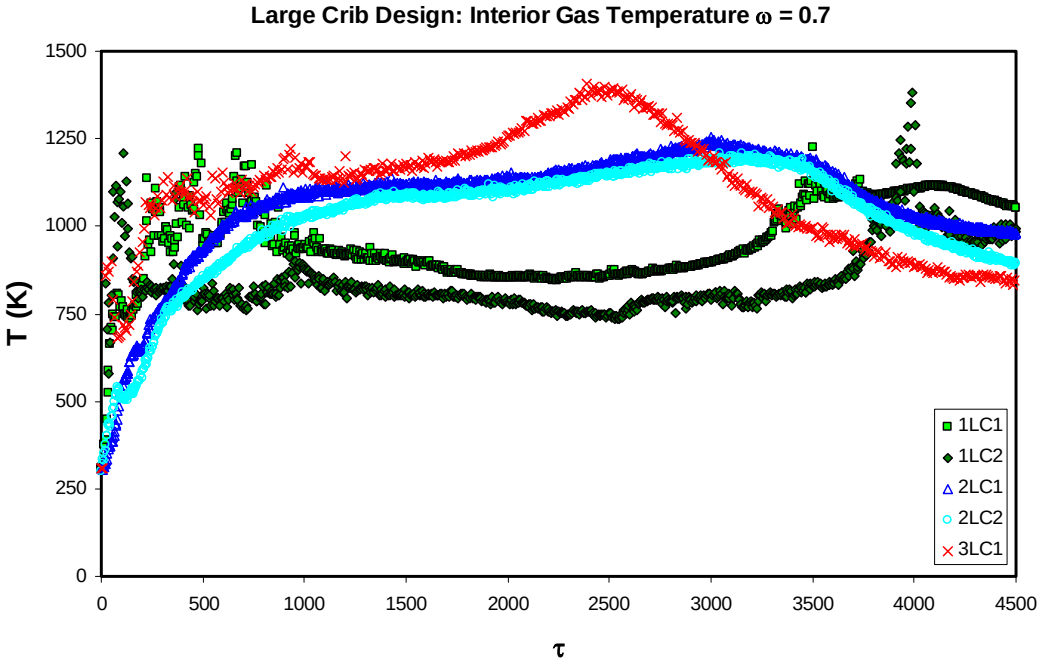

Figure 4.29c: Large Crib Design, Interior Gas Temperatures, ω = 0.7

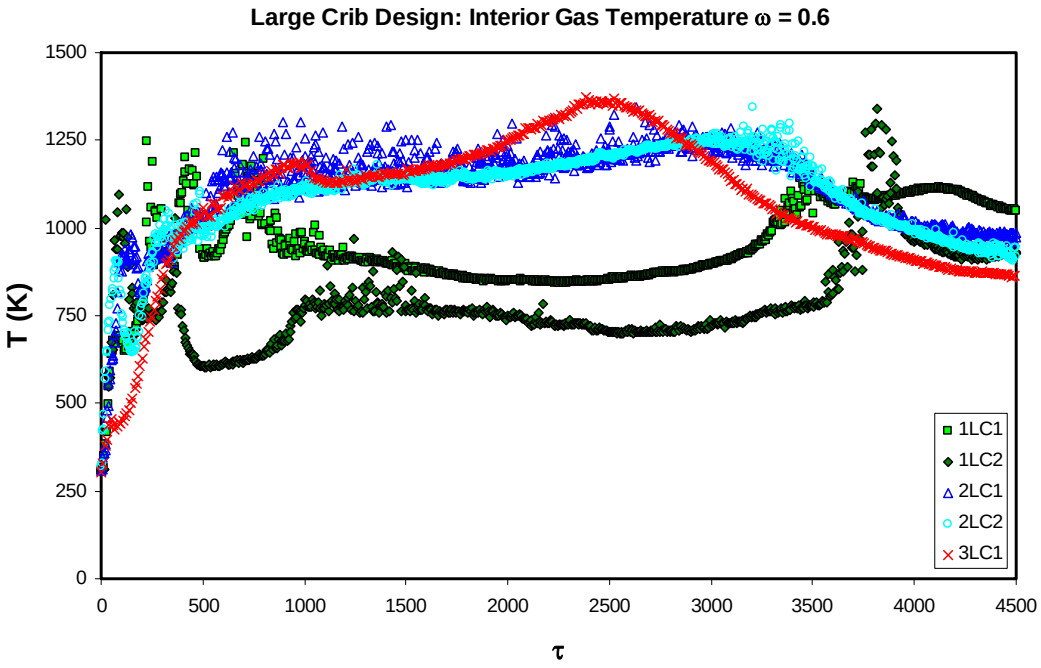

Figure 4.29d: Large Crib Design, Interior Gas Temperatures, ω = 0.6

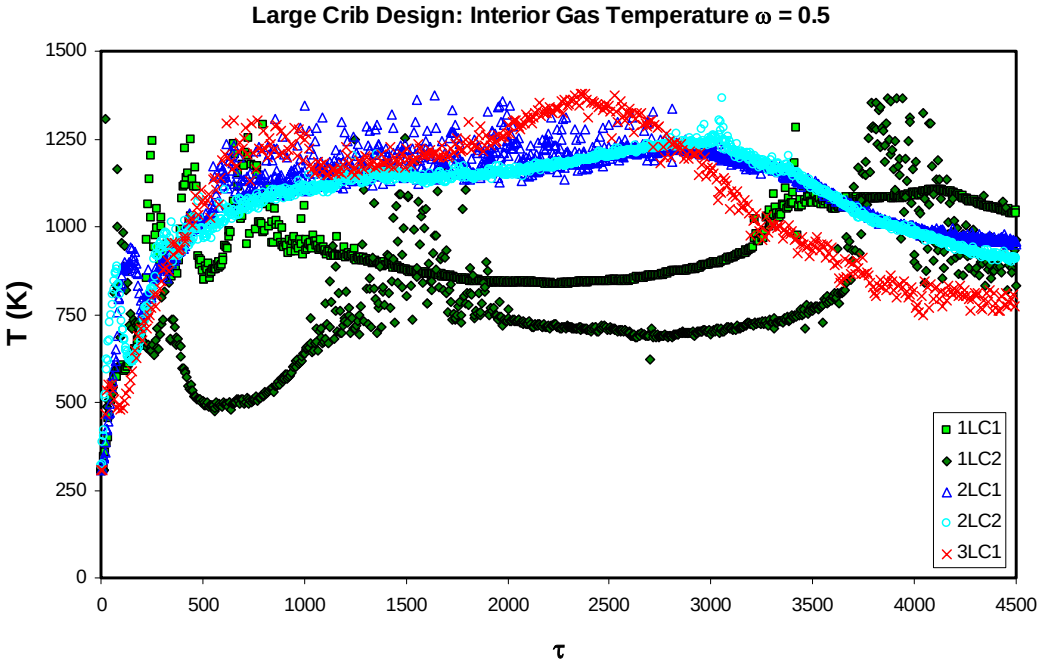

Figure 4.29e: Large Crib Design, Interior Gas Temperatures, ω = 0.5

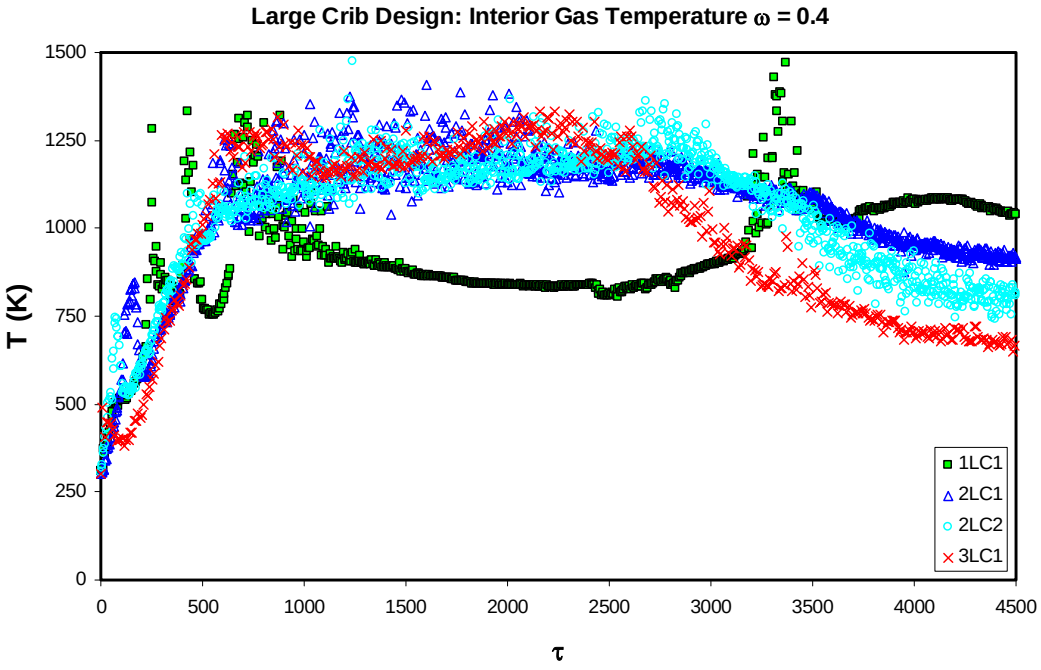

Figure 4.29f: Large Crib Design, Interior Gas Temperatures, ω = 0.4

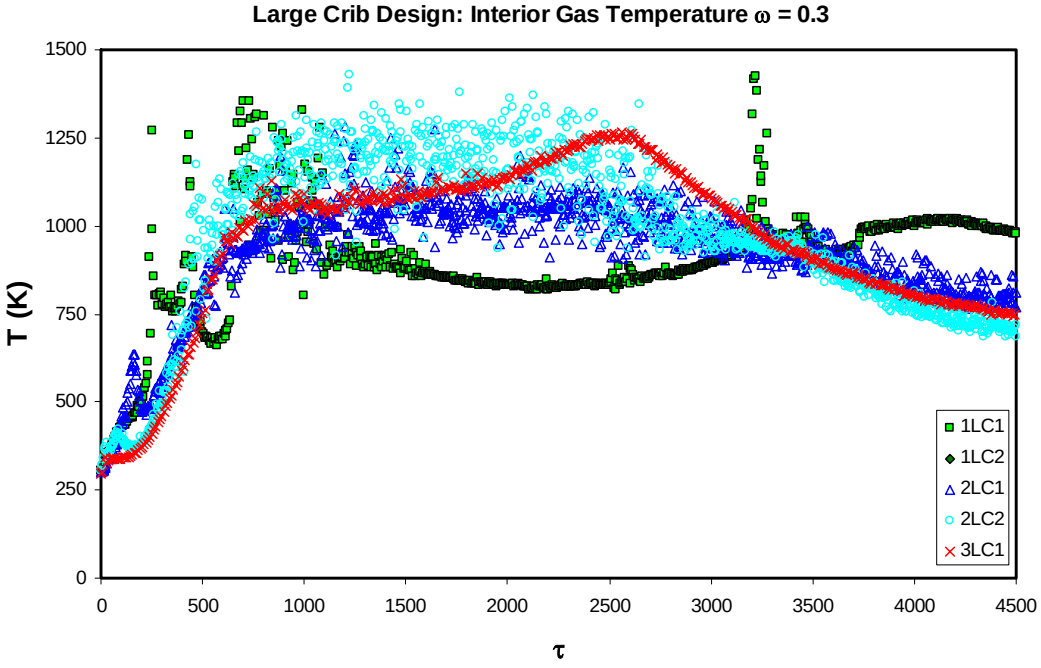

Figure 4.29g: Large Crib Design, Interior Gas Temperatures, ω = 0.3

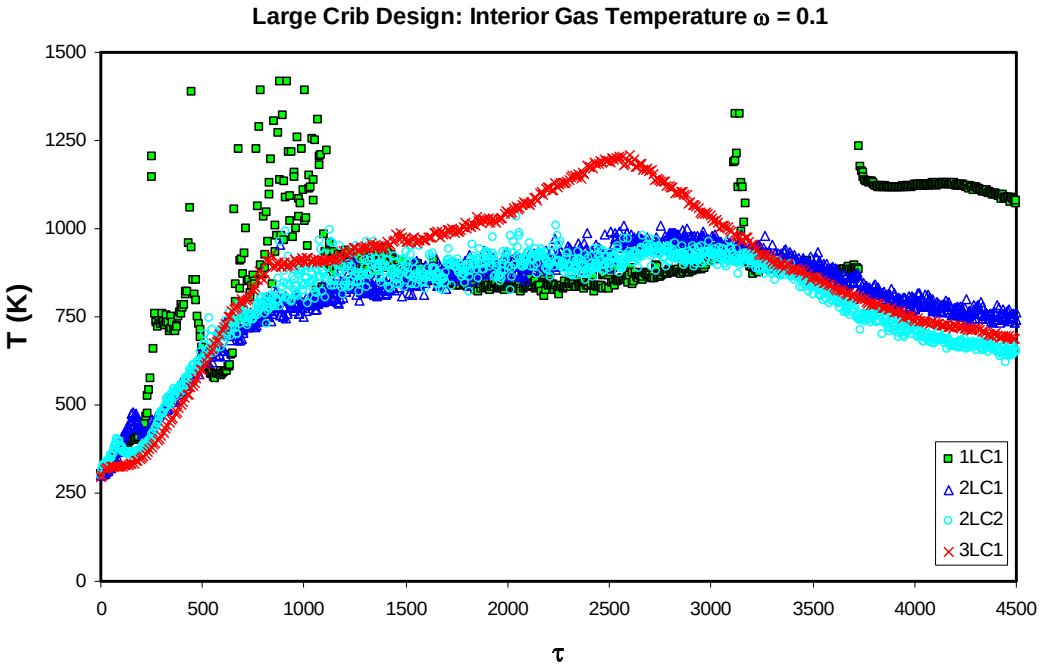

Figure 4.29h: Large Crib Design, Interior Gas Temperatures, ω = 0.1

Clearly the ventilation inconsistency translates into the 1/8 scale model for the large crib design. However, note the generally good agreement between the two larger scales. The large crib design produces a more uniform temperature profile throughout the gas. Note that Figure 4.29h demonstrates steady state temperatures on the order of 1000K. As in the case of the small crib design, an instantaneous temperature profile is used to portray this phenomenon.

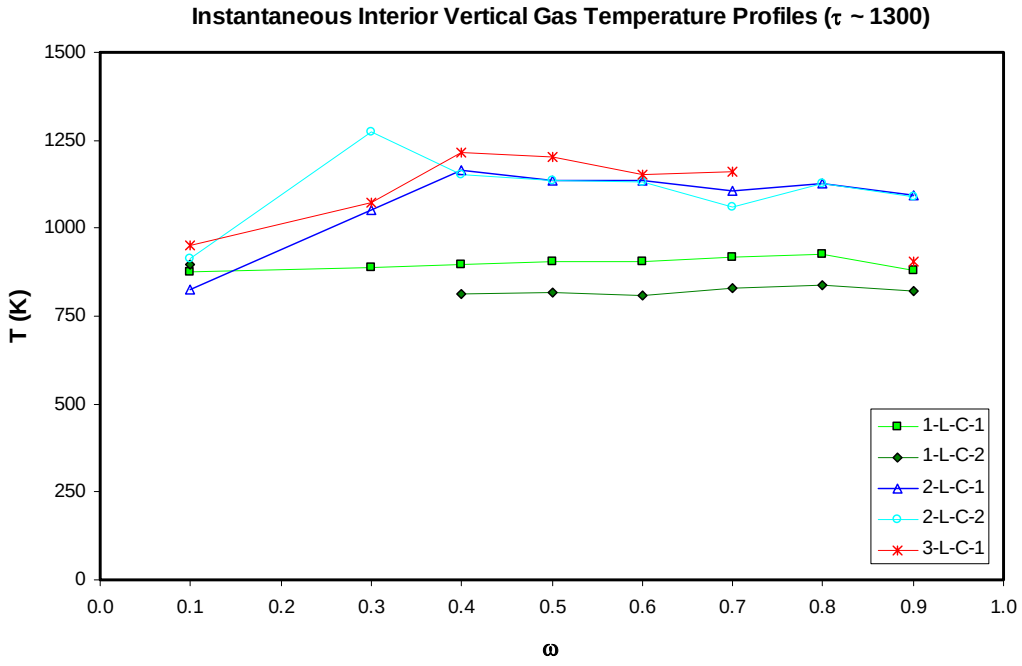

Figure 4.30: Large Crib Design, Interior Vertical Temperature Profiles, τ = 1300

The instantaneous temperature profiles reveal the furnace-like behavior of these compartment fires. The temperature is approximately uniform throughout the compartment in each case. Frequent fluctuations in the temperature readings are the product of turbulent fluctuations in the flame. The uppermost thermocouple in test 3-L-C-1 records a significantly lower temperature at steady state. Figure 4.29a shows that this temperature was consistently lower than those measured for the rest of the profile during the test. It is clear that this fire was ventilation limited. The upper layer consisted of a fuel rich mixture of gases. Recall that test 3-L-C-1 produced leakage of smoke through cracks in adjoining insulation boards as the test progressed in time. As the fire progressed, so did the slow expansion of the cracks. The sharp rise of the gas temperature at ω = 0.9 and τ = 2200 in this test was linked to the observation of ignition

of those leaking gases at the ceiling. Therefore, the rise in temperature was likely the product of ignition of this layer of unburned fuel near the thermocouple in question. A sharp increase in the fuel supply rate is also evident at this dimensionless time in Figure 4.22a. It seems that this leakage had a similar but much less pronounced effect on the thermocouple at $\omega = 0.7$. The lack of flame in the layer of fuel rich gases near $\omega = 0.9$ also provides an explanation for the significant decrease in scatter of the temperature data at this location.

The vertical temperature profile of the gas at the vent is presented below in Figures 4.31a through 4.31e for the large crib design.

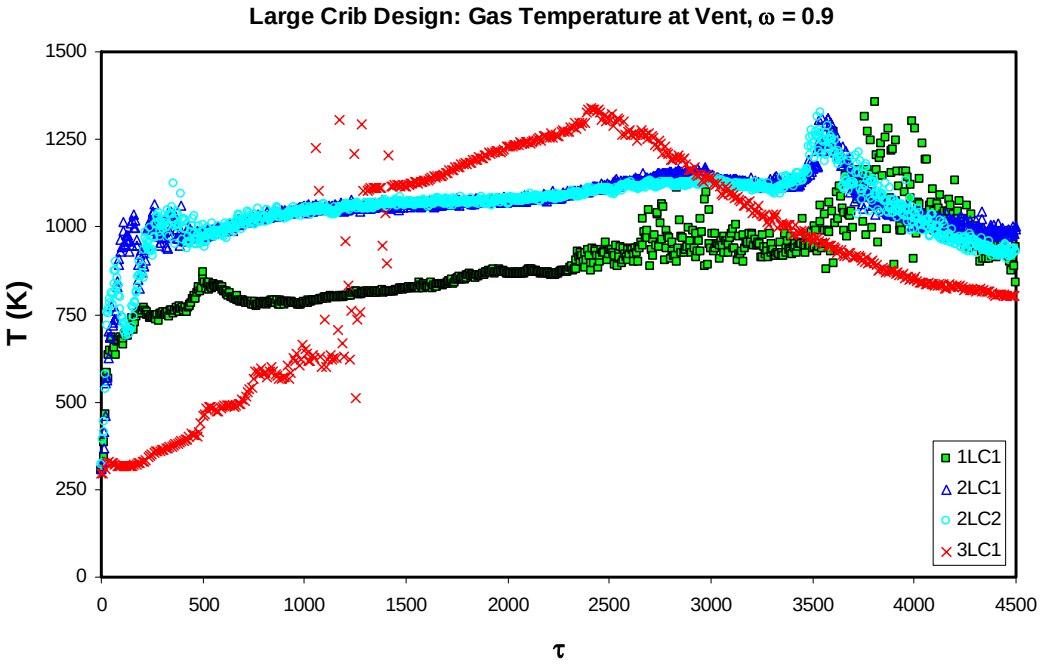

Figure 4.31a: Large Crib Design, Interior Gas Temperatures, $\omega = 0.9$

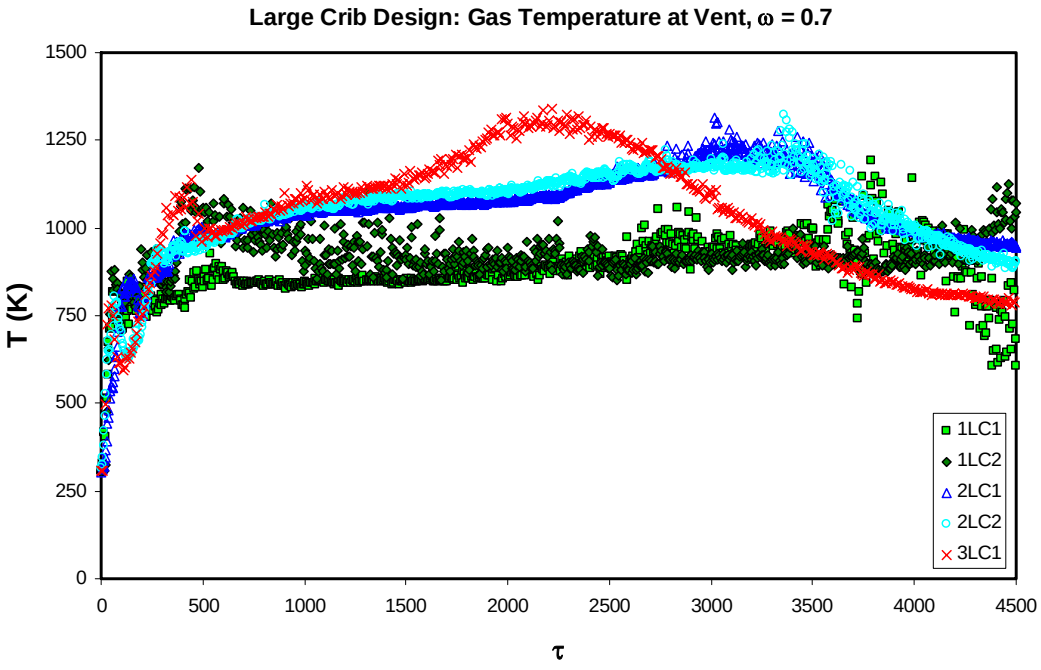

Figure 4.31b: Large Crib Design, Interior Gas Temperatures, ω = 0.7

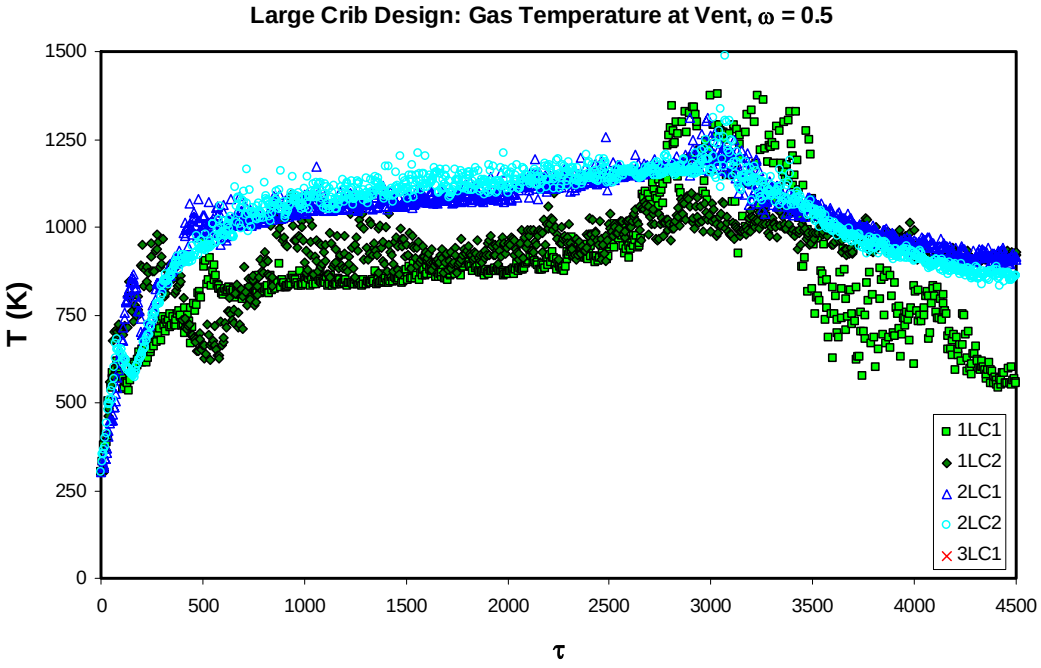

Figure 4.31c: Large Crib Design, Interior Gas Temperatures, ω = 0.5

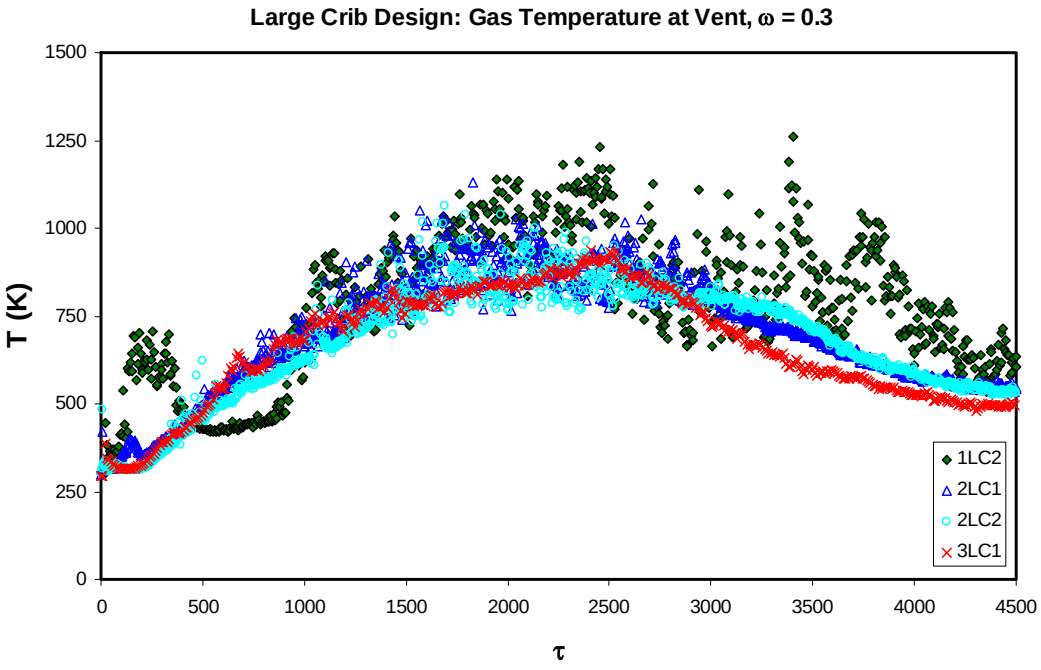

Figure 4.31d: Large Crib Design, Interior Gas Temperatures, ω = 0.3

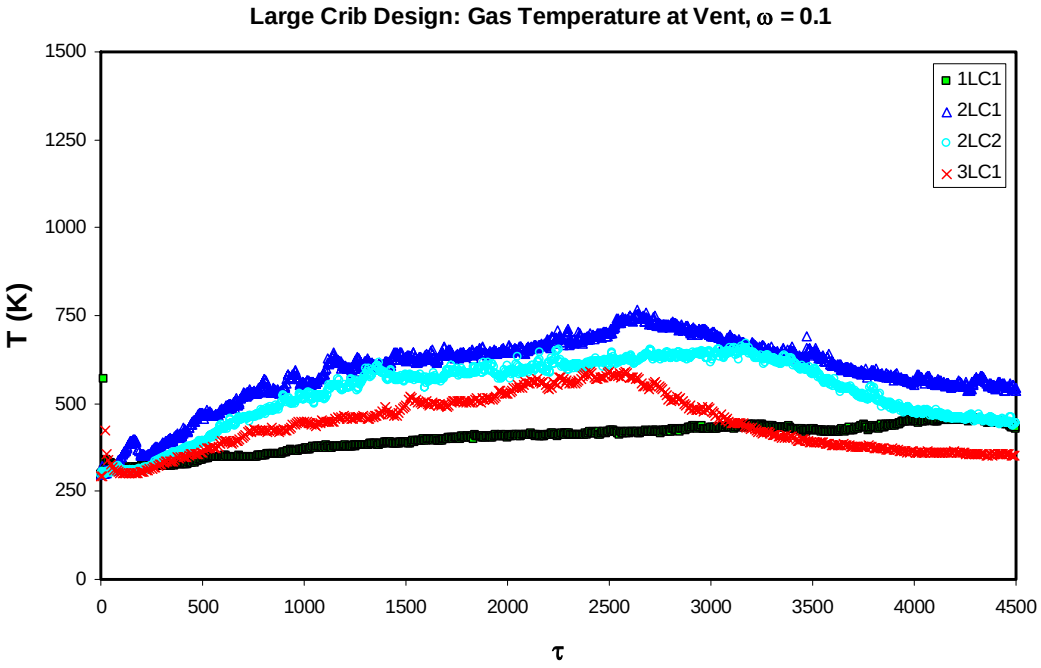

Figure 4.31e: Large Crib Design, Interior Gas Temperatures, ω = 0.1

The gas temperatures at the vent show the same trends as those measured in the interior of the compartment. Figure 4.31a illustrates a time lag in temperature rise for the uppermost thermocouple at the vent. This is further evidence of the presence of a layer of fuel rich gases keeping the probe relatively cool. The cool fuel rich layer is the most plausible explanation for the thermocouple at $\omega = 0.7$ measuring a higher temperature. However, the presence of flame at the vent suggests that a higher temperature should be found at $\omega = 0.9$. It could be that the probe has also strayed from the desired position and measurements are being taken slightly inside the compartment upper layer. An instantaneous set of temperature profiles at the vent is presented in Figure 4.32.

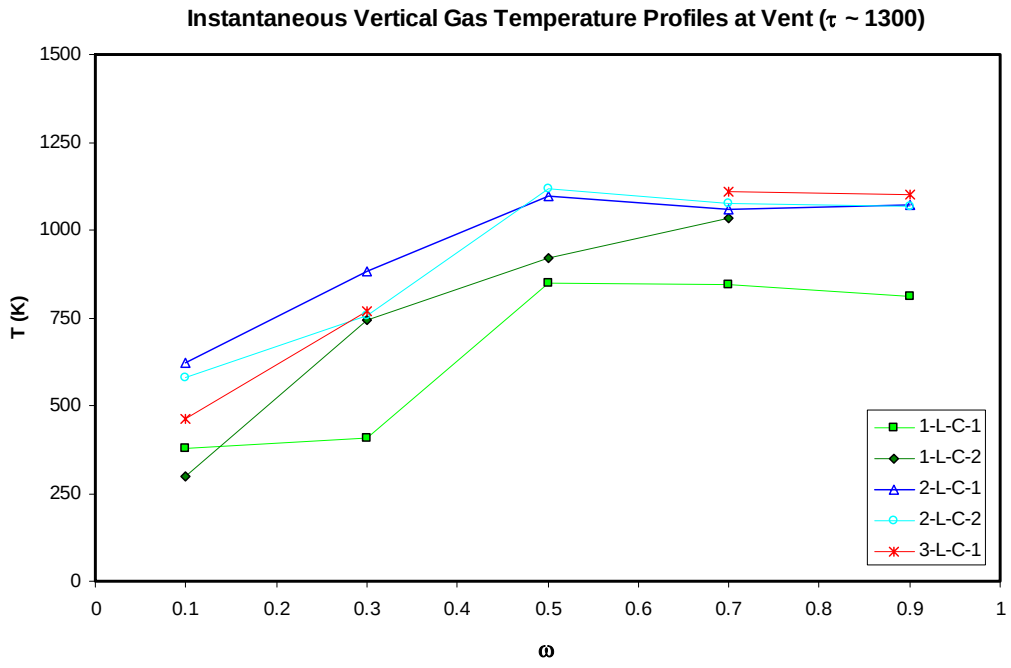

Figure 4.32: Large Crib Design, Gas Temperature Profiles at Vent, $\tau = 1300$

The data presented above reveals the presence of a cool lower layer at the vent. This is not the case for the interior of the compartment in which relatively uniform

temperatures were consistently found. This is evidence of a ventilation limited fire in which the cool fresh air entering through the lower portion of the vent directly determines the burning rate. As the air enters it is immediately mixed with hot fuel rich gases and a diffusion flame results.

Surface temperatures for the upper wall and ceiling are presented in Figures 4.33a and 4.33b. Note again that the ceiling measurements appear to be measuring gas temperatures. This will have consequences in the calculation of the net heat flux in section 4.2.6.

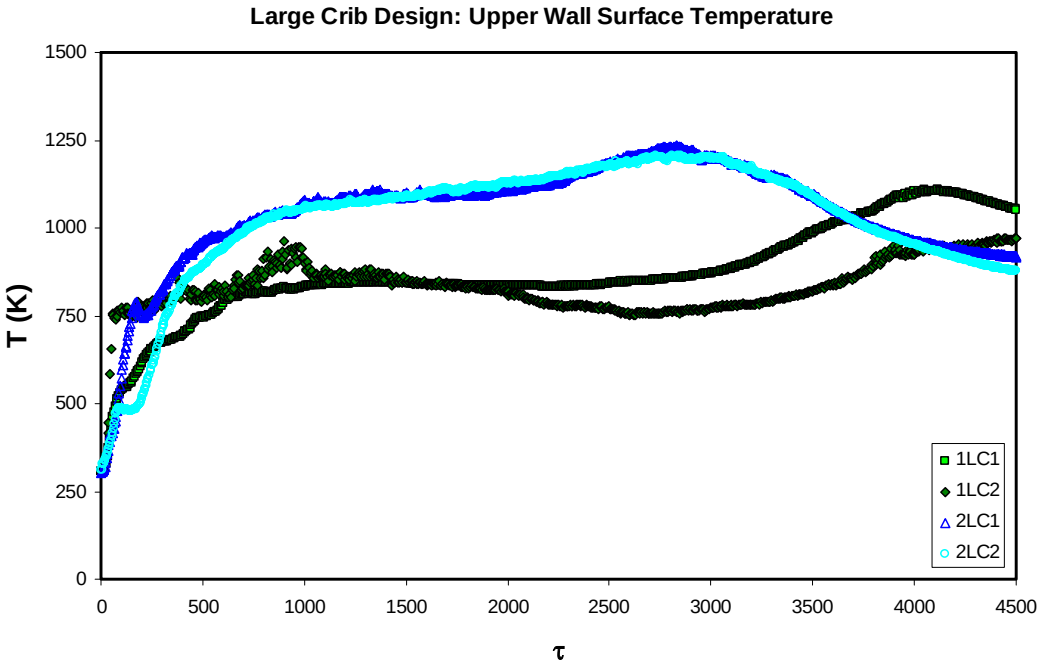

Figure 4.33a: Large Crib Design, Upper Wall Surface Temperatures

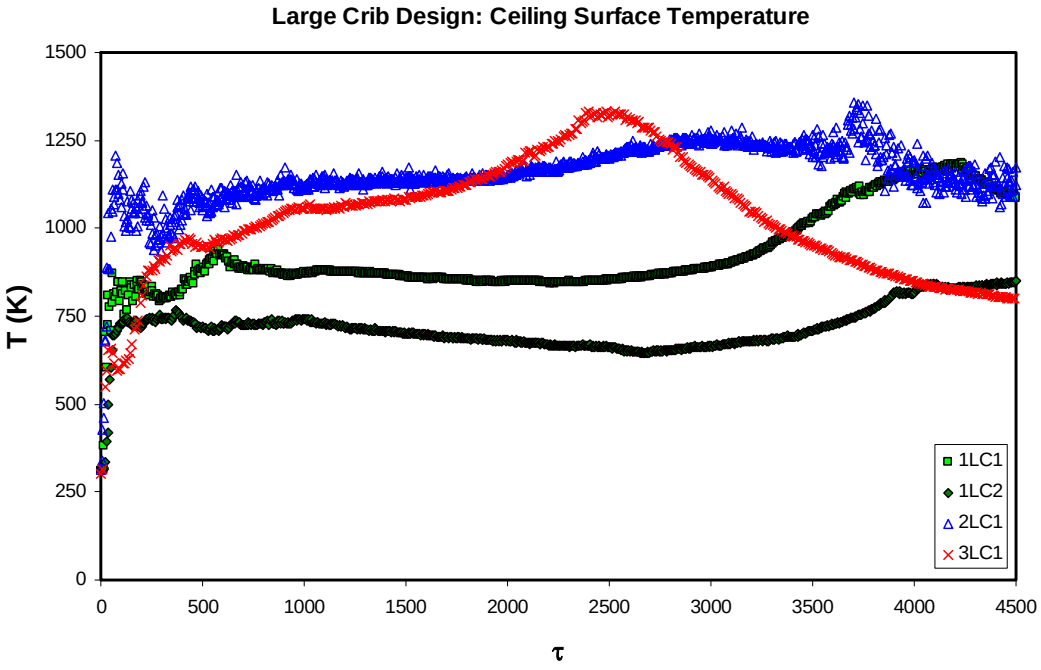

Figure 4.33b: Large Crib Design, Ceiling Surface Temperatures

The temperature results show a consistent gap between the 1/8 scale model and the larger compartments. This scaling inconsistency is due to the limitation on the burning rate caused by the inconsistency in the height of the vent at this scale. Higher temperatures are expected as the vent height is increased.

4.2.5 Gas Composition Results

Assuming a stoichiometric reaction, the global mechanism for oak burning with air as an oxidizer can be assumed to have the following form[30]:

$$CH_{1.7}O_{0.72}N_{0.001} + 1.765\left(O_2 + 3.76N_2\right) \Rightarrow 1.7CO_2 + 0.85H_2O + 6.636N_2 \qquad (4.6)$$

where a commonly used expression for simplified air composition of 21% Oxygen and 79% Nitrogen by volume has been assumed[31]. The chemical composition of oak was

taken from an experimentally determined value. The stoichiometric air to fuel ratio can be determined from the global mechanism.

$$\left(A/F\right)_{stoic} = \left.\frac{m_{air}}{m_{fuel}}\right|_{stoic} = \left(4.76\right)\left(1.765\right)\frac{MW_{air}}{MW_{fuel}} = 6.59 \qquad (4.7)$$

Incomplete combustion will produce some yield of Carbon Monoxide. In the case of ventilation limited fires, the yield of Carbon Monoxide is expected to be significant.

Gas was sampled from the compartments in order to determine the completeness of combustion at each scale. The upper sampling tube was located at $\omega = 0.9$ and the lower tube at $\omega = 0.1$ for all tests. The upper tube was tasked with measuring the concentrations of O_2, CO and CO_2 from the incoming sample gas. The lower tube measured only the concentration of O_2.

The scaling theory suggests that the yield of a given species is independent of scale. The gas analyzers output mole fractions of the various species[21]. In order to facilitate the clearest presentation, results are shown for transient mole fractions. The mole fractions are an appropriate representation of the $\pi_{species}$ model output for two reasons. The first is that specific heat (constant pressure), heat of combustion and ambient temperature used to define this dimensionless group are all assumed constant throughout the experiment and independent of scale. Thus, the only transient variable in the dimensionless group is the species yield. The second reason for using mole fractions is that there is no length scale present in the conversion from species yield to mole fraction. Therefore, the mole fraction is independent of scale.

Unfortunately, all of the gas sampling data from the 2/8 scale model was deemed unreliable due to small leakage pathways discovered in the tubing after testing. In

addition to the lack of data for the 2/8 scale model, a blockage in the lower layer tubing occurred during tests 1-S-C-2 and 3-S-C-1. The data acquired for the small crib design is extremely sparse. Results are presented in Figures 4.34a through 4.34d. The only comparison with respect to scaling is between the 1/8 and 3/8 scale models for the upper layer oxygen. The results of Figure 4.34a confirm that the fires are ventilation limited.

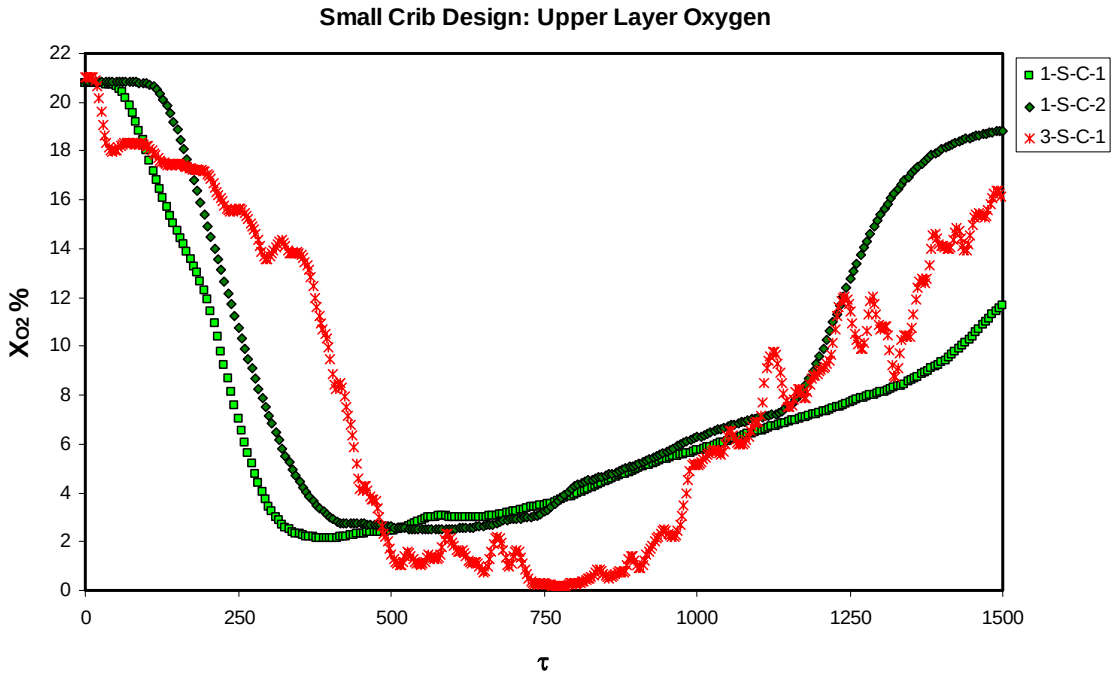

Figure 4.34a: Small Crib Design, Upper Layer O_2

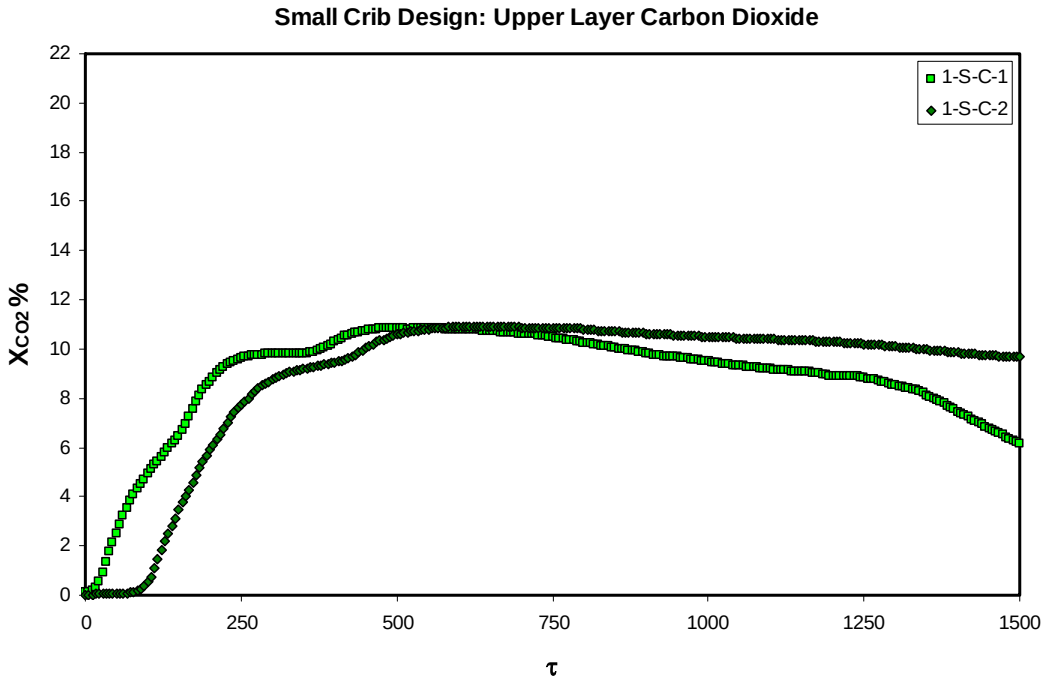

Figure 4.34b: Small Crib Design, Upper Layer CO_2

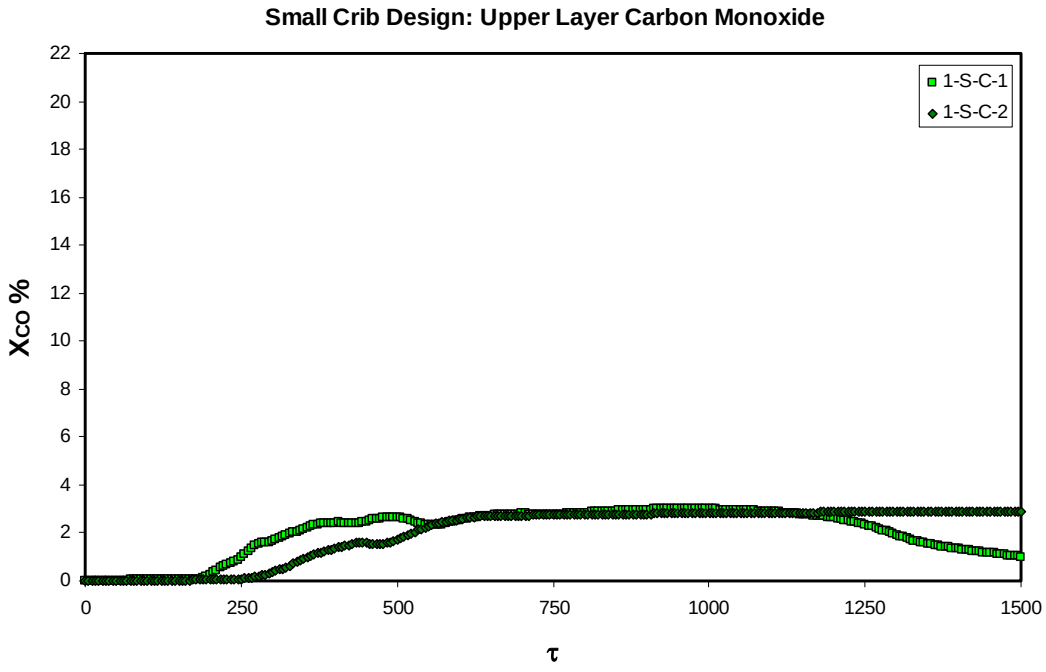

Figure 4.34c: Small Crib Design, Upper Layer CO

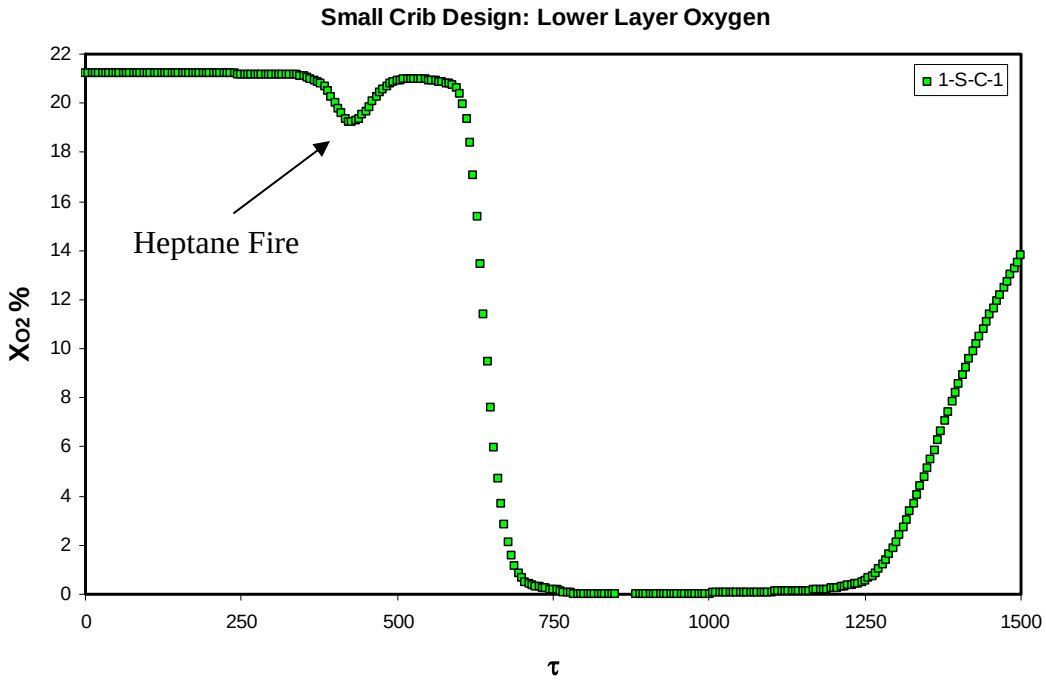

Figure 4.34d: Small Crib Design, Lower Layer O_2

The results for the 1/8 scale model oxygen concentration are quite surprising. The height of the tube in the lower layer is approximately equal to the height of the base of the crib at $\omega = 0.1$. It appears as though the compartment is lacking the amount of oxygen necessary to sustain combustion. A typical estimate of the critical mole fraction at the base of the fire is 10% [23]. It is important to note that the fire reaches a smoldering stage at $\tau \sim 900$. Based on the critical value, one would expect extinction at $\tau \sim 700$. However, this timing seems to be a natural progression of the decay phase in light of the comparison to the free burning experiment. Observations of the experiment highlight the fact that a flame was protruding through the vent throughout this stage of the fire. Due to the small vent width, no observations were possible for the compartment interior.

The timing of the sudden drop following the peak burning period in combination with the observation of flames at the vent introduces an intriguing explanation. It appears that enough heat had been stored inside the compartment to continue vaporizing solid fuel after the cessation of flame. As the fuel was produced it flowed out of the vent and met fresh air to produce a flame outside of the box.

The results for the large crib design are presented in Figures 4.35a through 4.35d. Once again, the presentation is without the 2/8 scale model data.

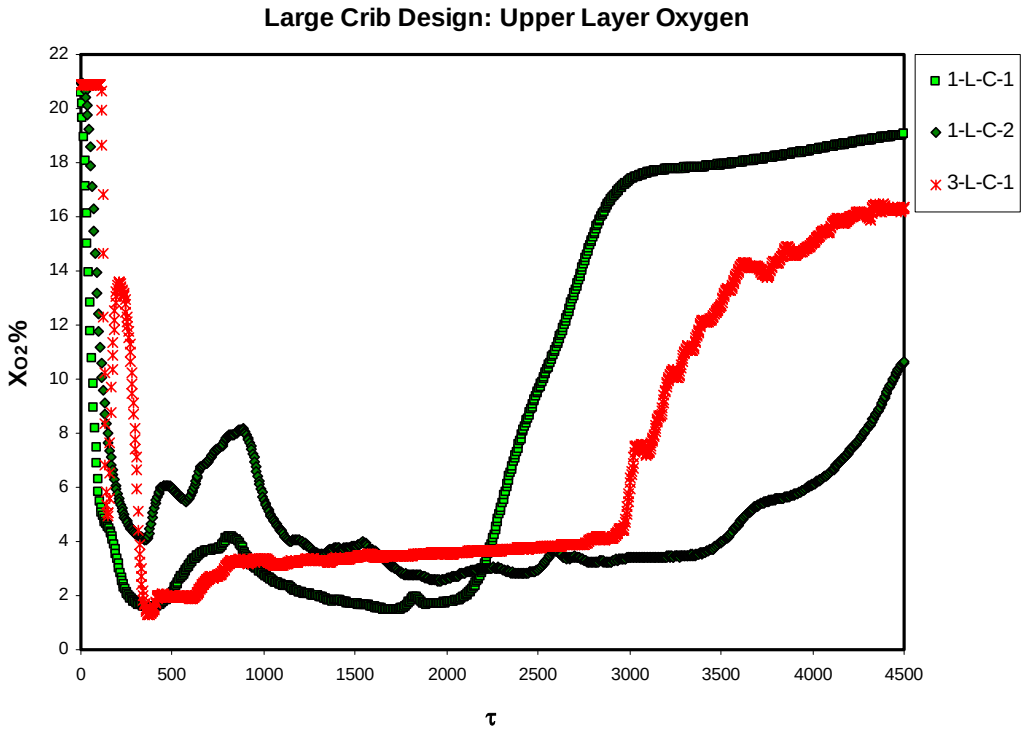

Figure 4.35a: Large Crib Design, Upper Layer O_2

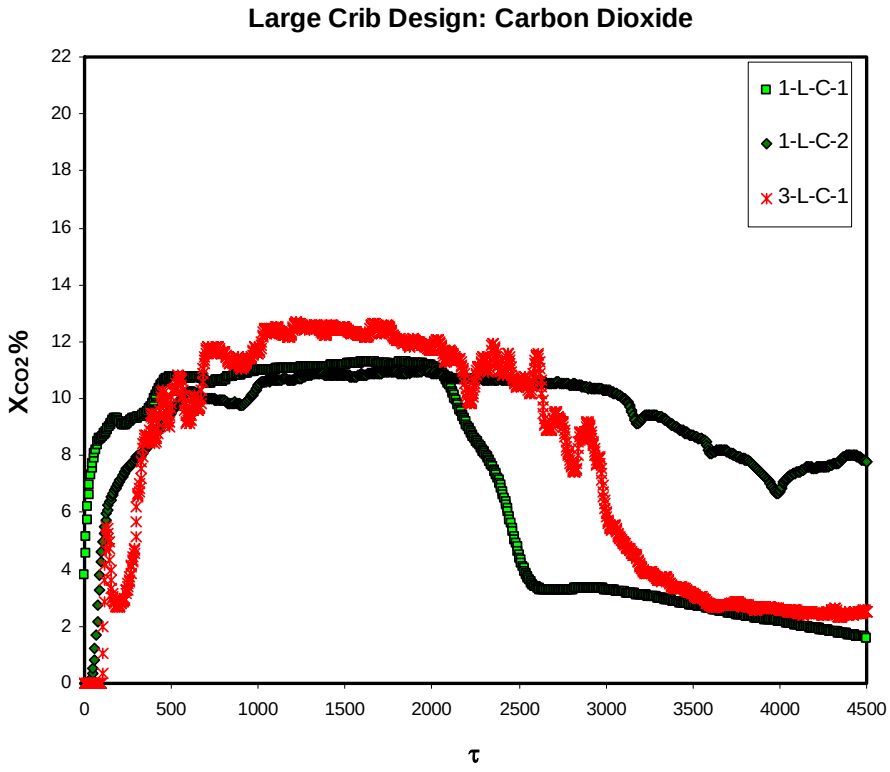

Figure 4.35b: Large Crib Design, Upper Layer CO_2

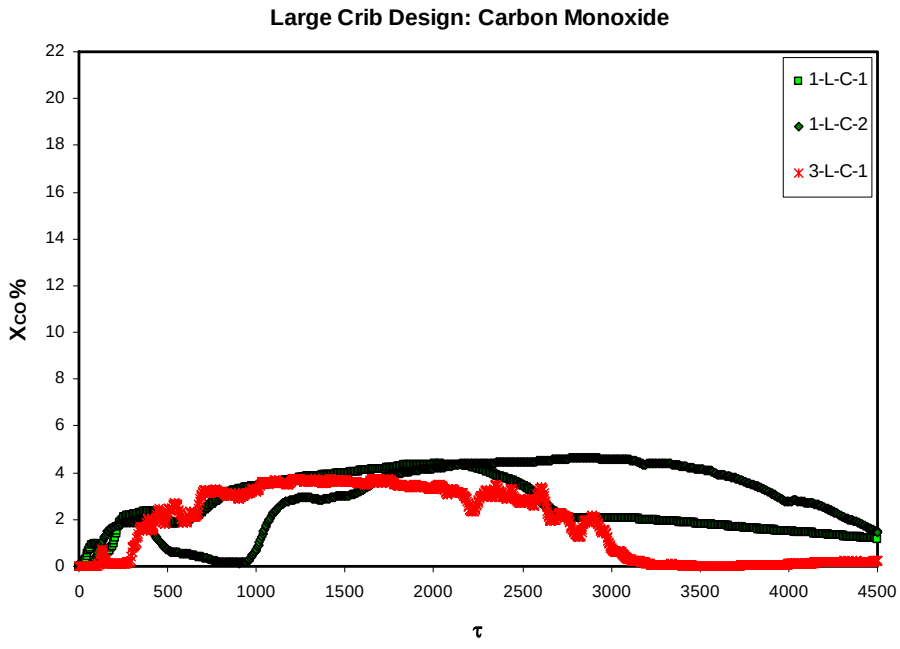

Figure 4.35c: Large Crib Design, Upper Layer CO

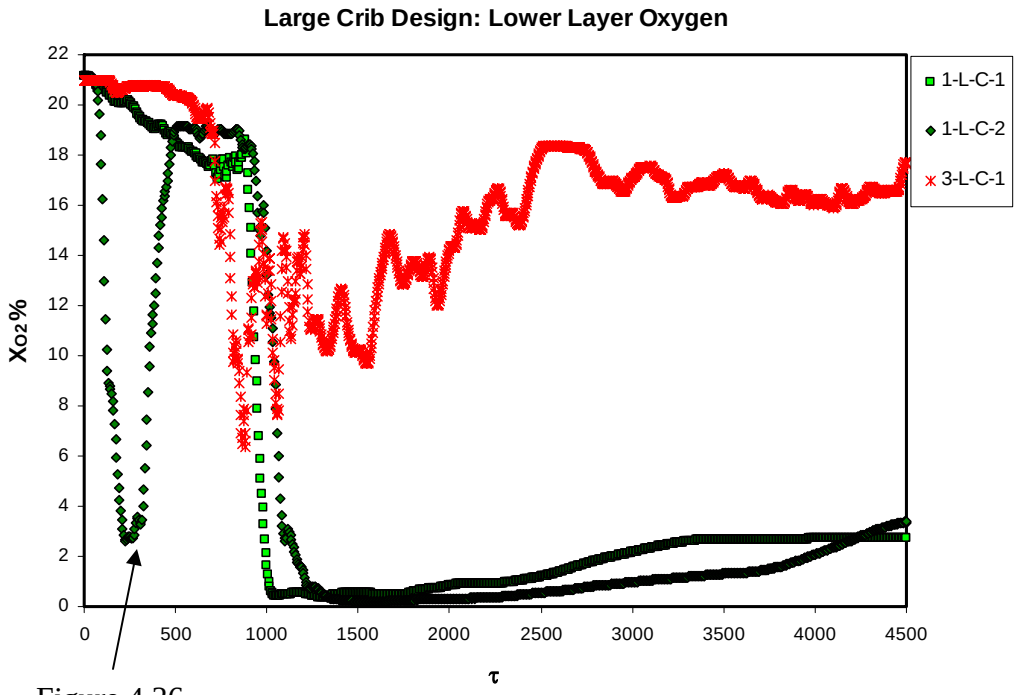

Figure 4.36

Figure 4.35d: Large Crib Design, Lower Layer O_2

The results for the 1/8 and 3/8 scale models show excellent agreement for the upper layer gas concentrations. The difference between the lower layer oxygen concentrations is likely due to the inconsistency in the height of the vent for the 1/8 scale model. Once again, the lower layer oxygen dips far below any reasonable definition of a critical value for sustained combustion in the 1/8 scale model. The duration of the large crib fires is $\tau \sim 3750$. The maximum values of the fuel supply rate occur consistently at $\tau \sim 1000$. The heptane fire occurs in the range of $\tau = 0 - 500$. With these reference points in mind, simple observations can explain the phenomena depicted by the data.

In test 1-L-C-2, the first dip below a critical value occurs during the heptane fire. Figure 4.36 is a photograph taken during this time period. Note the general absence of flame in the compartment. This corresponds to a plateau in the fuel supply rate shown in

Figure 4.14. The fact that this rate flattens rather than dropping to zero during this time is further evidence of the role of the crib core as a resistor to heat loss. The initial dip in oxygen is short lived. The heat that has already evolved in the compartment evaporates the heptane. The temperature of the wood is high enough to sustain ignition with the proper oxygen concentration. This occurs once the heptane is evaporated. The wood burns for a short period inside the compartment until the oxygen concentrations again fall below the critical value. At this point, the heat that has already evolved in the compartment is enough to continue vaporizing fuel and thus produce a flame at the vent. This is evidenced by the consistently higher temperatures recorded at the vent than in the compartment interior. The flame at the vent radiates energy back into the compartment and the process continues.

Recall that the combustion of the wood crib is heavily dependent on the radiation within the crib core. This radiation will act as a resistor to heat loss regardless of the presence of oxygen. Therefore a relatively small amount of energy is necessary to sustain combustion once the peak burning period has been reached.

Figure 4.36: Initial Dip of Oxygen in Test 1-L-C-2

Figure 4.34a shows a similar dip in lower layer oxygen concentration for test 3-L-C-1; however, the dip does not appear to be below the critical value of a 10% mole fraction. Once the flame outside the vent was established in that test, observations of processes inside the compartment were very difficult. It appears that a flaming combustion continued in the compartment to some extent throughout the test.

The sparseness of data for gas composition suggests the use of a mathematical model for purposes of estimation. Quintiere and McCaffrey devised a control volume analysis for a two zone model of a similar wood crib compartment fire[18]. Figure 4.37 depicts this analysis applied to the conservation of species in the compartment.

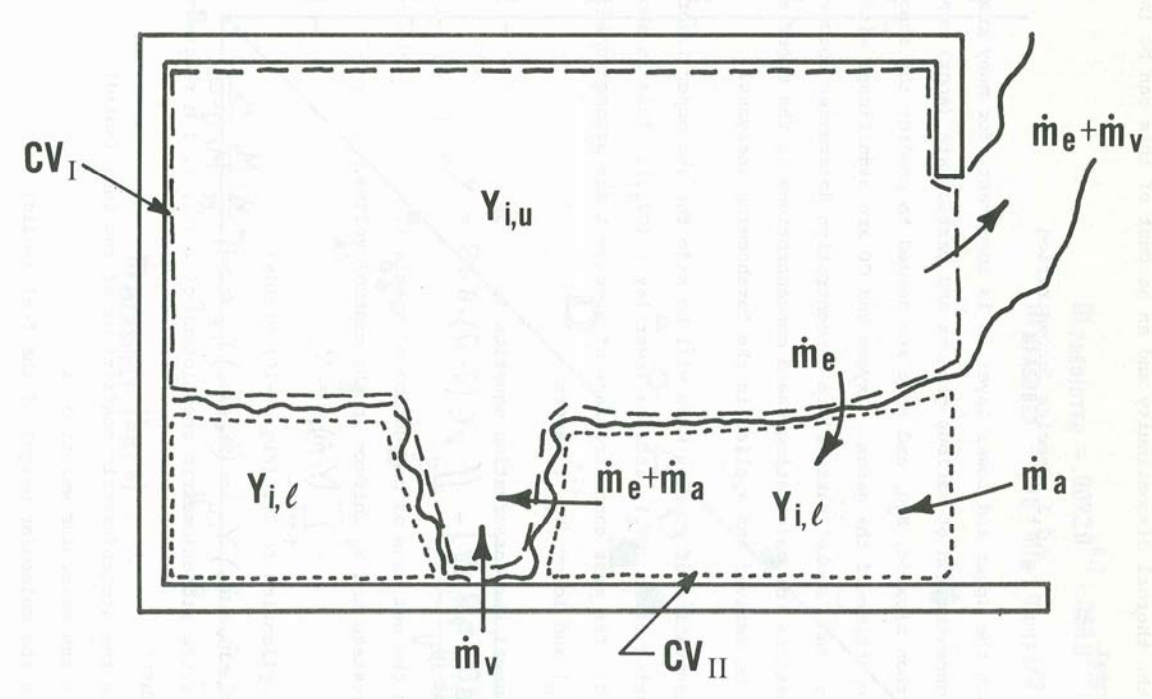

Figure 4.37: Conservation of Species, Two Zone Model[18]

The conservation of species in the compartment allows for the estimation of the lower layer oxygen concentration based simply on knowledge of the upper layer concentration and a gas temperature defined mixing ratio.

$$Y_{o_2,l} = \frac{0.23 + \left(\frac{\dot{m}_e}{\dot{m}_a}\right) Y_{o_2,u}}{1 + \left(\frac{\dot{m}_e}{\dot{m}_a}\right)} = \frac{0.23 + \left(\frac{T_{g,l} - T_a}{T_{g,u} - T_{g,l}}\right) Y_{o_2,u}}{1 + \left(\frac{T_{g,l} - T_a}{T_{g,u} - T_{g,l}}\right)} \tag{4.8}$$

Equation 4.9 calculates a mass fraction, which can be converted into a mole fraction. It is assumed that the molecular weight of the mixture is equal to that of air[18].

$$X_i = \frac{Y_i MW_{mix}}{MW_i} \tag{4.9}$$

If the equation is applied to this test at $\tau = 600$, an estimate for the peak lower layer oxygen concentration results. Selection of this specific time allows for the use of Figure 4.26 to estimate the temperatures and locations of the upper and lower layers respectively. Based on the location of the steepest gradient in this Figure, the lower layer is estimated to occur at and below $\omega = 0.3$. Therefore, the lower layer temperature is taken as an average of the two lowest thermocouples at this instant. The upper layer temperature is taken as an average of the remaining thermocouples. The result of the calculations is an estimate of 1% for the lower layer oxygen mole fraction at $\tau = 600$. Consultation of Figure 4.34d reveals that the lower layer mole fraction of oxygen in the 1/8 scale model is about to drop rapidly to zero at this dimensionless time. The curves may be slightly out of sync with respect to time, as was the case with the upper layer concentrations. Ultimately, the result of the model confirms similar behavior between the 1/8 and 3/8 scale models. Keep in mind, however, that the burning observed suggests that this estimate for oxygen concentration should not apply to the gas volume in front of the crib in close proximity to the vent.

Taking the control volume analysis one step further, an estimate can be made for the concentration of Carbon Dioxide in the upper layer for test 3-S-C-1 [18].

$$Y_{i,u} = \frac{\left(\frac{\nu_i MW_i}{\nu_f MW_f}\right)\left(\frac{\dot{m}_b}{1-\xi}\right)}{\dot{m}_a + \dot{m}_v} \tag{4.10}$$

Where the ventilation limited burning rate in the enclosure is defined as

$$\dot{m}_b = \dot{m}_a (A/F)_{stoic} \tag{4.11}$$

The stoichiometric reaction shown in Equation 4.6 is used to evaluate the molecular weights and coefficients of the molecules. The instantaneous fuel supply rate of 0.032 kg/s at $\tau = 600$ is used. Lastly, the fraction of the initial fuel mass at this instant corresponding to this dimensionless time is 0.59. The model produces an estimate of 13% for the mole fraction of CO_2 in the upper layer at $\tau = 600$. This compares quite favorably to the 11% magnitude of the 1/8 scale model tests at this time.

An adjustment of the vent height in the 1/8 scale model will ultimately increase the concentration of CO_2 at the expense of CO. The burning rate will also increase as the O_2 concentration throughout the compartment interior increases. The influence of decreased oxygen concentrations in the compartment on the fuel supply rate can be estimated from the model of Quintiere and McCaffrey[18].

$$\Delta \dot{m}_{ox} = -\dot{m}_{freeburn}\left(1 - \frac{Y_{ox,l}}{0.23}\right) \tag{4.12}$$

Based on Equation 4.12, if the change in burning rate due to decreased oxygen is evaluated at $\tau = 600$ for the measured lower layer mass fractions, it is obvious that the confined burning rate will be very near zero in most of these cases. The one recorded exception is that of test 3-L-C-1 where the lower layer oxygen concentration does not appear to drop below a critical value of 10% mole fraction. Evaluation of Equation 4.12 at this value of the mole fraction suggests that the free burning rate is cut in half by the oxygen limitation. The positive contribution from thermal feedback is not yet considered.

It is critical to understand, however that the magnitude of the ventilation limitation on the fuel supply rate is not equally severe throughout the compartment. Due

to the absence of flame away from the vent, the application of this model to these compartments is very sensitive to the location of the gas sampling tube. A relocation of the tube to the plane of the vent would capture concentrations indicative of gas phase combustion. Figure 4.23 demonstrates that the mass flow rate of air entering the compartment is properly scaled. Therefore, regardless of where the measurement is taken, the placement of the tube in homologous locations at different scales records similar concentrations. Thus, a mixing phenomenon is captured by the scaling.

4.2.5.2 Clean Burning

A phenomenon known as clean burning was observed in all three compartments for both the small and large crib designs. This essentially refers to the consumption of carbon particles lining the upper surfaces of the enclosure boundaries. The burning of carbon particles is not a new concept, but it is one that has to date received little attention in compartment fire research. The phenomenon is particularly germane to the fire investigator attempting to identify often ambiguous fire patterns in an effort to analytically, but very generally, reconstruct the dynamic fire environment. The following model offers one possible explanation for this phenomenon observed in these compartments.

In a simplified two-film model, combustion is considered in both the solid surface and gas phases[31]. The assumptions of the model are given as follows:

1) Quasi-steady state burning
2) Spherical Carbon particle burning in quiescent air
3) Infinite (unconfined) medium

4) Gas phase thermal conductivity, specific heat and product of density and mass diffusivity are all constants. The Lewis number is unity.
5) Neglect intra-particle diffusion
6) Uniform particle temperature, no radiation to particle from medium

The only somewhat troublesome assumption is that of an unconfined medium. However, it is assumed that the volume of the box is large enough with respect to the particulate.

The intriguing feature of the two-film model is that Carbon Dioxide acts as a global oxidizer. The global reaction at the carbon surface is given by

$$C + CO_2 \Rightarrow 2CO \tag{4.13}$$

The CO that is produced by this reaction is then consumed by the gas phase flame.

$$CO + \frac{1}{2}O_2 \Rightarrow CO_2 \tag{4.14}$$

The Carbon Dioxide produced at the flame then diffuses back toward the carbon surface and the consumption of the particulate continues. Figure 4.38 illustrates some general concepts of the model regarding the spatial variation of species mass fractions and temperatures.

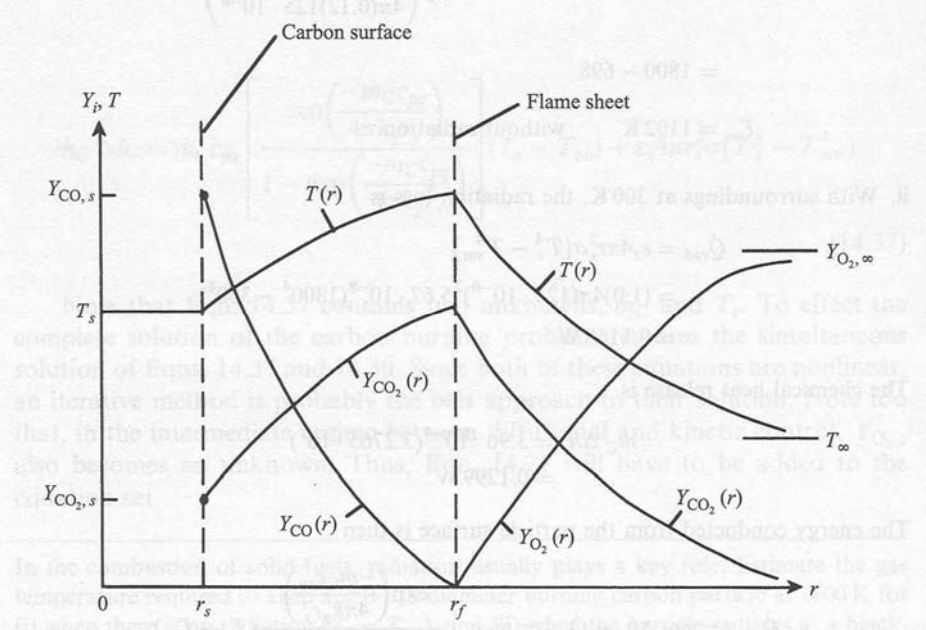

Figure 4.38: Two-Film Model, Species and Temperature Profiles[31]

The model dictates that both the temperature and the Carbon Dioxide concentration peak at the flame sheet. This suggests that the proper combination of these two variables is the driving force for consumption of the carbon.

The current research yields typical combinations of 15% Carbon Dioxide mass fraction and 1100K surface temperature. The scaling inconsistency of the vent which produced lower temperatures for the 1/8 scale model large crib design proves to be fortuitous in this explanation. Although the maximum CO_2 concentrations were not significantly different, the average upper wall surface temperatures did not exceed 800 K. The Carbon Dioxide concentration is not abnormally large for compartment fires, but its combination with high surface temperatures is significant. Often, clean burning is observed in an area of fire origin indicating close proximity of a wall surface to a flame[29]. This idea is consistent with the two-film model in that the close proximity of flame to a

wall surface provides it with the necessary combination of temperature and CO_2 concentration. However, in the case of the 1/8 scale model, it appears that the carbon on the upper walls was consumed at a relatively low temperature. Note, however that some of the carbon deposits were left on the walls after these tests, whereas at the higher temperatures recorded in the larger models, every last bit of carbon was consumed. Ultimately more research should be done to reveal the complexity of this process, but the preceding discussion does bring to light some pertinent concepts.

The color gradient of the insulation material ranging from white at the inner surface to dark brown at the outer surface is perhaps evidence of the presence of carbon in the original pigment of the material. The temperature gradient through the wall thickness at steady state likely leaves a carbon concentration gradient through the thickness of the board.

4.2.6 Heat Flux Results

For the limited ventilation enclosure fires there are competing influences on the burning rate of the fuel. In order to properly evaluate the thermal feedback influence on the fuel mass loss rate, the heat flux inside the compartment must be analyzed in two forms. Recall that the heat flux that is incident to the boundaries is expected to scale differently than that which is absorbed by the boundaries and subsequently lost via conduction to the ambient.

Inside the enclosure there is a radiant heat exchange occurring between the enclosure boundaries and the wood crib. The confined fire plume is also a contributing factor as it accumulates into a hot upper layer. This layer participates in the radiant

exchange between the upper boundaries of the enclosure and the fuel, as well as introducing a convective heating component. The total incident heat flux to the ceiling surface is identified as the sum of the radiant and convective heating components, while the incident flux to the floor is a sum of radiant heating from the upper layer and flame.

$$\dot{q}_{incident,ceiling} = \dot{q}_{rad,\,flame} + \dot{q}_{rad,layer} + \dot{q}_{conv,\,flame} + \dot{q}_{conv,layer} + \dot{q}_{walls} \tag{4.15a}$$

$$\dot{q}_{incident,\,floor} = \dot{q}_{rad,\,flame} + \dot{q}_{rad,layer} + \dot{q}_{walls} \tag{4.15b}$$

Recall that gauges were placed at the surface of both the compartment ceiling and floor for each of these fires. These gauges were responsible for measuring this incident flux to the surface. The location of the floor gauge at a surface adjacent to the cool lower layer indicates that the convective component of its incident flux should be quite small. The results of the measured incident flux are shown in Figures 4.39 through 4.42. As the vent size is increased in the 1/8 scale model, the height of the thermal discontinuity is expected to rise. An increase in the burning rate would be accompanied by an increased incident heat flux throughout the compartment. The increase in this rate of heat transfer suggests narrower incident heat flux curves corresponding more closely to data of the 2/8 and 3/8 scale models. Recall that the limiting influence of compartment ventilation was far more severe with the large crib design fires.

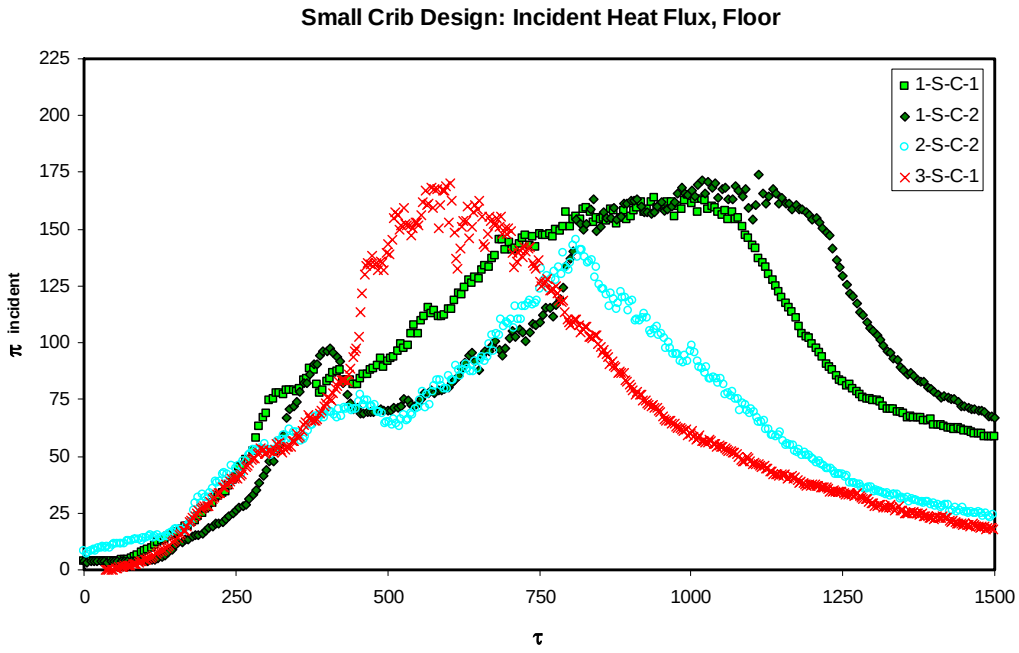

Figure 4.39: Small Crib Design: Incident Heat Flux to Floor Gauge

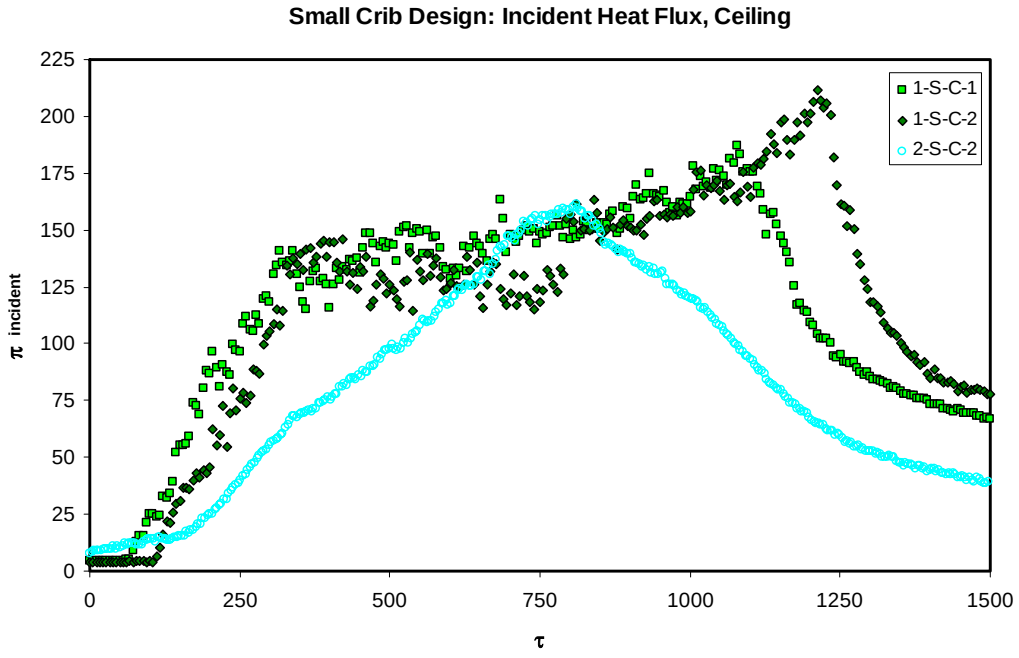

Figure 4.40: Small Crib Design: Incident Heat Flux to Ceiling Gauge

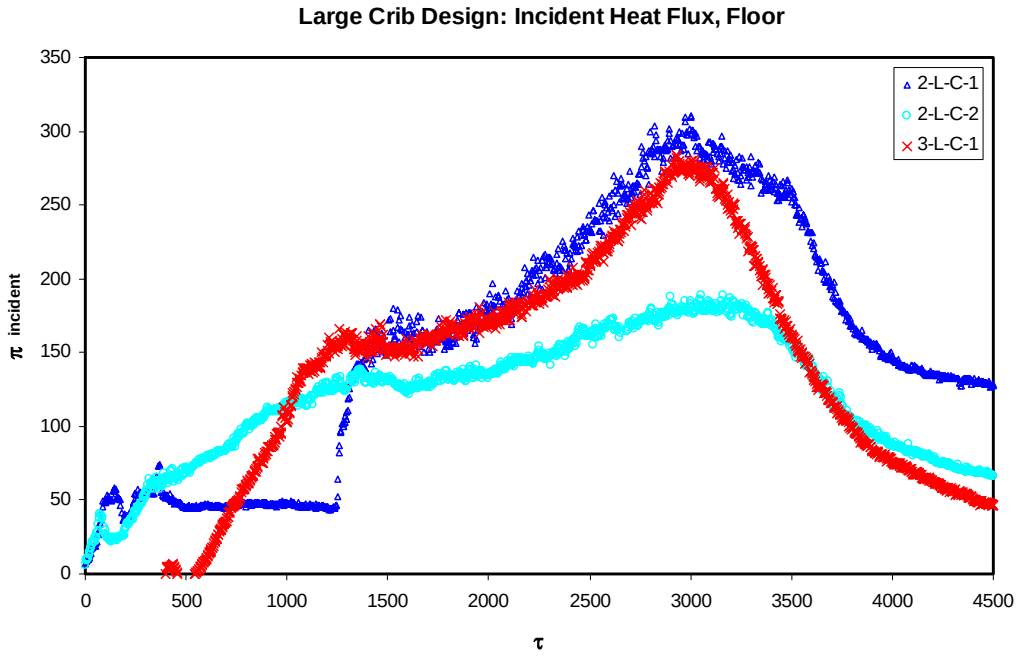

Figure 4.41: Large Crib Design: Incident Heat Flux to Floor Gauge

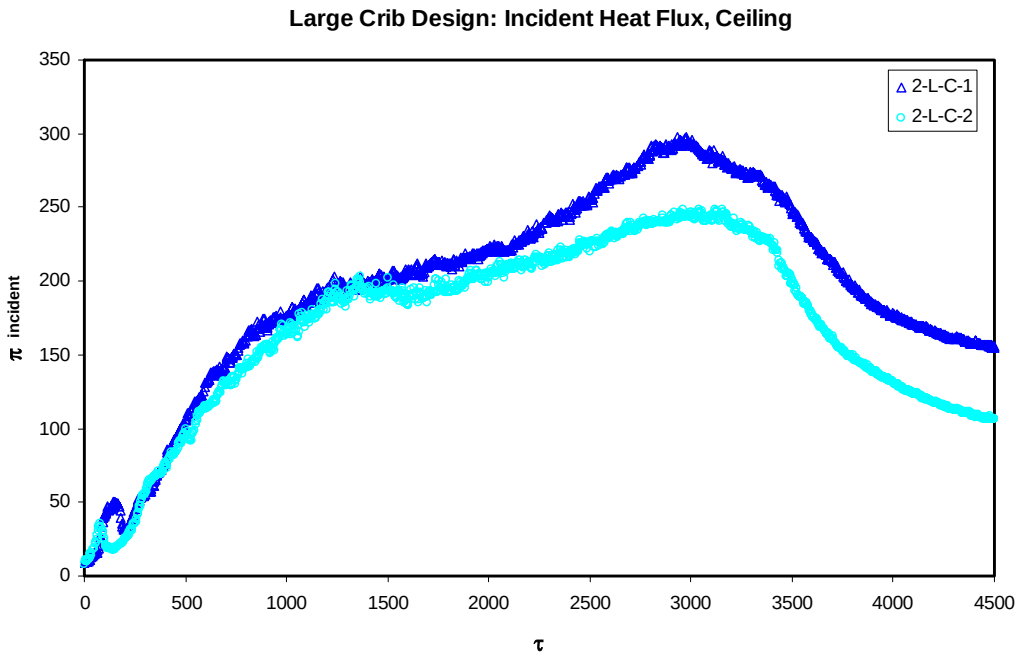

Figure 4.42: Large Crib Design: Incident Heat Flux to Ceiling Gauge

The results shown for the dimensionless incident heat flux essentially confirm the independence of this flux from length scale. It is important to appreciate the magnitude of this dimensionless group for comparison with the absorbed heat flux values, which presented in the following discussion.

A calculation of the net heat flux accounts for the water cooling provisions for the measuring instrument.

$$\dot{q}''_{net} = \dot{q}''_{gauge} - \sigma\left(T_s^4 - T_w^4\right) - h_c\left(T_s - T_w\right) \tag{4.16}$$

The convective coefficient for the enclosure fire can be modeled as turbulent natural convection on a heated vertical plate. The result of this assumption yields Equation 4.17 from which the convective coefficient can be calculated[23].

$$Nu = \frac{h_c H}{k} = 0.1 Ra^{1/3} \tag{4.17}$$

For each of these experiments, the surface temperature of the ceiling is very close to that of the adjacent gas layer throughout the steady state. Therefore, the net heat transfer to the surface is expected to be quite small. The surface temperature of the compartment floor was not recorded; however, in the cool lower layer of the compartment, much lower temperatures prevail and the gas temperature at $\omega = 0.1$ should serve as a reasonable estimate for the surface. The calculations of the absorbed heat flux to the floor and ceiling of the enclosures are shown in Figures 4.43 through 4.46.

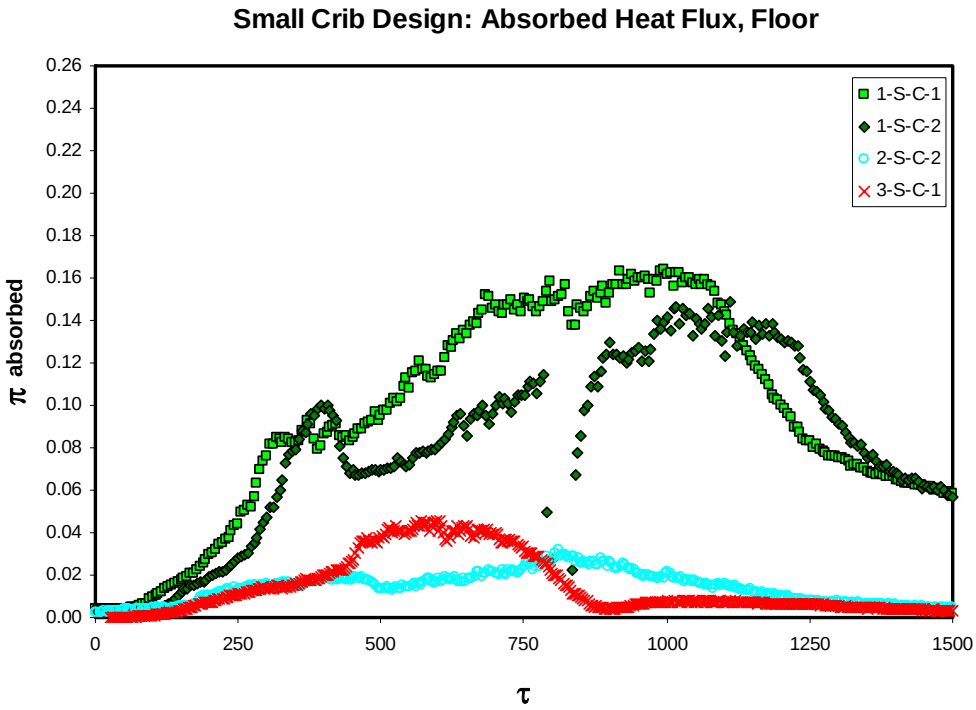

Figure 4.43: Small Crib Design, Absorbed Heat Flux, Floor

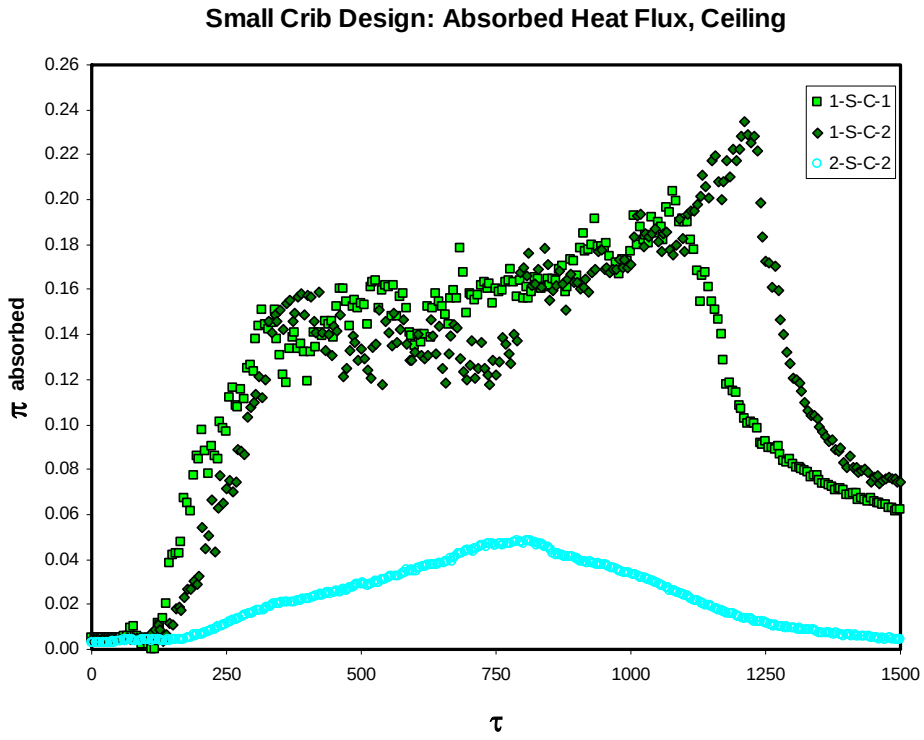

Figure 4.44: Small Crib Design, Absorbed Heat Flux, Ceiling

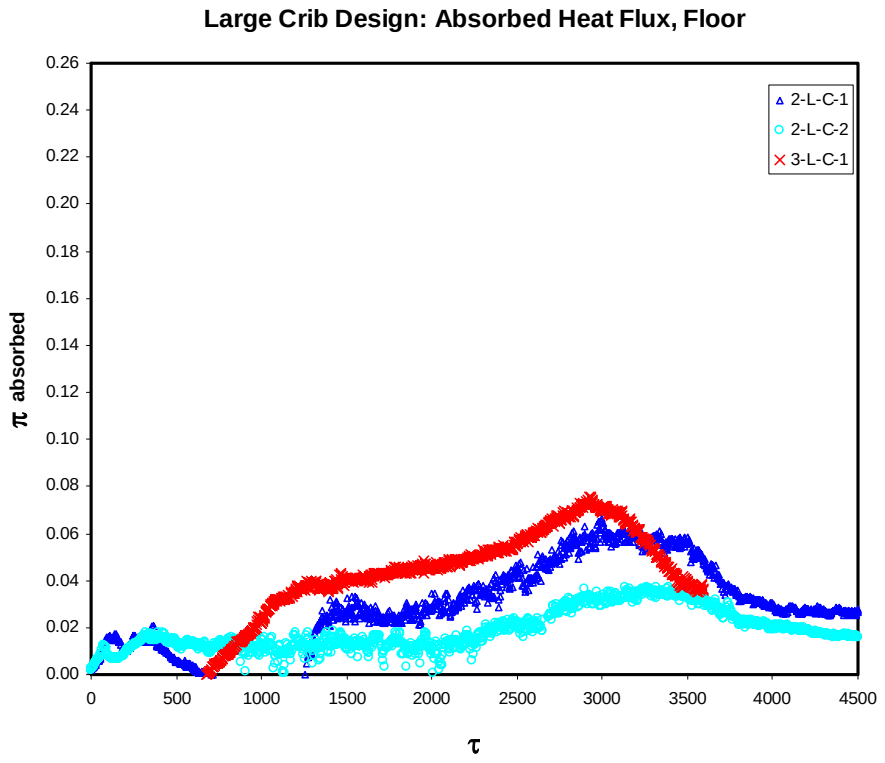

Figure 4.45: Large Crib Design, Absorbed Heat Flux, Floor

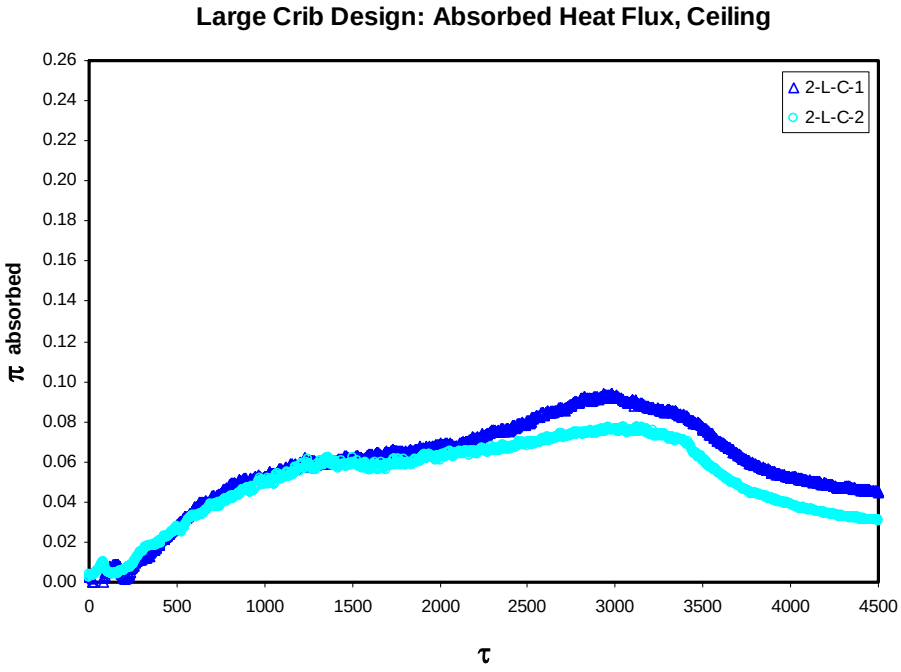

Figure 4.46: Large Crib Design, Absorbed Heat Flux, Ceiling

At first glance, it is not readily apparent how the net heat flux is related to length scale in these experiments; however, it is clear that the magnitude of this flux is quite small in comparison to the incident heat flux. The lack of a clear scaling relationship is likely the product of approximating solid surface temperatures with gas temperatures. In the case of the floor, this is done deliberately; however, in the case of the ceiling, it is questionable whether the measured temperatures correspond to the surface or the gas. In any case, the comparison between absorbed and incident flux confirms the notion that the primary resistor to heat loss is conduction through the walls of the compartments. The well insulated boundaries are absorbing only a very small amount of the tremendous incident heat flux. The heat that is therefore trapped inside the boundaries is fed back to the fuel and enhances the mass loss rate. Ultimately, more data must be collected to determine whether the relationship between this expression for the absorbed heat flux and length scale can be consistently modeled. This will be accomplished in future experiments.

4.2.7 Analysis of Uncontrolled Independent Variables

The application of the scaling theory presented in Chapter 3 reveals some inconsistencies in the preservation of both dimensionless radiant and convective heat transfer rates inside the compartment. These dimensionless groups can be quantified and their affects investigated with the help of a few rational assumptions. If the flow inside the compartment can be assumed to behave as a turbulent naturally convective flow over a heated vertical plate, Equation 4.17 can again be used to estimate the convective coefficient and consequently $\pi_{convection}$ as well. The Grashof number, which carries

significance for flow turbulence, may be calculated from Equation 3.14a based on the temperature rise in the compartment interior.

Given that the $\pi_{radiation}$ term varies only with length scale, the success of the radiant heat flux scaling is dependent on the emissivity of the upper layer. The mathematical model of Quintiere and McCaffrey can be used to approximate average peak values for this group for each scale[18]. Knowledge of the conservation of mass in the enclosure, the flame absorption coefficient and simple stoichiometry allows for an estimate of the smoke layer absorption coefficient.

$$\kappa_{gas} = \kappa_{flame}\left[\frac{\left(1+\left(A/F\right)_{stoic}\right)\dot{m}_f}{\dot{m}_a+\dot{m}_f}\right] \tag{4.18}$$

The flame absorption coefficient is taken to be 0.8 m^{-1} as determined by Quintiere and McCaffrey for their sugar pine wood cribs[18]. Average peak values are used for the fuel supply rate and mass flow rate of air into the compartment. The mass flow rate of air is calculated in Equation 4.4. Estimates for the scaling of the smoke layer absorption coefficient are made in Figures 4.47a and 4.47b.

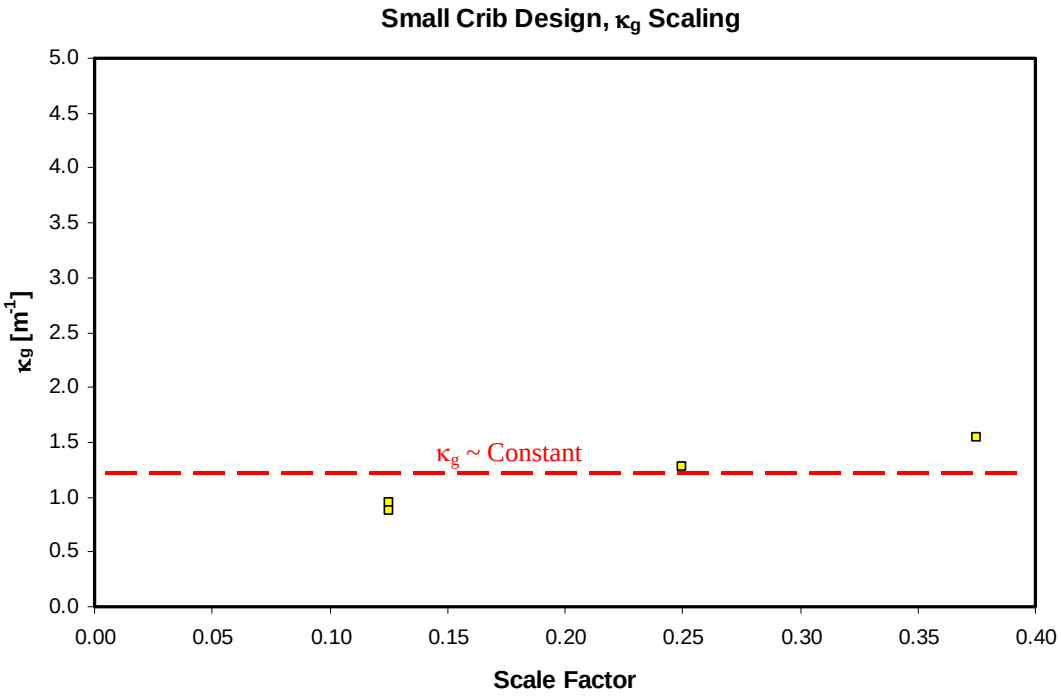

Figure 4.47a: Small Crib Design, κ_{gas} Estimation

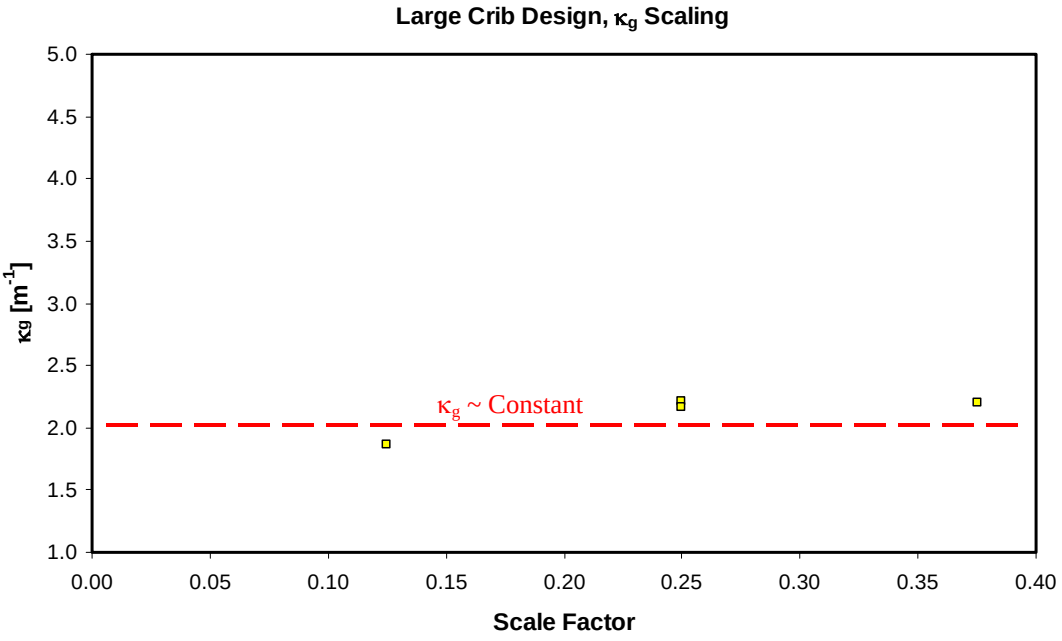

Figure 4.45b: Large Crib Design, κ_{gas} Estimation

The results shown above essentially show that the absorption coefficient is independent of scale. This is expected for the same fuel used at each length scale.

The mean beam length is simply a ratio of smoke layer volume to surface area as stated in Equation 3.35. This equation can be applied to a rectangular enclosure based on knowledge of the dimensions of the box and the position of the layer interface.

$$l_m = \frac{2WL_{enc}(H-D)}{(H-D)(W+L_{enc})+WL_{enc}} \tag{4.19}$$

The position of the layer interface is simply estimated based on the representative steady state snapshots of the interior gas temperature profiles taken in Figures 4.26 and 4.32. The height corresponding to the steepest temperature gradient is assumed to be the location of the thermal discontinuity. The estimations for the mean path length are shown in Figures 4.48a and 4.48b for the different crib design sets.

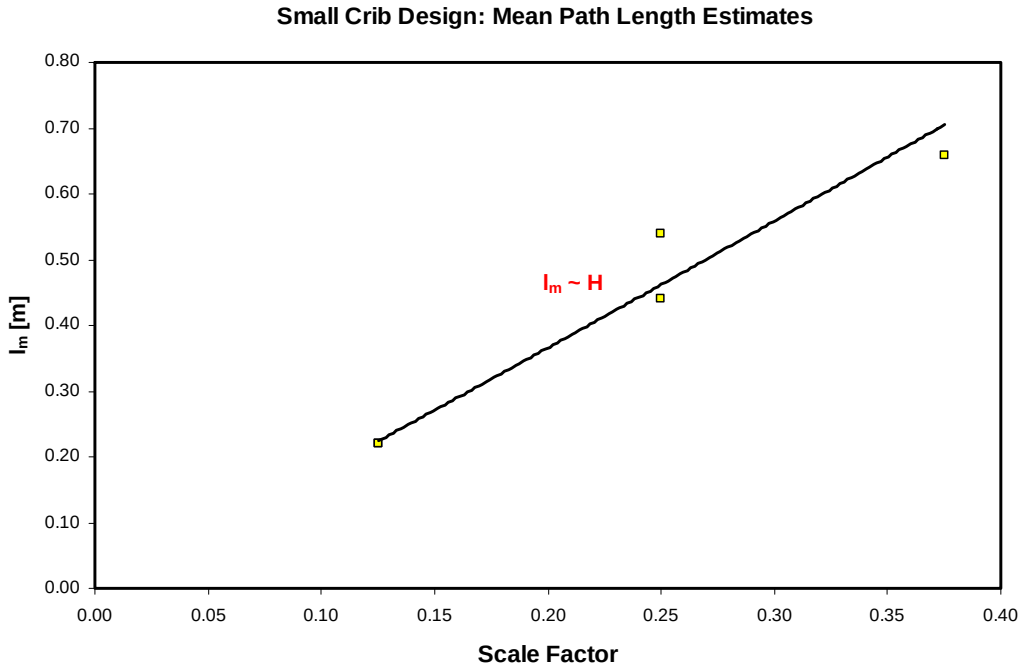

Figure 4.48a: Small Crib Design, Mean Path Length Estimations

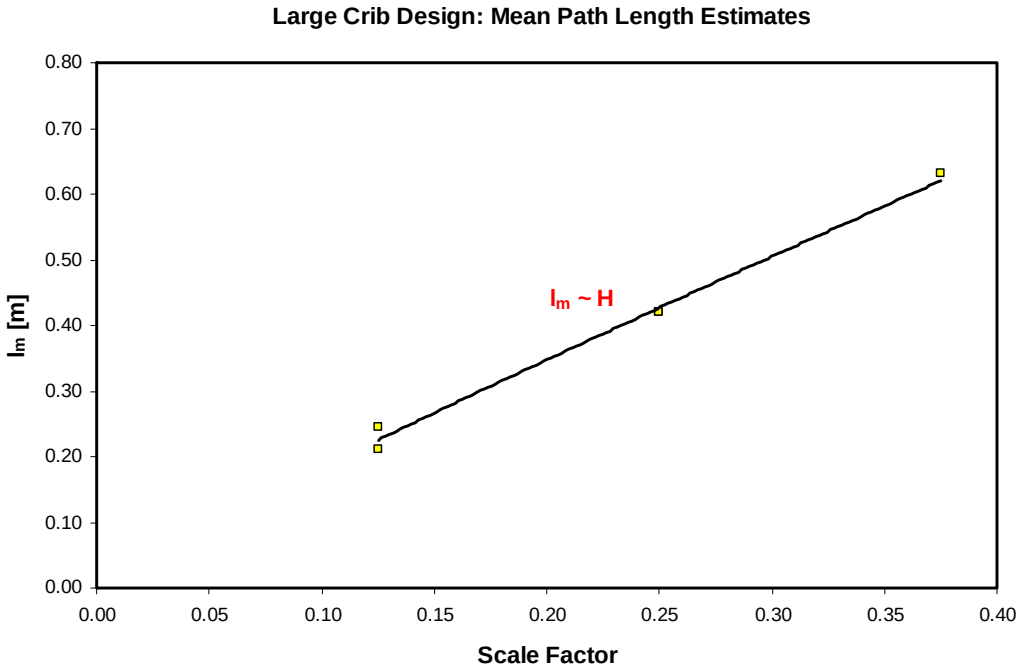

Figure 4.48b: Large Crib Design, Mean Path Length Estimations

The estimations for mean path length support the scaling theory, which suggests that this quantity scales geometrically. The combination of the absorption coefficient and the mean path length suggests the following results for the dimensionless groups related to radiant heat transfer:

$$\pi_{emissivity} = \kappa_g l_m \approx H \tag{4.20}$$

The above equation indicates that the net heat flux to the boundaries is scaling as $H^{1/2}$ as desired for the proper balance of the energy equation. However, there seems to be some ambiguity in the measured data. This could be due to assumption of the scaling theory that the walls of the compartment behave as blackbodies. Observations of clean burning during these experiments indicate that this may not be an accurate assumption for these enclosures. In addition, the affect of combustion products building up on the

surface of the gauges during testing may have altered the calibration data for the instruments even beyond attempts to recalibrate between tests.

Table 4.7 lists estimated average values for each of the uncontrolled independent variables in the model. The calculations of *Gr* and *Ra* utilize an ambient temperature of 300K and an average interior temperature of 1000K for all experiments. The emissivity groups are calculated using the data presented in Figures 4.48a and 4.48b.

			Small Cribs	Large Cribs	
Scale	$\pi_{convection}$	$\pi_{radiation}$	$\pi_{emissivity}$	$\pi_{emissivity}$	**Gr**
1/8	2.81E-04	7.17E-03	0.21	0.42	2.96E+09
2/8	4.97E-05	1.27E-03	0.56	0.97	2.37E+10
3/8	1.80E-05	4.60E-04	0.99	1.43	7.98E+10

Table 4.7: Quantification of Uncontrolled Independent Variables

The results for *Gr* show that turbulent flow is maintained at all scales. Therefore, the inconsistency in the scaling $\pi_{convection}$ is accepted as insignificant. Note that the magnitudes of $\pi_{convection}$ and $\pi_{radiation}$ are orders of magnitude less than $\pi_{conduction}$. This again confirms the role of conduction through the walls as a primary resistor to heat flow. The relative magnitudes of the convection and radiation terms show that radiation dominates over convection at the high temperatures measured in these experiments. The emissivity of the gas suggests an optically thick layer for both the large and small crib designs. Therefore, future experiments must consider the influence of this term on the scaling of the net heat flux.

5. Conclusions

The preceding report is part of a larger research effort to produce a physical scale model of the interaction between a fire and a structural steel frame in an enclosure. The goal of this particular study was to develop the foundation for the physical scale model of the enclosure fire. In recognition of the sensitivity of the performance of a structural frame to transient heating, the fire model was designed with a specific focus on transient accuracy. The following conclusions were drawn based on an analysis of the experimental results.

1. The driving mechanism for the sustained combustion of the wood crib is heating of the fuel by the flame. There exists a relationship between the internal and external geometry of the pile that is most closely approximated as a radiant exchange between a body and a surrounding enclosure. This interaction resists the loss of heat from the crib core to the ambient. The magnitude of this resistance is dependent on the relative size of the core with respect to the external members of the crib.
2. Non-uniform ignition of a wood crib is a common occurrence. In the event that the external surfaces of the crib outnumber the internal surfaces by some critical margin, the burning rate of the crib reveals twin maxima. The peaks correspond to unsynchronized burning of the crib interior and exterior. This is a significant pitfall for a scale model attempting to reproduce the transient burning rate of a larger prototype. The results of this research suggest a minimum of 5 sticks per layer and a minimum of 4 layers in the crib to avoid this burning rate behavior in the scale model.

3. The key to transient scaling is the direct link between the characteristic time and the characteristic length scale. The flow time was extracted from the conservation equations and its selection as the characteristic time was the cornerstone for the scale model. The differential equations expressing the conservation laws for the system all contain time as an independent variable. Therefore, every model design feature from the crib to the compartment is determined by the characteristic time.
4. It has been demonstrated that the transient burning rate of a free burning wood crib can be reproduced with excellent local and global accuracy in the data at multiple length scales. There is no longer a need for the use of time-averaged values in the scaling of wood cribs.
5. Thermal feedback from the compartment boundaries is one of the two major influences affecting the burning rate of fuel in an enclosure. There is a tremendous need for an extensive database of the thermal properties of materials at temperatures indicative of an enclosure fire environment. The thermal response of a material often varies significantly with temperature. In a fire compartment the temperature varies significantly with time. Compartment materials in scale models must be selected with this in mind.
6. It has been demonstrated that the transient burning rate of a wood crib burning in a ventilation limited enclosure can be reproduced with excellent local global accuracy in the data at multiple length scales. Ultimately, more data is needed to demonstrate consistent scaling of the fuel supply rate particularly with respect to the fire growth period; however, the potential of the method is intriguing.

7. Despite a scaling inconsistency in the ventilation of the 1/8 scale model, good agreement is found between the temperature fields in the models. This is particularly true for the small crib fires in which the ventilation played only a minor role in determining the fuel supply rate. The ability to reproduce the temperature field within the compartment paves the way for the introduction of the structural steel frame to the model.
8. Scaling inconsistencies have been acknowledged with respect to both convection and radiation inside the enclosure; however, it is recognized that the primary resistor to heat loss is conduction through the compartment walls. This is confirmed by comparison between the magnitudes of $\pi_{incident}$ and $\pi_{absorbed}$. Recognition of this condition along with the preservation of turbulent flow in each model, suggest that inconsistencies in scaling $\pi_{convection}$ and $\pi_{radiation}$ are insignificant. The emissivity of the gas holds the key to controlling the scaling of the net heat flux.
9. Although the data is sparse, there is experimental evidence that transient concentrations of O_2, CO_2 and CO in the upper layer as well as O_2 in the lower layer of the compartment can be predicted by the model. The ventilation limiting influence on the burning rate can therefore be accurately scaled.
10. The consistent consumption of soot throughout these compartments during testing has provided a hypothesis for the cause of what is often referred to as a clean burning fire pattern. The hypothesis is based the principle that at high temperatures, CO_2 will oxidize solid Carbon particles.

APPENDIX A: Correction for 3/8 Scale Model Compartment Weighing

Determination of the transient mass for the 3/8 scale model experiments 3-S-C-1 and 3-L-C-1 involved weighing the compartment and all of its contents. The mass loss rate is intended to reflect only the mass loss of the wood crib during the experiment. There are 2 additional influences on the measurement that must be considered when the compartment is weighed in this manner. The first of these influences is the moisture content of the compartment material. The high density of water means that its evaporation from the walls during testing will influence the mass data. Assuming that all of the moisture in the boundaries evaporates during the first experiment, consideration need only be for test 3-S-C-1, the first test conducted in the compartment. In order to account for moisture content, a sample of the *Kaowool S* material was placed in an oven at 105^{o}C for 1 week. The ratio of the weight at an ambient relative humidity of 60% versus the oven dry weight was used to estimate the moisture present in the compartment prior to the test. The results indicate a moisture content of 1.6% at the ambient relative humidity. Given the high temperatures of exposure in a fire compartment, the moisture must have evaporated completely from the material early in the test. Therefore, the mass of water represented by this 1.6% moisture content is simply subtracted from the initial mass of the compartment.

The second calculation considers the lifting affect of buoyant gas on a relatively enclosed compartment. Figure A.1 illustrates the problem as a force balance.

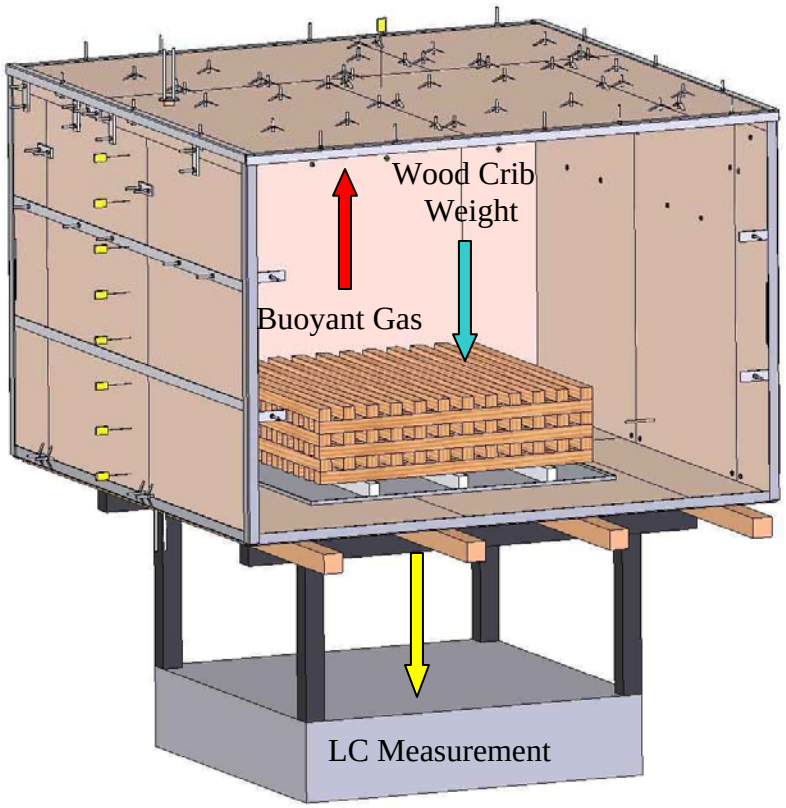

Figure A.1: Load Cell Force Balance

$$\sum Forces = LC - \left[\left(\rho_{gas} - \rho_{\infty}\right)Vg\right] + \left(mg\right)_{crib} = 0 \qquad \text{(A.1)}$$

The Load Cell measurement is known. The gas is assumed to be air which behaves as an ideal gas at these temperatures. The density of the air can therefore be calculated based on the interior temperature profile in the compartment using Equation A.2.

$$\rho_{air} = \frac{\left(\rho T\right)_{air,STP}}{T_{air,measured}} \qquad \text{(A.2)}$$

The measured air temperature is simply taken as the average temperature of the air in the compartment along the entire vertical profile at each time step. The result is a calculated transient air density. The transient crib mass is then found using the following values.

$$\rho_{\infty}(300K) = 1.18\frac{kg}{m^3} \qquad V = 1.893m^3 \qquad g = 9.81\frac{m}{s^2}$$

APPENDIX B: Correction for Transducer Response Times

Each of the measurement devices used in this report possesses an inherent response time. This is particularly important for the thermocouples given that different wire and bead sizes were used at the compartment interior and at the vent. Equation B.1 was used to adjust the voltage reading of the transducers to account for the response time delay. The signal is denoted as ψ and the subscripts denote the signal that is measured and that which is representative of the instantaneous phenomena in the compartment[32].

$$t_{response}\frac{d\psi_{meas}}{dt}+\psi_{meas}=\psi_{real} \tag{B.1}$$

The response time for the instrument is determined by placing it in an open flame and recording the rise in voltage. The time difference between the start of the exposure and the point at which steady state values are reached is used to calculate the response time according to Equation B.2.

$$\frac{\psi-\psi_{steady}}{\psi_0-\psi_{steady}}=e^{-t/t_{response}} \tag{B.2}$$

In addition to the response times, a delay time was measured for the gas analyzers. A pump was used to move gas through the sampling tube to the analyzer. The delay time was simply measured as the time required for pure Nitrogen, traveling from the compartment end of the tube, to cause a change in the voltage reading. The subsequent drop of the measured mole fraction of the particular gas (O_2, CO or CO_2) to zero was used in Equations B.1 and B.2 to calculate the analyzer response time[32].

References

1. Glanz, J. and Lipton, E., *City In The Sky: The Rise and Fall of the World Trade Center.* Times Books, Henry Holt and Company. 2003, New York.

2. Alpert, R.L. *Pressure Modeling of Transient Crib Fires.* Combustion Science and Technology, 1977. **15** (1-2) : p. 11-20.

3. Gross, A.F. and Robertson, D., *Experimental Fires in Enclosures.* Combustion Institute-Symposium on Combustion, 1965. p. 931-942.

4. Folk, F., *Experiments in Fire Extinguishment.* National Fire Protection Association Quarterly, 1937. **31**(2): p. 115-126.

5. Gross, D., *Experiments on the Burning of Cross Piles of Wood.* Journal of Research of the National Bureau of Standards-C. Engineering and Instrumentation, 1962. **66C** (2): p. 99-105.

6. Thomas, P.H. and Smith, P.G., *The Rate of Burning of Wood Cribs.* Fire Technology, 1970. **6**: p. 29-38.

7. Thomas, Webster and Raftery, *Some Experiments on Buoyant Diffusion Flames.* Combustion and Flame, 1961. **5** (4): p. 359-367.

8. Burke, S.P. and Schumann, T.E.W. *Diffusion Flames*. in *Proceedings of the Combustion Institute*. 1937. Michigan.

9. McCarter and Broido, *Radiative and Convective Energy from Wood Crib Fires.* Pyrodynamics, 1965. **2**: p. 65-85.

10. Block, J.A. *A Theoretical And Experimental Study of Non-propagating Free-Burning Fires*, in *Thirteenth Symposium (International) on Combustion*. 1971. Pittsburgh, Pennsylvania: The Combustion Institute.

11. Kays, W.M. and Crawford, M.E. *Convective Heat and Mass Transfer*. Third ed. McGraw-Hill Series in Mechanical Engineering, ed. Loyd. 1993, New York: McGraw-Hill.

12. Delichatsios, *Fire Growth Rates in Wood Cribs.* Combustion and Flame, 1976. **27**: p. 267-278.

13. Buchanan, A.H., *Structural Design for Fire Safety*. 1st ed. 2002, Chichester: John Wiley & Sons, LTD.

14. Gross, A.F. and Robertson, D., *Fire Load, Fire Severity and Fire Endurance*. 1970, American Society for Testing and Materials. p. 3-29.

15. Harmathy, T.Z., *A New Look at Compartment Fires, Parts I and II.* Fire Technology, 1972. **8** (196).

16. Thomas, P.H. and Heselden, J.M., *C.I.B. International Co-operative Programme on Fully-Developed Fires in Single Compartments: Comprehensive Analysis of Results*.

17. Tewarson, A., *Some Observations on Experimental Fires in Enclosures. Part I: Cellulosic Materials.* Combustion and Flame, 1972. **19**: p. 101-111.

18. Quintiere, J.G. and McCaffrey, B.M., *The Burning of Wood and Plastic Cribs in An Enclosure*, U.S.D.o. Commerce, Editor. 1980, National Bureau of Standards.

19. Heskestad, G., *Modeling of Enclosure Fires.* Journal of Fire and Flammability, 1975. **6** (3): p. 253-273.

20. Croce, P.A., *Modeling of Vented Enclosure Fires Part I. Quasi-Steady Wood-Crib Source Fire*. 1978, Factory Mutual Research Corporation: Norwood, Massachusetts.

21. Quintiere, J.G., *Fundamentals of Fire Phenomena*. 2002, University of Maryland, Department of Fire Protection Engineering.

22. Quintiere, J.G. (2003). Engineering Guide to Fire Exposures to Structural Elements, Ballot Draft. Society of Fire Protection Engineers.

23. Karlsson, B. and Quintiere, J.G. *Enclosure Fire Dynamics*. Environmental and Energy Engineering Series, ed. D.G.L. Ashwani K. Gupta. 2000, Washington, D.C.: CRC Press.

24. Janssens, M.L., *Fundamental Thermophysical Characteristics of Wood and their Role in Enclosure Fire Growth*. 1991, University of Gent (Belgium).

25. Drysdale, D., *An Introduction to Fire Dynamics*. Second ed, ed. J.W. Sons. 1998, Chichester.

26. Simpson, W. and Tenwolde, A., *Chapter 3 - Physical Properties and Moisture Relations of Wood*, in *Wood Handbook*. 1999.

27. Thermal Ceramics (2003-2004). *K-Source: Heatflow 4*. Atlanta, GA: Thermal Ceramics, 2001.

28. Harmathy, T.Z., *Properties of Building Materials at Elevated Temperatures*. 1983, National Research Council of Canada, Division of Building Research: Ottawa, Canada.1970, Ministry of Technology and Fire Offices' Committee Joint Fire Research Organization: Borehamwood, England.

29. *National Fire Codes*, in NFPA 921: *Guide for Fire and Explosion Investigations*. 1999.

30. Tewarson, A., *Generation of Heat and Chemical Compounds in Fires*, in *The SFPE Handbook of Fire Protection Engineering*, P.J. DiNenno, Editor. 1995, National Fire Protection Association: Quincy, Massachusetts.

31. Turns, S.R., *An Introduction to Combustion, Concepts and Applications*. Second ed. McGraw-Hill Series in Mechanical Engineering. 2000, Boston: McGraw-Hill.

32. Doebelin, E.O., *Measurement Systems Application and Design*. 3rd ed, Auckland: McGraw-Hill International Book Company.

33. Green, D.W., Winandy, J. E. and Kretschmann, D. E., *Chapter 4 - Mechanical Properties of Wood*, in *Wood Handbook*. 1999.

34. Harmathy, T.Z., *Mechanism of Burning of Fully-Developed Compartment Fires.* Combustion and Flame, 1978. **31**: p. 265-273.

35. Thomas, P.H., *Behavior of Fully Developed Fire in Enclosures.* Combustion and Flame, 1962. 6 (3): p. 133-135.